Modelling the Impact of Treatment and Adherence on Multi-Strain HIV Dynamics

by

Ashish Poonia

DEPARTMENT OF MATHEMATICS
INDIAN INSTITUTE OF TECHNOLOGY GUWAHATI
GUWAHATI-781039, INDIA

September, 2025

Modelling the Impact of Treatment and Adherence on Multi-Strain HIV Dynamics

A Thesis submitted
in partial fulfillment of the requirements
for the degree of

DOCTOR OF PHILOSOPHY

by

Ashish Poonia
(Roll Number: 196123102)

to the

DEPARTMENT OF MATHEMATICS
INDIAN INSTITUTE OF TECHNOLOGY GUWAHATI

September, 2025

Declaration

I hereby declare that the work contained in this thesis entitled **"Modelling the Impact of Treatment and Adherence on Multi-Strain HIV Dynamics"** was done by me, under the supervision of **Prof. Siddhartha Pratim Chakrabarty**, Professor, Department of Mathematics, Indian Institute of Technology Guwahati for the award of the degree of Doctor of Philosophy and this work has not been submitted elsewhere for a degree.

September, 2025

Ashish Poonia
Roll No. 196123102
Department of Mathematics
Indian Institute of Technology Guwahati

Certificate

It is certified that the work contained in this thesis entitled **"Modelling the Impact of Treatment and Adherence on Multi-Strain HIV Dynamics"** by **Ashish Poonia,** a student in Department of Mathematics, Indian Institute of Technology Guwahati, for the award of the degree of Doctor of Philosophy has been carried out under my supervision and this work has not been submitted elsewhere for a degree.

September, 2025

Prof. Siddhartha Pratim Chakrabarty
Professor
Department of Mathematics
Indian Institute of Technology Guwahati

To

My Family

Acknowledgements

I would like to express my heartfelt gratitude to everyone who supported and guided me throughout my research journey.

First and foremost, I would like to express my deepest gratitude to my supervisor, Prof. Siddhartha Pratim Chakrabarty, for his invaluable guidance, encouragement, and support throughout my Ph.D. journey. His constant encouragement and high academic standards have been instrumental in shaping this thesis and pushing me to deliver my best work. His guidance extended far beyond academic supervision, he has been incredibly patient and understanding, especially during the most challenging moments of my personal life over these years. His ability to recognize what a student might be going through, and his willingness to support me during those times, is something I deeply appreciate. His active involvement and concise yet insightful advice at critical stages of my research greatly shaped the direction and quality of this thesis. I am truly fortunate to have had him as my mentor.

I extend my sincere thanks to the members of my doctoral committee, Prof. Natesan Srinivasan, Dr. Sweta Tiwari, and Dr. Palash Ghosh, for their regular reviews, constructive feedback, and valuable suggestions, which significantly improved the quality of this thesis. Their insightful comments during progress presentations helped refine my research objectives and guided me toward a more focused and impactful direction. I am also grateful to all the faculty members of the Department of Mathematics, IIT Guwahati, for their direct and indirect support throughout my Ph.D. journey.

I would also like to express my heartfelt gratitude to my Master's project supervisor, Dr. Jai Prakash Tripathi, for laying the foundation of my research journey. His guidance during my Master's project not only sparked my interest in this field but also equipped me with the essential skills and mindset required to pursue research.

I am deeply grateful to my elder brother, Dr. Ankit Kumar, for his unwavering support, both academically and personally, throughout my journey. He has been a constant source of motivation and inspiration, and I have always aspired to follow in his footsteps. Our long discussions on completely random topics made this journey lighter and more enjoyable. During the most challenging phases of my life, he believed in me and encouraged me to keep going. I am truly fortunate and thankful to have such a supportive brother by my side.

I would also like to express my gratitude to my academic elder brother, Dr. Anupam Khatua, for his constant support and encouragement during my research journey. His willingness to discuss and help with any problem I encountered, no matter how small, was invaluable, especially during the later phases of this work. His guidance made a significant difference in shaping the final outcomes of this thesis. I am also thankful to Dr. Vijay Pal Bajiya for his early guidance during my Master's research, which laid a strong foundation for my Ph.D. work. I would further like to extend my thanks to my academic brothers-cum-friends, Deb Narayan Barik, Dr. Devang Sinha, and Amit Das, for their long discussions, light-hearted gossips, and memorable tea breaks, which brought much needed balance and joy to this journey.

I acknowledge the Council of Scientific and Industrial Research (CSIR), India, for providing me with financial support in the form of a JRF and SRF fellowship to pursue my thesis work. I would also like to extend my sincere gratitude to Prof. Tapan Kumar Kar for taking the time to evaluate my progress as an external examiner, which enabled the conversion of my fellowship from JRF to SRF.

I gratefully acknowledge the Indian Institute of Technology Guwahati for providing an excellent academic and research environment. I sincerely appreciate the technical staff, Mr Santanu Majumdar, Mr Pranpratim Borgohain, Mr Pranab Jyoti Boro, and the administrative staff for their consistent help and support throughout my time at the institute.

Further, I want to express my heartfelt thanks to my friends. First, I am grateful to Kailash Mohar and Aryan Bhambu, who have been like my brothers. Without their company, this journey would have felt much longer. I deeply appreciate the lifelong memories we have shared along the way. I would like to thank Sirshendu Pan and Dr. Shilpi Jain for their company and support, which made this journey truly complete. I always turned to you whenever I felt down, faced challenges, or needed to discuss anything. I extend my gratitude to all my batchmates—Anjali, Dr. Deepa, Dr. Gopinath, Madhab, Prakash, Ramendra, Rik, and Dr. Rupchand—for their encouragement and motivation throughout this journey. I also thank all fellow researchers in the department who, directly or indirectly, contributed to the completion of this work. I would like to extend my heartfelt thanks to my evergreen friends—Gaurav, Amandeep, Dr. Surjeet, Chiku, Gulashan, Hemant, Vikas, Heena, Garima, Pragya, Mohit, and Manoj—for their weekend company over the phone and for keeping me connected to home, so that no matter how far I was, it never felt like I was away from my hometown during this long journey. A special mention goes to the Krantikari group: Dr. Arnab Babak, Dr. Subhankar Nandi, Sagar Saha, Sirshendu, Bibakar and Aryan, whose unconditional support and readiness to help made a lasting impact. Finding such a remarkable group of friends at this stage has been an extraordinary blessing.

Most importantly, the note of thanks is incomplete without paying earnest and heartfelt gratitude to my family. Words cannot fully capture my appreciation for my respected grandparents Shri Bhagirath Singh, Smt. Sona Devi; my parents, Smt. Parbhati Devi and Mr. Rajendra Singh; my parents-in-law, Smt. Kamlesh Devi and Mr. Hemaram Mahala; my sister-in-law, Smt. Rakesh; my elder brother Mr. Ankit; and all members of my extended family, for their unconditional love, sacrifices, and unwavering belief in me. Their support has been the cornerstone of all my efforts.

Last but certainly not least, I offer my heartfelt thanks to my beloved life partner, and now my wife, Varsha. Her constant emotional support, patience, and understanding have carried me through the most challenging phases of this journey. Her unwavering belief in my ambitions, even during times when I doubted myself, has been my greatest source of strength. Thank you for standing by me through every high and low, for celebrating my small victories, for comforting me in moments of doubt, and for being my pillar of strength, my confidante, and my biggest cheerleader. This accomplishment is as much yours as it is

mine.

IIT Guwahati Ashish Poonia

Abstract

This thesis develops and analyzes a series of multi-strain mathematical models to investigate the transmission dynamics and control of Human Immunodeficiency Virus (HIV) in a community, with particular focus on the emergence of drug resistance, the role of treatment availability, and the impact of adherence to antiretroviral therapy (ART). Starting with a basic two-strain model in the absence of treatment, we establish that competitive exclusion prevents the coexistence of drug-sensitive and drug-resistant strains when only natural transmission pathways are considered. Extending this framework to include treatment availability and adherence, we demonstrate that coexistence becomes possible under certain conditions, and that treatment-related factors critically influence long-term epidemic outcomes. The models reveal the occurrence of transcritical and Hopf bifurcations, leading to periodic epidemic behavior within specific parameter ranges, and highlight the crucial role of transmission rates, disease-induced mortality, and treatment adherence in shaping epidemic trajectories. Building on this foundation, we further incorporate AIDS progression, diagnosis status, and treatment switching from first-line to second-line therapy. Analytical results establish conditions for the persistence or elimination of different strains, and sensitivity analyses identify key drivers of both short- and long-term dynamics, with parameter interactions exerting strong influence on epidemic outcomes. Optimal control theory is applied to design and compare multiple intervention strategies, including diagnosis-focused, treatment-focused, adherence-focused, balanced, and dynamic approaches. A dynamic optimization framework is proposed that achieves the UNAIDS 95-95-95 targets through efficient and adaptive allocation of healthcare resources. Cost-effectiveness analysis, adjoint-based sensitivity methods, and Shapley value analysis are employed to assess the economic viability of interventions and to quantify the relative contribution of each control measure. Overall, the results emphasize that while expanding treatment coverage remains important, the long-term success of HIV epidemic control depends critically on adherence-focused strategies and timely switching to second-line therapies. The models not only provide theoretical in-

sights into the mechanisms governing HIV dynamics but also deliver practical guidance for policy-makers in designing efficient, sustainable, and cost-effective intervention programs.

Contents

List of Figures

List of Tables

Chapter 1

Introduction

Infectious diseases have historically posed significant threats to human health, shaping the evolution of societies and their public health responses. From historical pandemics such as the Black Death to contemporary outbreaks like influenza, Ebola, COVID-19, and HIV, the emergence and transmission of infectious agents continue to challenge global health management. Infectious diseases are caused by the transmission of harmful pathogens, such as bacteria, viruses, fungi, or parasites, from an infected source to a susceptible host. Transmission pathways for these infections can be direct, involving physical contact (e.g., animal bites, sexual contact), or indirect, via contaminated media such as water, food, air, or disease-carrying vectors. The effective management and control of infectious diseases depend on the understanding of how pathogens spread within populations, how interventions can mitigate or remove their impact, and how resources can be optimally allocated to eliminate them.

Epidemiology, the study of the distribution and determinants of health-related conditions within populations, provides the fundamental framework for understanding the dynamics of diseases and formulating public health strategies. It examines patterns of diseases and health conditions at the population level, encompassing diverse areas such as disease transmission, outbreak investigation, surveillance, bio-monitoring, screening programs, and the evaluation of treatment interventions, including those conducted through clinical trials [1]. However, in general, the dynamics of infectious diseases are inherently nonlinear, shaped by a complex interplay of various biological, social, and environmental factors. These complexities often exceed beyond what descriptive statistics and empirical studies alone can capture. In such settings, mathematical modelling serves as a powerful tool to systematically analyze, predict, and interpret disease transmission patterns at both individual and population levels. These models abstract the key processes of disease transmission, progression, and control into quantifiable components. Mathematical models are not perfect replicas of biological reality, but structured simplifications of the processes involved, that reveal deeper insights into the

mechanisms and consequences of disease spread. With the advancement of computational tools and the increasing availability of high-quality epidemiological data, these models have become central to the design, evaluation, and optimization of disease control strategies.

In this thesis, we develop and analyze mathematical models to investigate the transmission dynamics of the Human Immunodeficiency Virus (HIV) at the community level, considering various factors that influence its spread. By integrating epidemiological data with theoretical analysis and control strategies, the thesis aims to provide insights into the design of more effective and sustainable public health intervention strategies for managing HIV. This work aligns with the broader use of mathematical modelling to inform infectious disease policy, intervention strategies, and optimize resource allocation for better public health strategies.

1.1 HIV/AIDS: A Global Health Challenge

Acquired Immunodeficiency Syndrome (AIDS) has remained one of the most persistent global public health challenges and a major contributor to worldwide mortality and morbidity since its emergence in the early 1980s [2]. AIDS is caused by HIV, a RNA retrovirus that primarily targets the immune system of the host and weakens its ability to defend against other opportunistic infections. Without treatment, the infection typically advances through multiple stages over several years, eventually resulting in AIDS. Despite decades of progress in biomedical research and intervention strategies, HIV/AIDS continues to pose significant health, social, and economic burdens worldwide.

The World Health Organization (WHO) classifies HIV infection as a global epidemic. According to the latest Joint United Nations Programme on HIV/AIDS (UNAIDS) reports, approximately 40.8 million people were living with HIV globally in 2024, with around 1.3 million new infections and 630,000 AIDS-related deaths reported in the same year [3]. Since the start of the epidemic, HIV has led to an estimated 91.4 million infections and 44.1 million deaths worldwide. Figure 1.1 illustrates global trends in the annual number of new HIV infections and the total population of people living with HIV (PLHIV) from 1990 to 2024. In India, where the epidemic is concentrated but heterogeneous across states, an estimated 2.6 million people are living with HIV as of 2024. Although the national incidence has declined markedly over the past two decades, specific geographic regions and high-risk groups, such as men who have sex with men (MSM), transgender individuals, female sex workers (FSW), and injecting drug users, continue to exhibit disproportionately high rates of transmission. India ranks third globally in terms of HIV burden after South Africa and Mozambique. These trends highlight the dynamic and region-specific nature of the HIV epidemic, emphasizing

the importance of tailoring public health interventions to local contexts, and the need for continued surveillance, treatment, and prevention efforts.

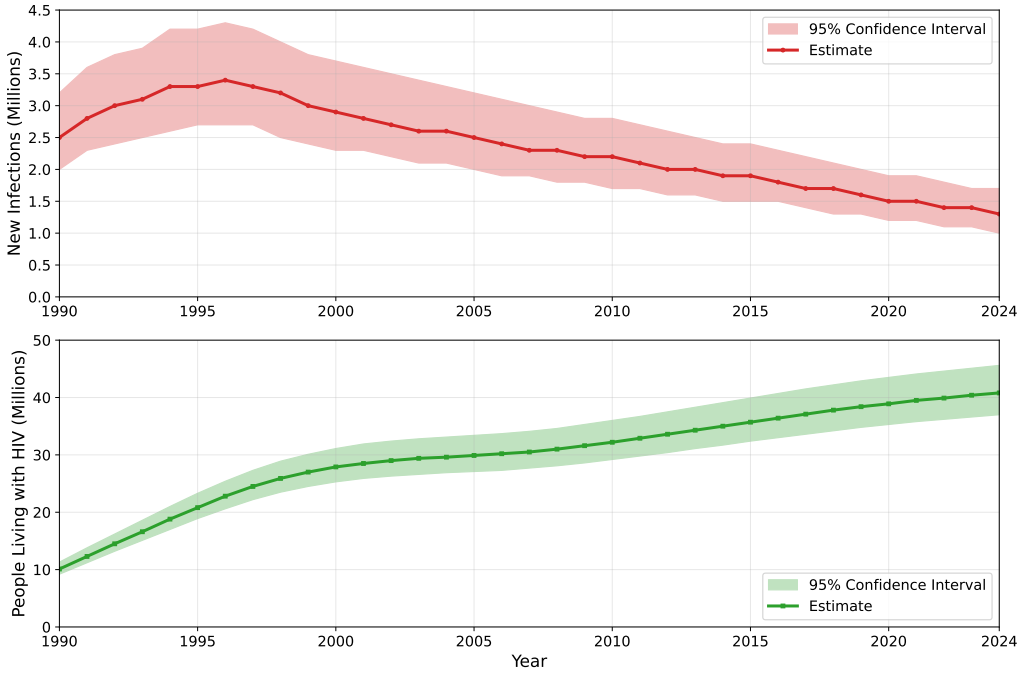

Figure 1.1: Temporal dynamics of the global HIV epidemic (1990-2024).

HIV is a biologically and epidemiologically complex disease, characterized by long latency periods, diverse disease outcomes, and highly variable transmission dynamics shaped by biological, behavioral, and socio-demographic factors. The long asymptomatic phase of the infection contributes to undetected transmission within communities, making early detection and timely intervention critical for epidemic control. It is further complicated by systemic influences such as healthcare access, stigma, mobility, and public health infrastructure. These multifaceted influences signify the importance of understanding the community-level mechanisms of its transmission for designing effective interventions and evaluating public health strategies. It is therefore essential to first understand the biological, clinical, and epidemiological characteristics of HIV before developing mathematical models that aim to represent the complex dynamics of its transmission at the community level.

1.2 Biological and Clinical Aspects of HIV Transmission

To provide a comprehensive overview of the multifaceted challenges posed by HIV, and the key factors that must be considered in developing mathematical models for HIV transmission, the following subsections describe the biological progression of HIV at the individual level, the mechanisms of its transmission within communities, and the critical roles of diagnosis, treatment, adherence, and drug resistance in shaping epidemic outcomes. These interconnected elements form the epidemiological foundation for the mathematical modelling framework developed in this thesis.

1.2.1 HIV progression and transmission dynamics

HIV is a chronic infection that can persist for 5 to 10 years without treatment, during which the immune system gradually deteriorates [4]. However, this duration can be extended to 30–40 years with treatment, depending on the quality and efficacy of the provided treatment. After initial exposure to HIV, the progression of infection in an individual typically divided into three stages: the acute phase, the chronic (or latent) phase, and the final progression to AIDS. Each stage is characterized by specific bio-indicators, particularly CD4+ T-cell counts and viral load, which reflect the state of immune function and viral activity [5]. The acute phase, which generally lasts for a few weeks post-infection, is characterized by a rapid increase in viral load and a corresponding sharp decline in CD4+ T-cell levels. Individuals in this phase often experience flu-like symptoms, but are highly infectious due to the elevated level of concentration of HIV in the bloodstream [6]. This is followed by the chronic or latent phase, which is typically asymptomatic and can last for several years. During this stage, the immune system initiates a response and stabilizes viral levels at a lower set point. Despite a relatively low viral load during this phase, individuals remain infectious. Most new HIV transmissions occur during this stage, particularly in long-term partnerships where individuals are unaware of their HIV status and are not receiving treatment [7]. Without any therapeutic intervention, CD4+ T-cell counts progressively decline over time, from healthy levels (approximately 800 to 1000 cells/mm^3) to below 200 cells/mm^3, in conjunction with the increase in viral load. This severe immunodeficiency characterizes the onset of AIDS, a condition associated with a high risk of other opportunistic infections. A detailed illustration of the time evolution of HIV infection is presented in [8]. This entire progression of infection typically takes 5 to 10 years in untreated individuals, though the timeline can vary across individuals due to biological and environmental factors such as host immunity, presence of

co-infections, and viral characteristics [4].

At the population level, the primary route for HIV transmission is sexual contact, but it can also spread via blood transfusion, needle sharing among injecting drug users, and vertical transmission from mother to child during pregnancy or breastfeeding. Heterosexual transmission remains the dominant route in most regions, accounting for approximately 70% of infections [9]. Although the probability of transmission per contact is relatively low for HIV compared to many other infectious diseases, but this is offset by the long duration of infectiousness and the often undiagnosed status of individuals in the chronic phase [10]. HIV transmission dynamics are also influenced by demographic, behavioural, socio-cultural, and socio-economic factors. Demographic factors, such as age distribution, gender, and migration patterns, affect both the level of exposure to HIV and access to healthcare services. Individual level behavioural factors, including number of sexual partners, condom use, and drug abuse, directly impact the likelihood of transmission. Socio-cultural factors, such as stigma, gender norms in society, and health-related beliefs, shape individual health-seeking behaviour and often can interrupt timely diagnosis and treatment. Similarly, socio-economic factors, including poverty, education level, and healthcare infrastructure, play a critical role in determining the ability to seek, afford, and adhere to HIV-related healthcare [11, 12]. All these factors shape the transmission dynamics of HIV at the community level and must be considered when developing realistic and effective intervention strategies.

1.2.2 Diagnosis and biomedical interventions

Early and accurate diagnosis of any infection is a fundamental step for effective disease management, as it enables timely initiation of preventive measures and appropriate treatment. Timely diagnosis of infection plays a key role in reducing onward transmission by encouraging behavioral change. However, despite global efforts to reduce HIV transmission, a significant proportion of people living with HIV (PLHIV) remain undiagnosed. According to UNAIDS estimates, around 5.3 million individuals were unaware of their HIV status in 2024, which is a major barrier to epidemic control [3]. Late diagnosis is a particularly concerning issue, as it is associated with higher risk of onward transmission, increased morbidity and mortality, and higher treatment costs as compared to timely diagnosis [13]. For HIV, late diagnosis is characterized by a CD4+ T-cell count ≤ 350 cells/mm^3 within 91 days of diagnosis [14]. The leading cause of late HIV diagnosis is insufficient testing, which is influenced by a complex network of societal, systemic, and individual factors. Structural or interpersonal discrimination based on sexual orientation, ethnicity, or age creates barriers to routine testing, health-seeking behaviours, and testing in response to symptoms of the disease [15].

Implementation of effective interventions to increase timely HIV testing can be achieved by identifying barriers in our local communities. Public education campaigns, wider availability of free or home-based testing kits, and policies aimed at reducing HIV-related stigma have shown promise in increasing testing uptake [10]. In addition, provider-initiated testing in clinical supervision and targeted testing strategies for high-risk groups are critical tools in expanding diagnostic coverage. The role of self-imposed behavioural modifications, driven by psychological fear and increased awareness through media and public health campaigns, has also been recognized as a key component in encouraging individuals to seek early testing and avoid high-risk behaviours [16, 17].

While prevention interventions are crucial prior to exposure, prompt initiation of treatment is essential following the diagnosis of infection to improve individual outcomes and reduce onward transmission by limiting opportunities for secondary infections. Ongoing efforts towards treatment and prevention have progressed significantly, but an definitive cure or preventive vaccine for HIV has yet to be developed. However, along with early diagnosis of infection, therapeutic interventions such as antiretroviral therapy (ART) have proven successful in substantially improving health outcomes and life expectancy for individuals living with HIV. ART involves the use of a combination of antiretroviral drugs that suppress viral replication significantly, reduce the viral load to undetectable levels, and allow for immune system recovery. As of December 2024, approximately 31.6 million people, representing around 77% of PLHIV, were receiving ART, a significant increase from 7.7 million in 2010 [3]. However, this figure remains below the global target of 34 million set for 2025. Although, the success of ART has significantly transformed HIV from a fatal infection into a manageable chronic disease, universal treatment coverage has not yet been achieved, and many individuals still lack consistent access due to economic, geographic, or structural barriers. The ART coverage still remains below the global target of 34 million set for 2025.

In addition to ART, biomedical prevention strategies have also emerged as powerful tools in reducing the incidence of HIV. One of the most widely adopted strategies is Pre-exposure Prophylaxis (PrEP), a preventive treatment involving the daily use of antiretroviral medications by individuals who are at high risk of acquiring HIV. PrEP has been shown to reduce the risk of sexual transmission by more than 90% and is recommended for individuals with HIV-positive partners, those with multiple sexual partners, or people who inject drugs [18]. Despite its proven effectiveness, challenges such as limited awareness, stigma, cost, and adherence issues continue to restrict PrEP uptake in many regions. Post-exposure prophylaxis (PEP) is an another HIV preventive tool, recommended only as an emergency intervention. It must be initiated within 72 hours of potential exposure, such as unprotected sex, needlestick injuries, or sexual assault. Apart from these biomedical interventions, behavioural and

structural strategies, such as consistent condom use, needle-exchange programs, and stigma-reduction initiatives, also play a crucial role in preventing HIV transmission, particularly in resource-limited and high-risk settings [19].

The modelling frameworks developed in this thesis are restricted to treatment-related interventions, while biomedical and behavioural prevention strategies are beyond the scope of the present study. The success of treatment depends on long-term adherence to the prescribed regimen. Interruptions in therapy or its sub-optimal adherence can reduce the effectiveness of ART and contribute to the emergence of drug-resistant strains, which remains a growing public health concern. These aspects of HIV treatment are further discussed in the following subsection.

1.2.3 Treatment adherence and emergence of drug resistance

Although ART has become increasingly available worldwide, HIV continues to disproportionately affect populations in low and middle-income countries, particularly in sub-Saharan Africa and parts of Asia, due to persistent challenges associated with treatment. ART is a lifelong therapy, and its effectiveness can be compromised by the occurrence of virologic failure. Virologic failure of ART is characterized by two consecutive assessments of viral load exceeding 200 copies/ml [20]. This failure can result from a combination of three broad categories of factors: patient-related, viral, and treatment-related. Among these, sub-optimal adherence to ART is the most common cause of virologic failure, which is related to the behaviour of patient [20]. Treatment adherence usually refers to the degree to which a patient adheres to the prescribed medications, and plays a vital role in the control of chronic diseases. Optimal adherence to ART ensures that sufficient drug concentrations are maintained in the bloodstream, thereby effectively suppressing viral replication [21]. It helps in preventing onward HIV transmission to others [22, 23], minimizing the emergence of drug resistance [24, 25] and brings down the HIV related mortality [26].

Depending on the treatment regimen, research suggests that maintaining an adherence rate of 80% to 85% or higher is typically sufficient for effective HIV viral suppression [27]. However, maintaining this level of adherence is often challenging due to a combination of personal attributes, institutional management, treatment related factors and psychological factors, in developing as well as developed countries [28]. The fear of disclosure of HIV diagnosis and subsequent stigma in the society [29–31], low self-efficacy and reading ability [32], as well as mental illness [30, 33] are some major concerning factors related to ART adherence. The situation gets exacerbated when two major diseases collide. In this context, the COVID-19 pandemic has severely affected the ART adherence in HIV patients. On one

hand, COVID-19 has interrupted the ART drug supply due to transportation difficulties (as most cities have implemented some form of lockdown), while on the other hand, overstretched health care system under COVID-19 resulted in lower quality of clinical care for HIV patients, in addition to suspension of HIV testing [34, 35]. It has also increased the cases of mental health issues such a depression and anxiety [36]. In July 2020, WHO announced that 73 countries have warned of being at risk of stock of ART medicines running out because of the COVID-19 pandemic, and 24 countries reported having either an extremely low stock of ARTs or disruptions in the supply of these vital medicines. Such interruptions in treatment provide an ideal environment for emergence of resistance to one or more components of the ART regimen. With the increasing accessibility of ART, maintaining optimal drug adherence is essential for controlling the emergence of drug-resistant strains of HIV.

The phenomenon of HIV drug resistance (HIVDR) continuously remains a major clinical and public health concern, as it can develop in newly infected patients (who access treatment) and be transmitted from infected individuals to others, posing a serious threat to treatment efficacy and disease control [20,37]. HIVDR can be classified as primary and secondary drug resistence. Primary HIVDR exists even before the initiation of ART. This type of resistance is usually transmitted from other drug-resistant infected person or acquired during previous treatment to eliminate vertical transmission of HIV or due to poor adherence to preventive methods like PrEP [38]. This leads to the failure of first-line regimens, especially when not identified at the time of ART initiation [39]. On the other hand, secondary HIVDR evolves through selection process between virus mutants. These drug-resistant mutants typically develop during treatment due to ongoing viral replication, which can result from either sub-optimal drug concentrations caused by poor adherence (patient-related factor) or from an inappropriate combination of ART regimens that fail to effectively suppress viral levels, even with good adherence (treatment-related factor) [25]. A study on drug-resistant mutations found a positive correlation between poor adherence to treatment and the number of drug-resistant HIV-infected individuals in the Leningrad region [40]. Risk factors associated with emergence of drug resistance are higher viral loads or lower CD4+ T-cell concentration, before initiation of treatment, particularly with less potent ART regimens. However, in some cases, the failure of viral suppression can be attributed to pharmacological factors, such as drug-drug or drug-food interactions, which result in sub-optimal pharmacokinetics and prevent sufficient serum concentrations of the antiretroviral agent [41].

ART is highly exposed to poor or sub-optimal drug adherence due to the various factors discussed above. Consequently, the risk of drug resistance is increasing in parallel with the global expansion of ART coverage. This increased risk not only compromises the effectiveness of first-line ART regimens but also necessitates timely clinical responses, including the

initiation of second-line or other alternative therapies. These treatment-switching strategies play a critical role in restoring viral suppression and are discussed in the following subsection.

1.2.4 Treatment switching

Timely switching of ART regimes is a critical component in the long-term disease management of HIV, particularly in the presence of virologic failure due to the emergence of drug-resistant strains. When the first-line ART regimens become ineffective, often due to poor adherence, suboptimal pharmacokinetics, or the development of resistant strains, continuing the same regimen can lead to further viral replication, immune deterioration, and increased risk of onward transmission. To prevent these outcomes, it is recommended to switch to second-line ART regimens as alternative therapeutic options, ideally composed of drugs with a different resistance profile and a higher genetic barrier to resistance [42]. The process of switching to second-line regimes is clinically complex and context-dependent. In developed regions, regular viral load monitoring and resistance testing enables timely identification of treatment failure and the prompt initiation of effective second-line regimens. However, in low and middle-income countries, such practices are either limited or unavailable, and treatment switching often depends on immunological indicators, which can delay the identification of virologic failure. Such delayed diagnosis of resistance increases the risk of transmitting drug-resistant HIV strains within the community.

Second-line ART regimens usually incorporate agents with stronger resistance barriers. Multiple large randomized controlled trials, particularly in resource-constrained settings where NNRTI-based regimens have been used as first-line therapy, have examined various options for second-line regimen combinations. These studies recommend prescribing at least two or three fully active ART drugs, with the potential addition of partially active drugs to leverage their immunologic and virologic benefits [42–44]. These studies further emphasized that second-line regimens should include agents with high resistance barrier, such as boosted protease inhibitors (PIs) or integrase strand transfer inhibitors (INSTIs) like dolutegravir (DTG), to minimize the risk of further resistance development.

While second-line regimens can effectively restore viral suppression in patients with first-line treatment failure and prevent disease progression, they often present significant practical challenges. These alternative regimes are usually more expensive, may have a higher pill burden or toxicity, and require close clinical monitoring [20]. These practical and economic constraints further complicate the timely implementation of switching treatments, particularly in resource-limited healthcare systems. Despite these limitations, second-line therapy remains essential for maintaining viral suppression and optimizing long-term treatment out-

comes in individuals with first-line ART failure. Note that, while the modelling approach in this thesis focuses on the population-level impact of treatment switching, a more detailed clinical understanding, including regimen selection, diagnostic criteria, and patient monitoring protocols, can be found in the *Guidelines for the Use of Antiretroviral Agents in Adults and Adolescents with HIV* [42]. A full clinical discussion is beyond the scope of this thesis.

The biological and clinical aspects discussed in this section, ranging from within-host disease progression and community-level transmission pathways to diagnosis, treatment, adherence, and resistance, represent critical components in understanding HIV dynamics at the population level. These factors are deeply interconnected and collectively influence the course of the infection, making them essential to consider when developing a modelling framework for HIV transmission dynamics. In the following section, we examine how mathematical modelling has evolved as a central tool in infectious disease epidemiology, with a particular focus on HIV.

1.3 Literature Review: Mathematical Modelling in HIV Epidemiology

Mathematical modelling has proven to be a powerful tool for understanding the dynamics of infectious diseases and informing effective public health policies. By translating various biological and epidemiological processes into mathematical equations, these models allow to simulate disease progression, assess intervention strategies, predict future outcomes under various scenarios, and identify the key determinants of disease dynamics. In the context of HIV, where the infection is characterized by prolonged and complex transmission dynamics, modelling plays a particularly crucial role in exploring epidemic patterns and optimizing control efforts. In this section, we first outline a brief history of mathematical modelling in epidemiology and then review major developments in the modelling of HIV infection. Particular emphasis is placed on the evolution of compartmental models, the incorporation of treatment and drug resistance dynamics, and the application of optimal control theory to resource allocation and public health interventions. By examining existing literature, this review aims to identify key trends, methodological advances, and gaps that motivate the modelling frameworks proposed in this thesis.

1.3.1 A brief history of mathematical modelling in epidemiology

Epidemiology has existed for centuries, but the systematic integration of mathematics to the study of infectious diseases began only a few hundred years ago. One of the earliest known

efforts to quantify disease outcomes was made by John Graunt in the 17th century [45]. His analysis of mortality data of plague disease in London laid the groundwork for statistical approaches to understanding modern life tables and demographic analysis. In the 18th century, Daniel Bernoulli proposed one of the first mathematical models in epidemiology, estimating the potential benefits of immunization with a living virus took from a mild case of smallpox, a foundational example of applying mathematics to evaluate public health interventions. A modern interpretation of Bernoulli's approach is developed using differential equations in [46]. The early 20th century marked a turning point for mathematical epidemiology. Ronald Ross, the father of modern mathematical epidemiology and renowned for his ground breaking work on malaria transmission [47], was among the first to use formal mathematical models to describe disease spread and control strategies. His work introduced the concept of a threshold condition for disease persistence, which is known today as the basic reproduction number. Ross was awarded the Nobel Prize in 1902 for his work on malaria. Subsequently, William Hamer applied principles from population dynamics to explain recurring patterns of measles outbreaks, emphasizing the role of contact rates in transmission. He was the first to apply the law of mass action to model the transmission of contagious diseases. Building on earlier efforts, however, the formal foundation of contemporary epidemic modelling was laid by the seminal work of Kermack and McKendrick in 1927 [48]. They introduced the SIR (Susceptible–Infectious–Removed) framework, a deterministic compartmental model that has since become the cornerstone of mathematical epidemiology. Their work demonstrated how disease dynamics could be captured using systems of differential equations, providing a theoretical foundation for understanding disease outbreak and its progression.

Since then, mathematical models have been extensively used to analyze diseases ranging from influenza [49] and Ebola [50] to HIV [51, 52] and COVID-19 [53, 54]. The inclusion of additional compartments, such as exposed, quarantined, hospitalized, or drug-resistant populations, has made these models more useful and better suited to inform public health decision-making. With the emergence of new pathogens and evolving public health challenges, the scope of modelling has expanded beyond deterministic approaches to include stochastic processes [55, 56], network models [57, 58], agent-based simulations [59], and models incorporating behavioral, social, and economic dimensions [60–63]. Modern modelling frameworks are often supported by empirical data drawn from clinical studies, surveillance systems, and unconventional sources like social media [64–66]. These models allow for estimation of key epidemiological parameters, simulate intervention scenarios, and evaluate strategies such as vaccination, treatment, contact tracing, and non-pharmaceutical interventions. Currently, mathematical modelling plays an important role in guiding responses to infectious disease outbreaks by providing real-time epidemic forecasting, resource alloca-

tion, and the design of effective control strategies. As data availability and computational tools are continuously improving, mathematical epidemiology is also becoming increasingly important as a critical pillar of evidence-based public health planning and intervention.

1.3.2 Mathematical modelling of HIV transmission

Modelling the spread of HIV poses unique challenges compared to many other infectious diseases. Unlike acute infections such as influenza or COVID-19, HIV is characterized by a long incubation period, chronic progression, and often years of asymptomatic infection. These characteristics contribute to increased transmissions, particularly when individuals remain undiagnosed. Furthermore, HIV transmission is strongly shaped by sexual behavior, patterns of partnerships, and social and structural factors such as stigma and healthcare access. To realistically capture the infection dynamics, these factors must be incorporated into mathematical models. The combination of biological complexity and strong behavioral components makes HIV fundamentally different from short-duration epidemics, requiring specialized modelling approaches.

After the emergence of HIV in the early 1980s, initial modelling efforts adapted classical SIR frameworks to explain the persistence of HIV within populations. Anderson and May [51, 67] were among the pioneers who made initial attempts to model the transmission of HIV within a community. They quantified key components of HIV spread such as contact rates, transmission probability, duration of infectiousness. Using a basic reproduction number based analysis, they concluded that reversing the epidemic would require substantial behavioral changes and increased control efforts. Subsequently, various refinements have been introduced to the modelling frameworks to capture the chronic nature of HIV by incorporating longer infectious periods, progressive stages of infection, variability in sexual contact structures. Jacquez et al. developed a stage-structured HIV transmission model showing that the high infectiousness during the acute phase plays a disproportionate role in accelerated early epidemic growth, suggesting that interventions targeting recent infections could substantially reduce transmission [68]. The infectiousness of HIV is not constant over time but varies markedly across different stages of infection. The epidemiological contribution of each phase of HIV infection is highly sensitive to the assumed mathematical relationship between viral load and transmissibility [69]. Estimates of relative infectiousness indicated that the primary and late stages are associated with substantially higher transmissibility than the long asymptomatic chronic phase [70]. However, the sexual contact patterns during the chronic phase of infection is also vital to access the long-term impact of the disease. In a classical work on the impact of concurrent (overlapping) sexual partnerships in HIV spread,

Morris et al. [71] used stochastic network simulations and demonstrated that concurrency can lead to a significantly higher prevalence of HIV compared to serial monogamy, even when individuals have the same number of lifetime partners. These studies highlighting the importance of modelling these distinct infection phases explicitly. Hyman et al. [72] developed a stage-progression model that explicitly incorporated the differential infectivity across distinct phases of HIV infection and emphasized the importance of early intervention efforts for effective control of the epidemic. The basic SIR-type modelling framework was further improved by introducing additional compartments to capture different forms of heterogeneity in the population [6, 7, 73, 74].

Furthermore, these extended models have been integrated with behavioural, social, and economic factors that influence the transmission dynamics of HIV within and across populations. Incorporating such factors into the design of prevention strategies has been recognized as essential for effective HIV control. Behavioural factors such as sexual risk-taking, concurrency of partnerships, and injecting drug use can generate disproportionate effects on epidemic growth. In a review article, Mishra et al. [75] studied behavioural heterogeneity and behaviour change among infected and high-risk individuals, incorporating factors such as condom use, contact rates, and mixing patterns between high- and low-risk groups. They concluded that individuals in high-risk groups who engage in frequent multiple or concurrent partnerships play a critical role in the establishment and persistence of heterosexual HIV epidemics and should therefore be a primary target for effective interventions. Beyond individual behavior, social and structural determinants such as stigma, gender inequality, and migration significantly influence HIV spread. Social stigma and discrimination reduce testing uptake and adherence to treatment, which indirectly increase the community-level prevalence of the infection. Migration and mobility patterns also reshape local epidemics by linking high and low-prevalence regions and by increasing high-risk sexual behaviors among migrants [76]. Models based on economic considerations such as treatment costs, healthcare budgets, and cost-effectiveness analyses further improve the outcomes and provide valuable insights for policymakers. In a review of the cost and impact of scaling up PrEP for HIV prevention, which examined key issues such as prioritization strategies, adherence, behavior change, toxicity, and resistance, it was concluded that PrEP can be a cost-effective HIV preventive method in specific settings, particularly when targeted at high-risk populations. However, its cost-effectiveness and affordability remain highly sensitive to drug prices, program coverage, and individual adherence levels [77].

Another important direction in the mathematical modelling of HIV transmission has been the study of co-infections with other pathogens, particularly tuberculosis (TB), hepatitis B (HBV), and hepatitis C (HCV) [78–84]. HIV infection suppresses the immune system of

the infected individual, increasing susceptibility to opportunistic infections, which in turn accelerate disease progression and complicate treatment outcomes. According to WHO, TB remains the leading cause of mortality among PLHIV with an estimated figure of 30% of all AIDS-related deaths worldwide. These models aim to examine the synergistic effects that arise when two or more epidemics co-occur and mutually reinforce each other. Studies incorporating HIV–TB comorbidity have examined the bidirectional interactions between the two pathogens, demonstrating how HIV infection accelerates the reactivation of latent TB, while TB co-infection further increases HIV-related morbidity and mortality [80, 84]. Similar modelling frameworks have also been extended to HIV–HBV and HIV–HCV co-infections, emphasizing the additional challenges posed by liver-related complications and the complexities of treatment interactions [81–83].

The development of mathematical modelling frameworks that integrate the aforementioned factors has provided valuable insights into the drivers of HIV transmission within communities. Building on this foundation, we now review key modelling advancements that explicitly incorporate prevention and treatment interventions, particularly ART, and explore how these have shaped our understanding of epidemic control.

Modelling of prevention and treatment interventions for HIV

The investigation of preventive measures and treatment options through mathematical modelling, along with the identification of feasible strategies for their implementation at both individual and population levels, has remained a central focus of epidemiological studies. For HIV, researchers have consistently translated both biomedical (direct) and behavioural (indirect) preventive interventions into quantifiable outcomes. The use of PrEP with sufficiently high adherence has been shown to substantially reduce HIV incidence in high-risk groups, such as MSM population and serodiscordant couples [85]. If targeted efficiently, PrEP can yield the largest reductions in HIV incidence and serves as a highly cost-effective preventive strategy. Similarly, other biomedical interventions such as PEP and condom use, along with harm-reduction strategies for people who inject drugs (PWID), also contribute to reducing the overall incidence of HIV infection. The role of condom use in reducing HIV burden has been highlighted in a comparative study of two mathematical models, where hypothetical increases in condom use within both spousal and nonspousal relationships were evaluated as an intervention strategy [86]. Further, Omondi et al. [87] developed and analyzed a deterministic model to capture cross-group transmission between commercial sex workers (CSWs) and PWID, evaluating the impact of combined interventions. Their findings indicated that integrated strategies, simultaneously reducing needle sharing among PWID

and unsafe sexual practices between CSWs and their clients, synergistically reduce HIV transmission more effectively than single-route interventions applied in isolation. Voluntary medical male circumcision, supported by randomized trials in southern and eastern Africa, has been shown to produce sustained reductions in HIV incidence when scaled up in high-prevalence regions [88]. Beyond biomedical and harm-reduction tools, models incorporating structural and behavioural factors, such as stigma reduction, lowering gender inequality, and risk-behaviour change through individual and educational campaigns, consistently demonstrate that targeting prevention efforts to the highest-risk groups yields the greatest efficiency [31, 89]. The effect of self-imposed behavioral changes due to psychological fear and awareness through media is very crucial in reducing the transmission of HIV worldwide in the absence of an effective biomedical intervention [16, 17].

Preventive measures are crucial before exposure to infection, while timely diagnosis followed by prompt treatment is essential for effectively curbing the disease. Early modelling analyses in the 1990s and 2000s explored the impact of ART initiation at different CD4+ T-cell thresholds [90]. Clinical guidelines for ART have evolved rapidly in response to the remarkable progress achieved in HIV therapeutics. A major paradigm shift occurred with the emergence of treatment as prevention (TasP), the concept that viral-load suppression through ART prevents onward transmission. This shift directed research attention to assess the impact of early ART initiation, which was shown to dramatically reduce sexual transmission within serodiscordant partnerships [23]. Various mathematical modelling approaches have been employed to investigate strategic ways of expanding ART coverage and identifying the most efficient methods for reducing community-level HIV incidence through ART. Test-and-treat is a well-studied approach that involves screening individuals at risk of HIV and providing prompt treatment to those who diagnosed with the infection. This early intervention reduces secondary infections and consequently lowers the overall disease burden [91]. In [92], the authors proposed a mathematical model to examine the impact of late diagnosis on the spread and control of HIV. Their findings highlighted the importance of encouraging early initiation of HIV treatment and promoting self-testing programs to increase the proportion of individuals who are aware of their HIV status.

Furthermore, In addition to the test-and-treat approach, mathematical models have been developed to study the role of treatment with the integration of various aspects of HIV transmission dynamics. Cai et al. [4] examined HIV/AIDS model with treatment by considering two different stages of the infection period as asymptomatic and symptomatic and compared the results with a time-delayed system in which treatment becomes effective after a certain time. A comprehensive global analysis of a Susceptible-Infected-Chronic-AIDS (SICA) compartmental model was carried out in [93]. The study concluded that substantial increase

in treatment coverage and transmission reduction were essential to meet the UNAIDS 2030 target of ending AIDS. Further, Gurski et al. [7] developed a dynamic compartmental model that captured staged HIV transmission within both casual and long-term partnerships, and incorporated treatment processes alongside partnership dynamics. Their analysis concluded that infection rates vary substantially by partner type and disease stage, indicating that long-term partnerships contribute uniquely to the overall transmission dynamics. Overall, while universal ART access combined with frequent testing could avert a large proportion of new infections, the outcomes depend strongly on adherence and retention in care.

Modelling of ART adherence and multi-strain HIV transmission dynamics

The effectiveness of treatment is strongly dependent on the degree to which individuals follow the prescribed medication plans. Suboptimal or poor adherence reduces the suppressive effect of ART, allowing viral replication to continue, which in turn accelerates the risk of developing drug-resistant HIV strains. Several modelling studies have provided insights into how adherence patterns affect the efficacy of ART, demonstrating that adherence acts as a threshold parameter for treatment success. Rosenbloom et al. [94] developed a within-host stochastic model to evaluate how the relationship between adherence and the likelihood of development of drug-resistance varies across different ART drug classes. Their results suggested that intermediate levels of adherence, where drug concentrations are sufficient to suppress drug-sensitive strains but insufficient to fully prevent replication, pose the highest risk for the emergence of resistant strains. This finding highlighted the nonlinear relationship between adherence and resistance, in which both very high and very low adherence minimize the probability of development of resistance, whereas moderate adherence creates the greatest risk. At the population level, Braithwaite et al. [95] used computational simulations to study the role of adherence in ART efficacy, showing that imperfect adherence not only compromises individual viral suppression but also reduces the broader prevention benefits of ART. In a recent study, Lai et al. [96] developed a dynamic transmission model incorporating CD4+ T-cell count based diagnosis, treatment, and adherence rates, while accounting for both transmitted and acquired drug resistance. Their findings showed that poor adherence can compromise the benefits of ART expansion and accelerate the spread of drug resistance. This underscores that maintaining adherence among treated individuals is as critical as expanding ART coverage to those not yet on treatment.

The emergence and spread of drug-resistant HIV strains has motivated the development of multi-strain mathematical models. The dynamics of multi-strain epidemics differ fundamentally from those of single-strain epidemics due to ecological competition between resistant

and sensitive strains, as well as differences in the processes that sustain them. While single-strain epidemics are fuelled solely by transmission, multi-strain epidemics are driven by both the emergence of resistance and its subsequent transmission [97]. Recent studies have applied multi-strain mathematical models to examine how ecological interactions and evolutionary mechanisms influence the transmission dynamics of infectious diseases [96, 98–101]. These models typically extend the classical compartmental frameworks by dividing the infected population into compartments for drug-sensitive and drug-resistant strains. Blower et al. [102] used a multi-strain transmission model combined with a statistical framework that incorporated high degree of uncertainty in the treatment effects of ART, changes in risky behaviour, and the rate of drug resistance emergence. It highlighted two potential long-term outcomes of widespread ART use. In the optimistic scenario, HIV elimination is achievable, whereas in the pessimistic scenario, driven by factors such as suboptimal adherence, a second wave of the epidemic may be sustained by multidrug-resistant strains. Sharomi et al. [98] developed a two-strain HIV model of six compartments with the inclusion of drug-sensitive and drug-resistant HIV-infected populations. In this study, the authors analyzed the impact of ART on HIV dynamics and concluded that the widespread use of ART, despite the risk of the development and transmission of drug-resistant strain, can lead to a significant reduction in disease burden or even eradicate the HIV infection from a community, under certain conditions. Further, Kuddus et al. [100] investigated a two-strain model for general infectious diseases that have a protracted infectious period with treatment. They suggested that the emergence of drug resistance could be reduced if the treatment rate is sufficient to eliminate the drug-sensitive strain from the population. Various recent studies have demonstrated that, in the long term, drug-sensitive strains often face competitive exclusion from the population in the presence of emerging drug-resistant strains [99,100]. Subsequent multi-strain models applied to the ART scale-up in sub-Saharan Africa confirmed that the spread of transmitted resistance could severely reduce the public health benefits of treatment if not carefully managed [96, 103]. Multi-strain frameworks thus serve as a valuable tool for exploring the trade-offs between expanding ART coverage and managing resistance. They further demonstrate the critical importance of timely access to second-line therapies.

To address how to detect treatment failure and determine when to switch to second-line ART, Keebler et al. [104] combined three independently developed transmission models to compare monitoring strategies. They found that routine viral load monitoring with defined thresholds enables earlier switching, leads to better health outcomes, and is often cost-effective compared to clinical or CD4+ T-cell-based monitoring in generalized epidemics. However, recent systematic reviews have shown that HIV models vary widely in how they incorporate viral load monitoring, highlighting that assumptions about testing intervals,

confirmatory testing, and loss to follow-up critically influence predicted switching rates and resistance dynamics [105–107]. To evaluate the effectiveness of second-line therapy, Shen et al. [108] developed an infection–age-structured mathematical model that examined the effects of ART initiation timing, frequency of acquired drug resistance, and second-line drug efficacy on both total and drug-resistant HIV incidence. Their results indicated that earlier ART initiation reduces the overall number of infections, including those with drug resistance, provided second-line therapy remains highly effective (greater than 80%). However, they also found that earlier initiation may increase the proportion of new infections that are drug resistant. Further, with the ongoing expansion of ART, the number of patients requiring second-line therapy is steadily increasing. Estill et al. [109] developed a simulation model to project the demand for second-line ART in adults in sub-Saharan Africa up to 2030, incorporating factors such as viral load monitoring availability, ART scale-up speed, and rates of retention and switching. Their projections suggested that, even under optimistic first-line performance, more than 2 million people in the region will be receiving second-line ART, while over 4 million will be in need by 2030.

Irrespective of ART scale-up strategies or patient management approaches, the demand for second-line drugs is expected to rise substantially in the future as countries increase access to routine viral load monitoring. In such scenarios, mathematical models that incorporate optimal control theory and strategic resource allocation frameworks become important for sustainable HIV management.

Optimal control and resource allocation models for HIV treatment

The application of optimal control theory to infectious disease dynamics has a long history for effective disease management. Early epidemiological studies explored vaccination, isolation, treatment or health promotion campaigns as control variables in simple SIR-type frameworks aiming to maximize health benefit subject to budget constrains [110–114]. As a progression, Lenhart and Workman provided a fundamental framework for applying Pontryagin's Maximum Principle to epidemic models [115]. These pioneering works established the mathematical foundation for determining time-dependent control strategies that minimize disease burden while balancing intervention costs. The central aim was to move beyond descriptive modelling toward providing quantitative guidance for strategic resource allocation and intervention planning to the policy makers.

With the emergence of the HIV epidemic, optimal control models gained special interest from the researchers due to the chronic nature of the infection, the high cost of long-term ART, the risk of drug resistance, and the wide range of available prevention and treatment

interventions. Early applications of optimal control theory to HIV treatment primarily focused on determining the optimal timing of ART initiation, aiming to maximize therapeutic benefits while minimizing drug toxicity. Kirschner et al. [116] introduced one of the earliest within-host HIV models using control theory to optimize the use of ART drugs, showing that structured treatment interruptions could, in principle, balance treatment efficacy and drug toxicity. Similar results were obtain in [117, 118]. Although such strategies were later rejected in clinical practice, these works highlighted the potential of optimal control methods in shaping HIV treatment strategies. Shechter et al. used a Markov decision process–based optimization model aimed at maximizing the quality-adjusted lifetime of a patient [119]. Their findings highlighted that early initiation and sustained continuation of treatment represent the optimal strategy for achieving this goal.

As ART coverage expanded globally, researchers focused on balancing coverage and adherence related factors, incorporating resource allocation into their models. Okosun et al. [120] developed an optimal control model to evaluate the combined impact of condom use, screening of unaware HIV-positive individuals, and treatment in a population with ongoing susceptible immigration. They concluded that undiagnosed HIV infections impose substantial burden on community-level costs. Moreover, implementing a combination of all three interventions was identified as the most cost-effective strategy for reducing HIV transmission. Takaidaza et al. proposed an optimal control model for HIV/AIDS transmission in communities affected by substance abuse [121]. Their framework examined the impact of strategies such as treating substance-abusing susceptibles, providing counselling, and implementing prevention measures to curb the spread of infection. In [122], the authors analyzed an optimal control model incorporating time-dependent ART allocation and demonstrated that prioritizing treatment for individuals in the early stages of infection is most effective in reducing new infections and total infection-years. In contrast, allocating resources to later-stage patients resulted in minimizing overall costs and HIV-related mortality. Further, Ayele et al. [123] developed an HIV/AIDS compartmental model that incorporated diagnosis and awareness as key factors, with the rates of becoming aware or unaware modelled as functions of media campaigns, while screening and treatment rates were assumed constant. Their analysis demonstrated that combining optimal control strategies substantially reduces the numbers of unaware susceptibles, undiagnosed infectives, diagnosed infectives, and individuals with AIDS symptoms. Moreover, they found that the joint implementation of preventive and screening strategies is the most cost-effective approach. In general, combining multiple intervention methods achieve better outcomes than relying on a single strategy, since HIV spreads through multiple transmission routes [123, 124]. Controlling the recruitment of susceptible individuals into the population can also serve as an effective strategy for

optimally reducing the disease burden [125]. Similar optimal control frameworks have also been extended to other modelling approaches, such as reaction–diffusion systems, fractional-order models and stochastic models, to capture spatial heterogeneity, memory effects, and randomness in biological dynamics [126–129].

Mathematical models with optimal control theory has also been extensively used to study HIV co-infections with other major diseases such as TB, HBV, HCV, malaria, and most recently COVID-19 [130–136]. Agusto and Adekunle developed an HIV–TB co-infection model with two TB strains and applied optimal control to evaluate treatment combinations [130]. They showed that integrated control strategies, targeting both diseases simultaneously, can substantially reduce the co-infection burden and improve cost-effectiveness compared to isolated interventions. Similarly, Silva et al. [131] showed that simultaneous implementation of ART and TB treatment minimise the disease prevalence and total intervention costs. Mallela et al. [132] applied optimal control theory to HIV–TB co-infection treatment and demonstrated that treatment timing and coordination were critical for reducing long-term infection levels. Further, Fatmawati et al. [133] studied an HIV–malaria co-infection model, applying multiple optimal control strategies such as ART, malaria treatment, and preventive interventions like bed nets. Their results emphasized that combined prevention and treatment yielded the most significant reductions in co-infection prevalence. Recently, Majumder et al. examined HIV–TB dynamics under the effects of COVID-19, introducing awareness campaigns and treatment saturation into an optimal control model [134]. They concluded that maintaining awareness and treatment programs was essential to prevent a resurgence of both epidemics during COVID-19 pandemic. Similar benefits of using optimal combinations of multiple treatments to manage co-infections of different diseases simultaneously have also been highlighted in [135, 136].

At the 20^{th} International AIDS Conference in 2014, UNAIDS introduced the 90-90-90 global targets as a strategic framework for HIV epidemic control [137]. These goals aimed for 90% of all individuals living with HIV to be diagnosed, 90% of those diagnosed to receive ART, and 90% of individuals on ART to achieve viral suppression by the end of 2020. Furthermore, UNAIDS has proposed the more ambitious 95-95-95 targets to be achieved by 2030, which are expected to result in approximately 86% overall viral suppression. Achieving these goals in an optimal manner remains a significant challenge, particularly for low and middle-income countries with a high prevalence of HIV. Xue et al. [17] incorporated the 90-90-90 framework by mathematically quantifying each step-diagnosis, treatment uptake, and viral suppression, within their compartmental model, and formulated the model with behavioral fear effects. They concluded that, while implementing the 90-90-90 targets significantly reduces new infections, it would still require approximately 26 years to eliminate new HIV

cases entirely. In addition, the optimal control to reduce the development and transmission of drug-resistant HIV strains introduces additional complexities, especially in the context of treatment strategies involving first- and second-line treatments.

Overall, these studies show that optimal control and resource allocation models provide valuable insights for controlling the infection. These frameworks not only quantify the benefits of multiple intervention options but also highlight critical trade-offs, such as early versus delayed treatment initiation, switching between first-line and second-line ART, and the long-term sustainability of intervention programs. By integrating cost-effectiveness analyses, these models extend their relevance beyond biological insights to the economic feasibility of interventions. This is particularly important in resource-limited healthcare systems, where budget optimization is essential for translating theoretical findings into practical policy recommendations.

1.4 Motivation and Research Questions

A central challenge in HIV public health policy lies in determining whether to universally expand treatment access, despite the risk of sub-optimal adherence and consequent emergence of drug resistance, or to adopt a more strategic allocation of resources that balances treatment coverage with adherence support. This dilemma is further complicated by the need for timely switching to second-line therapy, which is critical for managing treatment failure but imposes additional burdens on limited healthcare resources. Mathematical modelling has become an indispensable tool for analyzing the complex community-level dynamics of HIV transmission and for shaping effective public health policies. Despite the significant progress made in modelling frameworks to replicate the HIV transmission dynamics, these important challenges remain unaddressed or partially addressed. Many existing studies simplify the biological and clinical processes of HIV by neglecting the effects of treatment coverage, adherence, drug resistance, and treatment switching, or by considering them in isolation rather than as interconnected processes. Furthermore, while optimal control theory and resource allocation models provide valuable policy insights, there is still a need to tailor such approaches to integrate these processes simultaneously into the modelling framework to account for the practical constraints of healthcare systems. In line with the UNAIDS 95-95-95 targets for 2030, the need for such robust modelling frameworks becomes even more crucial. Achieving these ambitious targets requires not only expanding treatment coverage but also addressing adherence, resistance, and timely treatment switching. Addressing these challenges is the central motivation of this thesis.

Based on this motivation, this thesis seeks to address the following research questions

through various mathematical modelling frameworks:

1. **How can multi-strain models be formulated to capture the competition and coexistence of drug-sensitive and drug-resistant HIV strains at the community level, and what insights do they provide about the long-term persistence of resistance in a community?**
   Approach: To address this question, we develop and analyze a basic multi-strain SI-type model that incorporates both drug-sensitive and drug-resistant HIV infected individuals in the absence of treatment. By applying stability and bifurcation analysis, we investigate the conditions that govern the coexistence or competitive exclusion of strains, providing insights into the long-term epidemiological burden of drug resistance in absence of treatment.

2. **What is the impact of varying ART coverage and drug adherence levels on the emergence of drug resistance and the overall epidemic trajectory?**
   Approach: To explore this question, we extend the basic multi-strain SI-type model by incorporating ART coverage and adherence levels. Through qualitative analysis of the extended model, we examine how increasing treatment coverage with different adherence levels influence the emergence of resistance and the long-term epidemic outcomes. This approach highlights the trade-offs between expanding ART coverage and ensuring sufficient adherence.

3. **What role does the timely diagnosis and initiation of second-line ART play in reducing treatment failure? Which epidemiological parameters have the greatest influence on HIV transmission and model outcomes, and how can these insights guide effective policy design?**
   Approach: We extend previous modelling frameworks by explicitly incorporating diagnosis and second-line ART related classes to capture treatment failure and its management. We then apply both local and global sensitivity analysis to systematically assess the influence of epidemiological parameters on various disease outcomes. By ranking the influence of key parameters, we provide a guidance to where resources and efforts should be concentrated.

4. **What can be the optimal resource allocation strategies that balance treatment scale-up, adherence support, and second-line therapy provision in order to achieve sustainable epidemic control within constrained healthcare systems?**
   Approach: To explore this question, we apply optimal control theory to the extended

model in order to evaluate optimal intervention strategies that balance diagnosis, treatment scale-up, adherence support, and second-line ART provision. The framework allows for a systematic examination of trade-offs between competing priorities, identifying strategies that minimize both the health and economic burden of HIV. Further, a cost-effectiveness analysis is carried out to compare proposed strategies, thereby determining which strategies provide maximum benefit per unit cost. This combined approach ensures long-term sustainability of resource allocation under limited resource settings.

1.5 Biological and Mathematical Preliminaries

In this section, we present the fundamental biological and mathematical concepts, definitions, and terminologies that will be frequently used throughout this thesis. These preliminaries provide the essential foundation for formulating and analyzing viral dynamics within a mathematical modelling framework.

1.5.1 Compartmental modelling framework

In mathematical epidemiology, compartmental models provide a structured way to describe the dynamic spread and control of infectious diseases at both individual and population levels. The central idea is to divide the whole population into distinct groups or 'compartments', based on their individual characteristics related to disease status, and then describe the rules governing the transitions of individuals between these compartments over time. For example, in the classical SIR model, individuals are classified as susceptible (S), infected (I), or recovered/removed (R). The changes in these compartments are typically governed by systems of ordinary differential equations, where transition rates represent biological processes such as infection, recovery, or disease-induced mortality. Susceptible individuals become infected upon effective contact with an infectious individual, and infected individuals eventually recover or die from the disease. This process can be written as:

$$\begin{aligned} \frac{dS}{dt} &= -\beta SI, \\ \frac{dI}{dt} &= \beta SI - \gamma I, \\ \frac{dR}{dt} &= \gamma I, \end{aligned} \tag{1.5.1}$$

where β is the transmission rate and γ is the recovery or disease-induced mortality rate. The schematic representation of this model is presented in 1.2.

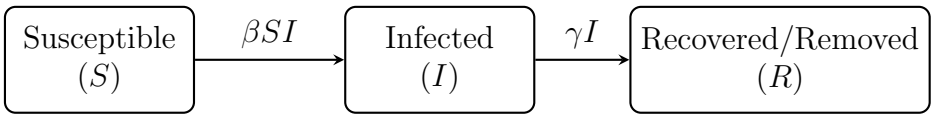

Figure 1.2: Schematic representation of the classical SIR model.

Further, additional compartments can be introduced to account for specific characteristics of a disease. For HIV, this might include acute infection, asymptomatic infection, AIDS, treatment classes, or drug-resistant strains. Likewise, the inclusion of demographic processes, such as birth, death, and migration, makes the model more realistic for long-term population studies. More detailed aspects of these fundamental models are discussed in [138].

1.5.2 Basic reproduction numbers

The basic reproduction number, generally denoted by R_0, is a threshold parameter in epidemic and viral dynamics models. It represents the average number of secondary infections generated by a single infectious individual during its entire infectious period, when introduced into a completely susceptible population. This dimensionless measure is an important indicator related to the potential spread of the disease within a community. Its importance lies in its role as a threshold parameter:

- If $R_0 < 1$, the infection cannot sustain itself and eventually dies out.
- If $R_0 > 1$, the infection persists in the population and may lead to an endemic state.

In literature, several approaches exist for calculating R_0. Among them, the next generation matrix method is one of the most widely applied due to its generality [139, 140]. In this method, we first separate the system into infected and non-infected compartments. Let the model consist of n compartments, with m of them representing infected classes. Denote the state vector by

$$Y = (y_1, y_2, \ldots, y_n),$$

where y_i gives the proportion of individuals in the i-th compartment. For the infected compartments, let $\mathcal{F}_i(Y)$ is the rate of arrival of susceptible individuals as new infections in the i-th compartment, and

$$\mathcal{V}_i(Y) = \mathcal{V}_i^-(Y) - \mathcal{V}_i^+(Y),$$

where $\mathcal{V}_i^-$ denotes the rate at which individuals leave the i-th compartment, and $\mathcal{V}_i^+$ represents the rate at which individuals enter the i-th compartment due to transitions from other compartments. At the disease-free equilibrium $Y = Y_0$, the matrices,

$$F = \left[\frac{\partial \mathcal{F}_i(Y_0)}{\partial y_j}\right], \qquad V = \left[\frac{\partial \mathcal{V}_i(Y_0)}{\partial y_j}\right], \quad i, j = 1, \ldots, m$$

are constructed. The *next generation matrix* is then defined as,

$$G = FV^{-1}.$$

Finally, the basic reproduction number is given by,

$$R_0 = \rho(G),$$

where $\rho(G)$ denotes the spectral radius (the largest eigenvalue in modulus) of G. Since G is a non-negative matrix, the spectral radius is real and non-negative, making R_0 a well-defined threshold quantity.

1.5.3 Dynamical system and its stability analysis

Dynamical systems, particularly those formulated through systems of ordinary differential equations, provide a natural framework to describe time-dependent processes in epidemiology and population biology. A general non-linear autonomous system can be expressed as

$$\frac{dX}{dt} = F(X), \quad X \in \mathbb{R}^n, \tag{1.5.2}$$

and $F(X)$ is a smooth vector-valued function governing their rates of change. Since $F \in \mathcal{C}^1$ (and hence locally Lipschitz), this system admits a unique local solution for any given initial condition.

Definition 1.5.1. ***Equilibrium points:*** *A point $X^* \in \mathbb{R}^n$ is called an equilibrium (or steady state) of system (1.5.2) if*

$$F(X^*) = 0.$$

In epidemiological modelling, equilibria often correspond to biologically meaningful scenarios. The disease-free equilibrium (DFE) represents the absence of infection in the population, whereas the endemic equilibrium (EE) characterizes a persistent state where infection coexists with the susceptible population. The stability of these equilibrium points plays a key role in determining the long-term dynamics of the system. If the DFE is stable, the infection eventually vanishes, while stability of the EE implies that the infection persists for a long time in the community.

Stability of equilibria

We recall the following definitions related to local and global stability of equilibrium points:

Definition 1.5.2. ***Local stability:*** *An equilibrium point* $\mathbf{X}^*$ *of the system* (1.5.2) *is said to be locally stable if, for any* $\epsilon > 0$*, there exists a* $\delta > 0$ *such that*

$$|\mathbf{X}(t_0) - \mathbf{X}^*| < \delta \quad \Rightarrow \quad |\mathbf{X}(t) - \mathbf{X}^*| < \epsilon, \ \ \forall t > t_0,$$

for every solution $\mathbf{X}(t)$ *of* (1.5.2)*. In other words, trajectories that start sufficiently close to the equilibrium remain close for all future times.*

Definition 1.5.3. ***Local asymptotic stability:*** *An equilibrium point* $\mathbf{X}^*$ *of the system* (1.5.2) *is said to be locally asymptotically stable if it is locally stable and, in addition, there exists a constant* $k > 0$ *such that,*

$$|\mathbf{X}(t_0) - \mathbf{X}^*| < k \quad \Rightarrow \quad \lim_{t\to\infty} |\mathbf{X}(t) - \mathbf{X}^*| = 0.$$

Thus, not only do trajectories remain close, but they also converge to the equilibrium as $t \to \infty$*. Further, an equilibrium point that is not stable is called unstable.*

Definition 1.5.4. ***Global stability:*** *An equilibrium point* $\mathbf{X}^*$ *of system* (1.5.2) *is said to be globally stable if, for every* $\epsilon > 0$*, there exists* $\delta > 0$ *such that*

$$\|\mathbf{X}(t_0) - \mathbf{X}^*\| < \delta \quad \Longrightarrow \quad \|\mathbf{X}(t) - \mathbf{X}^*\| < \epsilon, \quad \forall t > t_0,$$

for all initial conditions $\mathbf{X}(t_0) \in \mathbb{R}^n$*.*

Definition 1.5.5. ***Global asymptotic stability:*** *An equilibrium point* $\mathbf{X}^*$ *of system* (1.5.2) *is said to be globally asymptotically stable if it is globally stable and, in addition,*

$$\lim_{t\to\infty} |\mathbf{X}(t) - \mathbf{X}^*| = 0,$$

for all initial conditions $\mathbf{X}(t_0) \in \mathbb{R}^n$*. That is, global asymptotic stability ensures that all trajectories not only remain bounded near the equilibrium but also converge to it as time progresses.*

Global asymptotic stability describes that the solution trajectories converge to a unique equilibrium point regardless of their initial conditions. An equilibrium point may be globally stable without being globally asymptotically stable, as illustrated by systems with center dynamics [141]. Note that global stability of an equilibrium automatically implies its local stability.

The eigenvalue method

In order to understand the behaviour of the system in the neighborhood of an equilibrium point, we carry out the stability analysis. We define the perturbation variable $\mathbf{Y} = \mathbf{X} - \mathbf{X}^*$. By applying a first-order Taylor expansion about $\mathbf{X}^*$, the non-linear system (1.5.2) can be approximated by a linear form,

$$\frac{d\mathbf{Y}}{dt} = J\mathbf{Y}, \tag{1.5.3}$$

where J denotes the Jacobian matrix of the system (1.5.2) evaluated at the equilibrium $\mathbf{X}^*$. Explicitly, we can write

$$DF(\mathbf{X}^*)\,\mathbf{Y} = \sum_{i=1}^{n} Y_i \frac{\partial F}{\partial x_i}(\mathbf{X}^*). \tag{1.5.4}$$

The eigenvalues of the Jacobian matrix J are determined by solving the characteristic equation $\det(J - \lambda I) = 0$, where I is the n^{th} order identity matrix. The local stability of the system (1.5.2) near the equilibrium point $\mathbf{X}^*$ is governed by the signs of the real parts of these eigenvalues. This leads to the following result.

Theorem 1.5.6. *The equilibrium point $\mathbf{X}^*$ of the system (1.5.2) is locally asymptotically stable if all eigenvalues of its Jacobian matrix J are negative, or their real parts are strictly less than zero at $\mathbf{X}^*$.*

To determine the signs of the eigenvalues of the Jacobian matrix, we shall use the well-known Routh–Hurwitz criterion [142].

Theorem 1.5.7. ***Routh-Hurwitz stability criterion:*** *The necessary and sufficient condition for the negativity of the real parts of all the roots of the polynomial,*

$$\lambda^n + a_1\lambda^{n-1} + a_2\lambda^{n-2} + a_3\lambda^{n-3} + \cdots + a_n = 0,$$

with real coefficients, is the positivity of all the principal minors of the Hurwitz matrix,

$$H_n = \begin{bmatrix} a_1 & 1 & 0 & \dots & 0 \\ a_3 & a_2 & a_1 & \dots & 0 \\ a_5 & a_4 & a_3 & \dots & 0 \\ \vdots & \vdots & \vdots & \ddots & \vdots \\ 0 & 0 & 0 & \dots & a_n \end{bmatrix}.$$

Note that, the leading principal minors of H_n are,

$$D_1 = a_1 > 0, \quad D_2 = \begin{vmatrix} a_1 & 1 \\ a_3 & a_2 \end{vmatrix} > 0, \quad D_3 = \begin{vmatrix} a_1 & 1 & 0 \\ a_3 & a_2 & a_1 \\ a_5 & a_4 & a_3 \end{vmatrix}, \quad \dots, \quad D_n = \det(H_n).$$

Thus, the Routh-Hurwitz criterion for particular values of n are as follow:

(i) $n = 2$: $a_1 > 0,\ a_2 > 0,$

(ii) $n = 3$: $a_1 > 0,\ a_3 > 0,\ a_1 a_2 > a_3,$

(iii) $n = 4$: $a_1 > 0,\ a_3 > 0,\ a_4 > 0,\ a_1 a_2 a_3 > a_1^2 a_4 + a_3^2.$

Lyapunov's direct method

The physical validity of this method lies in the fact that the stability of a system is determined by its energy, which is expressed as a function of the system variables. Lyapunov's direct method involves constructing energy-like functions, called Lyapunov functions, which are not necessarily unique. Positive or negative definite functions play a central role in this approach. In this thesis, we use the following fundamental definitions and results related to Lyapunov stability and invariance, which form the foundation for establishing both local and global stability properties of the proposed models.

Definition 1.5.8. ***Positive or negative definite functions:*** *Let $S \subset \mathbb{R}^n$ be an open set containing the origin and let $L : \Omega \to \mathbb{R}$ be a continuously differentiable ($\mathcal{C}^1$) function. The function L is called positive definite on Ω if the following hold:*

(a) $L(0) = 0,$

(b) $L(\mathbf{X}) > 0$ *for all* $\mathbf{X} \in \Omega \setminus \{0\}$.

Similarly, L is said to be negative definite on Ω if $-L$ is positive definite.

Definition 1.5.9. ***Invariant set:*** *A set $\Omega \subset \mathbb{R}^n$ is said to be invariant if for every trajectory $\mathbf{X}(t)$ with $\mathbf{X}(t_0) \in \Omega$, it follows that*

$$\mathbf{X}(t) \in \Omega \quad \forall t \geq t_0.$$

That is, if a trajectory starts in Ω, it remains in Ω for all future time.

Theorem 1.5.10. ***LaSalle's invariance principle:*** *Let $\Omega \subset \mathbb{R}^n$ be a compact set that is positively invariant with respect to system (1.5.2). Let $L : \mathbb{R}^n \to \mathbb{R}$ be a continuously differentiable function such that $L(\mathbf{X})$ is positive definite and $\dot{L}(\mathbf{X}) \leq 0$ in Ω. Define*

$$M = \{\mathbf{X} \in \Omega \mid \dot{L}(\mathbf{X}) = 0\}.$$

Then, as $t \to \infty$, every trajectory tends to the largest invariant set contained in M. In particular, if M contains no invariant sets other than $\mathbf{X} = 0$, then the origin is globally asymptotically stable [143].

Definition 1.5.11. ***Lyapunov function:*** *Suppose $L : \Omega \to \mathbb{R}$ is positive definite in an open neighbourhood of the origin. Then L is referred to as a Lyapunov function for the system* (1.5.2) *if*

$$\dot{L}(\mathbf{X}) \leq 0, \quad \forall \mathbf{X} \in \Omega \setminus \{0\}.$$

Definition 1.5.12. ***Radially unbounded function:*** *A function $f : \mathbb{R}^n \to \mathbb{R}$ is said to be radially unbounded if*

$$f(\mathbf{X}) \to \infty \quad \textit{whenever} \quad \|\mathbf{X}\| \to \infty, \ \mathbf{X} \in \mathbb{R}^n.$$

Theorem 1.5.13. ***Lyapunov's stability theorem:*** *Consider the system* (1.5.2) *with equilibrium point $\mathbf{X}^* = 0$, and let L be a $\mathcal{C}^1$ positive definite function defined in a neighbourhood Ω of $\mathbf{X}^* = 0$. Then:*

(a) $\mathbf{X}^* = 0$ *is* locally stable *if $\dot{L}(\mathbf{X}) \leq 0$ for all $\mathbf{X} \in \Omega \setminus \{0\}$.*

(b) $\mathbf{X}^* = 0$ *is* locally asymptotically stable *if $\dot{L}(\mathbf{X}) < 0$ for all $\mathbf{X} \in \Omega \setminus \{0\}$.*

(c) $\mathbf{X}^* = 0$ *is* globally stable *if it is locally stable and L is radially unbounded.*

(d) $\mathbf{X}^* = 0$ *is* globally asymptotically stable *if it is locally asymptotically stable and L is radially unbounded.*

(e) $\mathbf{X}^* = 0$ *is* unstable *if $\dot{L}(\mathbf{X}) > 0$ for some $\mathbf{X} \in \Omega \setminus \{0\}$. (See [144] for more details on stability analysis)*

1.5.4 Limit cycles

A solution $X(t)$ of the system (1.5.2) is said to be periodic if there exists a positive constant T such that

$$X(t+T) = X(t), \quad \forall t \geq 0.$$

The constant T is called the period of the solution. If such a periodic solution is isolated, meaning that no other nearby trajectories are themselves periodic, then this closed trajectory is known as a limit cycle.

The stability of a limit cycle is determined by the behaviour of trajectories in its neighborhood:

- If all nearby trajectories approach the cycle as $t \to \infty$, it is called a stable (or attracting) limit cycle.

- If nearby trajectories move away from the cycle, it is called an unstable (or repelling) limit cycle.
- If trajectories approach the cycle from one side and diverge on the other, the limit cycle is referred to as semi-stable.

Limit cycles are significant because they describe sustained oscillations in nonlinear systems without requiring any external force. Such behaviour is observed in real-world biological, chemical, and physical systems. Examples include oscillations in heartbeat, rhythmic patterns in neural firing, circadian rhythms in living organisms, and periodic chemical reactions [145, 146].

1.5.5 Bifurcations

A bifurcation occurs in a dynamical system when a small variation in the value of a parameter produces a sudden change in the qualitative nature of its solutions. Such changes may affect the number or stability of equilibrium points, the appearance or disappearance of periodic orbits, or other invariant features of the system. The parameter responsible for these changes is called the bifurcation parameter, and the specific parameter values at which the changes occur are referred to as bifurcation points. In this section, we briefly discuss two important types of local bifurcations: transcritical and Hopf bifurcation.

Transcritical bifurcation

A transcritical bifurcation takes place when two equilibria of the system intersect and exchange their stability as the bifurcation parameter crosses a critical value. In this process, one equilibrium becomes stable while the other turns unstable, and vice versa. Notably, no equilibrium is created or annihilated in this bifurcation. Instead, the stability is interchanged between existing equilibria.

Hopf bifurcation

A Hopf bifurcation arises when an equilibrium of the system loses stability and a periodic orbit (limit cycle) is generated as the bifurcation parameter passes through its critical value. Mathematically, this occurs when a pair of complex-conjugate eigenvalues of the Jacobian matrix cross the imaginary axis. The bifurcation can be classified into two types:

- **Supercritical Hopf bifurcation:** a stable limit cycle emerges from the equilibrium point when it loses stability.

- **Subcritical Hopf bifurcation:** an unstable limit cycle arises, causing trajectories to diverge away from the cycle.

Hopf bifurcation is a fundamental mechanism through which non-linear systems exhibit self-sustained oscillations. See [146] for more details on bifurcations.

1.5.6 Optimal control theory

Optimal control theory provides a framework for determining a control strategy that minimizes (or maximizes) a given objective function while following the dynamics of the system and given constraints (for details see [115]). Consider the following general system of differential equations:

$$\begin{aligned} \dot{\mathbf{X}}(t) &= g(t, \mathbf{X}(t)), \quad t > 0, \\ \mathbf{X}(t_0) &= \mathbf{X}_0, \end{aligned} \tag{1.5.5}$$

where the state variable $\mathbf{X}(t) \in \mathbb{R}^n$ with initial condition $\mathbf{X}_0 \in \mathbb{R}^n$, and $g = (g_1, g_2, \ldots, g_n)^T$ is a continuously differentiable vector field. Introducing a control variable $\mathbf{u}(t) \in S \subseteq \mathbb{R}^m$, the system can be written as,

$$\begin{aligned} \dot{\mathbf{X}}(t) &= h(t, \mathbf{X}(t), \mathbf{u}(t)), \quad t > 0, \\ \mathbf{X}(t_0) &= \mathbf{X}_0, \end{aligned} \tag{1.5.6}$$

where h is also assumed to be continuously differentiable. The goal is to determine an admissible control $\mathbf{u}(t)$ that optimizes a given objective functional

$$\mathcal{J}(\mathbf{u}) = \int_{t_0}^{t_f} \Phi(t, \mathbf{X}(t), \mathbf{u}(t))\, dt, \tag{1.5.7}$$

subject to the control system (1.5.6). Here, Φ represents the instantaneous payoff (or cost) depending on time, states, and control variables.

To characterize the optimal control, the Hamiltonian function is defined as

$$\mathcal{H}(t, \mathbf{X}, \mathbf{u}, \lambda) = \Phi(t, \mathbf{X}(t), \mathbf{u}(t)) + \lambda^T h(t, \mathbf{X}(t), \mathbf{u}(t)), \tag{1.5.8}$$

where $\lambda(t)$ is the adjoint variable. The necessary condition for optimality requires

$$\frac{\partial \mathcal{H}}{\partial \mathbf{u}}(t, \mathbf{X}(t), \mathbf{u}^*(t), \lambda(t)) = 0, \tag{1.5.9}$$

together with the adjoint system

$$\dot{\lambda}(t) = -\frac{\partial \mathcal{H}}{\partial \mathbf{X}}(t, \mathbf{X}(t), \mathbf{u}^*(t), \lambda(t)), \tag{1.5.10}$$

and the transversality condition

$$\lambda(t_f) = 0.$$

For minimization problems, the Hamiltonian must be concave with respect to $\mathbf{u}$, i.e.,

$$\frac{\partial^2 \mathcal{H}}{\partial \mathbf{u}^2} > 0 \quad \text{at } \mathbf{u} = \mathbf{u}^*(t),$$

while for maximization problems it must be convex, i.e.,

$$\frac{\partial^2 \mathcal{H}}{\partial \mathbf{u}^2} < 0 \quad \text{at } \mathbf{u} = \mathbf{u}^*(t).$$

Pontryagin's maximum principle

Pontryagin's Maximum Principle is a fundamental tool for identifying optimal controls, providing necessary conditions that any optimal pair $(\mathbf{X}^*, \mathbf{u}^*)$ must satisfy. It reformulates the original optimal control problem as a two-point boundary value problem involving the state dynamics, the adjoint equations, and the optimality condition. For this, we have the following theorem:

Theorem 1.5.14. ***Pontryagin's Maximum Principle:*** *Let $\mathbf{X}^*(t)$ and $\mathbf{u}^*(t)$ denote the optimal state and control trajectories, then there exists a piecewise continuously differentiable adjoint variable $\lambda(t)$ such that*

$$\mathcal{H}(t, \mathbf{X}^*(t), \mathbf{u}(t), \lambda(t)) \leq \mathcal{H}(t, \mathbf{X}^*(t), \mathbf{u}^*(t), \lambda(t))$$

for all admissible controls $\mathbf{u}(t)$ and all $t \in [t_0, t_f]$. The corresponding adjoint equation is given by

$$\begin{aligned} \dot{\lambda}(t) &= -\frac{\partial \mathcal{H}}{\partial \mathbf{X}}(t, \mathbf{X}^*(t), \mathbf{u}^*(t), \lambda(t)), \\ \lambda(t_f) &= 0. \end{aligned}$$

Forward-backward sweep method

The forward-backward sweep method (FBSM) is a widely used numerical technique for solving optimal control problems governed by system of coupled non-linear differential equations and characterized by Pontryagin's Maximum Principle. A direct solution is generally intractable, since the state system evolves forward in time and the adjoint system evolves backward in time. The forward-backward sweep method provides an iterative procedure to approximate the optimal control, state, and adjoint trajectories simultaneously.

The main idea is to start with an initial estimate for the control variables, and solve the state system using the classical fourth-order Runge-Kutta method in forward direction over

the simulated time. Subsequently, with the state trajectories determined, the adjoint system is solved backward in time using the transversality conditions, again applying the Runge-Kutta fourth-order integration. The control variables are updated at each iteration using a convex combination of the previous control values and those derived from the characterization equations to improve numerical stability. This iterative procedure is repeated until successive iterations give negligible differences in the computed values of control variables (for details see [115]). The detailed algorithm for this method is as follows:

Algorithm 1 Forward–Backward Sweep Method for Optimal Control Problems

1: **Initialize:** Choose an initial guess for the control $\mathbf{u}^{(0)}(t)$ on $[t_0, t_f]$. Set iteration counter $k = 0$.
2: **repeat**
3: **Forward sweep:** Solve the state equation

$$\dot{\mathbf{X}}(t) = h(t, \mathbf{X}(t), \mathbf{u}^{(k)}(t)), \quad \mathbf{X}(t_0) = \mathbf{X}_0$$

to obtain the trajectory $\mathbf{X}^{(k)}(t)$.
4: **Backward sweep:** Solve the adjoint equation

$$\dot{\lambda}(t) = -\frac{\partial \mathcal{H}}{\partial \mathbf{X}}(t, \mathbf{X}^{(k)}(t), \mathbf{u}^{(k)}(t), \lambda(t)), \quad \lambda(t_f) = 0$$

backward in time to obtain $\lambda^{(k)}(t)$.
5: **Control update:** Update the control using the optimality condition

$$\mathbf{u}^{(k+1)}(t) = \arg\min_{\mathbf{u} \in S} \mathcal{H}(t, \mathbf{X}^{(k)}(t), \mathbf{u}, \lambda^{(k)}(t)).$$

6: **Relaxation:** Use a convex combination for numerical stability

$$\mathbf{u}^{(k+1)}(t) \leftarrow \theta \mathbf{u}^{(k+1)}(t) + (1 - \theta)\mathbf{u}^{(k)}(t), \quad \theta \in (0, 1].$$

7: **Increment:** Set $k \leftarrow k + 1$.
8: **until** The difference between successive controls satisfies $\|\mathbf{u}^{(k+1)} - \mathbf{u}^{(k)}\| < \varepsilon$, for a chosen tolerance ε.
9: **Output:** Approximate optimal state trajectory $\mathbf{X}^*(t)$, adjoint $\lambda^*(t)$, and optimal control $\mathbf{u}^*(t)$.

1.5.7 Sensitivity analysis

In epidemiological modelling, the state variables often exhibit complex and nonlinear dependence on model parameters. This results in uncertainty in model outcomes due to variations in input quantities such as parameter values, initial conditions, or model assumptions. Sensi-

tivity analysis provides a systematic approach to quantify the influence of such uncertainties in inputs on the variations of model outputs, also known as quantities of interest (QoI). Typical QoIs in epidemiological models include basic reproduction numbers, peak infection size, or cumulative infections over time. Sensitivity analysis methods are broadly classified into two categories: local and global.

Local sensitivity analysis

Local sensitivity analysis evaluates the effect of small perturbations of parameters around a nominal value. A commonly used measure is the normalized forward sensitivity index, defined as

$$\Upsilon_p^Q = \frac{\partial Q}{\partial p} \cdot \frac{p}{Q}, \tag{1.5.11}$$

where Q is the quantity of interest and p is the parameter being studied. This index gives the relative change in Q corresponding to a relative change in p. Local analysis is useful for initial screening of key parameters but does not capture non-linear interactions between them.

Global sensitivity analysis

Global sensitivity analysis, on the other hand, investigates the contribution of parameters to the uncertainty of model outputs over the entire parameter space. These methods account for nonlinear effects and interactions among parameters, and are typically based on sampling techniques. Common approaches include correlation-based methods such as the partial rank correlation coefficient (PRCC) and variance-based methods such as the Sobol indices.

- **Partial Rank Correlation Coefficient (PRCC):** This method evaluates the strength of the monotonic relationship between model outputs and parameters, while adjusting for the effect of other parameters. The PRCC is defined as,

$$\text{PRCC} = \frac{\text{Cov}(R_p, R_Q)}{\sqrt{\text{Var}(R_p) \cdot \text{Var}(R_Q)}}, \tag{1.5.12}$$

  where R_p and R_Q are the residuals obtained from rank regression of the parameter p and the output Q against all other parameters.

- **Sobol Indices:** These are variance-based measures which decompose the output variance into contributions from each parameter and their interactions. The first-order Sobol index, which measures the direct contribution of a parameter p_i to output variance, is defined as,

$$S_i = \frac{\text{Var}\big(\mathbb{E}[Q \mid p_i]\big)}{\text{Var}(Q)}, \tag{1.5.13}$$

where $\mathbb{E}[Q \mid p_i]$ denotes the conditional expectation of Q given p_i. The total-order Sobol index, which quantifies the overall effect of p_i including all interactions with other parameters, is defined as

$$S_{T_i} = 1 - \frac{\mathrm{Var}\big(\mathbb{E}[Q \mid p_{\sim i}]\big)}{\mathrm{Var}(Q)}, \tag{1.5.14}$$

where $p_{\sim i}$ denotes the set of all parameters except p_i.

Both local and global sensitivity analyses provide valuable insights into model dynamics. Local methods are computationally efficient and useful for preliminary exploration, while global methods are more comprehensive and account for parameter interactions. For further details on sensitivity analysis, see [147, 148].

1.5.8 Shapley value

The Shapley Value analysis is a tool from cooperative game theory, which provides a systematic approach to fairly distribute the total outcome of a cooperative game among its players based on their individual marginal impacts. Shapley values quantify the average marginal contribution of each player to a given outcome of the game, calculated across all possible combinations of the remaining players.

The calculation of Shapley values involves a combinatorial process that considers all possible coalitions of players. For a specific player p_i within a set of n players (P), its Shapley value $\phi(p_i)$, corresponding to the given outcome, is computed as the weighted average of its marginal contributions across all subsets S of P that exclude p_i. Mathematically, this is expressed as:

$$\phi(p_i) = \sum_{S \subseteq P \setminus p_i} \frac{|S|!(n - |S| - 1)!}{n!} \left(v(S \cup p_i) - v(S)\right), \tag{1.5.15}$$

where $v(S)$ denotes the value related to the given outcome under the coalition S, and the term $v(S \cup p_i) - v(S)$ represents the marginal contribution of player p_i when added to coalition S. The weighting factor $\frac{|S|!(n - |S| - 1)!}{n!}$ ensures fairness by accounting for all possible positions that player p_i could occupy in a permutation of the full set of players. This normalizes the contributions based on coalition size and ensures that each subset is weighted appropriately. For further details on the Shapley values, see [149–151].

1.6 Structure of the Thesis

This thesis is organized into six chapters. A brief overview of each chapter is provided below to guide the reader through the logical flow of the work.

Chapter 1 – This chapter highlights the global significance of HIV as a public health challenge and the need for mathematical modelling in understanding its transmission dynamics. It discusses the biological and clinical aspects of HIV, including disease progression, transmission pathways, diagnosis, treatment, adherence, drug resistance, and treatment switching. A comprehensive review of relevant literature on mathematical modelling of HIV transmission, treatment, and resource allocation is presented, identifying key research gaps. The chapter concludes by formulating the research questions and outlining the objectives of the thesis.

Chapter 2 – This chapter presents a basic two-strain SI-type model to study the competition between drug-sensitive and drug-resistant HIV strains in the absence of treatment. The basic reproduction numbers for both strains are derived using the next-generation matrix method. The existence and stability of the equilibrium points are analyzed to determine long-term outcomes, revealing that coexistence of both strains is not possible under these assumptions. A bifurcation analysis is carried out to identify parameter thresholds that determine strain persistence or elimination.

Chapter 3 – Building on the first model, this chapter extends the framework by incorporating treatment availability and adherence effects. A separate treatment compartment is introduced, and drug resistance is assumed to emerge both through transmission and through sub-optimal adherence. The basic reproduction numbers under treatment are derived, and the model is analyzed for the existence and stability of equilibria. Bifurcation analysis, including Hopf bifurcation, is performed to explore parameter regions leading to oscillatory epidemic dynamics. The results demonstrate that treatment availability combined with poor adherence can promote the persistence of drug resistance and induce cyclical epidemic patterns.

Chapter 4 – This chapter refines the model further by including an explicit AIDS compartment, allowing for the study of late-stage disease progression under treatment. The system is analyzed for the existence and stability of its equilibria, revealing that drug-resistant infections can persist even if drug-sensitive infections die out. The analysis shows that treatment availability alone is insufficient to control the epidemic if adherence is sub-optimal. A comprehensive bifurcation analysis is carried out with respect to treatment availability and adherence level, showing the potential for oscillatory epidemics under medium treatment coverage. The findings emphasize the critical importance of maintaining high adherence levels to prevent the occurrence of a drug-resistant endemic.

Chapter 5 – This chapter introduces diagnosis status and the possibility of switching to second-line treatment upon resistance detection. The model admits a disease-free equilibrium and two endemic equilibria, whose stability is analyzed. Extensive local and global sensitivity

analyses identify the most influential epidemiological parameters affecting disease dynamics. Optimal control theory is applied to evaluate five intervention strategies targeting diagnosis, treatment scale-up, and adherence support. A cost-effectiveness analysis is conducted to compare these strategies and to identify the most efficient allocation of limited resources. Furthermore, adjoint-based sensitivity analysis and Shapley value analysis are performed to inform resource prioritization beyond cost-effectiveness goals. The results underline that adherence-focused interventions, combined with timely treatment switching, are essential to achieving long-term epidemic control and meeting UNAIDS 95-95-95 targets.

Chapter 6 – The final chapter summarizes the key findings of the research presented in this thesis and highlights the main limitations of the study. It also outlines potential directions for future work, suggesting how the current modelling framework can be extended to address additional complexities and improve its applicability for public health decision-making.

Chapter 2

Multi-Strain HIV Dynamics Without Treatment

As a starting point, this chapter develops and analyses a basic multi-strain SI-type compartmental model that incorporates both drug-sensitive and drug-resistant HIV infections in the absence of treatment. In this setting, transmission from drug-resistant individuals is the only source of new resistant infections. This basic framework is important, as it isolates the role of transmission pathways in the persistence or eradication of resistance, before considering the additional complexities introduced by the treatment. The basic reproduction numbers for each strain are derived using the next-generation matrix approach. To see the long-term dynamics, equilibrium points are determined and their local and global stability are examined. In addition, bifurcation analysis is carried out to investigate how variations in critical parameters near threshold values affect the system dynamics. Several numerical simulations are performed to support these theoretical findings. This analysis provides insights into whether these strains exhibit coexistence or competitive exclusion, and highlights the potential epidemiological burden of drug resistance in the absence of treatment. The results from this baseline framework will also serve as a benchmark for comparison with treatment-inclusive models presented in subsequent chapters.

2.1 Formulation of the Mathematical Model

The model divides the total sexually active population into three mutually exclusive groups, namely, susceptible (S), infected individuals with the drug-sensitive strain (I_S), and infected individuals with the drug-resistant strain (I_R). We assume that the individuals are homogeneously distributed in the given population, implying that every susceptible individual has an equal chance of contacting infected individuals. The susceptible population increases through the process of recruitment of individuals, who enter into the sexually active class,

at a constant rate λ. Transmission of infection is modelled using a mass-action incidence function. Therefore, the susceptible population become infected after an effective contact either with the drug-sensitive infected or the drug-resistant infected individuals with the incidence rates of $\alpha I_S S$ and $\beta I_R S$, respectively. Here α and β represent the effective contact rates of susceptible with the drug-sensitive infected and the drug-resistant infected individuals, respectively. We further assume that an effective contact transmits the same type of strain in the newly infected person, and no cross-infection between the two strains is allowed. Consequently, an individual infected with the drug-sensitive strain cannot acquire resistance through contact with a drug-resistant individual, and vice versa. Individuals in all groups die naturally at the rate μ. Also, the drug-sensitive and drug-resistant infected populations experience disease-induced mortality at rates μ_S and μ_R, respectively. Since this model excludes treatment, the only mechanism for the emergence and persistence of resistance is through direct transmission from resistant individuals. A schematic representation for this type of HIV spread at community level is presented in Figure 2.1.

Taking into account the aforementioned assumptions, the population in each group is determined by the following deterministic system of coupled non-linear ordinary differential equations:

$$\begin{aligned} S' &= \lambda - \alpha I_S S - \beta I_R S - \mu S, \\ I_S' &= \alpha I_S S - (\mu + \mu_S) I_S, \\ I_R' &= \beta I_R S - (\mu + \mu_R) I_R, \end{aligned} \tag{2.1.1}$$

with the initial condition $(S(0), I_S(0), I_R(0))$ belonging to the region $\mathcal{R}$ defined as,

$$\mathcal{R} = \left\{ (S, I_S, I_R) \in \mathbb{R}^3_+ : 0 \leq S + I_S + I_R \leq \frac{\lambda}{\mu} \right\},$$

where $\mathbb{R}^3_+$ refers to the closed cube in the first octant. The biological meaning of the parameters used in the system (2.1.1) is provided in Table 2.1.

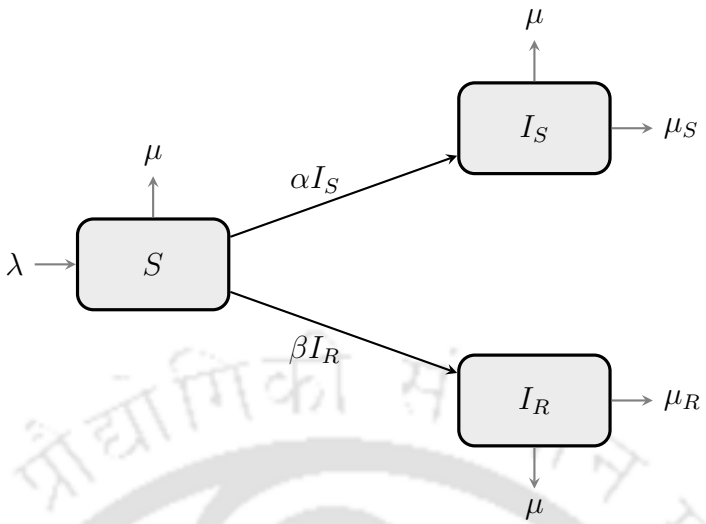

Figure 2.1: Schematic representation of the model (2.1.1).

Parameter	Biological Description
λ	Recruitment rate of susceptible individuals
α	Transmission rate per effective contact between a susceptible individual and a drug-sensitive infected individual
β	Transmission rate per effective contact between a susceptible individual and a drug-resistant infected individual
μ_S	Disease-induced death rate of drug-sensitive infected population
μ_R	Disease-induced death rate of drug-resistant infected population
μ	Natural death rate

Table 2.1: Model parameters and their biological descriptions for system (2.1.1).

2.2 Mathematical Analysis of the Model

In this section, we establish the uniqueness, non-negativity and boundedness of the solutions of the system (2.1.1), which ensures that it is biologically well-posed. To understand the long-term behaviour of the system and its sensitivity to changes in epidemiological parameters, we identify the equilibrium points and analyze their local and global stability. This analysis will provide us parameter conditions under which the disease either dies out or persists in the population. We investigate whether the two strains can coexist or exhibit competitive

exclusion, and determine the conditions under which one strain dominates over the other in the latter case. We also provide a theoretical analysis of possible bifurcations in this section.

2.2.1 Uniqueness, non-negativity and boundedness of the solutions

The right-hand side of the system (2.1.1) is continuous and Lipschitz on $[0, a]$, $a > 0$. Therefore, the system (2.1.1) with the initial condition $(S(0), I_S(0), I_R(0)) \in \mathbb{R}^3_+$ has a unique solution.

Since the state variables of the model represents the human population, the solution of system (2.1.1) needs to be non-negative (for all non-negative initial conditions) and bounded. We begin with the non-negativity part. Let t_1 denote the time at which the susceptible population S becomes extinct. Then $S(t_1) = 0$ and $S'(t_1) = \lambda > 0$. Therefore $\nexists$ any $\epsilon > 0$ such that $S(t_1) = 0$ and $S(t_1 + \epsilon) < 0$. Hence $S(t_1) \geq 0$, $\forall t_1 > 0$ and $S(0) \geq 0$. Now, from the second and third equation of (2.1.1), we have,

$$I_S(t) = I_S(0) \exp\left[\int_0^t (\alpha S(\tau) - (\mu + \mu_S))\, d\tau\right] \geq 0 \text{ for } I_S(0) \geq 0,$$

$$I_R(t) = I_R(0) \exp\left[\int_0^t (\beta S(\tau) - (\mu + \mu_R))\, d\tau\right] \geq 0 \text{ for } I_R(0) \geq 0,$$

respectively.

For the boundedness part, we define $W = S + I_S + I_R$. Then,

$$\begin{aligned} W' &= S' + I'_S + I'_R \\ &= \lambda - \mu W - \mu_S I_S - \mu_R I_R \\ &\leq \lambda - \mu W, \end{aligned}$$

which implies that $W \leq \dfrac{\lambda}{\mu} := M_1$ (say). This shows that W is bounded by M_1. Therefore S, I_S, and I_R are also bounded by M_1. From these results, we can now state the following Theorem.

Theorem 2.2.1. *The biologically feasible region $\mathcal{R}$ defined by:*

$$\mathcal{R} = \left\{(S, I_S, I_R) \in \mathbb{R}^3_+ : 0 \leq S + I_S + I_R \leq \frac{\lambda}{\mu}\right\},$$

where $\mathbb{R}^3_+$ denotes the closed cube in the first octant, is positively invariant for the system (2.1.1) with non-negative initial conditions.

2.2.2 Equilibrium points and local stability analysis

For the system given by equation (2.1.1), there exists three equilibrium points, as enumerated below.

(A) Disease free equilibrium point: $E_0^{(1)}\left(\frac{\lambda}{\mu}, 0, 0\right)$.

(B) Drug-sensitive equilibrium point: $E_1^{(1)} = (S_1, I_{S_1}, 0) = \left(\frac{\mu+\mu_S}{\alpha}, \frac{\lambda\alpha - \mu(\mu+\mu_S)}{\alpha(\mu+\mu_S)}, 0\right)$, which exists provided $\frac{\lambda}{\mu} > \frac{\mu+\mu_S}{\alpha}$.

(C) Drug-resistant equilibrium point: $E_2^{(1)} = (S_2, 0, I_{R_2}) = \left(\frac{\mu+\mu_R}{\beta}, 0, \frac{\lambda\beta - \mu(\mu+\mu_R)}{\beta(\mu+\mu_R)}\right)$, which exists provided $\frac{\lambda}{\mu} > \frac{\mu+\mu_R}{\beta}$.

Now, in order to determine the "Basic Reproduction Number", for system (2.1.1), we consider, the next generation matrix as,

$$FV^{-1} = \begin{pmatrix} \frac{\alpha\lambda}{\mu(\mu+\mu_S)} & 0 \\ 0 & \frac{\beta\lambda}{\mu(\mu+\mu_R)} \end{pmatrix}.$$

Hence the "Basic Reproduction Number" for the drug-sensitive strain and the drug-resistant strain are given by $R_0^{(S)} = \frac{\alpha\lambda}{\mu(\mu+\mu_S)}$ and $R_0^{(R)} = \frac{\beta\lambda}{\mu(\mu+\mu_R)}$, respectively. We denote the ratio of $R_0^{(S)}$ and $R_0^{(R)}$, as $R_0^{(SR)} := \frac{\alpha(\mu+\mu_R)}{\beta(\mu+\mu_S)}$.

Finally, we present the stability analysis for system (2.1.1), for which we consider the following Jacobian,

$$J_1 = \begin{bmatrix} -\alpha I_S - \beta I_R - \mu & -\alpha S & -\beta S \\ \alpha I_S & \alpha I_S - \mu - \mu_S & 0 \\ \beta I_R & 0 & \beta S - \mu - \mu_R \end{bmatrix}.$$

(A) The eigenvalues of the Jacobin matrix, evaluated at $E_0^{(1)}$ are

$$\lambda_{01} = -\mu,\ \lambda_{02} = \frac{\alpha\lambda - \mu^2 - \mu\mu_S}{\mu},\ \lambda_{03} = \frac{\beta\lambda - \mu^2 - \mu\mu_R}{\mu}.$$

So the disease free equilibrium $E_0^{(1)}$ is locally stable if, $\alpha\lambda - \mu^2 - \mu\mu_S < 0$ and $\beta\lambda - \mu^2 - \mu\mu_R < 0$, *i.e*, $R_0^{(S)} < 1$ and $R_0^{(R)} < 1$, respectively. This is equivalent to the condition $\max\left(R_0^{(S)}, R_0^{(R)}\right) < 1$. Note that under these conditions $E_1^{(1)}$ and $E_2^{(1)}$ do not exist.

(B) One of the eigenvalues of the Jacobin matrix, evaluated at $E_1^{(1)}$ is given by,

$$\lambda_{11} = -\mu - \mu_R + \frac{\beta(\mu + \mu_S)}{\alpha}.$$

The remaining two eigenvalues are the solutions of the characteristic equation,

$$x^2 + \frac{\alpha\lambda}{\mu + \mu_S}x - \mu(\mu + \mu_S) + \alpha\lambda = 0,$$

which have negative real parts provided $\alpha\lambda > \mu(\mu + \mu_S) \iff R_0^{(S)} > 1$ (this condition is already satisfied from the existential condition of $E_1^{(1)}$). Note that the first eigenvalue λ_{11} is negative, provided,

$$\frac{\mu + \mu_S}{\alpha} < \frac{\mu + \mu_R}{\beta} \iff R_0^{(SR)} > 1.$$

Therefore the equilibrium point $E_1^{(1)}$ is locally stable if and only if $R_0^{(SR)} > 1$.

(C) One of the eigenvalues of the Jacobin matrix, evaluated at $E_2^{(1)}$ is given by,

$$\lambda_{21} = -\mu - \mu_S + \frac{\alpha(\mu + \mu_R)}{\beta}.$$

The remaining two eigenvalues are the solution of the characteristic equation,

$$x^2 + \frac{\beta\lambda}{\mu + \mu_R}x - \mu(\mu + \mu_R) + \beta\lambda = 0,$$

which have negative real parts provided $\beta\lambda > \mu(\mu + \mu_R) \iff R_0^{(R)} > 1$ (this condition is already satisfied from the existential condition of $E_2^{(1)}$). Note that the first eigenvalue λ_{21} is negative, provided,

$$\frac{\mu + \mu_R}{\beta} < \frac{\mu + \mu_S}{\alpha} \iff R_0^{(SR)} < 1.$$

Therefore the equilibrium point $E_2^{(1)}$ is locally stable if and only if $R_0^{(SR)} < 1$.

The summary of existence and stability conditions for different equilibrium points are presented in Table 2.2 and Figure 2.2.

Existent equilibrium points and their stability in different cases, are presented in Table 2.3, for which we define,

$$P_1 := \frac{\mu + \mu_S}{\alpha},\ P_2 := \frac{\mu + \mu_R}{\beta},\ P_3 := \frac{\lambda}{\mu}.$$

Equilibrium Point	Existence Condition	Stability Condition
$\left(\frac{\lambda}{\mu}, 0, 0\right)$	Always	$\max\{R_0^{(S)}, R_0^{(R)}\} < 1$
$\left(\frac{\mu+\mu_S}{\alpha}, \frac{\lambda\alpha-\mu(\mu+\mu_S)}{\alpha(\mu+\mu_S)}, 0\right)$	$R_0^{(S)} > 1$	$R_0^{(SR)} > 1$
$\left(\frac{\mu+\mu_R}{\beta}, 0, \frac{\lambda\beta-\mu(\mu+\mu_R)}{\beta(\mu+\mu_R)}\right)$	$R_0^{(R)} > 1$	$R_0^{(SR)} < 1$

Table 2.2: Existence and stability conditions for the equilibrium points.

Case	Basic Reproduction Numbers	Existing Equilibria	Stable (S) / Unstable (US)
$P_1 < P_2 < P_3$	$R_0^{(S)} > 1, R_0^{(R)} > 1, R_0^{(SR)} > 1$	$E_0^{(1)}, E_1^{(1)}, E_2^{(1)}$	$S = \{E_1^{(1)}\}, US = \{E_0^{(1)}, E_0^{(2)}\}$
$P_1 < P_3 < P_2$	$R_0^{(S)} > 1, R_0^{(R)} < 1, R_0^{(SR)} > 1$	$E_0^{(1)}, E_1^{(1)}$	$S = \{E_1^{(1)}\}, US = \{E_0^{(1)}\}$
$P_2 < P_1 < P_3$	$R_0^{(S)} > 1, R_0^{(R)} > 1, R_0^{(SR)} < 1$	$E_0^{(1)}, E_1^{(1)}, E_2^{(1)}$	$S = \{E_2^{(1)}\}, US = \{E_0^{(1)}, E_1^{(2)}\}$
$P_2 < P_3 < P_1$	$R_0^{(S)} < 1, R_0^{(R)} > 1, R_0^{(SR)} < 1$	$E_0^{(1)}, E_2^{(1)}$	$S = \{E_2^{(1)}\}, US = \{E_0^{(1)}\}$
$P_3 < P_1 < P_2$	$R_0^{(S)} < 1, R_0^{(R)} < 1, R_0^{(SR)} > 1$	$E_0^{(1)}$	$S = \{E_0^{(1)}\}, US = \Phi$
$P_3 < P_2 < P_1$	$R_0^{(S)} < 1, R_0^{(R)} < 1, R_0^{(SR)} < 1$	$E_0^{(1)}$	$S = \{E_0^{(1)}\}, US = \Phi$

Table 2.3: Existence and stability of equilibrium points under different parameter settings.

2.2.3 Global stability analysis

Theorem 2.2.2. *The equilibrium point $E_0^{(1)}$ is globally asymptotically stable with $R_0 < 1$.* $\left(\textit{here } R_0 = \max\{R_0^{(S)}, R_0^{(R)}\}\right)$

Proof. We define the Lyapunov function as:

$$L_1(t) = L_1(S(t), I_S(t), I_R(t)) = \left(1 - R_0^{(R)}\right) I_S + \left(1 - R_0^{(S)}\right) I_R$$

Then $L_1\left(E_0^{(1)}\right) = 0$ and $L_1(x) > 0, x \neq E_0^{(1)}$. The derivative of $L_1(t)$ along the solution of system (2.1.1) gives,

$$\begin{aligned}
\frac{dL_1}{dt} &= \left(1 - R_0^{(R)}\right) I_S' + \left(1 - R_0^{(S)}\right) I_R' \\
&= \left(1 - R_0^{(R)}\right) (\alpha I_S S - (\mu + \mu_S) I_S) + \left(1 - R_0^{(S)}\right) (\beta I_R S - (\mu + \mu_R) I_R) \\
&\leq \left(1 - R_0^{(R)}\right) \left(\frac{\alpha\lambda}{\mu} I_S - (\mu + \mu_S) I_S\right) + \left(1 - R_0^{(S)}\right) \left(\frac{\beta\lambda}{\mu} I_R - (\mu + \mu_R) I_R\right) \\
&= -(I_S(\mu + \mu_S) + I_R(\mu + \mu_R)) \left(R_0^{(S)} - 1\right) \left(R_0^{(R)} - 1\right) \\
&\leq 0, \quad \text{if } R_0 < 1.
\end{aligned}$$

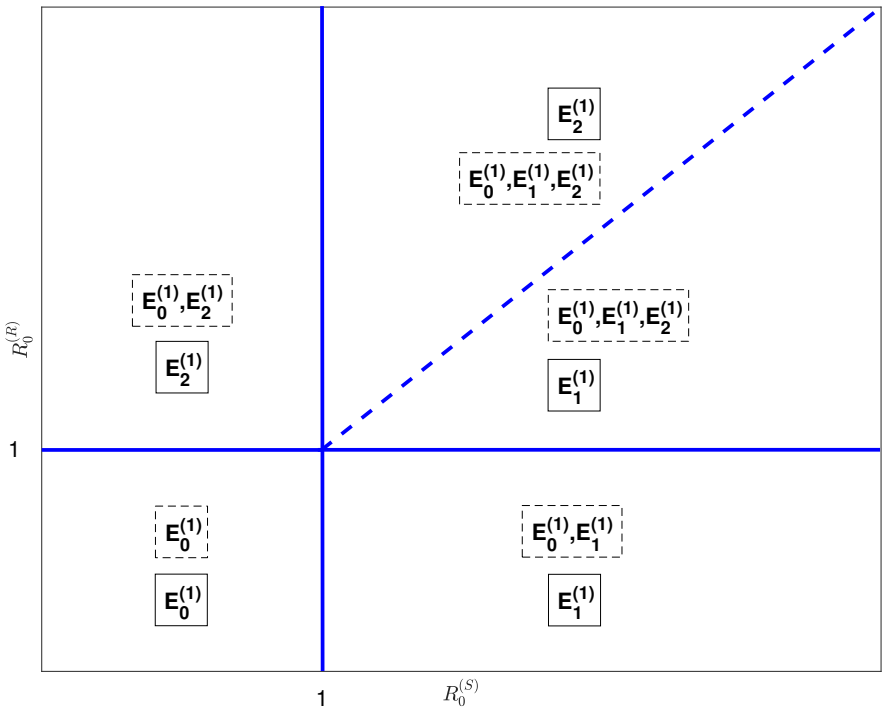

Figure 2.2: Two parameter bifurcation diagram showing existence and stability regions for different equilibrium points of model (2.1.1). The dashed boxes contain total existing equilibrium point while solid boxes contain only stable equilibrium points. The dashed blue line represents $R_0^{(S)} = R_0^{(R)}$.

Therefore, by LaSalle's invariance principle, $E_0^{(1)}$ is globally asymptotically stable if $R_0 < 1$. □

Remark 2.2.3. *In LaSalle's invariance principle, the equality $\dot{L}(t) = 0$ holds at equilibrium points and may also hold on larger invariant sets, such as periodic orbits or centers, where the Lyapunov function remains constant along solution trajectories.*

Theorem 2.2.4. *The equilibrium point $E_1^{(1)}$ is globally asymptotically stable whenever it exists if $R_0^{(SR)} > 1$.*

Proof. We consider the Lyapunov function as:

$$L_2(t) = L_2(S(t), I_S(t), I_R(t)) = S - S_1 - S_1 \ln\left(\frac{S}{S_1}\right) + I_S - I_{S_1} - I_{S_1} \ln\left(\frac{I_S}{I_{S_1}}\right) + I_R$$

The derivative of $L_2(t)$ along the solution of system (2.1.1) gives

$$\begin{aligned}
\frac{dL_2}{dt} &= \left(1-\frac{S_1}{S}\right)S' + \left(1-\frac{I_{S_1}}{I_S}\right)I'_S + I'_R \\
&= \left(1-\frac{S_1}{S}\right)(\lambda - \alpha I_S S - \beta I_R S - \mu S) + I_S\left(1-\frac{I_{S_1}}{I_S}\right)(\alpha S - \mu - \mu_S) \\
&\quad + I_R(\beta S - \mu - \mu_R) \\
&= \lambda - \mu S - \frac{\lambda S_1}{S} + I_R\left(\frac{\beta(\mu+\mu_S)(\mu+\mu_R)}{\alpha(\mu+\mu_R)}\right) - I_R(\mu+\mu_R) \\
&\quad - \alpha I_{S_1} S + I_{S_1}(\mu+\mu_S) + \frac{\mu(\mu+\mu_S)}{\alpha} \\
&= -\mu S - \frac{\lambda S_1}{S} + \frac{\lambda\alpha + \mu(\mu+\mu_S)}{\alpha} + I_R(\mu+\mu_R)\left(\frac{R_0^R}{R_0^S} - 1\right) - \alpha I_{S_1} S + I_{S_1}(\mu+\mu_S) \\
&= -\frac{(\lambda - \mu S R_0^S)^2}{\mu S R_0^S} + I_R(\mu+\mu_R)\left(\frac{R_0^R}{R_0^S} - 1\right) \\
&\leq 0, \quad \text{if } R_0^{(SR)} > 1.
\end{aligned}$$

Therefore, by LaSalle's invariance principle, $E_1^{(1)}$ is globally asymptotically stable if $R_0^{(SR)} > 1$. □

Theorem 2.2.5. *The equilibrium point $E_2^{(1)}$ is globally asymptotically stable whenever it exists if $R_0^{(SR)} < 1$.*

Proof. We define the Lyapunov function as,

$$L_3(t) = L_3(S(t), I_S(t), I_R(t)) = S - S_2 - S_2 \ln\left(\frac{S}{S_2}\right) + I_S + I_R - I_{R_2} - I_{R_2}\ln\left(\frac{I_R}{I_{R_2}}\right).$$

The remaining proof is similar to the proof in Theorem 2.2.4. □

2.2.4 Bifurcation analysis

Theorem 2.2.6. *The system (2.1.1) undergoes through transcritical bifurcation at:*

$$\alpha = \alpha_*^{(1)} = \frac{\mu(\mu+\mu_S)}{\lambda}$$

if $\beta\lambda - \mu^2 - \mu\mu_R < 0$ ($R_0^{(R)} < 1$). Here, equilibrium points $E_0^{(1)}$ and $E_1^{(1)}$ exchange their stability at $\alpha = \alpha_*^{(1)}$ (or $R_0^{(S)} = 1$).

Proof. Let $\alpha = \alpha_*^{(1)} = \dfrac{\mu(\mu+\mu_S)}{\lambda}$, then

$$J_1(E_0^{(1)})\,\big|_{\alpha=\alpha_*^{(1)}} = \begin{bmatrix} -\mu & -(\mu+\mu_S) & -\dfrac{\beta\lambda}{\mu} \\ 0 & 0 & 0 \\ 0 & 0 & \dfrac{\beta\lambda - \mu^2 - \mu\mu_R}{\mu} \end{bmatrix},$$

and

$$J_1^T(E_0^{(1)})\,\big|_{\alpha=\alpha_*^{(1)}} = \begin{bmatrix} -\mu & 0 & 0 \\ -(\mu+\mu_S) & 0 & 0 \\ -\dfrac{\beta\lambda}{\mu} & 0 & \dfrac{\beta\lambda-\mu^2-\mu\mu_R}{\mu} \end{bmatrix}.$$

Notice that one eigenvalue of matrix $J_1(E_0^{(1)})\,\big|_{\alpha=\alpha_*^{(1)}}$ becomes zero at $\alpha = \alpha_*^{(1)}$ and the remaining two eigenvalues are negative only if $\beta\lambda - \mu^2 - \mu\mu_R < 0$. Now, we choose,

$$v = \begin{bmatrix} v_1 \\ v_2 \\ v_3 \end{bmatrix} = \begin{bmatrix} -\left(\frac{\mu+\mu_S}{\mu}\right) \\ 1 \\ 0 \end{bmatrix}, \quad w = \begin{bmatrix} w_1 \\ w_2 \\ w_3 \end{bmatrix} = \begin{bmatrix} 0 \\ 1 \\ 0 \end{bmatrix}$$

as the eigenvectors corresponding to the zero eigenvalues of the matrices $J_1(E_0^{(1)})\,\big|_{\alpha=\alpha_*^{(1)}}$ and $J_1^T(E_0^{(1)})\,\big|_{\alpha=\alpha_*^{(1)}}$, respectively. We rewrite the system (2.1.1) as

$$\frac{dX}{dt} = \begin{bmatrix} f(S, I_S, I_R) \\ g(S, I_S, I_R) \\ h(S, I_S, I_R) \end{bmatrix} = F(E^{(1)}(S, I_S, I_R)).$$

Then,

$$F_\alpha(E_0^{(1)}, \alpha_*^{(1)}) = \begin{bmatrix} 0 \\ 0 \\ 0 \end{bmatrix}, \tag{2.2.1}$$

and

$$DF_\alpha(E_0^{(1)}, \alpha_*^{(1)}) \cdot v = \begin{bmatrix} -\frac{\lambda}{\mu} \\ \frac{\lambda}{\mu} \\ 0 \end{bmatrix}. \tag{2.2.2}$$

Also, $D^2F(E^{(1)}, \alpha) \cdot (v, v) =$

$$\begin{bmatrix} f_{SS}v_1v_1 + f_{SI_S}v_1v_2 + f_{SI_R}v_1v_3 + f_{I_SS}v_2v_1 + f_{I_SI_S}v_2v_2 + f_{I_SI_R}v_2v_3 + f_{I_RS}v_3v_1 + f_{I_RI_S}v_3v_2 + f_{I_RI_R}v_3v_3 \\ g_{SS}v_1v_1 + g_{SI_S}v_1v_2 + g_{SI_R}v_1v_3 + g_{I_SS}v_2v_1 + g_{I_SI_S}v_2v_2 + g_{I_SI_R}v_2v_3 + g_{I_RS}v_3v_1 + g_{I_RI_S}v_3v_2 + g_{I_RI_R}v_3v_3 \\ h_{SS}v_1v_1 + h_{SI_S}v_1v_2 + h_{SI_R}v_1v_3 + h_{I_SS}v_2v_1 + h_{I_SI_S}v_2v_2 + h_{I_SI_R}v_2v_3 + h_{I_RS}v_3v_1 + h_{I_RI_S}v_3v_2 + h_{I_RI_R}v_3v_3 \end{bmatrix}$$

So,

$$D^2F(E_0^{(1)}, \alpha_*^{(1)}) \cdot (v, v) = \begin{bmatrix} \dfrac{2(\mu+\mu_S)^2}{\lambda} \\ -\dfrac{2(\mu+\mu_S)^2}{\lambda} \\ 0 \end{bmatrix}. \tag{2.2.3}$$

Now, from equations (2.2.1), (2.2.2) and (2.2.3), we can conclude that,

(A) $w^T F_\alpha(E_0^{(1)}, \alpha_*^{(1)}) = 0,$

(B) $w^T[DF_\alpha(E_0^{(1)}, \alpha_*^{(1)}) \cdot v] = \dfrac{\lambda}{\mu} \neq 0,$

(C) $w^T[D^2F(E_0^{(1)}, \alpha_*^{(1)}) \cdot (v, v)] = -\dfrac{2(\mu+\mu_S)^2}{\lambda} \neq 0.$

Therefore, F satisfies all the transversality conditions (from Sotomayor's theorem [144]) for transcritical bifurcation at $\alpha = \alpha_*^{(1)} = \dfrac{\mu(\mu+\mu_S)}{\lambda}$. □

Theorem 2.2.7. *The system (2.1.1) undergoes through transcritical bifurcation at:*

$$\beta = \beta_*^{(1)} = \frac{\mu(\mu+\mu_R)}{\lambda}$$

if $\alpha\lambda - \mu^2 - \mu\mu_S < 0$ $(R_0^{(S)} < 1)$. *Here, equilibrium points* $E_0^{(1)}$ *and* $E_2^{(1)}$ *exchange their stability at* $\beta = \beta_*^{(1)}$ *(or* $R_0^{(R)} = 1$*).*

Proof. The proof of this theorem is similar to the proof in Theorem 2.2.6. □

2.3 Epidemiological Parameter Values

In this section, we will estimate the parameter values for the models (2.1.1) based on the real data from the Indian population and some previous literature related to HIV spread. The recruitment rate (λ) can be estimated as the sum of new individuals, who enter in the sexually active class and number of net migrated individuals, during the whole year, at the initial time. In India, we assume that most of the adults become sexually active during the age interval of $18-30$ years. We set the base year to be 2019, for the purpose of our simulation. The number of individuals recruited in the susceptible class during base year is equal to the average net births during the period $1989-2001$, in addition to the net migration in the base year. The net births are total number of births adjusted with the infant deaths in a year. According to United Nations World Population Prospectus [152], the average birth rate and average infant mortality rate in India during time period $1989-2001$ was 29.38 per thousand population per year and 78.87 per thousand live births per year, respectively. Further, the average total population of India during this time period was 955.29 million. Also, the net migration into India in 2019 was -0.54 million.
Therefore, the constant recruitment rate (λ) can be estimated as follows:

$$\begin{aligned}
\lambda &= \text{(avg. population)} \times \text{(avg. birth rate)} \times \text{(1 - avg. infant mortality rate)} \\
&\quad + \text{(net migration rate)} \\
&= (955.29 \times 0.02938 \times (1 - 0.07887)) - 0.54 \\
&= 25.31 \text{ million per year.}
\end{aligned}$$

The transmission rate α represents the rate of change of drug-sensitive infected population in presence of unit susceptible and unit drug-sensitive infected population. According to

India HIV Estimate 2019 Report, NACO [153], there were 69200 new HIV cases reported with total 2.35 million cases. The population in age group 20-50 can be considered as total susceptible population since it includes most of the sexually active people. According to [152], in 2019, India had 625.19 million people in the age group of 20-50. Therefore, the transmission rate is given by,

$$\alpha = \frac{0.06922}{625.19 \times 2.35} = 0.000047134 \text{ million}^{-1}\text{year}^{-1}.$$

According to United Nations World Population Prospectus [152], in India, around 7.2 persons died for every 1000 individuals during 2019. Therefore, the natural death rate (μ) is 0.007 per year in 2019. The disease induced death rates can be estimated by using the life expectancy of an HIV infected person. In [154], the authors have concluded that the life expectancy of an HIV infected patient reduces about 38 years from the general population at the exact age of 20. In India, the life expectancy from birth was 69.50 years in 2019 [152]. From this we can conclude that the life expectancy of an HIV infected person without any treatment would be around 11 years. Therefore, 1 in every 11 HIV infected person will die every year. Thus, we estimate that, $\mu_S = \frac{1}{11} = 0.0909$ per year. The remaining parameters related to the drug-resistant infected class would be varied within a suitable range, considering the corresponding parameter values associated with the drug-sensitive infected class. For each of the parameters, the unit, estimated value and range of variation has been included in Table 2.4.

Parameter	**Unit**	**Estimated Value**	**Range of Variation**
λ	million year^{-1}	25.31	fixed
α	million^{-1} year^{-1}	4.7134×10^{-5}	$[2.5 \times 10^{-5}, 3.0 \times 10^{-4}]$
β	million^{-1} year^{-1}	assumed	$[1.0 \times 10^{-5}, 7.0 \times 10^{-5}]$
μ	year^{-1}	7.0×10^{-3}	$[4.0 \times 10^{-3}, 7.0 \times 10^{-3}]$
μ_S	year^{-1}	9.09×10^{-2}	fixed
μ_R	year^{-1}	assumed	$[6.0 \times 10^{-2}, 2.0 \times 10^{-1}]$

Table 2.4: Units and values (estimates and ranges) of model parameters.

2.4 Numerical Simulation

In this section, we will numerically illustrate the analytic results on existence and stability of the equilibrium points and bifurcations, through several numerical illustrations. For this, we fix $\lambda = 25.31, \mu = 0.007, \mu_S = 0.0909, \mu_R = 0.06$, and vary parameters α and β. We choose

the initial population as 625 million for susceptible, 2.2 million for drug-sensitive infected and 1 million (assumption) for drug-resistant infected individuals, $ic_1 = (625, 2.2, 1)$, which is based on the number of individuals in different classes in the base year. We also choose two other initial conditions to validate the global stability results: $ic_2 = (300, 30, 20)$ and $ic_3 = (1000, 80, 100)$.

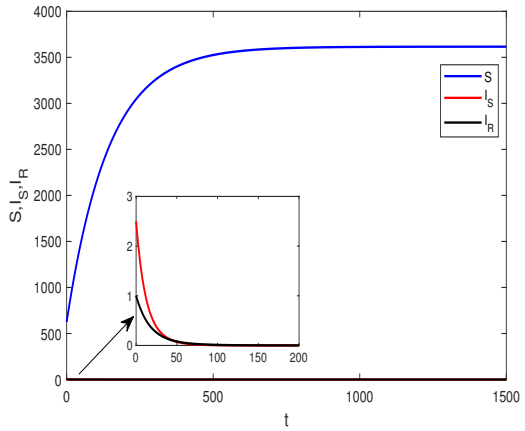

(a) $\alpha = 0.000025,\ \beta = 0.000015$

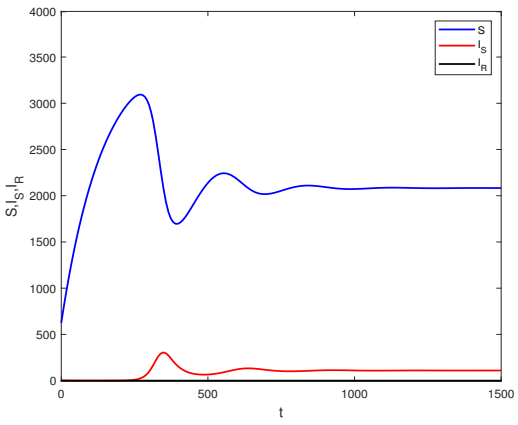

(b) $\alpha = 0.000047,\ \beta = 0.00002$

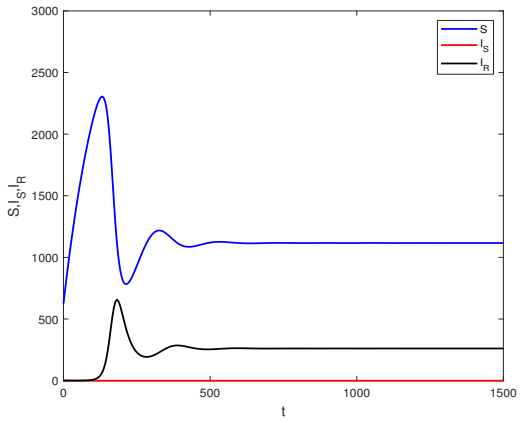

(c) $\alpha = 0.000047,\ \beta = 0.00006$

Figure 2.3: Time series plot for each population of the model system (2.1.1) with other parameter values as $\lambda = 25.31, \mu = 0.007, \mu_S = 0.0909, \mu_R = 0.06$ and initial condition $[625, 2.2, 1]$.

First we consider $\alpha = 0.000025$ and $\beta = 0.000015$ for which $R_0^{(S)} = 0.92$ and $R_0^{(R)} = 0.81$. The solutions are represented in Figure (2.3a) which points out the local asymptotic stable behaviour of the disease free equilibrium point $E_0^{(1)}(3615.7, 0, 0)$, as expected, since $R_0^{(S)} < 1$ and $R_0^{(R)} < 1$. The population level of susceptible individuals for different initial

values converges to λ/μ ($= 3615.7$) while the drug-sensitive and drug-resistant population decrease continuously and eventually get extinct (see Figure (2.4a)). This ensures the global asymptotic stability of equilibrium point $E_0^{(1)}$ and supports the theoretical result in Theorem 2.2.2. These time series and phase portrait plots indicate that when the transmission rates of both strains are below their respective threshold values, the infection cannot be sustained in the population. Consequently, the solutions converge to the disease-free equilibrium, and the majority of the population remains healthy in the long term.

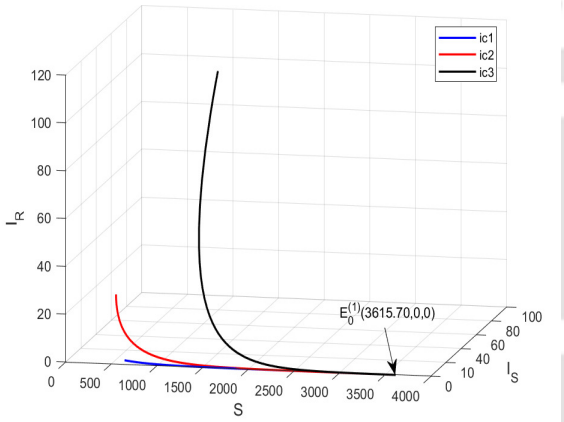

(a) $\alpha = 0.000025,\ \beta = 0.000015$

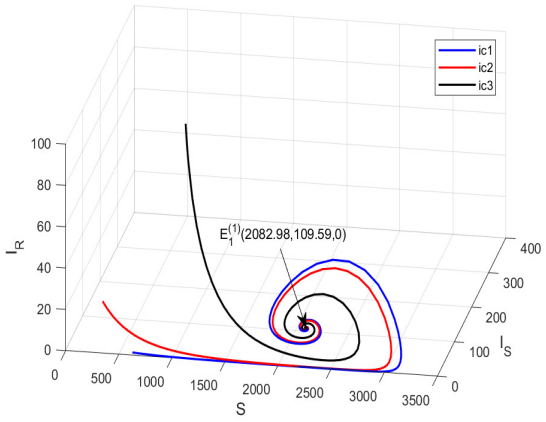

(b) $\alpha = 0.000047,\ \beta = 0.00002$

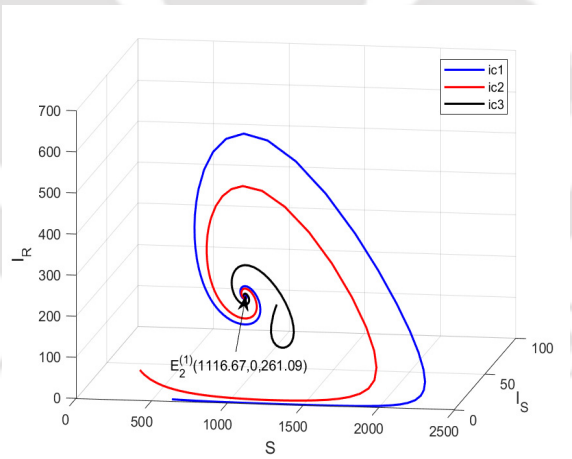

(c) $\alpha = 0.000047,\ \beta = 0.00006$

Figure 2.4: Phase portrait for model (2.1.1) with various initial conditions assuring the global stability of each equilibrium point. Other parameter values as $\lambda = 25.31, \mu = 0.007, \mu_S = 0.0909, \mu_R = 0.06$.

In order to illustrate the case $R_0^{(S)} > 1$ and $R_0^{(SR)} > 1$, we choose $\alpha = 0.000047$ and $\beta = 0.00002$ which results in $R_0^{(S)} = 1.74$ and $R_0^{(R)} = 1.08$. The dynamics for these parame-

ter values is represented in Figure (2.3b) which indicates the persistence of susceptible and drug-sensitive infected population and extinction of drug-resistant infected population after a certain time. It is seen from the Figure (2.4b), that the population levels of susceptible and drug-sensitive infected individuals for different initial conditions exhibit oscillatory behaviour before stabilizing at the level 2082.98 and 109.59, respectively, while the drug-resistant infected population becomes extinct in a very short period of time. This also suggests the global asymptotic stability of drug-sensitive mutant dominant equilibrium point $E_1^{(1)}$ and is in agreement with the theoretical result of Theorem 2.2.4. Note that the basic reproduction number of drug-resistant infected population is greater than 1 but still this population gets wiped out from the system. This is because of a higher basic reproduction number of drug-sensitive mutant which makes it dominant in comparison to the drug-resistant mutant.

Further, in order to illustrate the case $R_0^{(R)} > 1$ and $R_0^{(SR)} < 1$, we choose $\alpha = 0.000047$ and $\beta = 0.00006$ which leads to $R_0^{(S)} = 1.74$ and $R_0^{(R)} = 3.24$. The solution trajectories are drawn in Figure (2.3c) which shows that the susceptible and drug-resistant infected population saturate to a positive level and the drug-sensitive infected population dies out after some time. The global stability of drug-resistant mutant dominant equilibrium point $E_2^{(1)}(1116.67, 0, 261.09)$, as already obtained theoretically in Theorem 2.2.5, can be confirmed from Figure (2.4c) which also depicts an oscillatory behaviour of the susceptible and drug-resistant infected population before progressing to a steady state. The drug-resistant infected population dominates the drug-sensitive infected population due to its higher basic reproduction number. However, the basic reproduction number for both infected populations is greater than one. This analysis indicates that both the infected populations can be controlled by their transmission rate and disease induced death rate. A higher transmission rate of an infected population is in favor of its persistence at a higher level, while a higher disease induced death rate can cause its extinction from the system. We also observed that the coexistence of both infected populations is not possible because they share the only resource available to them, that is, the susceptible population.

Now we choose the parameters as $\lambda = 25.31, \mu = 0.007$ and $\mu_S = \mu_R = 0.0909$ to illustrate the transcritical bifurcation when equilibrium point $E_0^{(1)}$ exchanges its stability with equilibrium point $E_1^{(1)}$ $\left(\text{or } E_2^{(1)}\right)$. Also, we vary the parameter α (or β) to show the exchange of stability between equilibrium point $E_0^{(1)}$ and $E_1^{(1)}$ $\left(\text{or } E_2^{(1)}\right)$. In Figure (2.5a), we observe that the equilibrium point $E_0^{(1)}$ bifurcates and losses its stability at $\alpha = \alpha_*^{(1)}$ (or $\beta = \beta_*^{(1)}$) $= 2.71 \times 10^{-5}$ and a new stable equilibrium point $E_1^{(1)}$ $\left(\text{or } E_2^{(1)}\right)$ comes into the picture. We also demonstrated this bifurcation behaviour between these equilibrium points with respect to basic reproduction number $R_0^{(S)}$ $\left(\text{or } R_0^{(R)}\right)$. For this, we fix $\alpha = \beta = 0.000047$ and vary

the basic reproduction number $R_0^{(S)}$ and $R_0^{(S)}$ by changing common parameters λ and μ. Figure (2.5b) depicts that if $R_0^{(S)}$ $\left(\text{or } R_0^{(R)}\right) < 1$, only one equilibrium point exists, that is $E_0^{(1)}$, which is locally asymptotically stable. On $R_0^{(S)}$ $\left(\text{or } R_0^{(R)}\right) = 1$, a new equilibrium point $E_1^{(1)}$ $\left(\text{or } E_2^{(1)}\right)$ emerges and $E_0^{(1)}$ exchanges its stability with this new equilibrium point provided that $R_0^{(R)}$ $\left(\text{or } R_0^{(S)}\right) < 1$. These numerical results support Theorem 2.2.6 and Theorem 2.2.7.

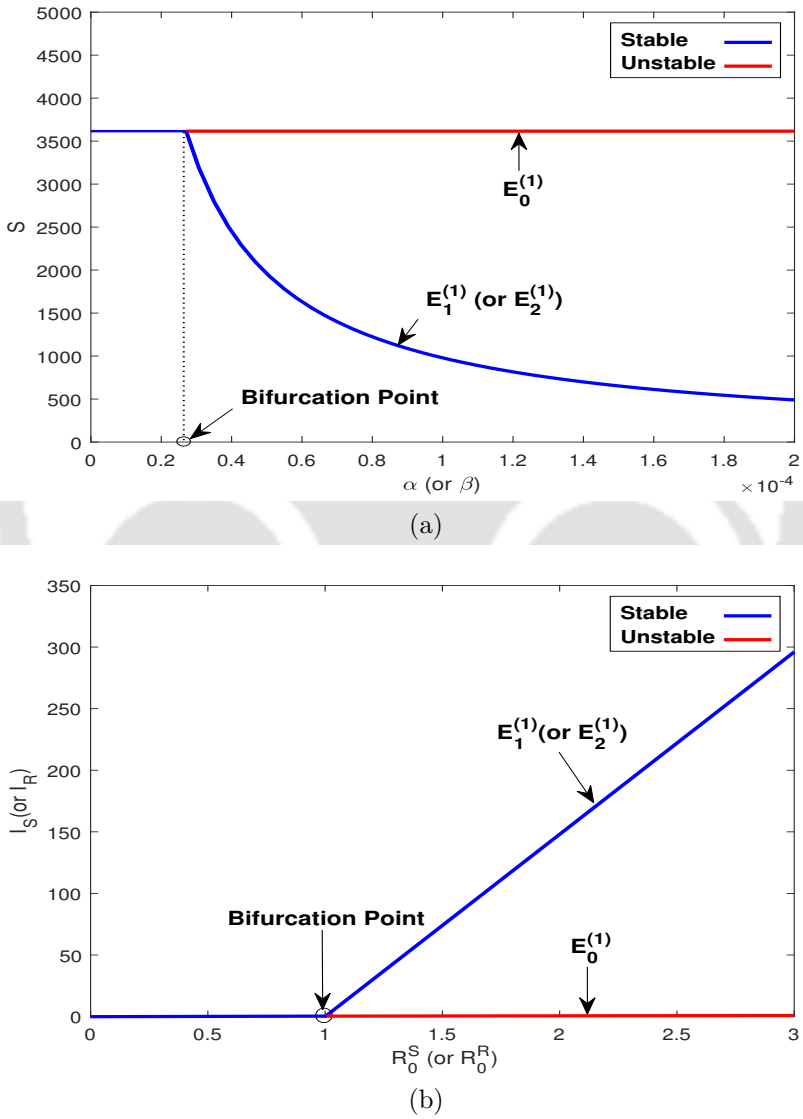

Figure 2.5: Transcritical bifurcation diagrams with respect to parameters (a). α(or β) and (b). $R_0^{(S)}$ $\left(\text{or } R_0^{(R)}\right)$.

2.5 Conclusion

In this chapter, we formulated a mathematical model to understand the community-level dynamics of multiple strains of HIV spread without any treatment options. In absence of treatment, there is no development of drug resistance. The only way of getting drug resistance is transmission from already drug-resistant infected population. For the proposed model, we obtained the basic reproduction number for drug-sensitive ($R_0^{(S)}$) and drug-resistant ($R_0^{(R)}$) strains with the help of the next generation matrix. The existence of equilibrium points and their stability is totally controlled by these basic reproduction numbers. The stability analysis of equilibrium points provides us with three possible scenarios:

(A) Both type of infected population dies out when $R_0^{(S)} < 1$ and $R_0^{(R)} < 1$.

(B) Only drug-sensitive infected population survives when $R_0^{(S)} > 1$ and $R_0^{(SR)} > 1$.

(C) Only drug-resistant infected population survives when $R_0^{(R)} > 1$ and $R_0^{(SR)} < 1$.

In all of the above cases, we observe that the co-existence of all populations is impossible due to the competitive selection process. This happens because both infected populations with drug-sensitive and drug-resistant strains share their common source (susceptible population) of growth and have a strong competition type relationship. The strongest and the fittest one will win this battle and survive for long time. The bifurcation analysis shows that the transmission rate and disease induced death rate of both strains are the determining factors for the elimination of the disease from the system. The lower transmission rate or higher disease induced death rate from certain threshold values makes the system disease free after some time. On the other hand, a greater transmission rate or a lower disease induced death rate of a strain from these threshold values is directly related to the increased fitness of that strain.

Chapter 3

Multi-Strain HIV Dynamics With Treatment

In the absence of treatment, the coexistence of both drug-sensitive and drug-resistant strains is generally not sustainable, as competitive selection typically favors one strain over the other. However, once treatment and related factors are introduced, a broader range of epidemiological outcomes becomes possible. The effectiveness of ART in suppressing viral replication depends not only on timely initiation but also on sustained adherence to prescribed regimens. In this chapter, we extend the treatment-free model of Chapter 2 by incorporating treatment and its adherence levels. To capture the development of drug resistance, we introduce an additional treatment compartment and account for the fact that resistant infections may arise both through direct transmission from drug-resistant individuals and through the emergence of resistance due to suboptimal adherence among treated individuals. The long-term dynamics of the system are investigated by determining equilibrium points and analyzing their local and global stability. A detailed bifurcation analysis is then conducted to explore how threshold parameters govern the qualitative behavior of the system. The theoretical results are further illustrated and explained with numerical simulations.

3.1 Formulation of the Mathematical Model

Sub-optimal adherence reduces treatment efficacy and accelerates the emergence of drug-resistant strains, which can then spread within the community alongside the drug-sensitive virus. This dynamic introduces a feedback loop: while ART reduces transmission when taken properly, poor adherence can increase resistance, complicating epidemic control. Capturing this dual role of ART, both as a suppressor of infection and as a potential driver of emergence of drug resistance, is essential for assessing its population-level impact through mathematical modelling. To mathematically model this dynamics, the total sexually active population is

partitioned into four mutually exclusive groups: susceptible individuals (S), those infected with the drug-sensitive strain (I_S), those receiving treatment (T), and those infected with the drug-resistant strain (I_R). We assume that the individuals are homogeneously distributed in the given population. As in Chapter 2, we assume that the susceptible population increases through constant recruitment at a rate λ, and individuals move to the infected classes upon effective contact with the drug-sensitive infected and the drug-resistant infected individuals at contact rates α and β, respectively. We assume that an effective contact transmits the same type of strain in the newly infected person. The primary reason for the drug resistance in the infected population is its acquisition from the failure of treatment, and not the transmission [97]. Therefore, we do not consider the cross-transmission of resistance between drug-sensitive and drug-resistant infected population. The poor economic condition of infected patients, in addition to limited medical infrastructure, restricts the reach of treatment to only a fraction (η) of the whole drug-sensitive infected population with a rate of γ. Further, we assume that only a fraction (ϵ) of total population under treatment adheres to it, as directed. The remaining fraction $(1-\epsilon)$ of the treatment class is non-adherent to the prescribed drugs, which causes this population to develop a drug-resistant strain of the virus. As a result, $(1-\epsilon)$ fraction of the treatment class will transfer to the drug-resistant infected class at the rate of ρ. Also, these remaining fraction of the population in the drug-sensitive infected $(1-\eta)$ and treatment $(1-\epsilon)$ compartments die with disease induced death rate of μ_S. This population also develops drug resistance because of the sub-optimal adherence to the treatment. Here we are considering only the sub-optimal adherence to the treatment as the reason for the development of drug resistance. The drug-resistant infected population dies with the disease induced death rate of μ_R. We also assume that a drug-resistant infected individual is at 100% drug resistance level. In other words, the treatment does not work at all on drug-resistant infected population. Individuals in each of the groups die naturally at the rate μ. A schematic representation for this type of HIV spread is presented in Figure 3.1.

Taking into account the aforementioned assumptions, the population in each group is determined by the following deterministic system of coupled non-linear ordinary differential equations:

$$\begin{aligned} S' &= \lambda - \alpha I_S S - \beta I_R S - \mu S, \\ I_S' &= \alpha I_S S - \gamma\eta I_S - \mu_S(1-\eta) I_S - \mu I_S, \\ T' &= \gamma\eta I_S - \rho(1-\epsilon)T - \mu_S(1-\epsilon)T - \mu T, \\ I_R' &= \beta I_R S + \rho(1-\epsilon)T - \mu_R I_R - \mu I_R, \end{aligned} \tag{3.1.1}$$

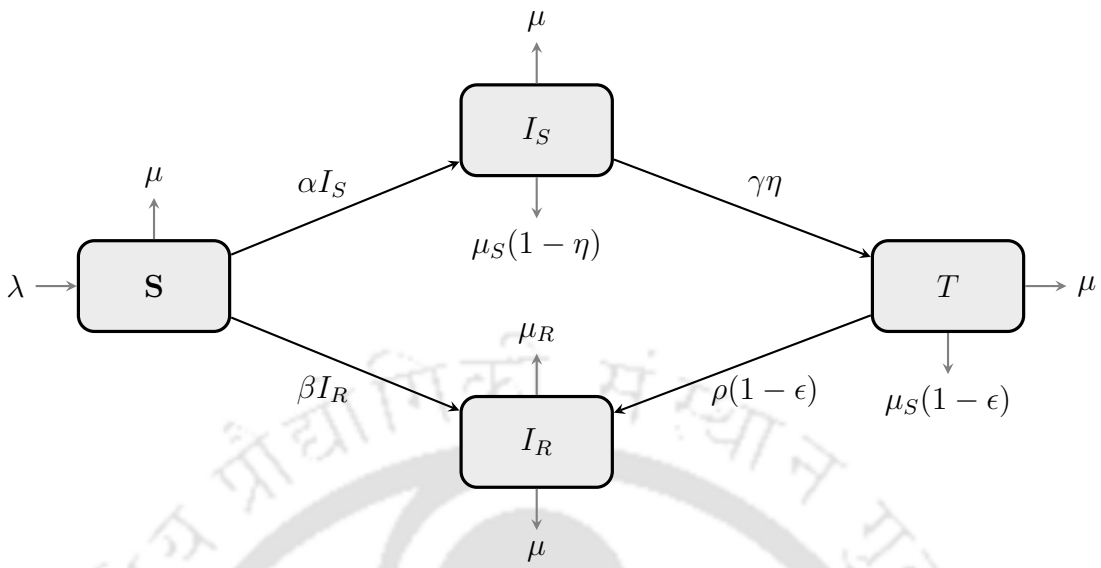

Figure 3.1: Schematic representation of the model (3.1.1).

with the initial condition $(S(0), I_S(0), T(0), I_R(0))$ belonging to the region $\mathcal{R}$ defined as,

$$\mathcal{R} = \left\{ (S, I_S, T, I_R) \in \mathbb{R}^4_+ : 0 \leq S + I_S + T + I_R \leq \frac{\lambda}{\mu} \right\},$$

where $\mathbb{R}^4_+$ refers to the non-negative cone along with its lower-dimensional faces. The biological meaning of the parameters used in the system (3.1.1) is provided in Table 3.1.

3.2 Mathematical Analysis of the Model

In this section, we first establish the biological well-posedness of the system (3.1.1) by proving the uniqueness, non-negativity, and boundedness of its solutions. We then identify the equilibrium points and study their local and global stability to understand the long-term behavior of the system. This analysis provides parameter-dependent conditions that determine the possible epidemic outcomes. In particular, we explore whether the two strains can coexist or whether one will competitively exclude the other. Finally, we carry out a theoretical investigation of potential bifurcations to capture threshold-driven changes in system dynamics.

3.2.1 Uniqueness, non-negativity and boundedness of the solutions

We define these new parameters for further analysis of the model (3.1.1):

$$a := \gamma\eta + \mu_S(1-\eta) + \mu, b := \rho(1-\epsilon) + \mu_S(1-\epsilon) + \mu \text{ and } c := \mu + \mu_R.$$

Parameter	Biological Description
λ	Recruitment rate of susceptible individuals
α	Transmission rate per effective contact between a susceptible individual and a drug-sensitive infected individual
β	Transmission rate per effective contact between a susceptible individual and a drug-resistant infected individual
γ	Treatment initiation rate for drug-sensitive infected population
ρ	Rate of emergence of drug resistance in non-adherent population
η	Proportion of HIV infected population which is receiving treatment
ϵ	Proportion of under treatment population which is adherent
μ_S	Disease-induced death rate of drug-sensitive infected population
μ_R	Disease-induced death rate of drug-resistant infected population
μ	Natural death rate

Table 3.1: Model parameters and their biological descriptions for the system (3.1.1).

The right-hand side of the system (3.1.1) is continuous and Lipschitz on $[0, a]$, $a > 0$. Therefore, the system (3.1.1) with the initial condition $(S(0), I_S(0), T(0), I_R(0)) \in \mathcal{R}$ has a unique solution.

Let t_1 denote the time at which the susceptible population S becomes extinct. Then $S(t_1) = 0$ and $S'(t_1) = \lambda > 0$. Therefore $\nexists$ any $\epsilon > 0$ such that $S(t_1) = 0$ and $S(t_1 + \epsilon) < 0$. Hence $S(t_1) \geq 0$, $\forall t_1 > 0$ as $S(0) \geq 0$. Now, from the second equation of (3.1.1), we have,

$$I_S(t) = I_S(0) \exp\left[\int_0^t (\alpha S(\tau) - a)\, d\tau\right] \geq 0 \text{ for } I_S(0) \geq 0.$$

In an analogous manner, from the third and fourth equation of (3.1.1), we have,

$$T(t) \geq T(0) \exp\left[\int_0^t (-b) d\tau\right] \geq 0 \text{ for } T(0) \geq 0,$$

$$I_R(t) = I_R(0) \exp\left[\int_0^t (\beta S(\tau) - c)\, d\tau\right] \geq 0 \text{ for } I_R(0) \geq 0,$$

respectively.

For the boundedness part, we define $W = S + I_S + T + I_R$. Then,

$$\begin{aligned} W' &= S' + I_S' + T' + I_R' \\ &= \lambda - \mu W - \mu_S(1-\eta)I_S - \mu_S(1-\epsilon)T - \mu_R I_R \\ &\leq \lambda - \mu W, \end{aligned}$$

which implies that $W \leq \dfrac{\lambda}{\mu} := M_1$ (say). This shows that W is bounded by M_1. Therefore S, I_S, T and I_R are also bounded by M_1. From these results, we can now state the following Theorem.

Theorem 3.2.1. *The biologically feasible region $\mathcal{R}$ defined by:*

$$\mathcal{R} = \left\{ (S, I_S, T, I_R) \in \mathbb{R}^4_+ : 0 \leq S + I_S + T + I_R \leq \frac{\lambda}{\mu} \right\},$$

where $\mathbb{R}^4_+$ denotes the non-negative cone and its lower dimensional faces, is positively invariant for the system (3.1.1) with non-negative initial conditions.

3.2.2 Equilibrium points and local stability analysis

For the system given by equation (3.1.1), there exist three equilibrium points as enumerated below:

(A) Disease free equilibrium point: $E_0^{(2)}\left(\dfrac{\lambda}{\mu}, 0, 0, 0\right)$.

(B) Planar equilibrium point: $E_1^{(2)}\left(\bar{S}_1, 0, 0, \bar{I}_{R_1}\right) = \left(\dfrac{c}{\beta}, 0, 0, \dfrac{\beta\lambda - \mu c}{c\beta}\right)$.

(C) Interior equilibrium point: $E_*^{(2)} = (S_*, I_{S_*}, T_*, I_{R_*})$, where,

$$S_* = \frac{a}{\alpha}, \quad I_{S_*} = \frac{b(c\alpha - a\beta)(\lambda\alpha - a\mu)}{a\alpha(bc\alpha - ab\beta + (1-\epsilon)\gamma\rho\beta\eta)},$$

$$T_* = \frac{\gamma\eta(c\alpha - a\beta)(\alpha\lambda - a\mu)}{a\alpha(bc\alpha - ab\beta + (1-\epsilon)\gamma\rho\beta\eta)}, \quad I_{R_*} = \frac{\gamma\rho\eta(1-\epsilon)(\alpha\lambda - a\mu)}{a(bc\alpha - ab\beta + (1-\epsilon)\gamma\rho\beta\eta)}.$$

Here, the parameters a, b and c are as defined in Section 3.2.1.

Now, we determine the "Basic Reproduction Number", for the system (3.1.1), by considering the next generation matrix as,

$$FV^{-1} = \begin{pmatrix} \frac{\alpha\lambda}{a\mu} & 0 \\ 0 & \frac{\beta\lambda}{c\mu} \end{pmatrix}.$$

Hence the "Basic Reproduction Number" for the sensitive strain and the drug-resistant strain are given by $\bar{R}_0^{(S)} = \dfrac{\alpha\lambda}{a\mu}$ and $\bar{R}_0^{(R)} = \dfrac{\beta\lambda}{c\mu}$, respectively. In particular, the "Basic Reproduction Number" for the system (3.1.1) is $\bar{R}_0 = \max\{\bar{R}_0^{(S)}, \bar{R}_0^{(R)}\}$. We denote the ratio of $\bar{R}_0^{(S)}$ and $\bar{R}_0^{(R)}$, as $\bar{R}_0^{(SR)} := \dfrac{\alpha c}{\beta a}$.

For the presentation of the stability analysis, we consider the following Jacobian,

$$J_2 = \begin{bmatrix} -\alpha I_S - \beta I_R - \mu & -\alpha S & 0 & -\beta S \\ \alpha I_S & \alpha S - a & 0 & 0 \\ 0 & \gamma\eta & -b & 0 \\ \beta I_R & 0 & \rho(1-\epsilon) & \beta S - c \end{bmatrix}.$$

The stability analysis for each of the equilibria is enumerated below:

(A) The eigenvalues of the Jacobin matrix, evaluated at $E_0^{(2)}$ are,

$$\lambda_{01} = -b,\ \lambda_{02} = -\mu,\ \lambda_{03} = \frac{\alpha\lambda - a\mu}{\mu},\ \lambda_{04} = \frac{\beta\lambda - c\mu}{\mu}.$$

Therefore, the disease free equilibrium $E_0^{(2)}$ is locally stable, provided, $\alpha\lambda - a\mu < 0$ and $\beta\lambda - c\mu < 0$, *i.e,* $\bar{R}_0^{(S)} < 1$ and $\bar{R}_0^{(R)} < 1$, respectively.

(B) The eigenvalues of the Jacobin matrix, evaluated at $E_1^{(2)}$ are given by,

$$\lambda_{11} = -b,\ \lambda_{12} = \alpha\bar{S}_1 - a,\ \lambda_{13} = \frac{A_1 + \sqrt{A_1^2 - 4B_1}}{2},\ \lambda_{14} = \frac{A_1 - \sqrt{A_1^2 - 4B_1}}{2},$$

where $A_1 := c - \beta\bar{S}_1 + \dfrac{\lambda}{\bar{S}_1}$ and $B_1 := \beta^2\bar{I}_{R_1}\bar{S}_1 + \dfrac{\lambda c}{\bar{S}_1} - \beta\lambda$. All the eigenvalues are either negative or have negative real part provided $\bar{S}_1 < \dfrac{a}{\alpha}$ and $A_1 > 0$, which are equivalent to $\bar{R}_0^{(SR)} < 1$, and the existential condition for $E_1^{(2)}$, namely $\bar{R}_0^{(R)} > 1$. Thus, the equilibrium point $E_1^{(2)}$ is stable, provided $\bar{R}_0^{(S)} < \bar{R}_0^{(R)}$.

(C) Finally, the eigenvalues of the interior equilibrium point $E_*^{(2)}$ are given by the roots of the following characteristic equation of the Jacobian matrix, evaluated at $E_*^{(2)}$:

$$x^4 + A_* x^3 + B_* x^2 + C_* x + D_* = 0, \tag{3.2.1}$$

where

$$\begin{aligned} A_* &= b + c - \beta S_* + \frac{\lambda}{S_*}, \\ B_* &= bc + \alpha^2 I_{S_*} S_* - b\beta S_* + \beta^2 I_{R_*} S_* + \frac{b\lambda}{S_*} + \frac{c\lambda}{S_*} - \beta\lambda, \\ C_* &= I_{S_*} S_* (b\alpha^2 + c\alpha^2 - S_*\alpha^2\beta) + b\beta^2 I_{R_*} S_* + \frac{bc\lambda}{S_*} - b\beta\lambda, \\ D_* &= bc\alpha^2 I_{S_*} S_* - b\alpha^2\beta I_{S_*} S_*^2 + (1-\epsilon)\alpha\beta\gamma\rho\eta I_{S_*} S_*. \end{aligned}$$

By the Routh-Hurwitz criterion, all the eigenvalues will have negative real part if,

(A) $A_* > 0, B_* > 0, C_* > 0, D_* > 0$,

(B) $A_*B_* - C_* > 0$,

(C) $A_*B_*C_* - A_*^2D_* - C_*^2 > 0$.

The coefficients of the characteristic equation, in terms of the Basic Reproduction Numbers are given by,

$$
\begin{aligned}
A_* &:= \frac{\alpha(ab+\alpha\lambda) + a^2\beta\left(\bar{R}_0^{(SR)} - 1\right)}{a\alpha}, \\
B_* &:= \frac{a\beta(ab+\alpha\lambda)\left(\bar{R}_0^{(SR)} - 1\right) + b\alpha^2\lambda}{a\alpha} + \frac{a^2b\mu\left(\bar{R}_0^{(S)} - 1\right)\left(\bar{R}_0^{(SR)} - 1\right)}{ab\left(\bar{R}_0^{(SR)} - 1\right) + \gamma\rho\eta(1-\epsilon)} \\
&\quad + \frac{a(1-\epsilon)\left(\bar{R}_0^{(S)} - 1\right)\beta\gamma\rho\eta\mu}{\alpha\left(ab\left(\bar{R}_0^{(SR)} - 1\right) + \gamma\rho\eta(1-\epsilon)\right)}, \\
C_* &:= b\lambda\beta\left(\bar{R}_0^{(SR)} - 1\right) + \frac{a^2b^2\mu\left(\bar{R}_0^{(S)} - 1\right)\left(\bar{R}_0^{(SR)} - 1\right)}{ab\left(\bar{R}_0^{(SR)} - 1\right) + \gamma\rho\eta(1-\epsilon)} \\
&\quad + \frac{a^3b\beta\mu\left(\bar{R}_0^{(S)} - 1\right)\left(\bar{R}_0^{(SR)} - 1\right)^2}{\alpha\left(ab\left(\bar{R}_0^{(SR)} - 1\right) + \gamma\rho\eta(1-\epsilon)\right)} + \frac{ab(1-\epsilon)\left(\bar{R}_0^{(S)} - 1\right)\beta\gamma\rho\eta\mu}{\alpha\left(ab\left(\bar{R}_0^{(SR)} - 1\right) + \gamma\rho\eta(1-\epsilon)\right)}, \\
D_* &:= \frac{a^2b\beta\mu\left(\bar{R}_0^{(S)} - 1\right)\left(\bar{R}_0^{(SR)} - 1\right)}{\alpha}.
\end{aligned}
$$

The condition (A) has already been satisfied since the interior equilibrium point $E_*^{(2)}$ exists if and only if $\bar{R}_0^{(S)} > 1$ and $\bar{R}_0^{(SR)} > 1$. For condition (B), we have,

$$
\begin{aligned}
A_*B_* - C_* = & \\
& \frac{(b\alpha + a\beta(\bar{R}_0^{(SR)} - 1))(ab(\bar{R}_0^{(SR)} - 1) + \gamma\rho\eta(1-\epsilon))(ab+\alpha\lambda)(a^2\beta(\bar{R}_0^{(SR)} - 1) + \alpha^2\lambda)}{\alpha^2a^2(ab(\bar{R}_0^{(SR)} - 1) + \gamma\rho\eta(1-\epsilon))} \\
& + \frac{a^2\mu(\bar{R}_0^{(S)} - 1)(a^2\beta^2\gamma\rho\eta(1-\epsilon)(\bar{R}_0^{(SR)} - 1) + \alpha^2(ab\alpha(\bar{R}_0^{(SR)} - 1) + \beta\gamma\rho\eta(1-\epsilon))\lambda)}{\alpha^2a^2(ab(\bar{R}_0^{(SR)} - 1) + \gamma\rho\eta(1-\epsilon))} \\
> & \ 0,
\end{aligned}
$$

which shows that condition (B) also holds whenever $E_*^{(2)}$ exists. So, we are left only with condition (C) to obtain a locally stable interior equilibrium point.

The summary of existence and stability conditions for different equilibrium points of model (3.1.1) are presented in Table 3.2 and Figure 3.2.

Equilibrium Point	Existence Condition	Stability Condition
$E_0^{(2)}\left(\frac{\lambda}{\mu},0,0,0\right)$	Always	$\max\{\bar{R}_0^{(S)},\bar{R}_0^{(R)}\}<1$
$E_1^{(2)}(\bar{S}_1,0,0,\bar{I}_{R_1})$	$\bar{R}_0^{(R)}>1$	$\bar{R}_0^{(SR)}<1$
$E_*^{(2)}(S_*,I_{S_*},T_*,I_{R_*})$	$\bar{R}_0^{(S)}>1$ and $\bar{R}_0^{(SR)}>1$	$A_*B_*C_*-A_*^2D_*-C_*^2>0$

Table 3.2: Existence and stability conditions for the equilibrium points of model (3.1.1).

3.2.3 Global stability analysis

Theorem 3.2.2. *The equilibrium point $E_0^{(2)}$ is globally asymptotically stable with $\bar{R}_0<1$, where $\bar{R}_0=\max\left(\bar{R}_0^{(S)},\bar{R}_0^{(R)}\right)$.*

Proof. From the system (3.1.1), we have,

$$I_S'=(\alpha S-a)\,I_S$$

which can be integrated to give,

$$I_S(t)=I_S(0)\exp\left[\int_0^t \alpha S(\tau)d\tau-at\right],\qquad \forall\ t\geq 0.$$

After using the upper bound of $S(t)$, which is $\dfrac{\lambda}{\mu}$, we obtain

$$\begin{aligned} I_S(t) &\leq I_S(0)\exp\left[\left(\frac{\alpha\lambda}{\mu}-a\right)t\right]\\ &= I_S(0)\exp\left[a\left(\bar{R}_0^{(S)}-1\right)t\right]. \end{aligned}$$

It follows then that $I_S(t)\to 0$ as $t\to\infty$, if $\bar{R}_0^{(S)}<1$. Therefore, the hyperplane $I_S=0$ attracts all solutions of the system (3.1.1) originating in domain $\mathcal{R}$.
Since $I_S(t)\to 0$ as $t\to\infty$ for $\bar{R}_0^{(S)}<1$, from the system (3.1.1), we have,

$$T'=-bT\implies T(t)=T(0)\exp(-bt).$$

It follows then that $T(t)\to 0$ as $t\to\infty$, if $\bar{R}_0^{(S)}<1$ and the hyperplane $T=0$ attracts all solution of the system (3.1.1) originating in domain $\mathcal{R}$. Similarly, if $\bar{R}_0^{(R)}<1$, $I_R(t)\to 0$ as $t\to\infty$, since $I_S(t)\to 0$ and $T(t)\to 0$ as $t\to\infty$ and the hyperplane $I_R=0$ attracts all solution of the system (3.1.1) originating in domain $\mathcal{R}$. Now, it is simple to show that if $I_S\to 0$ and $I_R\to 0$, then $S\to\dfrac{\lambda}{\mu}$. Therefore, the equilibrium point $E_0^{(2)}$ is globally asymptotically stable when $\bar{R}_0<1$. □

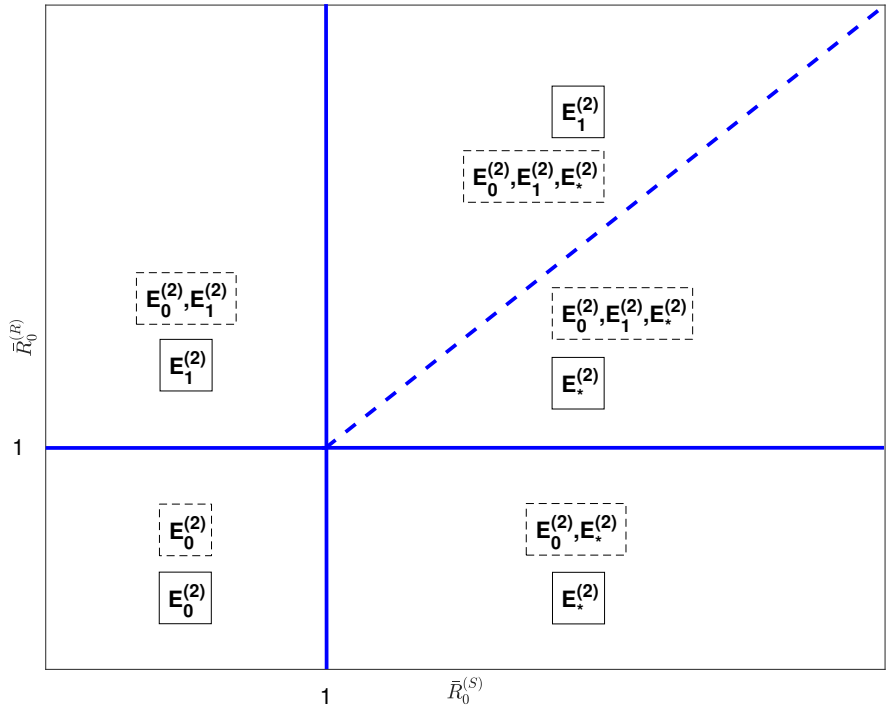

Figure 3.2: Two parameter bifurcation diagram showing existence and stability regions for different equilibrium points of model (3.1.1). The dashed boxes contain total existing equilibrium point while solid boxes contain only stable equilibrium points. The dashed blue line represents $\bar{R}_0^{(S)} = \bar{R}_0^{(R)}$. The interior equilibrium point is not stable in the whole region showed in the above figure, instead it is stable only in a sub-region of above stability region where condition (C) holds.

Theorem 3.2.3. *The equilibrium point $E_1^{(2)}$ is globally asymptotically stable whenever it exists if $\bar{R}_0^{(SR)} < 1$.*

Proof. From the second and last equations of the system (3.1.1), we have:

$$I_S' = (\alpha S - a)\, I_S, \tag{3.2.2}$$

$$I_R' = (\beta S - c)\, I_R + \rho(1-\epsilon)T. \tag{3.2.3}$$

Now, we divide equations (3.2.2) and (3.2.3) by I_S and I_R, respectively, and obtain

$$\frac{d(logI_S)}{dt} = \alpha S - a, \tag{3.2.4}$$

$$\frac{d(logI_R)}{dt} = \beta S - c + \rho(1-\epsilon)\frac{T}{I_R}. \tag{3.2.5}$$

Here, equations (3.2.4) and (3.2.5) lead to the following relation:

$$S = \frac{1}{\alpha}\frac{d(logI_S)}{dt} + \frac{a}{\alpha} = \frac{1}{\beta}\frac{d(logI_R)}{dt} + \frac{c}{\beta} - \frac{\rho(1-\epsilon)T}{\beta I_R},$$

and immediately obtain the following inequality:

$$\frac{1}{\alpha}\frac{d(logI_S)}{dt} + \frac{a}{\alpha} \leq \frac{1}{\beta}\frac{d(logI_R)}{dt} + \frac{c}{\beta}.$$

Now, integrating both sides of the above inequality yields,

$$\left(\frac{I_S(t)}{I_S(0)}\right)^{\frac{1}{\alpha}} \exp\left(\frac{at}{\alpha}\right) \leq \left(\frac{I_R(t)}{I_R(0)}\right)^{\frac{1}{\beta}} \exp\left(\frac{ct}{\beta}\right),$$

which we rearrange in the following form,

$$\begin{aligned}\left(\frac{I_S(t)}{I_S(0)}\right)^{\frac{1}{\alpha}} &\leq \left(\frac{I_R(t)}{I_R(0)}\right)^{\frac{1}{\beta}} \exp\left(\left(\frac{c}{\beta} - \frac{a}{\alpha}\right)t\right) \\ &= \left(\frac{I_R(t)}{I_R(0)}\right)^{\frac{1}{\beta}} \exp\left(\frac{c}{\beta}\left(1 - \frac{1}{\bar{R}_0^{(SR)}}\right)t\right).\end{aligned}$$

Finally, as we take the limit as $t \to \infty$, since both $I_S(t)$ and $I_R(t)$ are bounded, we get:

$$\lim_{t\to\infty}\left(\frac{I_S(t)}{I_S(0)}\right)^{\frac{1}{\alpha}} \leq \lim_{t\to\infty}\left(\frac{I_R(t)}{I_R(0)}\right)^{\frac{1}{\beta}} \exp\left(\frac{c}{\beta}\left(1 - \frac{1}{\bar{R}_0^{(SR)}}\right)t\right) \to 0, \quad \text{if } \bar{R}_0^{(SR)} < 1.$$

Therefore, all solutions of the system (3.1.1) converge to the hyperplane $I_S = 0$ when $\bar{R}_0^{(SR)} < 1$. Consequently, all solutions of this system converge to the hyperplane $T = 0$ also, as proved in Theorem 3.2.2.

Next, we construct the Lyapunov function to show the globally asymptotically stable behaviour of the equilibrium point $E_1^{(2)}$ on the hyperplanes $I_S = 0$ and $T = 0$. We consider the Lyapunov function as,

$$L_4(t) = L_4(S(t), I_S(t), T(t), I_R(t)) = S - \bar{S}_1 - \bar{S}_1 \log\left(\frac{S}{\bar{S}_1}\right) + I_R - \bar{I}_{R_1} - \bar{I}_{R_1} ln\left(\frac{I_{R_1}}{\bar{I}_{R_1}}\right).$$

Then $L_4(E_1^{(2)}) = 0$ and $L_4(x) > 0, x \neq E_1^{(2)}$. The derivative of $L_4(t)$ along the solution of system (3.1.1) gives,

$$\frac{dL_4}{dt} = \left(1 - \frac{\bar{S}_1}{S}\right)(\lambda - \beta I_R S - \mu S) + \left(1 - \frac{\bar{I}_{R_1}}{I_R}\right)(\beta I_R S - c I_R). \tag{3.2.6}$$

Now, at the equilibrium point $E_1^{(2)}$, we have,

$$\lambda = \beta \bar{I}_{R_1} \bar{S}_1 + \mu \bar{S}_1.$$

Replacing the λ in equation (3.2.6), we obtain,

$$\begin{aligned}\frac{dL_4}{dt} &= \mu\bar{S}_1\left(2-\frac{\bar{S}_1}{S}-\frac{S}{\bar{S}_1}\right)+c\bar{I}_{R_1}\left(2-\frac{\bar{S}_1}{S}-\frac{S}{\bar{S}_1}\right)\\ &= \left(2-\frac{\bar{S}_1}{S}-\frac{S}{\bar{S}_1}\right)(\mu S_1+c\bar{I}_{R_1}).\end{aligned}$$

Since the arithmetic mean is always greater than or equal to the geometric mean, we obtain $\frac{dL_4}{dt}\leq 0$. Therefore, by LaSalle invariance principle, it follows that the equilibrium point $E_1^{(2)}$ is globally asymptotically stable whenever it exists if $\bar{R}_0^{(SR)}<1$. □

Remark 3.2.4. *The global behaviour of the interior equilibrium point $E_*^{(2)}$ is uncertain, since we are unable to construct any suitable Lyapunov function for it. However, we have numerically shown that for a given set of parameter values, this equilibrium point is an attractor for solutions starting from a wide range of initial conditions (see Figure 3.4).*

3.2.4 Bifurcation analysis

Theorem 3.2.5. *The system (3.1.1) undergoes a transcritical bifurcation at:*

$$\beta=\beta_*^{(2)}=\frac{\mu c}{\lambda}\ (or\ \bar{R}_0^{(R)}=1)$$

if $\bar{R}_0^{(S)}<1$. Here, equilibrium points $E_0^{(2)}$ and $E_1^{(2)}$ exchange their stability at $\beta=\beta_*^{(2)}$.

Proof. Since the equilibrium point $E_0^{(2)}$ becomes non-hyperbolic at $\beta=\beta_*^{(2)}$, therefore linearization is inconclusive. We use the center manifold theory to study the local behaviour of this non-hyperbolic equilibrium point at $\beta=\beta_*^{(2)}$. It also describes the existence of another equilibrium point $E_1^{(2)}$, which is bifurcated from the non-hyperbolic equilibrium. The Jacobian matrix of model system (3.1.1) around the equilibrium $E_0^{(2)}$ evaluated at $\beta=\beta_*^{(2)}$, represented by $J_2\left(E_0^{(2)}\right)\Big|_{\beta=\beta_*^{(2)}}$, gives one simple zero eigenvalue and all the other eigenvalues have negative real parts if $\bar{R}_0^S<1$. Therefore, we can apply center manifold theory. We calculate the right eigenvector u and left eigenvector v corresponding to the zero eigenvalue of the matrix $J_2\left(E_0^{(2)}\right)\Big|_{\beta=\beta_*^{(2)}}$, which are given by $u=\left[-\frac{c}{\mu},0,0,1\right]^T$ and $v=\left[0,\frac{(1-\epsilon)\gamma\rho\eta\mu}{b(a\mu-\alpha\lambda)},\frac{\rho(1-\epsilon)}{b},1\right]^T$. Now, we rewrite the system (3.1.1) as

$$\frac{dX}{dt}=F(X,\beta),\ F:\mathbb{R}^4\times\mathbb{R}\to\mathbb{R}^4 \text{ and } F\in\mathcal{C}^2(\mathbb{R}^4\times\mathbb{R}),$$

where $X=[x_1,x_2,x_3,x_4]^T=[S,I_S,T,I_R]^T$ and $F=[f_1,f_2,f_3,f_4]^T$.

Let

$$f = \sum_{k,i,j=1}^{4} u_k v_i v_j \frac{\partial^2 f_k}{\partial x_i \partial x_j}\left(E_0^{(2)}, \beta_*^{(2)}\right),$$

$$g = \sum_{k,i=1}^{4} u_k v_i \frac{\partial^2 f_k}{\partial x_i \partial \beta}\left(E_0^{(2)}, \beta_*^{(2)}\right).$$

Further, by calculating the partial derivatives of the functions associated with model system (3.1.1) at equilibrium point $E_0^{(2)}$ and $\beta = \beta_*^{(2)}$, we get $f = -\dfrac{2c^2}{\lambda} < 0$ and $g = \dfrac{\lambda}{\mu} > 0$. Therefore, from Theorem 4.1(iv) of [155], we conclude that the model system (3.1.1) undergoes a transcritical bifurcation at $\beta = \beta_*^{(2)}$. □

Theorem 3.2.6. *The equilibrium point $E_*^{(2)}$ changes its stability through a Hopf-bifurcation when the real part of eigenvalues of $J_2(E_*^{(2)})$ intersects the imaginary axis at $\eta = \eta_H^{(2)}$, where $\eta_H^{(2)}$ is a root of the equation*
$A_*B_*C_* - A_*^2D_* - C_*^2 = 0$.

Proof. The characteristic equation of the matrix $J_2(E_*^{(2)})$ has purely imaginary roots if:

(A) $A_* > 0, B_* > 0, C_* > 0, D_* > 0$,

(B) $A_*B_* - C_* > 0$,

(C) $A_*B_*C_* - A_*^2D_* - C_*^2 = 0$,

and the system becomes structurally unstable in the neighborhood of the equilibrium point $E_*^{(2)}$, at $\eta = \eta_H^{(2)}$ where $\eta_H^{(2)} \in [0, 1]$ is a root of equation $A_*B_*C_* - A_*^2D_* - C_*^2 = 0$. Further, this equilibrium point will change its stability at $\eta = \eta_H^{(2)}$ through a Hopf-bifurcation if conditions (A), (B) and (C) satisfied along with the transversality condition $\mathrm{Re}\left(\dfrac{d}{d\eta}\left[x(\eta)\right]\Big|_{\eta=\eta_H^{(2)}}\right) \neq 0$ [156], where x is the root of characteristic equation (3.2.1) and $\mathrm{Re}(\cdot)$ denotes the real part of a complex number. Now differentiating equation (3.2.1) with respect to η, we have:

$$4x^3\frac{dx}{d\eta} + x^3\frac{dA_*}{d\eta} + 3A_*x^2\frac{dx}{d\eta} + x^2\frac{dB_*}{d\eta} + 2B_*x\frac{dx}{d\eta} + x\frac{dC_*}{d\eta} + C_*\frac{dx}{d\eta} + \frac{dD_*}{d\eta} = 0$$

Therefore,

$$\frac{dx}{d\eta} = -\frac{x^3\dfrac{dA_*}{d\eta} + x^2\dfrac{dB_*}{d\eta} + x\dfrac{dC_*}{d\eta} + \dfrac{dD_*}{d\eta}}{4x^3 + 3A_*x^2 + 2B_*x + C_*}$$

Since x is purely imaginary at $\eta = \eta_H^{(2)}$ (say $x = \pm i\omega$), we get:

$$\mathrm{Re}\left(\frac{d}{d\eta}\left[x(\eta)\right]\Big|_{\{x=\pm i\omega,\eta=\eta_H^{(2)}\}}\right) = \frac{\left(\frac{dD_*}{d\eta} - \omega^2\frac{dB_*}{d\eta}\right)(C_* - 3\omega^2 A_*) + \left(\omega\frac{dC_*}{d\eta} - \omega^3\frac{dA_*}{d\eta}\right)(2\omega B_* - 4\omega^3)}{(C_* - 3\omega^2 A_*)^2 + (2\omega B_* - 4\omega^3)^2} \tag{3.2.7}$$

where A_*, B_*, C_* and D_* are as defined in previous section. In order to satisfy the transversality condition, the numerator (say $N(\eta)$) must be non-zero at $\eta = \eta_H^{(2)}$. It is extremely difficult to simplify this expression furthermore, therefore we choose a set of parameter values and then investigate the existence of the Hopf-bifurcation numerically. This analysis has been done in the next section. □

3.3 Epidemiological Parameter Values

For simulation purposes, we adopt the same parameter values as in Chapter 2 for all common parameters, namely $\lambda, \alpha, \beta, \mu_S, \mu_R$, and μ. To estimate the parameter γ, representing the treatment initiation rate for drug-sensitive infected individuals, we account for the total time between infection and the start of appropriate treatment. This period includes both the time to diagnosis after infection and the time from diagnosis to treatment initiation. A recent systematic review and meta-analysis study of high- and upper-middle-income countries estimated that people live with undiagnosed HIV infection for an average of 3 years before receiving a diagnosis [157]. However, despite improved HIV testing facilities, the average time from infection to diagnosis can still range widely, from 0.69 to 10.15 years, depending on different interacting groups and regional factors [158–160]. Further, for the expected time taken to initiate appropriate treatment after the diagnosis of infection, a systematic review and meta-analysis suggest that it can vary from 5 to 40 days, influenced by factors such as age and gender of patient, and the economic conditions of the country [161]. Another study indicates a broader range, from 20 to 108 days [162]. Therefore, we consider the treatment initiation rate γ to be ranging from 0.25 to 2 year^{-1}.

The transmission rate ρ quantifies the average time taken in emergence of drug-resistance in an infected individual who is under treatment and does not adhere the treatment optimally. In a study, it has been shown that a small proportion of patients have developed resistance within 6 months after initiation of the treatment for HIV [163]. We assume that the resistance can develop in a non-adherent patient anywhere from 6 months to 2 years after starting the treatment. Therefore, the parameter ρ varies between 0.5 to 2 per year depending on the sub-optimality level to the treatment. Further, we have seen that due to the enhanced accessibility to medical facilities, around 73% of individuals living with HIV had started ART by the end of 2020 [164]. Therefore, we assume $\eta = 0.7$ for most of the numerical

simulations carried out. Also, we assume that 75% of the population in the treatment class follows the prescribed treatment properly. We will vary parameters in the provided range to simulate different possible scenarios. For each of the parameters, the unit, estimated value and range of variation has been included in Table 3.3.

Parameter	Unit	Baseline Value	Range of Variation
λ	million year^{-1}	25.31	fixed
α	million^{-1} year^{-1}	47.134×10^{-6}	$[2.5 \times 10^{-5},\ 3 \times 10^{-4}]$
β	million^{-1} year^{-1}	assumed	$[1 \times 10^{-5},\ 7 \times 10^{-5}]$
α	year^{-1}	1	$[0.25,\ 2]$
ρ	year^{-1}	1	$[0.5,\ 2]$
μ	year^{-1}	0.007	$[0.004,\ 0.007]$
μ_S	year^{-1}	0.0909	fixed
μ_R	year^{-1}	assumed	$[0.06,\ 0.2]$
η	unitless	0.7	$[0,\ 1]$
ϵ	unitless	0.75	$[0,\ 1]$

Table 3.3: Units and values (estimate and range) of various parameters.

3.4 Numerical Simulation

In this section, we validate the analytical results on the existence and stability of equilibria, as well as bifurcations, through several numerical illustrations. For that, we fix $\lambda = 25.31, \gamma = 1, \rho = 1, \mu_S = 0.0909, \epsilon = 0.75, \eta = 0.7$ and vary other parameters to illustrate all the possible existence and stability scenarios for the system (3.1.1). We choose the initial population as 625 million for susceptible, 2.2 million for drug-sensitive infected, 1.5 million for under treatment and 1 million (assumption) for drug-resistant infected individuals, $ic_1 = (625, 2.2, 1.5, 1)$, which is based on the number of individuals in different classes in the base year as discussed in Chapter 2. We also choose two other initial conditions to validate the global stability results: $ic_2 = (300, 30, 20, 20)$ and $ic_3 = (1000, 80, 50, 100)$.

We consider $\alpha = 0.000047, \beta = 0.000015, \mu = 0.007$ and $\mu_R = 0.06$ and get the corresponding basic reproduction numbers as $\bar{R}_0^{(S)} = 0.23\ (< 1)$ and $\bar{R}_0^{(R)} = 0.81\ (< 1)$. The dynamics for these parameter values is represented in Figure 3.3a. Clearly, the compartment of infected and under treatment individuals become empty at a very early stage, while the susceptible population increase continuously and eventually reach to its highest level $\lambda/\mu\ (= 3615.7)$. The phase portraits in the Figure 3.4a and 3.4b confirms the global stability of disease free equilibrium point $E_0^{(2)}$. Next, we choose $\alpha = 0.0003, \beta = 0.00003, \mu = 0.007$ and $\mu_R = 0.06$ to illustrate the case when $R_0^{(R)}(= 1.62) > 1$ and $R_0^{(SR)}(= 0.91) < 1$. In

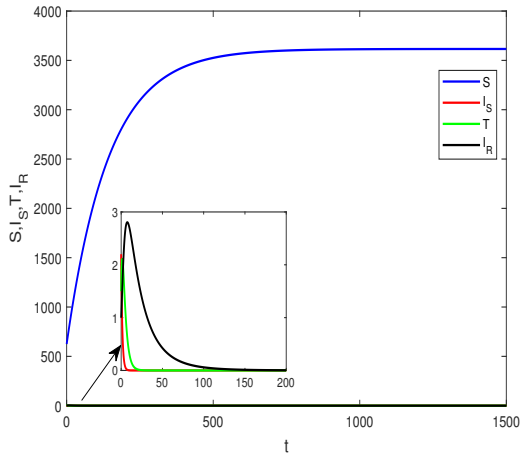

(a) $\alpha = 0.000047, \beta = 0.000015, \mu = 0.007, \mu_R = 0.06$

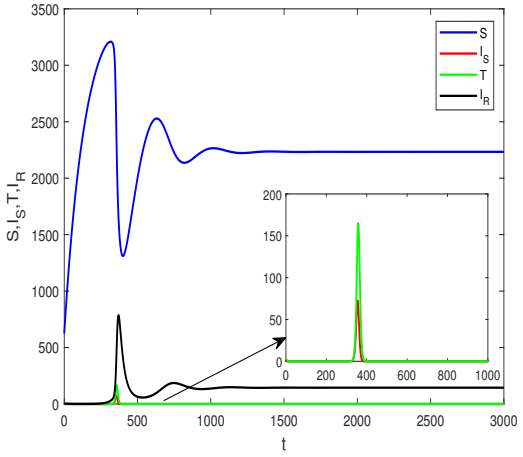

(b) $\alpha = 0.0003, \beta = 0.00003, \mu = 0.007, \mu_R = 0.06$

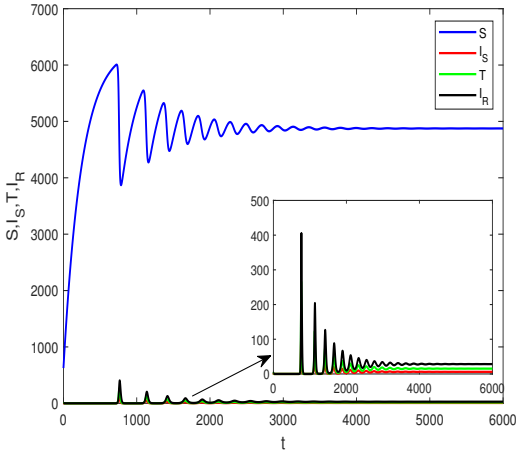

(c) $\alpha = 0.00015, \beta = 0.00001, \mu = 0.004, \mu_R = 0.18$

Figure 3.3: Time series plot for each population of the model system (3.1.1) with other parameter values as $\lambda = 25.31, \gamma = 1, \rho = 1, \mu_S = 0.0909, \epsilon = 0.75, \eta = 0.7$ and initial condition $[625, 2.2, 1.5, 1]$.

this case, the drug-resistant mutant dominant equilibrium point behaves like a sink and only the susceptible and drug-resistant infected populations are able to survive for long run. The dynamics for this case is illustrated in Figure 3.3b and the global stability of $E_1^{(2)}(2233.33, 0, 0, 144.43)$ is shown in Figure 3.4c and 3.4d. Note that the drug-sensitive infected population is wiped out from the system after some time, although it has basic reproduction number greater than one. This happens since the drug-resistant infected population has a higher basic reproduction number than drug-sensitive infected population. In other words we can say that the transmission rate of drug-sensitive infected population is not enough for its survival. Finally, we choose $\alpha = 0.00015, \beta = 0.00001, \mu = 0.004$ and $\mu_R = 0.18$. This set of parameter values results in $\bar{R}_0^{(S)}(= 1.29) > 1$, $\bar{R}_0^{(SR)}(= 3.77) > 1$ and $A_*B_*C_* - A_*^2D_* - C_*^2(= 2.02 \times 10^{-6}) > 0$. Figure 3.3c represents the long time dynamics of the model (3.1.1) and suggests that each population converges to the interior equilibrium point $E_*^{(2)}(4875.13, 6.06, 15.32, 28.32)$ after some initial oscillations. Further, the phase portraits in Figure 3.4e and 3.4f show that the phase point converges to the interior equilibrium point for various initial conditions. It also indicates that the equilibrium point $E_*^{(2)}$ is an attractor for a large region around it.

We observe similar transcritical bifurcation patterns for system (3.1.1) with respect to the bifurcation parameter β as in system (2.1.1) of Chapter 2, under the same parameter values, where the disease-free equilibrium $E_0^{(2)}$ exchanges stability with the axial equilibrium $E_1^{(2)}$. These numerical results support Theorem 3.2.5.

For the set of parameter values: $\lambda = 25.31, \alpha = 0.00025, \beta = 0.000025, \gamma = 1, \rho = 1, \mu = 0.005, \mu_S = 0.0909, \mu_R = 0.08, \eta = 0.37$ and $\epsilon = 0.75$, we observe that condition $A_*B_*C_* - A_*^2D_* - C_*^2 > 0$ is not satisfied. Therefore, the interior equilibrium point $E_*^{(2)}$ of model system (3.1.1) is not locally asymptotically stable for this set of parameter values. Our numerical simulation shows that the solution curves of this system admits periodic behaviour and converge to a stable limit cycle. The time series plot of each population for the above set of parameter values is shown in Figure 3.5a, which assures the existence of the periodic nature of the solutions and predicts that the interior equilibrium point $E_*^{(2)}$ is unstable. In Figure 3.5b, solutions starting from different initial values are converging to a stable limit cycle.

Considering η as a bifurcation parameter, we note that the solutions of equation $A_*B_*C_* - A_*^2D_* - C_*^2 = 0$ for η are $\eta_{H1}^{(2)} = 0.3422$ and $\eta_{H2}^{(2)} = 0.8191$, which lies in the interval $[0, 1]$. The set of eigenvalues for these values corresponding to Jacobian matrices $J_2(E_*^{(2)})\big|_{\eta=\eta_{H1}^{(2)}}$ and $J_2(E_*^{(2)})\big|_{\eta=\eta_{H2}^{(2)}}$ are $(-0.2765, -0.0611, 2.2551 \times 10^{-17} \pm 0.0559i)$ and $(-0.2777, -0.0085, -2.7322 \times 10^{-17} \pm 0.0154)$, respectively. These sets consist only either negative real or

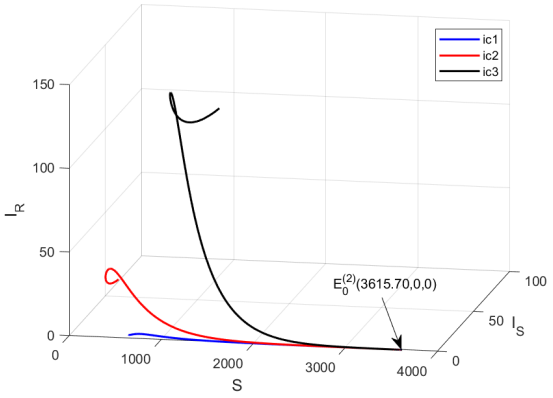

(a) $\alpha = 0.000047, \beta = 0.000015, \mu = 0.007, \mu_R = 0.06$

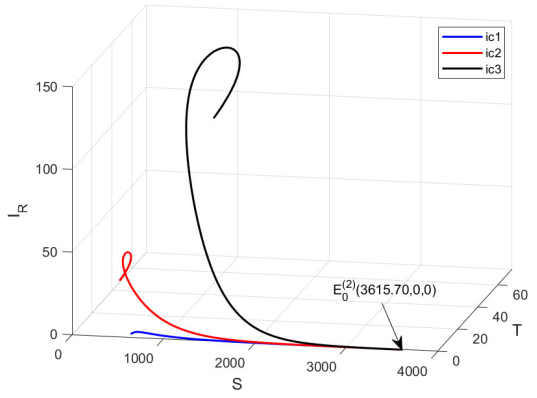

(b) $\alpha = 0.000047, \beta = 0.000015, \mu = 0.007, \mu_R = 0.06$

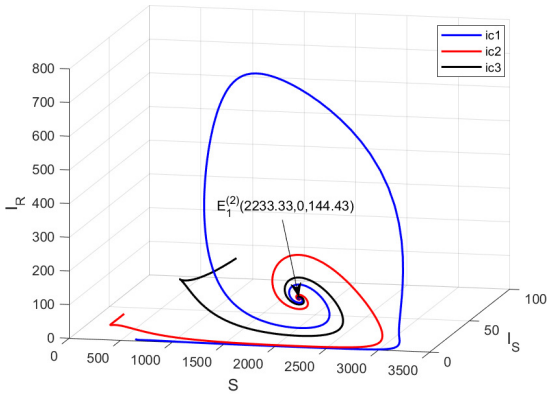

(c) $\alpha = 0.0003, \beta = 0.00003, \mu = 0.007, \mu_R = 0.06$

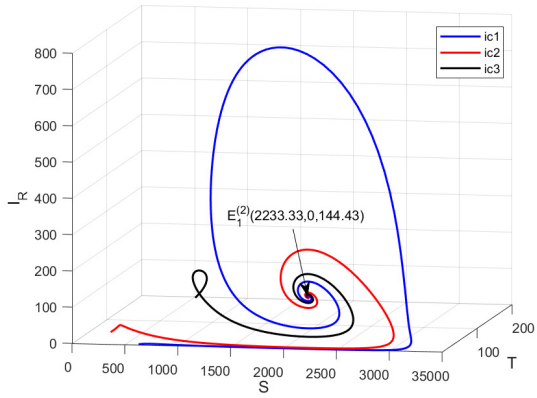

(d) $\alpha = 0.0003, \beta = 0.00003, \mu = 0.007, \mu_R = 0.06$

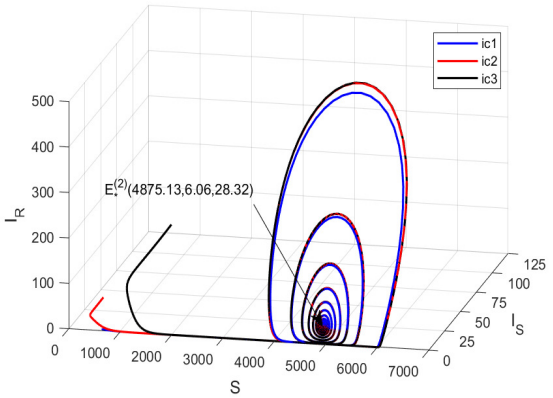

(e) $\alpha = 0.00015, \beta = 0.00001, \mu = 0.004, \mu_R = 0.18$

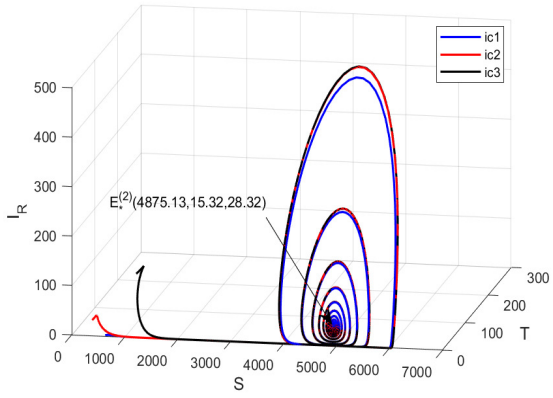

(f) $\alpha = 0.00015, \beta = 0.00001, \mu = 0.004, \mu_R = 0.18$

Figure 3.4: Phase portrait for model (3.1.1) with various initial conditions assuring the global stability of existing equilibrium points (except $E_*^{(2)}$). Other parameter values are $\lambda = 25.31, \gamma = 1, \rho = 1, \mu_S = 0.0909, \epsilon = 0.75, \eta = 0.7$.

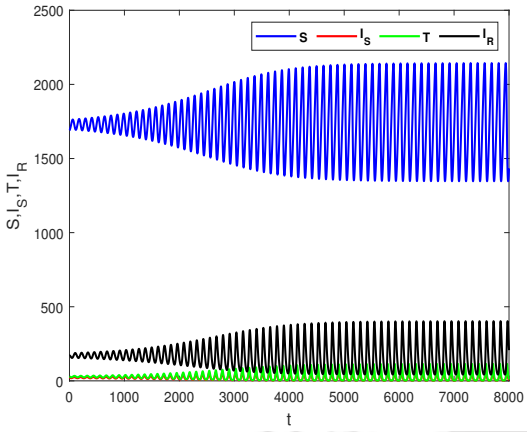

(a) Initial condition: $(1690, 22, 30, 170)$.

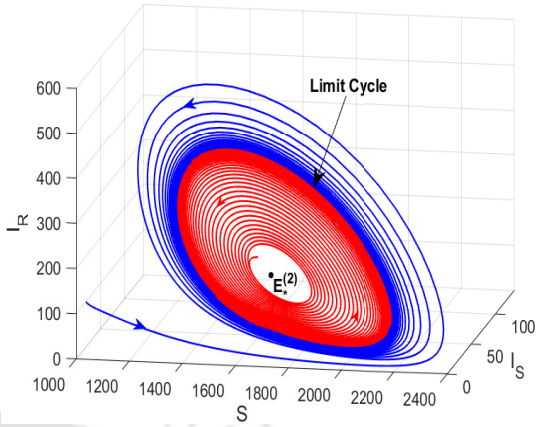

(b) Initial condition (for red): $(1630, 30, 40, 200)$, Initial condition (for blue): $(1000, 20, 25, 100)$.

Figure 3.5: (a). Time series plot for each population of the model system (3.1.1) showing periodic nature of solutions. (b). Phase portrait for the model system (3.1.1) with two different initial conditions assuring the existance of a stable limit cycle for the parameter values: $\lambda = 25.31, \alpha = 0.00025, \beta = 0.000025, \gamma = 1, \rho = 1, \mu = 0.005, \mu_S = 0.0909, \mu_R = 0.08, \eta = 0.37$ and $\epsilon = 0.75$.

almost pure imaginary eigenvalues. Further, we have $N\left(\eta_{H1}^{(2)}\right) = -2.18682 \times 10^{-7} \neq 0$ and $N\left(\eta_{H2}^{(2)}\right) = 5.4698 \times 10^{-9} \neq 0$, which is in agreement with the transversality condition (3.2.7). Here $N(\eta)$ is as discussed in Theorem 3.2.6. So, the equilibrium point $E_*^{(2)}$ changes its stability through Hopf-bifurcations at bifurcation points $\eta_{H1}^{(2)} = 0.3422$ and $\eta_{H2}^{(2)} = 0.8191$. Figure 3.6 and Figure 3.7 confirm the occurrence of Hopf-bifurcation at points $\eta_{H1}^{(2)}$ and $\eta_{H2}^{(2)}$. In Figure 3.6, the curves before the bifurcation point $\eta_{H1}^{(2)}$ and after the bifurcation point $\eta_{H2}^{(2)}$ show the population levels for different values of the parameter η. The limit cycles occur between these two bifurcation points and the red coloured dots represent the lowest population level, while the blue coloured dots represent the highest population level, at a specific value of the parameter η.

In addition, Figure 3.7 shows the periodic nature of solutions of system (3.1.1) for different values of parameter η. We can conclude from Figure 3.5b, Figure 3.7 and stability of coexistence equilibrium point $E_*^{(2)}$ that solutions of model system (3.1.1) achieve steady state at $E_*^{(2)}$ for $\eta < \eta_{H1}^{(2)}$ and $\eta > \eta_{H2}^{(2)}$ while converge to a stable limit cycle for $\eta \in [\eta_{H1}^{(2)}, \eta_{H2}^{(2)}]$. This confirms that Hopf-bifurcation is supercritical in nature.

Further, we have plotted density plots for each population on the $\epsilon\eta-$plane to know the best possible scenario to minimize the infected populations and maximize the under treatment population. We used parameter values: $\lambda = 25.31, \alpha = 0.0003, \beta = 0.00007, \gamma =$

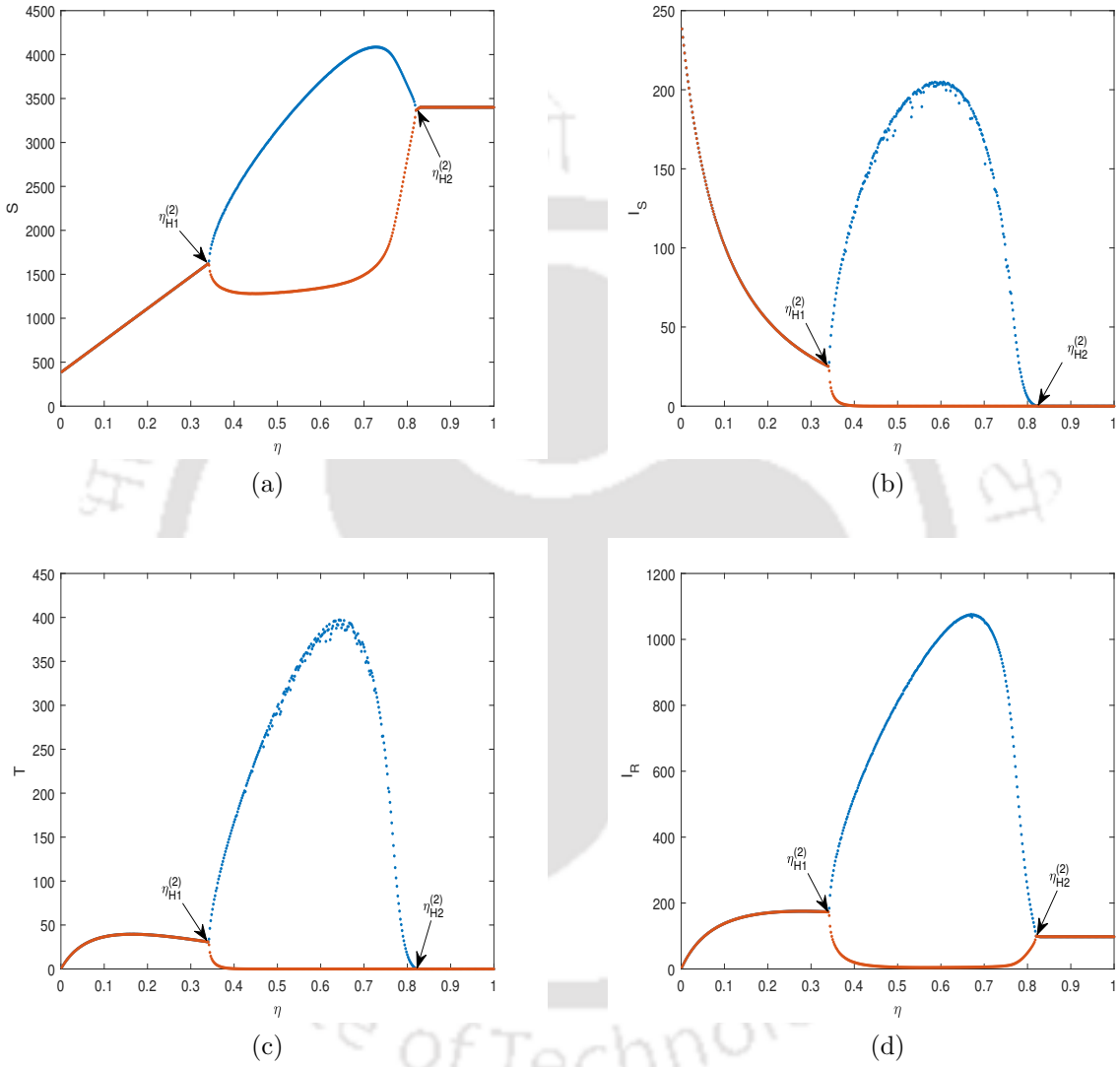

Figure 3.6: The bifurcation diagram of each population of the model system (3.1.1) with respect to the Hopf-bifurcation parameter η. The other parameters are $\lambda = 25.31, \alpha = 0.00025, \beta = 0.000025, \gamma = 1, \rho = 1, \mu = 0.005, \mu_S = 0.0909, \mu_R = 0.08, \epsilon = 0.75$.

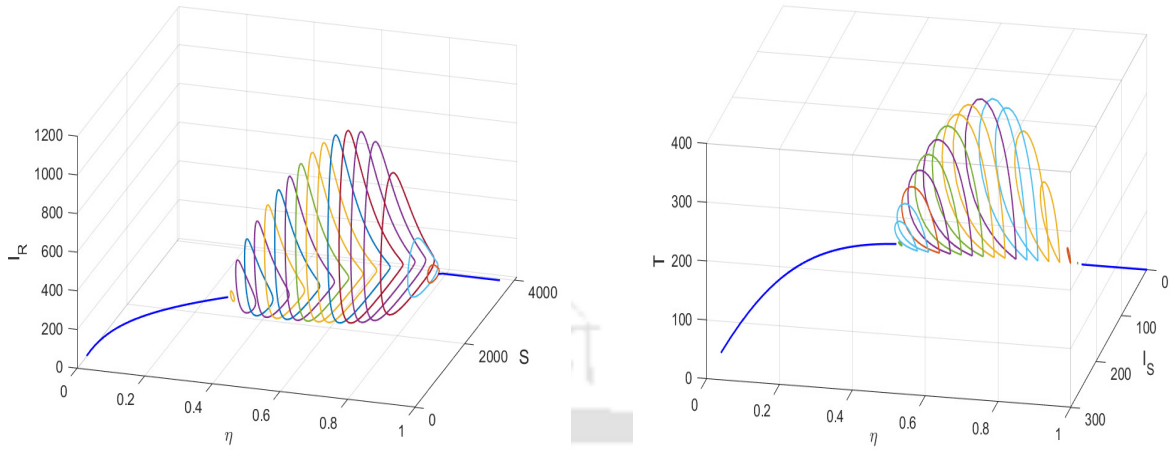

(a) (b)

Figure 3.7: The existence of limit cycle for the model system (3.1.1) corresponding to variation in Hopf-bifurcation parameter η. The other parameters are $\lambda = 25.31, \alpha = 0.00025, \beta = 0.000025, \gamma = 1, \rho = 1, \mu = 0.005, \mu_S = 0.0909, \mu_R = 0.08, \epsilon = 0.75$.

$1, \rho = 1, \mu = 0.007, \mu_S = 0.0909, \mu_R = 0.2$ for these density plots. Figure 3.8a suggests that lower treatment rate will minimize the susceptible population. This happens because lower treatment levels lead to a major increase in total infected population which we can observe in Figure 3.8b. It is observed from Figure 3.8c and Figure 3.8d that perfect adherence with medium treatment rate is an optimal scenario for maximizing the population under treatment. On the other hand, Figure 3.8e depicts that a medium treatment rate with imperfect adherence lead to a greater risk of emergence of drug resistance, while extremely low or high treatment rate minimizes this risk. In addition, a perfect drug adherence can also hold the drug-resistant infected population at lower levels.

3.5 Conclusion

In this chapter, we formulated a mathematical model to understand the dynamics of HIV spread under treatment in presence of drug-sensitive and drug-resistant infected population. We considered that the drug resistance transmits from drug-resistant infected population to susceptible via direct contact. Also, drug resistance can develop through improper drug adherence. We calculated the basic reproduction number for drug-sensitive $\bar{R}_0^{(S)}$ and drug-resistant $\bar{R}_0^{(R)}$ strains for treatment model to analyze it. We analyzed all existing equilibrium points and their stability. The treatment model also shows three different possible scenarios for infected population:

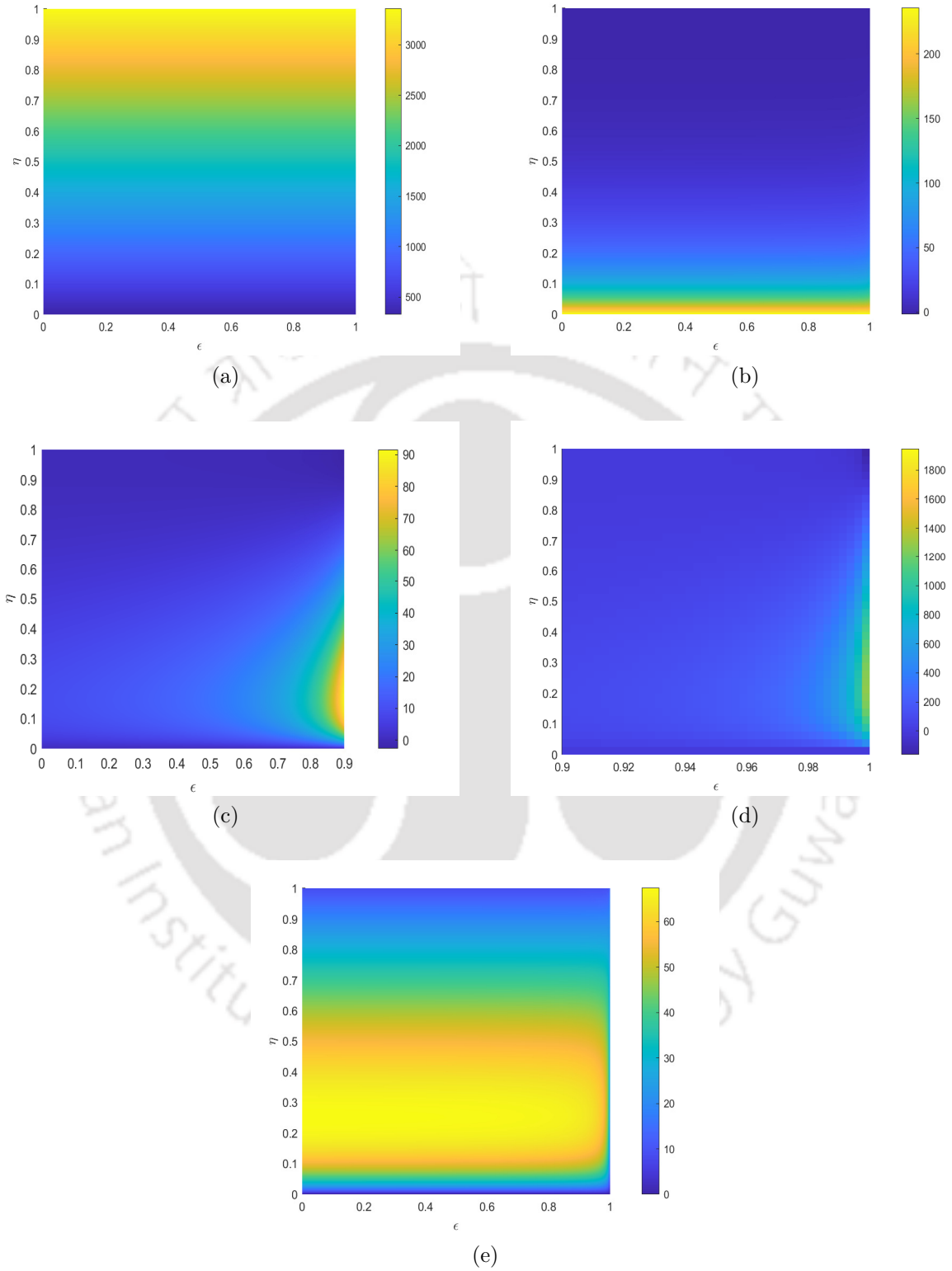

Figure 3.8: Density Plot for $(a)S,\ (b)I_S,\ (c)T,\ (d)T$ and $(e)I_R$ on $\epsilon\eta-$plane. The other parameters are $\lambda = 25.31, \alpha = 0.0003, \beta = 0.00007, \gamma = 1, \rho = 1, \mu = 0.007, \mu_S = 0.0909, \mu_R = 0.2$.

(A) Both type of infected population dies out when $\bar{R}_0^{(S)} < 1$ and $\bar{R}_0^{(R)} < 1$.

(B) Only drug-resistant infected population survives when $\bar{R}_0^{(R)} > 1$ and $\bar{R}_0^{(SR)} < 1$.

(C) drug-sensitive and drug-resistant infected population co-exist when $\bar{R}_0^{(S)} > 1$ and $\bar{R}_0^{(SR)} > 1$.

From this, we can conclude that the system becomes disease free at lower reproductive capacities of both the strains. At the same time, a higher basic reproduction number is not enough for the survival of the drug-sensitive infected population, since the drug-resistant infected population out-competes the former, if $\bar{R}_0^{(SR)} < 1$. This could be a result of high transmission rate or low disease induced death rate of drug-resistant infected class and a higher number of infected individuals in treatment class. These results are consistent with observations in a prior two-strain disease model [100]. We also found that the population in the drug-resistant infected class faces survival risk only at their lower reproductive capacity, in absence of drug-sensitive infected population. We observed that the drug resistance infected population remains in the system, even at its lower reproductive capacity, if the number of individuals in drug-sensitive infected and treatment class are at a positive level. This shows that a better treatment availability is responsible for the emergence of drug resistance. Therefore, one could question the sustainability of the treatment of the drug-sensitive infected population at the expense of an increment in the drug-resistant individuals in the community [165]. However, during the initial phase, such resistant strains have low fitness levels and are less transmissible than their drug-susceptible counterparts [166]. So an early awareness campaign in non-adherent patients may reduce the risk of emergence of the drug-resistant strain. From the existence condition of the interior equilibrium point, we conclude that the co-existence of both the infected populations, under better treatment availability, demands a high transmission rate in drug-sensitive infected population compare to the other one.

Finally, we have performed an extensive analysis of possible bifurcations for treatment model. We found that the system undergoes a transcritical bifurcation at a critical transmission rate of drug-resistant infected population. The system remains at disease-free state if the transmission rate remains below this threshold value, without which the system goes to the only drug-resistant strain endemic equilibrium point. A lower disease induced death rate of drug-resistant infected population also contributes in this transformation from disease-free to endemic state of the system. We also found that the co-existence endemic equilibrium point changes its stability through Hopf-bifurcation at a critical value of parameter η and the system shows periodic behaviour. Numerical simulation suggests that all solutions converge

to a stable limit cycle for a range of parameter values of η. Extremely low or high treatment availability makes the co-existence endemic equilibrium point stable. On the other hand, a large range of medium treatment availability forces the system to show a periodic behaviour, eventually approaching to a limit cycle. In this case, it is extremely difficult for policy makers to reach any concluding strategy to control the spread of the disease if the ratio of number of individuals in each class changes continuously. Therefore, a medium range of treatment availability is not an efficient way to control the disease. We also observed that both basic reproduction numbers are independent of the proportion of population which properly adheres to the treatment, but the stability condition of co-existence endemic equilibrium point depends on it. Sharomi et al. [98] concluded that the widespread use of ART could significantly reduce the disease burden, despite the risk of the development and transmission of drug-resistant strain. But, our study suggests that the drug-adherence to the treatment also plays a vital role in determining the dynamics and is responsible for periodic behavior. The density plot for treatment model shows that a medium level of treatment availability with sub-optimal drug adherence is suitable template for emergence of the drug resistance. This result can be a stepping stone for public health debates [165] regarding the potential benefits and dangers of providing ART to the infected population at risk for the emergence of drug-resistance in patients.

In summary, these results show that when treatment is provided to the infected population, the drug-sensitive infected population either face competitive exclusion or co-exist with drug-resistant infected population. The number of infected patients under treatment and patients who follow the treatment properly are the main determining factors of the dynamics of disease spread. Also, a higher transmission rate of drug-sensitive strain with enough treatment availability and its improper adherence ultimately supports the growth of the drug-resistant infected population. Our analysis shows that policy makers should focus on providing better conditions to the patients to adhere their treatment properly. Otherwise, a higher treatment availability with sub-optimal drug adherence could lead us to a danger of increased number of drug-resistant infected population, or an endemic of drug-resistant infection in the worst of conditions.

Chapter 4

Multi-Strain HIV Dynamics With AIDS Class

HIV is a chronic disease which persists for a long time. In the absence of ART, chronic HIV infection typically advances into AIDS over a period of 10 years or more. Although ART can slow down this progression, it cannot completely eliminate the infection. In this chapter, we introduce a new compartment representing HIV-infected individuals diagnosed with AIDS, thereby capturing the transmission dynamics of HIV/AIDS more precisely. Unlike previous model, we do not include a separate compartment for treated individuals, allowing us to investigate novel aspects of HIV transmission dynamics within a reduced-complexity framework. The chapter thus presents a new two-strain non-linear mathematical model designed to assess the impact of treatment availability and adherence on the spread of HIV in a community. First, we establish the well-posedness of the proposed model in an epidemiological context. The basic reproduction number for both the strains are determined by the next-generation matrix approach. The local and global analysis of existent equilibrium points using stability and bifurcation theory suggests that the drug-sensitive infected population faces competitive exclusion at lower relative transmission rates of this strain. For higher relative transmission rates of the infection, both infected populations co-exist for a long time. The system exhibits transcritical bifurcation and Hopf-bifurcation at multiple points with respect to various model parameters. Finally, we validate all the analytical results with an extensive numerical analysis. In summary, this chapter provides various conditions for applying different strategies to control the overall disease burden from the system.

4.1 Formulation of the Mathematical Model

To construct a mathematical model for HIV/AIDS transmission, we categorized the whole sexually active population into four mutually exclusive classes based on their disease sta-

tus, namely, susceptible individuals (S), infected individuals with the drug-sensitive strain (I_S), infected individuals with the drug-resistant strain (I_R), and infected individuals who have been diagnosed with AIDS (A). The individuals in each group are homogeneously distributed. We assume that the susceptibility to HIV infection is solely attributed to sexual exposure. The susceptible population increases at a constant rate λ as new individuals continuously join the sexually active group. The incidence rate or force of infection, expressed as a function of both the susceptible and infected individuals, plays a pivotal role in epidemiological modelling. The basic expression for the incidence rate can be derived from the principle of mass action. As a result, the infection is assumed to spread at a rate described by αSI, where α represents the per capita contact rate. In our model, we assume that α_S and α_R are the per capita contact rates for drug-sensitive and drug-resistant infected individuals with susceptible population, respectively, where a contact results in the transmission of the same strain to newly infected individuals. We neglected the exchange of drug sensitivity due to any effective contact between these two infected populations as the drug resistance primarily arises from treatment failure rather than transmission [97]. Further, we assume that a fraction (η) of whole drug-sensitive infected population access the treatment for HIV due to limited medical infrastructure and other restrictions. The infection in untreated population develops to its final stage in a mean time $\frac{1}{\beta_S}$ and consequently, drug-sensitive individuals move to the AIDS class with rate β_S. We do not consider a separate compartment for the individuals undergoing treatment, since we assume that ART does not result in a substantial reduction in the transmission of the infection. As some patients are unable to follow the treatment properly and develop the drug-resistant strain, we assume that only a proportion ϵ of the whole population receiving treatment follow it properly, and the rest will develop the drug resistance with the rate ρ. We assume that the given class of drugs are completely ineffective on the drug-resistant infected population, and they develop their disease status to the AIDS after a certain time at the rate β_R. The adherent population under treatment moves to the AIDS class with the rate γ. The natural death rate for individuals in each class is μ. As treatment cannot prevent the progression to the AIDS stage, infected individuals must reach the final stage of the infection before dying from the disease, unless they die naturally beforehand. Therefore, we assume that infected individuals die due to infection only if they are diagnosed with AIDS and consider the disease-induced death rate to be μ_d. The schematic illustration of the population flow among these compartments is presented in Figure 4.1.

The deterministic system of coupled non-linear ordinary differential equations which rep-

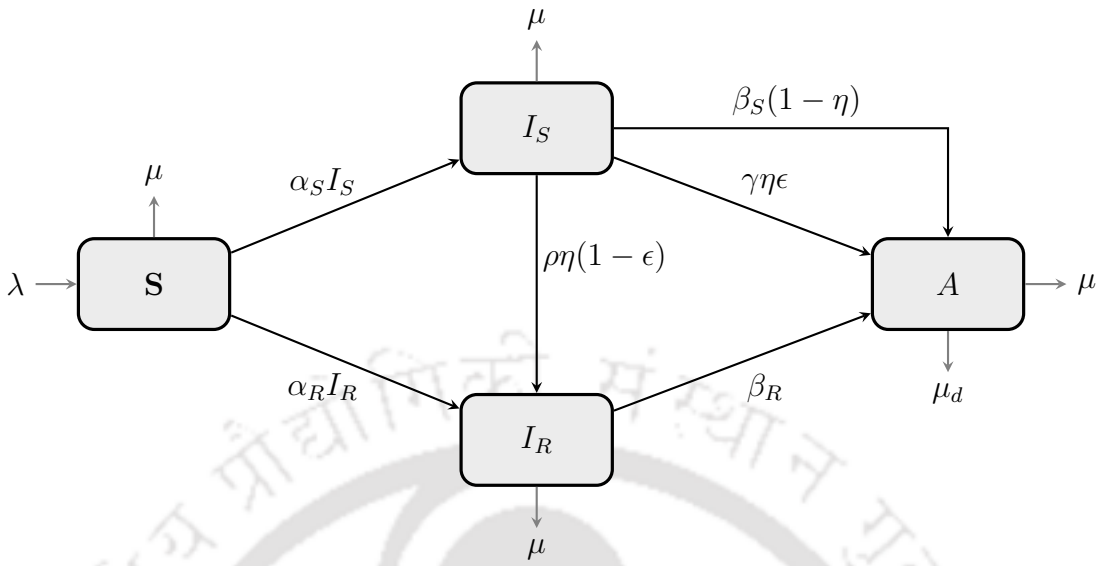

Figure 4.1: Flow diagram of the model (4.1.1).

resents the model is given by

$$\begin{aligned}
S' &= \lambda - \alpha_S I_S S - \alpha_R I_R S - \mu S,\\
I_S' &= \alpha_S I_S S - \rho\eta(1-\epsilon) I_S - \gamma\eta\epsilon I_S - \beta_S(1-\eta) I_S - \mu I_S,\\
I_R' &= \alpha_R I_R S + \rho\eta(1-\epsilon) I_S - \beta_R I_R - \mu I_R,\\
A' &= \gamma\eta\epsilon I_S + \beta_S(1-\eta) I_S + \beta_R I_R - \mu_d A - \mu A,
\end{aligned} \tag{4.1.1}$$

with the initial condition $(S(0), I_S(0), I_R(0), A(0))$ belonging to the region $\mathcal{R}$ defined as,

$$\mathcal{R} = \left\{ (S, I_S, I_R, A) \in \mathbb{R}^4_+ : 0 \leq S + I_S + I_R + A \leq \frac{\lambda}{\mu} \right\},$$

where $\mathbb{R}^4_+$ refers to the non-negative cone along with its lower-dimensional faces. The biological meaning of the parameters used in the system (4.1.1) is provided in Table 4.1.

4.2 Mathematical Analysis of the Model

In this section, we first establish the biological well-posedness of the system (4.1.1) by proving the uniqueness, non-negativity, and boundedness of its solutions. We then identify the equilibrium points and study their local and global stability to understand the long-term behaviour of the system. Finally, we carry out a theoretical investigation of potential bifurcations to capture threshold-driven changes in system dynamics.

Parameter	Biological Description
λ	Rate of recruitment of susceptible population
α_S	Rate of infection per effective contact between susceptible population and drug-sensitive infected population
α_R	Rate of infection per effective contact between susceptible population and drug-resistant infected population
μ	Natural death rate of population
η	Proportion of HIV infected population which is receiving treatment
ϵ	Proportion of under treatment population which is adherent
ρ	Rate of emergence of drug resistance in non-adherent population
β_S	Conversion rate from drug-sensitive infected population to AIDS population
β_R	Conversion rate from drug-resistant infected population to AIDS population
γ	Conversion rate of untreated drug-sensitive infected population to AIDS population
μ_d	Disease induced death rate

Table 4.1: Parameter description of the system (4.1.1).

4.2.1 Uniqueness, non-negativity and boundedness of the solutions

The right-hand side of the system (4.1.1) is continuous and Lipschitz on $[0, a]$, $a > 0$. Therefore, the system (4.1.1) with the initial condition $(S(0), I_S(0), T(0), I_R(0)) \in \mathbb{R}^4_+$ has a unique solution.

Further, we state the following theorem ensuring the biological well-posedness of the proposed model (4.1.1).

Theorem 4.2.1. *The biologically feasible region for the solutions, defined as $\mathcal{R}$, is a positively invariant set for the system (4.1.1). In other words, the solution $(S(t), I_S(t), I_R(t), A(t))$ of the system (4.1.1) starting from any initial condition $(S(0), I_S(0), I_R(0), A(0)) \in \mathcal{R}$, will remain in the region $\mathcal{R}$ for all $t > 0$.*

Proof. We rewrite the system (4.1.1) in the vector notation as,

$$\frac{dy(t)}{dt} = p(y(t)), \tag{4.2.1}$$

where $y(t) = (S(t), I_S(t), I_R(t), A(t))$ and $p(y(t)) = (p_1(y(t)), p_2(y(t)), p_3(y(t)), p_4(y(t)))$ is defined according to (4.1.1). We know that a compact set Γ is invariant for the system

$\frac{dy(t)}{dt} = p(y(t))$ if at each point x on the boundary $\partial\Gamma$ (of Γ), the vector $p(x)$ is either a tangent or pointing inwardly to the set [167].

Let us consider $(S(0), I_S(0), I_R(0), A(0)) \in \mathcal{R}$. Further, we break the whole boundary $\partial\mathcal{R}$ into 5 separate hyperplanes. These hyperplanes and their corresponding outer normal vectors are as follows:

$\partial\mathcal{R}_1 = \{(S, I_S, I_R, A) \in \mathcal{R} : S = 0\}$ and $\eta_1 = (-1, 0, 0, 0)$,
$\partial\mathcal{R}_2 = \{(S, I_S, I_R, A) \in \mathcal{R} : I_S = 0\}$ and $\eta_2 = (0, -1, 0, 0)$,
$\partial\mathcal{R}_3 = \{(S, I_S, I_R, A) \in \mathcal{R} : I_R = 0\}$ and $\eta_3 = (0, 0, -1, 0)$,
$\partial\mathcal{R}_4 = \{(S, I_S, I_R, A) \in \mathcal{R} : A = 0\}$ and $\eta_4 = (0, 0, 0, -1)$,
$\partial\mathcal{R}_5 = \left\{(S, I_S, I_R, A) \in \mathcal{R} : S + I_S + I_R + A = \frac{\lambda}{\mu}\right\}$ and $\eta_5 = \frac{1}{2}(1, 1, 1, 1)$.

Now, we consider a point $x \in \partial\mathcal{R}$, and obtain following cases:

Case 1: When $S = 0$, we have $\langle p(x), \eta_1\rangle = -\lambda < 0$. Therefore, $S(t) \geq 0, \forall\ t \geq 0$.

Case 2: When $I_S = 0$, we have $\langle p(x), \eta_2\rangle = 0$. Therefore, $I_S(t) \geq 0, \forall\ t \geq 0$.

Case 3: When $I_R = 0$, since $I_S \geq 0$, we have $\langle p(x), \eta_3\rangle = -\rho\eta(1-\epsilon)I_S \leq 0$. Therefore, $I_R(t) \geq 0, \forall\ t \geq 0$.

Case 4: When $A = 0$, since $I_S \geq 0, I_R \geq 0$, we have $\langle p(x), \eta_4\rangle = -\gamma\eta\epsilon I_S - \beta_S(1-\eta)I_S - \beta_R I_R \leq 0$. Therefore, $A(t) \geq 0, \forall\ t \geq 0$.

Case 5: When $S + I_S + I_R + A = \frac{\lambda}{\mu}$, since $A \geq 0$, we have

$$\langle p(x), \eta_5\rangle = \frac{1}{2}(\lambda - \mu(S + I_S + I_R + A) - \mu_d A) = -\frac{1}{2}(\mu_d A) \leq 0.$$

Therefore, $(S(t), I_S(t), I_R(t), A(t)) \leq \frac{\lambda}{\mu}, \forall\ t \geq 0$.

Thus, $\mathcal{R}$ is a positively invariant set for the system (4.1.1). □

Remark 4.2.2. *In the proof of Theorem 4.2.1, cases 1 to 4 confirm the positivity, while case 5 confirms the boundedness of the solutions of the system (4.1.1). Thus, the system (4.1.1) is biologically well posed.*

4.2.2 Equilibrium points and their stability properties

The equilibrium points are the intersection points of zero growth isoclines for each population of the system. Here, first three equations of the system (4.1.1) are independent of the AIDS

class (A). Therefore, we study the reduced system,

$$\begin{aligned}
\frac{dS}{dt} &= \lambda - \alpha_S I_S S - \alpha_R I_R S - \mu S; \\
\frac{dI_S}{dt} &= \alpha_S I_S S - a I_S; \\
\frac{dI_R}{dt} &= \alpha_R I_R S + \rho\eta(1-\epsilon) I_S - b I_R,
\end{aligned} \tag{4.2.2}$$

where $a = \rho\eta(1-\epsilon) + \gamma\eta\epsilon + \beta_S(1-\eta) + \mu$ and $b = \beta_R + \mu$.

Disease elimination

In this subsection, we discuss the conditions under which disease will get eliminated from the system. First, we derive the value of the basic reproduction number, which represents the expected number of secondary cases generated by one infected individual within a population entirely susceptible to the disease. We use the basic reproduction number to determine the local and global stability properties of the existing equilibrium points of the system (4.2.2).

When the system lacks HIV infected individuals of both strains, we have the disease-free equilibrium (DFE) point of the system (4.2.2) as:

$$E_0 = (S_0, I_{S_0}, I_{R_0}) = \left(\frac{\lambda}{\mu}, 0, 0\right).$$

Lemma 4.2.3. *The basic reproduction number for the system (4.2.2) is*

$$R_0 = \max\left\{\frac{\lambda\alpha_S}{a\mu}, \frac{\lambda\alpha_R}{b\mu}\right\}.$$

Moreover, the individual basic reproduction numbers related to the drug-sensitive strain and the drug-resistant strain are $\frac{\lambda\alpha_S}{a\mu}$ *and* $\frac{\lambda\alpha_R}{b\mu}$*, respectively.*

Proof. We use the next generation matrix method to calculate the basic reproduction number for the system (4.2.2). Since, we have two infectious compartments in the system, denoted by I_S and I_R, we write the sub-system of infected populations in the following form:

$$\begin{aligned}
\frac{dI_S}{dt} &= \mathcal{F}_1(S, I_S, I_R) - \mathcal{V}_1(S, I_S, I_R), \\
\frac{dI_R}{dt} &= \mathcal{F}_2(S, I_S, I_R) - \mathcal{V}_2(S, I_S, I_R),
\end{aligned}$$

where functions $\mathcal{F}_1$ and $\mathcal{F}_2$ represent the rate of arrival of susceptible individuals into the infected compartments I_S and I_R, respectively. On the other hand, functions $\mathcal{V}_1$ and $\mathcal{V}_2$ represent the rate of transfer in between, and out of the infected compartments I_S and

I_R, respectively. Therefore, $\mathcal{F}_1(S, I_S, I_R) = \alpha_S I_S S$, $\mathcal{F}_2(S, I_S, I_R) = \alpha_R I_R S$, $\mathcal{V}_1(S, I_S, I_R) = aI_S$ and $\mathcal{V}_2(S, I_S, I_R) = bI_R - \rho\eta(1-\epsilon)I_S$.

So, we obtain,

$$F = \begin{pmatrix} \frac{\partial \mathcal{F}_1}{\partial I_S}(E_0) & \frac{\partial \mathcal{F}_1}{\partial I_R}(E_0) \\ \frac{\partial \mathcal{F}_2}{\partial I_S}(E_0) & \frac{\partial \mathcal{F}_2}{\partial I_R}(E_0) \end{pmatrix} = \begin{pmatrix} \frac{\lambda\alpha_S}{\mu} & 0 \\ 0 & \frac{\lambda\alpha_R}{\mu} \end{pmatrix}, \tag{4.2.3}$$

and

$$V = \begin{pmatrix} \frac{\partial \mathcal{V}_1}{\partial I_S}(E_0) & \frac{\partial \mathcal{V}_1}{\partial I_R}(E_0) \\ \frac{\partial \mathcal{V}_2}{\partial I_S}(E_0) & \frac{\partial \mathcal{V}_2}{\partial I_R}(E_0) \end{pmatrix} = \begin{pmatrix} a & 0 \\ -\rho\eta(1-\epsilon) & b \end{pmatrix}. \tag{4.2.4}$$

Therefore, the next generation matrix is obtained as:

$$FV^{-1} = \begin{pmatrix} \frac{\lambda\alpha_S}{a\mu} & 0 \\ 0 & \frac{\lambda\alpha_R}{b\mu} \end{pmatrix}.$$

The basic reproduction number, denoted as R_0, is described as the spectral radius of the next generation matrix FV^{-1}. Therefore,

$$R_0 = \max\left\{\frac{\lambda\alpha_S}{a\mu}, \frac{\lambda\alpha_R}{b\mu}\right\}.$$

Biologically, we can conclude that the basic reproduction numbers related to the drug-sensitive strain $\left(R_0^{(S)}\right)$ and the drug-resistant strain $\left(R_0^{(R)}\right)$ are $\frac{\lambda\alpha_S}{a\mu}$ and $\frac{\lambda\alpha_R}{b\mu}$, respectively. □

Analysis of the basic reproduction numbers: We write the basic reproduction number related to the drug-sensitive strain and the drug-resistant strain in the form of original parameters as:

$$R_0^{(S)} = \frac{\lambda\alpha_S}{(\rho\eta(1-\epsilon) + \gamma\eta\epsilon + \beta_S(1-\eta) + \mu)\mu}$$

and

$$R_0^{(R)} = \frac{\lambda\alpha_R}{(\beta_R + \mu)\mu},$$

respectively. Now, we define the "Relative" basic reproduction number $\left(R_0^{(SR)}\right)$ as the ratio of $R_0^{(S)}$ and $R_0^{(R)}$, which represents the relative fitness of these two type of strains. The relative basic reproduction number for the system (4.2.2) is given by:

$$R_0^{(SR)} = \frac{R_0^{(S)}}{R_0^{(R)}} = \frac{b\alpha_S}{a\alpha_R} = \frac{\alpha_S(\beta_R + \mu)}{\alpha_R(\rho\eta(1-\epsilon) + \gamma\eta\epsilon + \beta_S(1-\eta) + \mu)}.$$

Biologically, the recruitment rate of the susceptible population has a direct positive impact on both type of infected populations. Similarly, an increased transmission rate of drug-sensitive (drug-resistant) strain results in an increased drug-sensitive (drug-resistant) infected population, as expected.

On the other hand, the basic reproduction number related to drug-sensitive strain is negatively related to the transfer rates ρ, γ and β_S, which is biologically reasonable as these parameters represent the rate of transfer of drug-sensitive infected population out of its compartment. Likewise, the basic reproduction number related to drug-resistant strain is indirectly proportional to the transfer rate β_R. Also, the natural death rate affects the basic reproduction number negatively, for both strains. Interestingly, the basic reproduction number related to the drug-sensitive strain is not uniformly dependent on the drug adherence level (ϵ) and the treatment availability (η), which makes these parameters more crucial for the analysis of our model (4.1.1).

To understand the impact of the treatment on the population dynamics of the system, we assume that the infected population is not receiving any treatment, i.e., $\eta = 0$. Then,

$$R_0^{(S_\eta)} = R_0^{(S)}\Big|_{\eta=0} = \frac{\lambda\alpha_S}{(\beta_S+\mu)\mu},$$

and we define a new parameter $\mathcal{H}$, where,

$$\mathcal{H} = \frac{R_0^{(S)}}{R_0^{(S_\eta)}} = \frac{\beta_S+\mu}{\rho\eta(1-\epsilon)+\gamma\eta\epsilon+\beta_S(1-\eta)+\mu}.$$

The treatment provided to the drug-sensitive infected population reduces the overall burden of the disease if it follows the inequality $\mathcal{H} < 1$, which implies:

$$\beta_S+\mu < \rho\eta(1-\epsilon)+\gamma\eta\epsilon+\beta_S(1-\eta)+\mu,$$

or

$$\beta_S < \rho(1-\epsilon)+\gamma\epsilon. \tag{4.2.5}$$

Also, we have,

$$\frac{\partial R_0^{(S)}}{\partial\eta} = \frac{\lambda\alpha_S(\beta_S-\rho(1-\epsilon)-\gamma\epsilon)}{\mu(\rho\eta(1-\epsilon)+\gamma\eta\epsilon+\beta_S(1-\eta)+\mu)^2}.$$

Here, $\dfrac{\partial R_0^{(S)}}{\partial\eta} < 0$ under the condition (4.2.5), which suggests a positive effect of the availability of treatment in eradicating the drug-sensitive strain from the system. In a system, the primary goals of the policy makers are to reduce the disease burden and control the risk factors associated with it. In the presence of treatment, equation (4.2.5) suggests that β_S is a more impactful parameter as compared to ρ and γ.

Lemma 4.2.4. *The matrix F is a non-negative and matrix V is a non-singular M-matrix. Further, $\rho(FV^{-1}) = R_0 < 1$ if and only if the matrix $(F - V)$ have all eigenvalues with negative real part.*

Proof. The proof is trivial from the expressions of matrices F and V (see [140]). □

Theorem 4.2.5. *The disease-free equilibrium point E_0 is locally asymptotically stable if the basic reproduction number $R_0 < 1$. Otherwise, it is unstable if $R_0 > 1$.*

Proof. The proof is a direct consequence of the Theorem 1 in [140]. □

To study the global behaviour of the DFE, although, we can use the most common approach by constructing an appropriate Lyapunov function. But here we follow a more general approach using basic reproduction number.

Theorem 4.2.6. *The disease-free equilibrium point E_0 is globally asymptotically stable in the region $\mathcal{R}$ if $R_0 < 1$.*

Proof. Since $\mathcal{R}$ is a positively invariant set for the system (4.1.1) and the DFE is locally asymptotically stable if $R_0 < 1$, it is sufficient to show that all solutions starting from inside the region $\mathcal{R}$, will ultimately fall into any given $\epsilon-$neighbourhood of E_0 intersected with $\mathcal{R}$. That is, for all $y(0) \in \mathcal{R}$,

$$\lim_{t\to\infty} S(t) = \frac{\lambda}{\mu}, \qquad \lim_{t\to\infty} I_S(t) = 0, \qquad \lim_{t\to\infty} I_R(t) = 0.$$

We derive the subsequent inequality from the first equation of system (4.2.2),

$$\frac{dS}{dt} \leq \lambda - \mu S.$$

Now, using the comparison lemma, for any given $\delta_1 > 0$, there exists a time $t_1 > 0$, such that $S(t) \leq \frac{\lambda}{\mu} + \delta_1$ for all $t \geq t_1$. Therefore,

$$\limsup_{t\to\infty} S(t) \leq \frac{\lambda}{\mu}. \tag{4.2.6}$$

Then, using this result, we get the following subsystem of the system (4.2.2) for $t \geq t_1$

$$\begin{aligned} \frac{dI_S}{dt} &\leq \alpha_S I_S \left(\frac{\lambda}{\mu} + \delta_1\right) - aI_S, \\ \frac{dI_R}{dt} &= \alpha_R I_R \left(\frac{\lambda}{\mu} + \delta_1\right) + \rho\eta(1-\epsilon)I_S - bI_R. \end{aligned}$$

Now, we consider the following system with $u_1(t_1) = I_S(t_1)$ and $u_2(t_1) = I_R(t_1)$,

$$\begin{aligned}\frac{du_1}{dt} &= \alpha_S u_1\left(\frac{\lambda}{\mu}+\delta_1\right) - au_1,\\ \frac{du_2}{dt} &= \alpha_R u_2\left(\frac{\lambda}{\mu}+\delta_1\right) + \rho\eta(1-\epsilon)u_1 - bu_2,\end{aligned}$$

that is represented as:

$$\frac{du}{dt} = (F_{\delta_1} - V_{\delta_1})u,$$

where $u = (u_1, u_2)^\top$ and matrices F_{δ_1} and V_{δ_1} are as defined in equations (4.2.3) and (4.2.4), respectively, evaluated at the point $y_{\delta_1}(0) = \left(\frac{\lambda}{\mu}+\delta_1, 0, 0\right)$. We obtain $\rho(F_{\delta_1}V_{\delta_1}^{-1}) < 1$ for a sufficiently small $\delta_1 > 0$ as $\mathcal{R}_0 = \rho(FV^{-1}) < 1$. Since F_{δ_1} is non-negative and V_{δ_1} is a non-singular M-matrix, we use Lemma 4.2.4 to obtain that the matrix $(F_{\delta_1} - V_{\delta_1})$ have all eigenvalues with negative real part. It follows that, for any given initial condition in the region $\mathcal{R}$, we have $\lim_{t\to\infty} u(t) = 0$. Therefore,

$$\lim_{t\to\infty} I_S(t) = 0 \qquad \text{and} \qquad \lim_{t\to\infty} I_R(t) = 0. \tag{4.2.7}$$

Now, for any given $\delta_2 > 0$, there exists a time $t_2 > 0$ such that for any $t \geq t_2$, $I_S(t) < \delta_2$ and $I_R(t) < \delta_2$. So, from the first equation of the system (4.2.2), we get the following inequality for $t \geq t_2$:

$$\frac{dS}{dt} \geq \lambda - (\delta_2(\alpha_S - \alpha_R) + \mu)S.$$

Again, using the comparison lemma, for any given $\delta_3 > 0$, there exists a time $t_3 > 0$, such that for all $t \geq t_3$,

$$S(t) \geq \frac{\lambda}{\mu + \delta_2(\alpha_S - \alpha_R)} - \delta_3.$$

Therefore,

$$\liminf_{t\to\infty} S(t) \geq \frac{\lambda}{\mu + \delta_2(\alpha_S - \alpha_R)}.$$

Since δ_2 is arbitrary, therefore we obtain,

$$\liminf_{t\to\infty} S(t) \geq \frac{\lambda}{\mu}. \tag{4.2.8}$$

Accordingly, equations (4.2.6) and (4.2.8) yield,

$$\lim_{t\to\infty} S(t) = \frac{\lambda}{\mu}.$$

□

Disease persistence

In this subsection, we discuss a couple of scenarios where disease persists for a very long time. We inspect different possibilities for the uniform persistence of different virus strains individually as well as simultaneously. The disease persists when atleast one type of infected population, either with drug-sensitive or drug-resistant strain, remains at a positive level even after a long time. We investigate the existence of equilibrium points which include the drug-sensitive and/or drug-resistant infected population. Further, we determine the local as well as global behaviour of these equilibrium points to analyze the endemic scenario of the disease. In system (4.2.2), there are two endemic equilibrium points as following:

(A) The drug-resistant strain endemic equilibrium point.

(B) The co-existence endemic equilibrium point.

Elimination of the drug-sensitive infected population: When we consider no drug-sensitive infected individual initially, we get the drug-resistant strain endemic equilibrium point of the system (4.2.2) as

$$E_1 = (S_1, I_{S_1}, I_{R_1}) = \left(\frac{b}{\alpha_R}, 0, \frac{\lambda\alpha_R - b\mu}{b\alpha_R}\right) = \left(\frac{b}{\alpha_R}, 0, \frac{\mu}{\alpha_R}\left(R_0^{(R)} - 1\right)\right),$$

which exists only if $R_0^{(R)} > 1$. Now, to determine the local behaviour of the solutions near drug-resistant strain endemic equilibrium point, we consider the Jacobian matrix evaluated at the point E_1, that is,

$$J\,\big|_{E_1} = \begin{pmatrix} -\frac{\lambda\alpha_R}{b} & -\frac{b\alpha_S}{\alpha_R} & -b \\ 0 & \frac{b\alpha_S}{\alpha_R} - a & 0 \\ \mu(R_0^{(R)} - 1) & \rho\eta(1-\epsilon) & 0 \end{pmatrix}.$$

The characteristic equation of the Jacobian matrix $J\,\big|_{E_1}$ is as following:

$$\det\left[xI_3 - J\,\big|_{E_1}\right] = \left(x^2 + \frac{\lambda\alpha_R}{b}x + b\mu(R_0^{(R)} - 1)\right)\left(x + a - \frac{b\alpha_S}{\alpha_R}\right) = 0, \tag{4.2.9}$$

where I_3 is the identity matrix of order 3. Now, zeros of the characteristic equation (4.2.9) has negative real part if and only if $\frac{b\alpha_S}{a\alpha_R} < 1 \left(\text{ or } \frac{R_0^{(S)}}{R_0^{(R)}} < 1\right)$, since it is provided that $R_0^{(R)} > 1$ (from the existential condition of the equilibrium point E_1). Therefore, the equilibrium point E_1 is locally asymptotically stable whenever it exists, provided $R_0^{(S)} < R_0^{(R)}$. We propose the following theorem based on above findings.

Theorem 4.2.7. *The drug-resistant strain endemic equilibrium point* $E_1 = (S_1, I_{S_1}, I_{R_1})$ *exists only if* $R_0^{(R)} > 1$. *Further, it is locally asymptotically stable if* $R_0^{(S)} < R_0^{(R)}$. *Also,* E_1 *is unstable if* $R_0^{(S)} > R_0^{(R)}$.

For the global behaviour of the drug-resistant strain endemic equilibrium point E_1, we present the following theorem.

Theorem 4.2.8. *The drug-resistant strain endemic equilibrium point* $E_1 = (S_1, I_{S_1}, I_{R_1})$ *is globally asymptotically stable whenever it exists if* $R_0^{(S)} < R_0^{(R)}$.

Proof. In order to prove this theorem, first, we show that all the solutions of the system (4.2.2) converge to the hyperplane $I_S = 0$ whenever $R_0^{(S)} < R_0^{(R)}$. Further, we construct a suitable Lyapunov function to demonstrate the globally attracting behaviour of E_1 on the hyperplane $I_S = 0$. The proof is similar to the proof of Theorem 3.2.3 of Chapter 3. □

Remark 4.2.9. *The transmission rates associated with the drug-sensitive strain do not impact the existence of the equilibrium point* E_1. *However, the stability of this equilibrium state relies on the relative transmission rate from the susceptible class to the infected class (the ratio of* α_S *and* α_R*), which must be limited by a threshold value to ensure stability.*

Co-existence of the drug-sensitive and drug-resistance infected population: Here, we explore the existence and stability of the co-existence endemic equilibrium point of the system (4.2.2), where drug-sensitive and drug-resistant infected population co-exist together along with the susceptible population. To establish the existence of this equilibrium point, we solve the following system,

$$\begin{aligned} &\lambda - \alpha_S I_S S - \alpha_R I_R S - \mu S = 0, \\ &\alpha_S I_S S - a I_S = 0, \\ &\alpha_R I_R S + \rho\eta(1-\epsilon) I_S - b I_R = 0, \end{aligned} \tag{4.2.10}$$

which yields

$$\begin{aligned} E_* &= (S_*, I_{S_*}, I_{R_*}) \\ &= \left(\frac{a}{\alpha_S}, -\frac{(a\alpha_R - b\alpha_S)(a\mu - \lambda\alpha_S)}{a\alpha_S(a\alpha_R - \eta\rho\alpha_R + \epsilon\eta\rho\alpha_R - b\alpha_S)}, \frac{\eta\rho(1-\epsilon)(a\mu - \lambda\alpha_S)}{a(a\alpha_R - \eta\rho\alpha_R + \epsilon\eta\rho\alpha_R - b\alpha_S)} \right). \end{aligned}$$

Also, we write the equilibrium point E_* in terms of the reproduction numbers as follows:

$$E_* = \left(\frac{a}{\alpha_S}, \frac{\mu\left(R_0^{(SR)} - 1\right)\left(R_0^{(S)} - 1\right)}{\alpha_S\left(R_0^{(SR)} - 1 + \frac{\eta\rho(1-\epsilon)}{a}\right)}, \frac{\eta\rho\mu(1-\epsilon)\left(R_0^{(S)} - 1\right)}{a\alpha_R\left(R_0^{(SR)} - 1 + \frac{\eta\rho(1-\epsilon)}{a}\right)} \right),$$

which exists only if $R_0^{(S)} > 1$ and $R_0^{(SR)} > 1$. These existence conditions indicate that we can control the co-existence of both strains by manipulating the fitness of the drug-sensitive strain alone. As we have seen in the previous section, the fitness of the drug-sensitive strain is strongly dependent on the treatment availability and the drug adherence level. Therefore, these two parameters play a significant role in determining the dynamics of the system.

Now, in order to determine the local stability behaviour of the equilibrium point E_*, we linearize the system (4.2.2) near it. The Jacobian matrix evaluated at the point E_* is given by,

$$J\Big|_{E_*} = \begin{pmatrix} -\frac{\lambda}{S_*} & -\alpha_S S_* & -\alpha_R S_* \\ \alpha_S I_{S_*} & 0 & 0 \\ \alpha_R I_{R_*} & \rho\eta(1-\epsilon) & \alpha_R S_* - b \end{pmatrix},$$

and the corresponding linearized system in the vector form is $Y' = J\Big|_{E_*} Y$, where Y represents the vector of state variables of the system (4.2.2). The characteristic equation of the Jacobian matrix $J\Big|_{E_*}$ is,

$$\det\left[xI_3 - J\Big|_{E_*}\right] = x^3 + A_1x^2 + A_2x + A_3 = 0, \tag{4.2.11}$$

where I_3 is the identity matrix of order 3 and

$$\begin{aligned} A_1 &= b + \frac{\lambda}{S_*} - \alpha_R S_*, \\ A_2 &= \alpha_S^2 S_* I_{S_*} + \alpha_R^2 S_* I_{R_*} - \lambda\alpha_R + \frac{b\lambda}{S_*}, \\ A_3 &= b\alpha_S^2 S_* I_{S_*} + \alpha_S\alpha_R\eta\rho(1-\epsilon)S_* I_{S_*} - \alpha_S^2\alpha_R S_*^2 I_{S_*}. \end{aligned}$$

We can also write these coefficients of the characteristic equation (4.2.11) in terms of the basic reproduction numbers as follows,

$$\begin{aligned} A_1 &= \frac{a^2\alpha_R\left(R_0^{(SR)} - 1\right) + \lambda\alpha_S^2}{a\alpha_S}, \\ A_2 &= \lambda\alpha_R\left(R_0^{(SR)} - 1\right) + \frac{\mu\left(R_0^{(S)} - 1\right)\left(\eta\rho(1-\epsilon)\alpha_R + a\alpha_S\left(R_0^{(SR)} - 1\right)\right)}{\alpha_S\left(\frac{\eta\rho(1-\epsilon)}{a} + R_0^{(SR)} - 1\right)}, \\ A_3 &= \frac{a^2\mu\left(R_0^{(S)} - 1\right)\left(R_0^{(SR)} - 1\right)\alpha_R}{\alpha_S}. \end{aligned}$$

Now, by Routh-Hurwitz criterion [142], the co-existence endemic equilibrium point is locally asymptotically stable if $A_i > 0$ for $i = 1, 2, 3$ and $A_1A_2 - A_3 > 0$. Note that $R_0^{(S)} > 1$ and $R_0^{(SR)} > 1$, from the existence condition of E_*. Therefore, $A_1 > 0$, $A_2 > 0$ and $A_3 > 0$ whenever the interior equilibrium point exists.

From the above discussion, we present the following theorem about the existence and the local stability of the co-existence endemic equilibrium point E_*.

Theorem 4.2.10. *The co-existence endemic equilibrium point $E_* = (S_*, I_{S_*}, I_{R_*})$ exists only if $R_0^{(S)} > 1$ and $R_0^{(SR)} > 1$. Further, it is locally asymptotically stable if $A_1A_2 - A_3 > 0$, where A_1, A_2 and A_3 are as discussed above. Also, E_* is unstable if $A_1A_2 - A_3 < 0$.*

Now, we investigate the global stability of the co-existence endemic equilibrium point by considering a suitable Lyapunov function.

Theorem 4.2.11. *The co-existence endemic equilibrium point (E_*) is globally asymptotically stable if the following conditions hold:*

(A) $4(a\mu - \lambda\alpha_S) > {\alpha_S}^2 (S_* - I_{S_*})^2$,

(B) $\mu \left(\left(a - \dfrac{\lambda\alpha_S}{\mu} \right) \left(b - \dfrac{\lambda\alpha_R}{\mu} \right) - \dfrac{1}{4}(\rho\eta(1-\epsilon))^2 \right)$
$-\dfrac{1}{4} \left(b{\alpha_S}^2 (S_* - I_{S_*})^2 + \alpha_S\alpha_R\rho\eta(1-\epsilon)(S_* - I_{S_*})(S_* - I_{R_*}) + a{\alpha_R}^2 (S_* - I_{R_*})^2 \right) > 0.$

Proof. We set the Lyapunov function as:

$$L(t) = L(S(t), I_S(t), I_R(t)) = \frac{1}{2}(S - S_*)^2 + \frac{1}{2}(I_S - I_{S_*})^2 + \frac{1}{2}(I_R - I_{R_*})^2,$$

which is a positive definite function in any given neighbourhood of the equilibrium point E_*. Now, differentiating the Lyapunov function L with respect to 't' along the solution of system (4.2.2) gives,

$$\begin{aligned} \frac{dL}{dt} &= (S - S_*)\frac{dS}{dt} + (I_S - I_{S_*})\frac{dI_S}{dt} + (I_R - I_{R_*})\frac{dI_R}{dt} \\ &= (S - S_*)(\lambda - \alpha_S I_S S - \alpha_R I_R S - \mu S) + (I_S - I_{S_*})(\alpha_S I_S S - aI_S) \\ &\quad + (I_R - I_{R_*})(\alpha_R I_R S + \rho\eta(1-\epsilon)I_S - bI_R). \end{aligned} \tag{4.2.12}$$

Now, using the solutions of system (4.2.10), the equation (4.2.12) can be written as,

$$\begin{aligned} \frac{dL}{dt} &= (S - S_*)(-(\mu + \alpha_S I_S + \alpha_R I_R)(S - S_*) - \alpha_S S_* (I_S - I_{S_*}) - \alpha_R S_* (I_R - I_{R_*})) \\ &\quad + (I_S - I_{S_*})((-a + \alpha_S S)(I_S - I_{S_*}) + \alpha_S I_{S_*}(S - S_*)) \\ &\quad + (I_R - I_{R_*})((-b + \alpha_R S)(I_R - I_{R_*}) + \rho\eta(1-\epsilon)(I_S - I_{S_*}) + \alpha_R I_{R_*}(S - S_*)) \\ &= -\left((\mu + \alpha_S I_S + \alpha_R I_R)(S - S_*)^2 + (a - \alpha_S S)(I_S - I_{S_*})^2 + (b - \alpha_R S)(I_R - I_{R_*})^2\right) \\ &\quad - ((\alpha_S I_{S_*} - \alpha_S S_*)(S - S_*)(I_S - I_{S_*}) + (\alpha_R I_{R_*} - \alpha_R S_*)(S - S_*)(I_R - I_{R_*})) \\ &\quad - (\rho\eta(1-\epsilon))(I_S - I_{S_*})(I_R - I_{R_*}) \\ &= -P^{-1}QP, \end{aligned} \tag{4.2.13}$$

where $P = [(S - S_*), (I_S - I_{S_*}), (I_R - I_{R_*})]^\top$ and

$$Q = \begin{pmatrix} \mu + \alpha_S I_S + \alpha_R I_R & \frac{1}{2}\alpha_S (S_* - I_{S_*}) & \frac{1}{2}\alpha_R (S_* - I_{R_*}) \\ \frac{1}{2}\alpha_S (S_* - I_{S_*}) & a - \alpha_S S & -\frac{1}{2}\rho\eta(1-\epsilon) \\ \frac{1}{2}\alpha_R (S_* - I_{R_*}) & -\frac{1}{2}\rho\eta(1-\epsilon) & b - \alpha_R S \end{pmatrix}.$$

The principal minors of the matrix Q are positive if conditions (A) and (B) satisfied. Therefore, the matrix Q becomes positive definite as per the Sylvester's criterion [168], and $\frac{dL}{dt} < 0$. By applying the LaSalle invariance principle, the co-existence endemic equilibrium point (E_*) is globally asymptotically stable under the conditions (A) and (B). □

Remark 4.2.12. ***Strain replacement:*** *From the stability conditions of equilibrium points E_1 and E_*, we observe the relative reproduction number $(R_0^{(SR)})$ strongly influences the dynamics of the system. The possibility of strain replacement is feasible as E_* replaces its stability with E_1. Strain replacement depends on the relative fitness of both strains instead of the fitness of any single strain. From the previous subsection, we have,*

$$R_0^{(SR)} = \frac{\alpha_S(\beta_R + \mu)}{\alpha_R(\rho\eta(1-\epsilon) + \gamma\eta\epsilon + \beta_S(1-\eta) + \mu)},$$

which indicates the following results related to the strain replacement: (A) a relatively higher transmission rate for the drug-resistant infected population from the susceptible population (α_R) is directly linked to the strain replacement, and (B) a relatively lower transmission rate from drug-resistant infected population to the AIDS population (β_R) is also responsible for the strain replacement.

4.2.3 Bifurcation analysis

From the previous subsection, we have observed the possibility of change in number of existing equilibrium points and their stability as we vary the value of a parameter resulting into an increased or decreased reproduction number. It shows a sudden change in the dynamics of the system at some critical values of these parameters. Theorems 4.2.6 and 4.2.8 confirm that the system exists with a stable disease-free equilibrium point when $R_0^{(S)} < 1$ and has a stable drug-resistant strain endemic equilibrium point when $R_0^{(R)} > 1$ and $R_0^{(SR)} > 1$, which indicates to the existence of a forward bifurcation. Furthermore, Theorem 4.2.10 shows that the co-existence endemic equilibrium point may loose its stability after a critical value achieved by a parameter and solutions of the system (4.2.2) exhibit a periodic behaviour. This type of bifurcation which separates a branch of equilibrium points from a branch of periodic oscillations is called Hopf bifurcation. In this section, we investigate the critical values of certain parameters at which the dynamics of the system (4.2.2) changes

drastically. Since the direct use of the reproduction number as a bifurcation parameter is often inconvenient, we have used other parameters to get the bifurcation points.

Transcritical bifurcation

Theorem 4.2.13. *The system (4.2.2) experiences transcritical bifurcation in forward direction between the equilibrium points E_0 and E_1 at $\alpha_R = \alpha_R^{tc} = \dfrac{b\mu}{\lambda}$, if $R_0^{(S)} < 1$.*

Proof. Let's re-write the system (4.2.2) as,

$$\frac{dY}{dt} = F(Y, \alpha_R),\ F : \mathbb{R}^3 \times \mathbb{R} \to \mathbb{R}^3 \text{ and } F \in \mathbb{C}^2(\mathbb{R}^4 \times \mathbb{R}),$$

where $Y = [y_1, y_2, y_3]^T = [S, I_S, I_R]^T$ and $F = [f_1, f_2, f_3]^T$. Observe that,

$$R_0^{(R)} = 1 \iff \alpha_R = \frac{b\mu}{\lambda} \qquad (\text{say } \alpha_R^{tc}).$$

Then the Jacobian matrix of the system (4.2.2) calculated at E_0 with $\alpha_R = \alpha_R^{tc}$ is given as,

$$J(E_0, \alpha_R^{tc}) = \begin{pmatrix} -\mu & -\frac{\lambda\alpha_S}{\mu} & -b \\ 0 & -a + \frac{\lambda\alpha_S}{\mu} & 0 \\ 0 & \rho\eta(1-\epsilon) & 0 \end{pmatrix}.$$

The Jacobian matrix $J(E_0, \alpha_R^{tc})$ has a simple zero eigenvalue and remaining two eigenvalues are $-\mu$ (< 0) and $\dfrac{\lambda\alpha_S - a\mu}{\mu}$, which is negative only if $R_0^{(S)} < 1$. We use the center manifold theory to deal with this non-hyperbolic nature of the equilibrium point E_0 at $\alpha_R = \alpha_R^{tc}$. Note that, the right eigenvector and left eigenvector of the matrix $J(E_0, \alpha_R^{tc})$ corresponding to the zero eigenvalue are,

$$U = [u_1, u_2, u_3]^T = \left[-\frac{b}{\mu}, 0, 1\right]^T \text{ and } V = [v_1, v_2, v_3]^T = \left[0, \frac{\rho\eta\mu(1-\epsilon)}{a\mu - \lambda\alpha_S}, 1\right]^T,$$

respectively. Further, we obtain,

$$\begin{aligned}
\tau_1 =& V^T \left[F_{\alpha_R}(E_0, \alpha_R^{tc})\right] = 0, \\
\tau_2 =& V^T \left[DF_{\alpha_R}(E_0, \alpha_R^{tc})U\right] = \frac{\lambda}{\mu} > 0\ (\neq 0), \\
\tau_3 =& V^T \left[D^2F(E_0, \alpha_R^{tc})(U, U)\right] = -\frac{2b^2}{\lambda} < 0\ (\neq 0),
\end{aligned}$$

where DF and F_{α_R} represent the matrices of all partial derivatives of the components of vector F with respect to the components of vector Y and the parameter α_R, respectively. From Sotomayor's Theorem [144], the disease-free equilibrium point (E_0) exchange its stability with the drug-resistance strain endemic equilibrium point (E_1) through transcritical bifurcation at $\alpha_R = \alpha_R^{tc} = \dfrac{b\mu}{\lambda}$. Also, from similar condition of Theorem 4.1 in [155], the direction of this bifurcation is forward as $\tau_3 < 0$. □

Hopf-bifurcation

In Theorem 4.2.13, the bifurcation is characterized by intersecting branches of equilibrium points. However, it has been observed that a single equilibrium point alone may change its stability properties corresponding to a varying parameter. In this subsection, we identify a threshold condition for the drug adherence level (ϵ) and the treatment availability (η), which splits down the whole range for this parameter based on the oscillatory behaviour of the solution curves of system (4.2.2) around the co-existence endemic equilibrium point. It shows the occurrence of the Hopf-bifurcation into the system and we present the results related to the Hopf-bifurcation in the following theorem.

Theorem 4.2.14. *The co-existence endemic equilibrium point E_* changes its stability through the Hopf-bifurcation at the threshold $\epsilon = \epsilon^H$ under following conditions:*

(A) $H(\epsilon^H) = A_1(\epsilon^H)A_2(\epsilon^H) - A_3(\epsilon^H) = 0$,

(B) $\left.\dfrac{dH(\epsilon)}{d\epsilon}\right|_{\epsilon=\epsilon^H} \neq 0$ *where A_1, A_2 and A_3 are functions of parameter ϵ used as in Theorem 4.2.10.*

Proof. The Jacobian matrix $J(E_*)$ has a conjugate pair of complex eigenvalues with zero real part if,

$$A_1A_2 - A_3 = 0 \tag{4.2.14}$$

Let $\epsilon = \epsilon^H$ be the solution of equation (4.2.14). Therefore, according to the Hopf-bifurcation theorem [169], the transversality condition for the equilibrium point to change its stability through Hopf-bifurcation at $\epsilon = \epsilon^H$ is $\mathrm{Re}\left\{\dfrac{d}{d\epsilon}\left[x_j(\epsilon)\right]\Big|_{\epsilon=\epsilon^H}\right\} \neq 0$, where x_j $(j = 1, 2, 3)$ are roots of the equation (4.2.11). From the equation (4.2.11) and (4.2.14), we have,

$$x_{1,2}(\epsilon^H) = \pm\sqrt{A_2(\epsilon^H)},\ x_3(\epsilon^H) = -A_1(\epsilon^H) < 0.$$

Now, differentiating equation (4.2.11) with respect to ϵ, we get,

$$\left.\frac{d}{d\epsilon}\left[x(\epsilon)\right]\right|_{\epsilon=\epsilon^H} = -\left.\frac{x^2\dfrac{dA_1}{d\epsilon} + x\dfrac{dA_2}{d\epsilon} + \dfrac{dA_3}{d\epsilon}}{3x^2 + 2A_1x + A_2}\right|_{\epsilon=\epsilon^H}$$

which gives,

$$\mathrm{Re}\left\{\left.\frac{d}{d\epsilon}\left[x_j(\epsilon)\right]\right|_{\epsilon=\epsilon^H}\right\} = \left.\frac{\dfrac{dA_3}{d\epsilon} - \left(A_2\dfrac{dA_1}{d\epsilon} + A_2\dfrac{dA_2}{d\epsilon}\right)}{2(A_1^2 + A_2)}\right|_{\epsilon=\epsilon^H} = -\left.\frac{\dfrac{dH(\epsilon)}{d\epsilon}}{2(A_1^2 + A_2)}\right|_{\epsilon=\epsilon^H};\ j = 1, 2.$$

Therefore, the transversality conditions hold if $\left.\frac{dH(\epsilon)}{d\epsilon}\right|_{\epsilon=\epsilon^H} \neq 0$, and E_* changes its stability through the Hopf-bifurcation at the threshold $\epsilon = \epsilon^H$. We have investigated these conditions further numerically in the next section. □

Theorem 4.2.15. *The co-existence endemic equilibrium point E_* changes its stability through the Hopf-bifurcation at the threshold $\eta = \eta^H$ under following conditions:*

(A) $H(\eta^H) = A_1(\eta^H)A_2(\eta^H) - A_3(\eta^H) = 0$,

(B) $\left.\frac{dH(\eta)}{d\eta}\right|_{\eta=\eta^H} \neq 0$ *where A_1, A_2 and A_3 are functions of parameter η used as in Theorem 4.2.10.*

Proof. The proof is similar to the proof of Theorem 4.2.14. □

Remark 4.2.16. *There may exist multiple roots of the equation (4.2.14). However, the occurrence of Hopf-bifurcation is limited to points where the equilibrium point E_* exists.*

Remark 4.2.17. *Based on the above discussion, we summarise the existence and stability conditions, based on the basic reproduction number, of all equilibrium points in Table 4.2.*

Value of $\mathbf{R_0^{(S)}}$	Value of $\mathbf{R_0^{(R)}}$	Value of $\mathbf{R_0^{(SR)}}$	Existing EP	Stable EP
< 1	< 1	< 1 or > 1	E_0	E_0
< 1 or > 1	> 1	< 1	E_0, E_1	E_1
> 1	< 1	> 1	E_0, E_*	E_* or stable limit cycle
> 1	> 1	> 1	E_0, E_1, E_*	E_* or stable limit cycle

Table 4.2: Existence and stability conditions of equilibrium points of model (4.2.2).

4.3 Epidemiological Parameter Values

In this section, our focus will be on estimating the parameter values for model (4.1.1) using real data based on some existing studies. Most of the parameters are calculated based on the results provided in multiple experimental and meta-analysis studies, while a few are taken directly from the literature and previous chapters. Further, the parameter values related to the drug-resistant infected class are assumed based on the corresponding parameter values associated with the drug-sensitive infected class. We have not used any explicit method for estimating these parameters, as they represent the rate of transfer from one compartment to another. In this case, we can use the average time an individual spends in one compartment.

In general, the recruitment rate (λ) signifies the rate at which new individuals join a specific population (susceptible to HIV infection), typically through processes like birth, immigration, or other similar mechanisms. In Chapter 2, the recruitment rate is estimated by considering the average number of new individuals joining the sexually active class, in addition to accounting for the net migrated population. Also, the value of λ was estimated as 25.31 million year^{-1}. The transmission rate α_S (α_R) quantifies how quickly the drug-sensitive (drug-resistant) infected population changes in presence of one unit each of susceptible individuals and drug-sensitive (drug-resistant) infected individuals. We take $\alpha_S = 4.7134 \times 10^{-5}$ million^{-1}year^{-1} as suggested in Chapter 2. We vary the parameter α_R within a suitable range around the parameter α_S, as it is related to the newly emerged resistant strain which may have different transmission rate. In India, there was an approximate mortality rate of 7.2 individuals per 1000 persons in the year 2019 [152], consequently establishing the natural death rate (μ) as 0.007 per year. The transmission rate ρ quantifies the average time taken in emergence of drug-resistance in an infected individual who is under treatment and does not adhere the treatment optimally. In a study, it has been shown that a small proportion of patients have developed resistance within 6 months after initiation of the treatment for HIV [163]. We assume that the resistance can develop in a non-adherent patient anywhere from 6 months to 2 years after starting the treatment. Therefore, the parameter ρ varies between 0.5 to 2 per year depending on the sub-optimality level to the treatment. A comprehensive meta-analysis study has revealed that the HIV infection progresses to AIDS within 10 years in 74% patients without any treatment [170]. Therefore, we assume that the transmission rates β_S is 0.1 per year. We also assume that no treatment is effective on drug-resistent infected population and they move into the AIDS class with same transmission rate as untreated drug-sensitve infected population, that is, $\beta_R = 0.1$ per year. On the contrary, an adherent patient under ART takes significantly longer time to move in AIDS class as compared to the resistant population. Based on multiple research studies, individuals who are HIV-positive have an average life expectancy of 37.3 years and 29.0 years from starting ART at the age of 20 and 35 years, respectively [171]. Thus, we take the parameter γ in the range of 0.025 to 0.04 per year. In [170], authors have also concluded that the survival probability of a patient decreases from 0.48 to 0.26 within 2 to 4 years after the onset of AIDS. Consequently, we consider the disease induced death rate (μ_d) to be 0.5 per year. At the end of 2022, approximately 76% people living with HIV were receiving the ART [172]. Therefore, for most of our numerical simulation purpose, we consider $\eta = 0.75$ and $\epsilon = 0.7$. Since our main focus is to understand the role of treatment and its adherence on the emergence of the drug-resistance, we vary the parameters η and ϵ with some other parameters in a suitable range to illustrate all possible scenarios. The parameters, their associated units,

estimated values, and the corresponding ranges of variation has been presented in the Table 4.3.

Parameter	Unit	Baseline Value	Range of Variation	Reference(s)
λ	million year^{-1}	25.31	fixed	see Chapters 2, 3
α_S	million^{-1} year^{-1}	4.7134×10^{-5}	$[4 \times 10^{-5},\ 3 \times 10^{-4}]$	see Chapters 2, 3
α_R	million^{-1} year^{-1}	2.0×10^{-5}	$[1 \times 10^{-5},\ 1 \times 10^{-4}]$	assumed
μ	year^{-1}	0.007	fixed	[152]
ρ	year^{-1}	1	[0.5, 2]	[163]
β_S	year^{-1}	0.1	fixed	[170]
β_R	year^{-1}	0.1	[0.05, 0.1]	assumed
γ	year^{-1}	0.03	[0.025, 0.04]	[171]
μ_d	year^{-1}	0.5	fixed	[170]
η	unitless	0.75	[0, 1]	[172]
ϵ	unitless	0.7	[0, 1]	assumed

Table 4.3: Various parameters of the system (4.1.1) along with their units, estimated values, range of variations and references.

4.4 Numerical Simulation

In this section, we will validate the analytical findings regarding the existence and stability of equilibrium points and explore various bifurcations using multiple numerical examples. We fix the parameters as estimated above for most of our simulations and vary some of them within their range of variation to discuss all the possible scenarios. The system (4.1.1) has three possible equilibrium points. The analytical findings indicate that the stability of two equilibrium points does not manifest simultaneously. The disease-free equilibrium point E_0 always exists and it is locally as well as globally asymptotically stable if $R_0 < 1$. We choose the values of parameters as given in Table 4.3. For this set of values, the basic reproduction numbers related to the drug-sensitive and the drug-resistant strain are 0.62 (< 1) and 0.68 (< 1), respectively. Consequently, the equilibrium point E_0 is asymptotically stable in accordance with Theorem 4.2.5 and Theorem 4.2.6. A time series plot for this scenario has represented in Figure 4.2a, where the solution starts from the initial condition $ic_1 = (625, 2.5, 1, 0.25)$ based on the population in each compartment at the starting time. To illustrate the global behaviour of solutions, we choose another three different initial conditions : $ic_2 = (3000, 500, 500, 20)$, $ic_3 = (1500, 100, 800, 10)$ and $ic_4 = (300, 100, 300, 100)$. Figure 4.2b shows the global asymptotically stable behaviour of the equilibrium point $E_0(3615.71, 0, 0, 0)$ where solutions starting from various initial conditions

converge to it. Note that, we have not included the AIDS class (A) in any phase portrait, since this does not influence the existence and stability of any equilibrium point.

To show the existence and stability of the drug-resistance strain endemic equilibrium point E_1, we change the parameter α_R to 0.00008 and rest of the parameters are same as in Table 4.3. For this set of parameter, the basic reproduction numbers related to the drug-sensitive and the drug-resistant strain are 0.62 (< 1) and 2.7 (> 1), respectively, which clearly show the dominance of the drug-resistant strain in the system. The time series plot with initial condition ic_1 is illustrated in Figure 4.2c, where the drug-sensitive infected population reaches to extinction within a very short time and all other compartments remain populated for all time. The phase portrait in Figure 4.2d shows the global asymptotically stability of the equilibrium point E_1. In Figure 4.2d, all the solution trajectories originating from various initial conditions are converging to the equilibrium point $E_1(1337.5, 0, 149.04, 29.40)$. Here, the disease-free equilibrium point exists but does not fulfil the criteria for the stability.

Further, we increase the rate of infection due to drug-sensitive infected population and choose $\alpha_S = 0.003$ while considering all other parameters same as in Table 4.3. For this increased infection rate, we get $R_0^{(S)} = 3.98$ (> 1), $R_0^{(R)} = 0.68$ and $R_0^{(SR)} = 5.85$ (> 1). These values of basic reproduction numbers assure the existence of the co-existence endemic equilibrium point (E_*). Moreover, the coefficients of the characteristic equation (4.2.11) are $A_1 = 0.11665 > 0$, $A_2 = 0.00739 > 0$ and $A_3 = 0.00051 > 0$. Therefore, $A_1A_2 - A_3 = 0.00036 > 0$, which satisfies the Routh-Hurwitz condition provided in the Theorem 4.2.10 for the local asymptotic stability of the equilibrium point E_*. The time series plot in Figure 4.2e indicates that each population show an oscillatory behaviour for some time with decreasing magnitude and then settle down on their respective equilibrium state. The long term phase portrait is depicted in Figure 4.2f which shows the global asymptotic stable behaviour of the equilibrium point $E_*(909.17, 59.43, 150.54, 94.16)$. This numerical analysis shows that the infection rates of drug-sensitive as well as drug-resistant infected population have a noticeable impact on the overall dynamics of the system. For lower infection rates, the infected population die out after some time and system reaches to a disease-free state. While, for higher infection rates, the system dynamics depends on the relative magnitudes of these rates. The co-existence of all populations is possible only if the infection rate due to drug-sensitive strain is significantly high as compare to the drug-resistant strain.

Furthermore, α_R is an important parameter in order to determine the existence and stability of equilibrium points. We vary the parameter α_R from 0 to 0.0001 and fix all other parameters as in Table 4.3. For this set of parameter values, the basic reproduction number $R_0^{(S)} < 1$ and we get the bifurcation point $\alpha_R = \alpha_R^{tc} = 0.00002959$ when $R_0^{(R)}$ passes from 1. Figure 4.3a and 4.3b show that E_0 is the only existing equilibrium point for $\alpha_R < \alpha_R^{tc}$

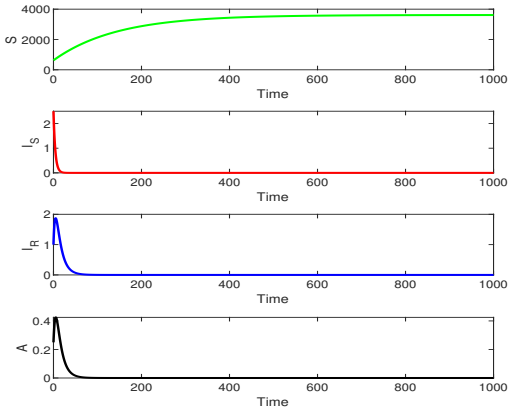

(a) $\alpha_S = 0.00004713, \alpha_R = 0.00002$

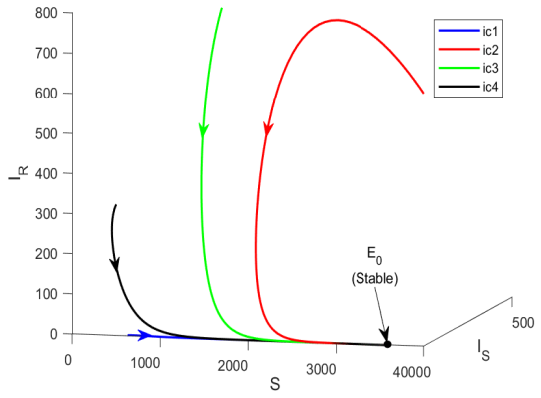

(b) $\alpha_S = 0.00004713, \alpha_R = 0.00002$

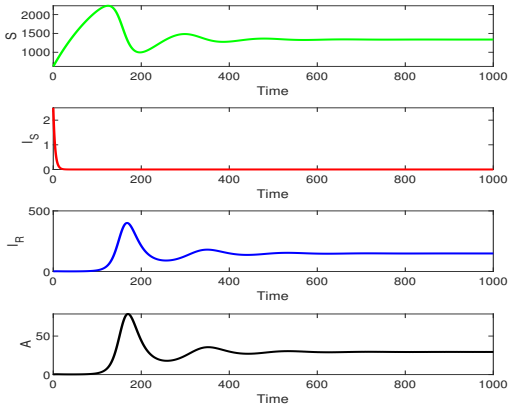

(c) $\alpha_S = 0.00004713, \alpha_R = 0.00008$

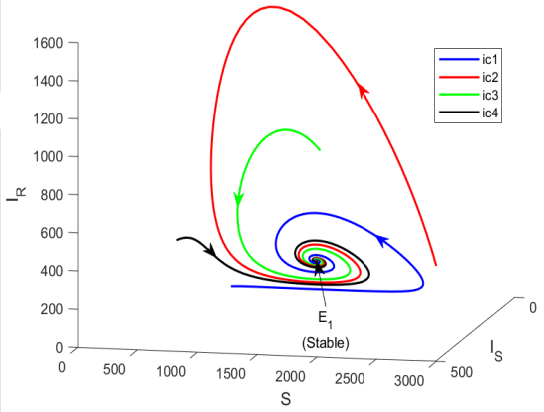

(d) $\alpha_S = 0.00004713, \alpha_R = 0.00008$

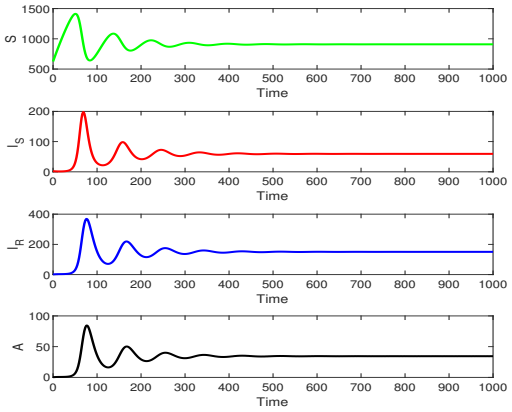

(e) $\alpha_S = 0.0003, \alpha_R = 0.00002$

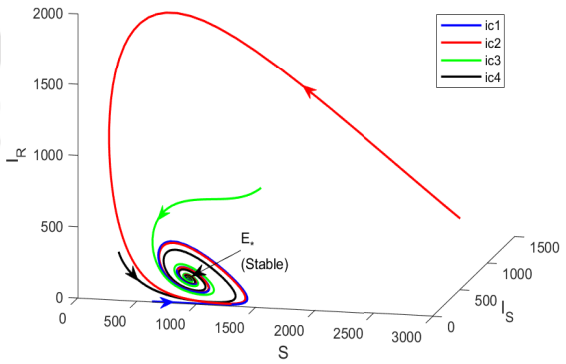

(f) $\alpha_S = 0.0003, \alpha_R = 0.00002$

Figure 4.2: Time series plots and phase portraits for model (4.1.1) under various initial conditions. The remaining values of parameters are as in Table 4.3.

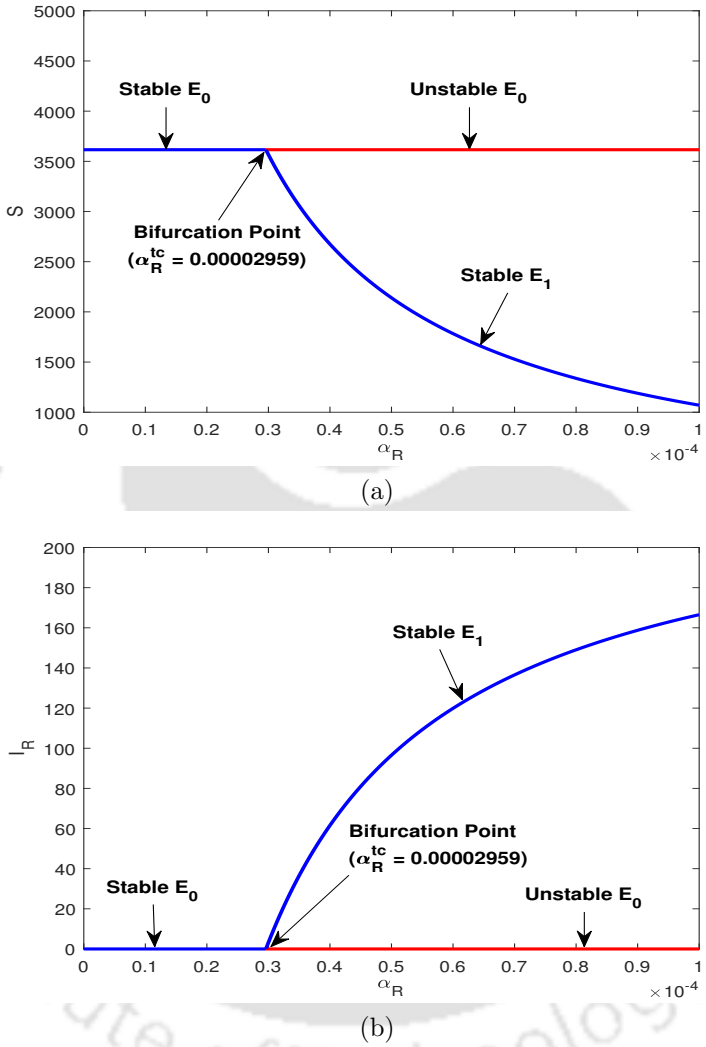

Figure 4.3: Transcritical bifurcation diagrams with respect to parameter α_R. The blue and red curves show the corresponding population level at the existing stable and unstable equilibrium points, respectively. Rest of the parameter values are same as described in Table 4.3.

and it is stable. As we increase the value of α_R and it crosses α_R^{tc}, a new equilibrium point E_1 occurs into the system with positive drug-resistant infected population level. Also, E_0 becomes unstable and exchange its stability with E_1 at $\alpha_R = \alpha_R^{tc}$. This set of parameter values provides the numerical values for the coefficients denoted as τ_2 and τ_3 in Theorem 4.2.13, with the specific values being 3615.71 (> 0) and -9.047×10^{-4} (< 0), respectively. This confirms that the bifurcation is progressing in the forward direction. These numerical results and Figure 4.3 are in accordance with Theorem 4.2.13.

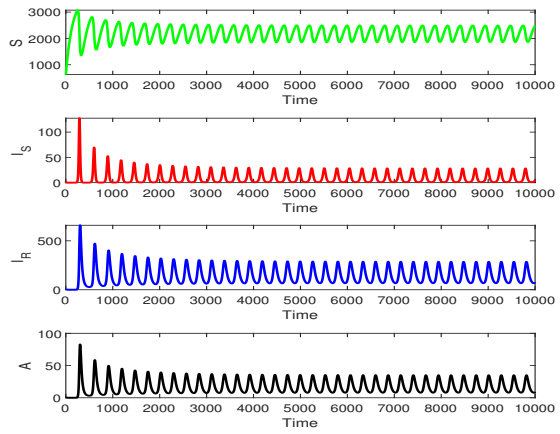

(a) $\alpha_S = 0.000125,\ \alpha_R = 0.000025,\ \beta_R = 0.059$

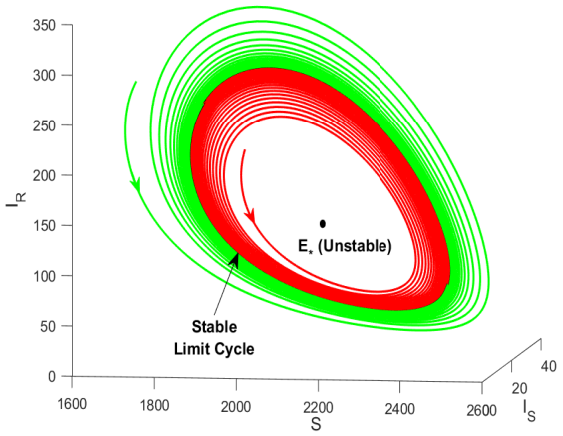

(b) $\alpha_S = 0.000125,\ \alpha_R = 0.000025,\ \beta_R = 0.059$

Figure 4.4: (a) Time series plots for different compartments of the system (4.1.1) revealing oscillatory behaviour of solutions. (b) Phase portrait for the system (4.1.1) using two distinct initial conditions confirming the existence of a stable limit cycle around the co-existence endemic equilibrium point. Rest of the parameter values are same as described in Table 4.3.

Now we consider a new set of parameters to illustrate the periodic behaviour of the solutions of the system (4.1.1). Let $\alpha_S = 0.000125,\ \alpha_R = 0.000025,\ \beta_R = 0.059$ and other parameters are same as in Table 4.3. For this set of parameters, the basic reproduction numbers are $R_0^{(S)} = 1.66 > 1$, $R_0^{(R)} = 1.37 > 1$, $R_0^{(SR)} = 1.21 > 1$ and the system exhibits three equilibrium points $E_0(3615.71, 0, 0, 0)$, $E_1(2640, 0, 103.48, 12.04)$ and $E_*(2182, 7.46, 146.66, 25.16)$. Also, the coefficients of the characteristic equation (4.2.11) are $A_1 = 0.023 > 0$, $A_2 = 5.8728 \times 10^{-4} > 0$, $A_3 = 1.4364 \times 10^{-5} > 0$ and $A_1A_2 - A_3 = -8.27584 \times 10^{-7} \approx 0$, which does not satisfy the Routh-Hurwitz condition provided in the Theorem 4.2.10. Therefore, all three existing equilibrium points are unstable. The time series plot with initial condition ic_1 in Figure 4.4a shows the periodic behaviour of the solutions. Further, the phase portrait in Figure 4.4b confirms the existence of a stable limit cycle around the equilibrium point E_* as both solutions with initial conditions $(1700, 15.7, 277.5, 33.5)$ (in green color) and

$(2000, 5.8, 221.7, 20)$ (in red color) are converging to the limit cycle (in black color).

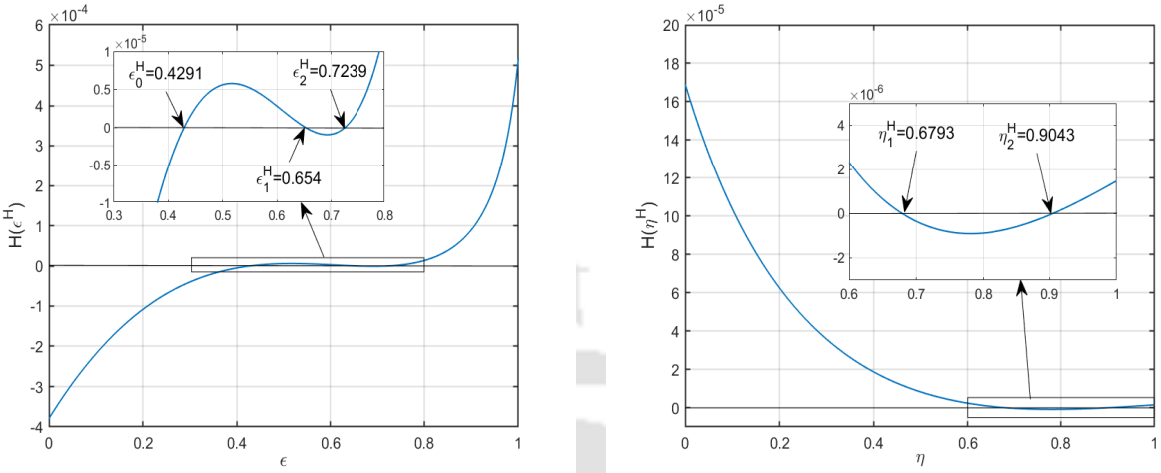

(a) (b)

Figure 4.5: (a). Plot for the equation $H(\epsilon^H) = 0$ on ϵH-plane for the parameter values $\alpha_S = 0.000125,\ \alpha_R = 0.000025,\ \beta_R = 0.059,\ \eta = 0.75$. (b). Plot for the equation $H(\eta^H) = 0$ on ηH-plane for the parameter values $\alpha_S = 0.000125,\ \alpha_R = 0.000025,\ \beta_R = 0.059,\ \epsilon = 0.7$. Rest of the parameteric values are same as described in Table 4.3.

Given that the co-existence endemic equilibrium point losses its stability on the occurrence of the limit cycle, we look for the existence of Hopf-bifircation with respect to the parameters ϵ and η. For above set of parameters, the equation $H(\epsilon^H) = 0$ in Theorem 4.2.14 has three roots $\epsilon_0^H = 0.4291,\ \epsilon_1^H = 0.654$ and $\epsilon_2^H = 0.7239$ in the interval $[0, 1]$ as shown in Figure 4.5a, where the blue curve represents the equation $H(\epsilon^H) = 0$. Also, note that the existence condition for the equilibrium point E_*, that is $\min\{1, R_0^{(S)}, R_0^{(RS)}\} = 1$, satisfied only for $\epsilon \in [0.6213, 1]$ (see Figure 4.6). Therefore, the Hopf-bifucation will occur only at bifurcation points $\epsilon = \epsilon_1^H$ and $\epsilon = \epsilon_2^H$. The sets of eigenvalues of the Jacobian matrix $J\big|_{E_*}$ at $\epsilon = \epsilon_1^H$ and $\epsilon = \epsilon_2^H$ are $(-0.507, -0.0151, -2.2551\times10^{-17}\pm0.0179i)$ and $(-0.507, -0.0273, -1.5612\times 10^{-17} \pm 0.0274i)$, respectively. Note that, the real parts of these eigenvalues are either negative or almost zero. The transversality condition for the Hopf-bifurcation also satisfies as $\left.\frac{dH(\epsilon)}{d\epsilon}\right|_{\epsilon=\epsilon_1^H} = -1.9161 \times 10^{-5} (\neq 0)$ and $\left.\frac{dH(\epsilon)}{d\epsilon}\right|_{\epsilon=\epsilon_2^H} = 1.3042 \times 10^{-5} (\neq 0)$. Therefore, we conclude from Theorem 4.2.14 that the co-existence equilibrium point changes its stability through the Hopf-bifurcation at $\epsilon_1^H = 0.654$ and $\epsilon_2^H = 0.7239$. Similarly, if we fix $\epsilon = 0.7$ and vary η in the interval $[0, 1]$, we observe that the equilibrium point E_* exists throughout the interval as shown in Figure 4.6. The equation $H(\eta^H) = 0$ in Theorem 4.2.15 has two roots $\eta_1^H = 0.6793$ and $\eta_2^H = 0.9043$ in this interval (see Figure 4.5b). The sets of eigenvalues of the

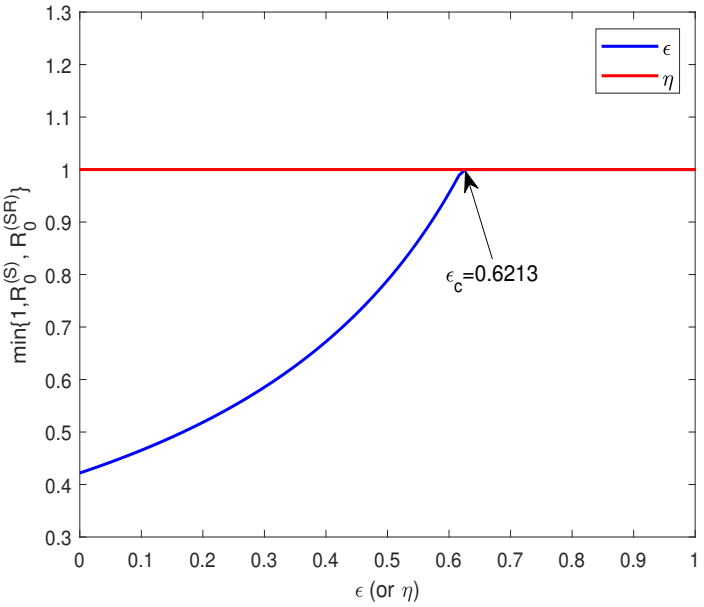

Figure 4.6: Plot for the $\min\{1, R_0^{(S)}, R_0^{(RS)}\}$ corresponding to different values of parameters ϵ (blue) or η (red) in the interval $[0, 1]$. The parameter values for red curve are $\alpha_S = 0.000125$, $\alpha_R = 0.000025$, $\beta_R = 0.059$, $\eta = 0.75$ and for blue curve are $\alpha_S = 0.000125$, $\alpha_R = 0.000025$, $\beta_R = 0.059$, $\epsilon = 0.7$. Rest of the parameter values are same as described in Table 4.3.

Jacobian matrix $J\big|_{E_*}$ at $\eta = \eta_1^H$ and $\eta = \eta_2^H$ are $(-0.507, -0.0269, -4.3368\times10^{-18}\pm0.0272i)$ and $(-0.507, -0.0149, -1.7347\times10^{-17}\pm0.0177i)$, respectively, which have eigenvalues with real parts as either negative or almost zero. Also, we get the transversality conditions $\left.\frac{dH(\eta)}{d\eta}\right|_{\eta=\eta_1^H} = -1.9161\times10^{-5}(\neq 0)$ and $\left.\frac{dH(\eta)}{d\eta}\right|_{\eta=\eta_2^H} = 1.3042\times10^{-5}(\neq 0)$. Therefore, all the conditions in Theorem 4.2.15 have been satisfied for the existence of the Hopf-bifurcation in the system and we conclude that the equilibrium point E_* changes its stability at $\eta_1^H = 0.6793$ and $\eta_2^H = 0.9043$. These results have been illustrated geometrically in Figure 4.7 and Figure 4.8. In these figures, the the red dots before and after bifurcation points show the corresponding population level at the equilibrium point E_*. The red and blue dots in between both bifurcation points show the minimum and maximum level of the corresponding population in a limit cycle. These bifurcation diagrams indicate that the equilibrium point E_* is stable until the bifurcation parameter (ϵ or η) reaches to the first bifurcation point (ϵ_1^H or η_1^H). The stable limit cycle occurs into the system after this critical value of the bifurcation point and the equilibrium point becomes unstable. Once the bifurcation parameter crosses the second bifurcation point (ϵ_2^H or η_2^H), the solutions of the system (4.1.1) lose their periodic nature and converge to the stable equilibrium point E_*. This analysis suggests that the nature of the Hopf-bifurcation is supercritical.

4.5 Conclusion

In this chapter, we proposed a novel non-linear mathematical model of susceptible, drug-sensitive infected, drug-resistant infected and AIDS infected population to understand the impact of the treatment availability and adherence to the treatment in controlling the HIV spread in a community. We have assumed that the susceptibility to HIV infection is only due to sexual exposure, and effective sexual contact transmits the same strain to newly infected individuals. We have also assumed that ART is not substantially effective in reducing the transmission of the infection and, therefore, have not considered a separate compartment for the individuals undergoing treatment. We found that the proposed system exhibits one disease-free and two endemic equilibrium points. In the endemic equilibrium state, the drug-sensitive infected population may become extinct, but the drug-resistant infected population always remains on a positive level. We determined the basic reproduction number related to drug-sensitive ($R_0^{(S)}$) and drug-resistant ($R_0^{(R)}$) strain by using the next generation matrix approach. The local and global stability analysis has been carried out for these equilibrium points. These findings align with observations made in the previous two strain models [100]. The disease free equilibrium point is locally as well as globally asymptotically stable if both

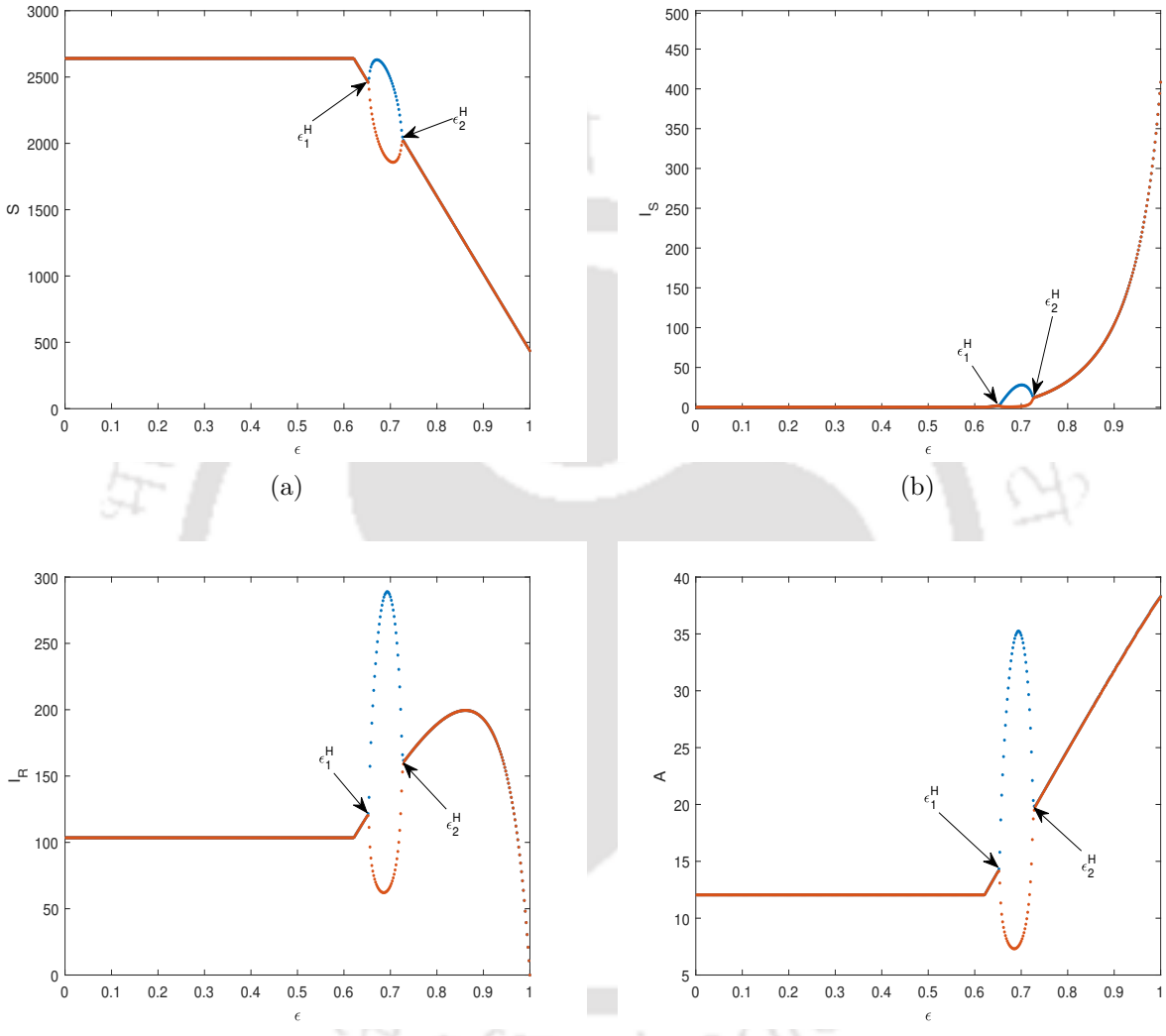

Figure 4.7: The Hopf-bifurcation diagram for each population of the system (4.1.1) with respect to parameter ϵ for $\alpha_S = 0.000125$, $\alpha_R = 0.000025$, $\beta_R = 0.059$, $\eta = 0.75$. Rest of the parameteric values are same as described in Table 4.3.

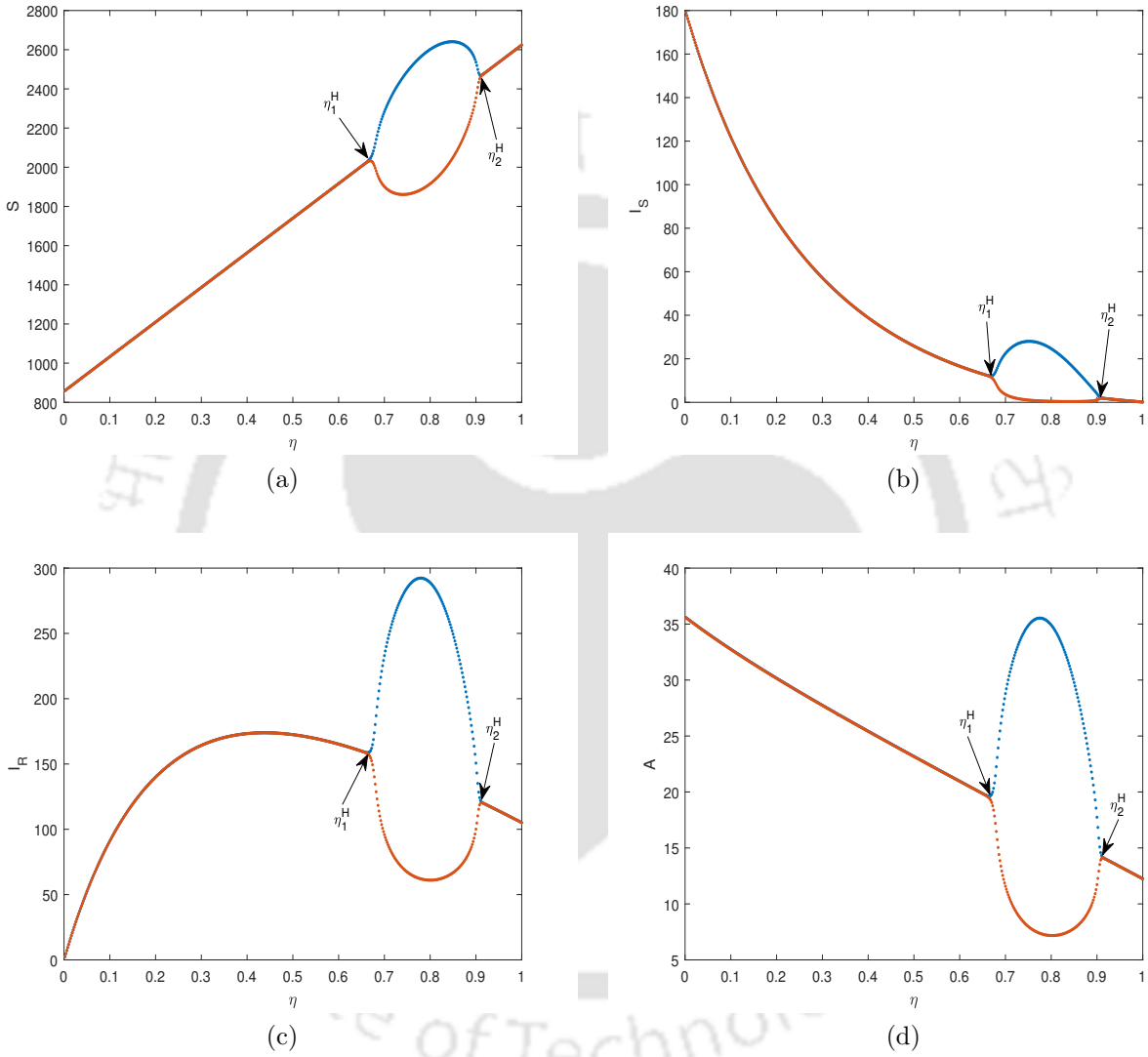

Figure 4.8: The Hopf-bifurcation diagram for each population of the system (4.1.1) with respect to parameter η for $\alpha_S = 0.000125$, $\alpha_R = 0.000025$, $\beta_R = 0.059$, $\epsilon = 0.7$. Rest of the parameter values are same as described in Table 4.3.

$R_0^{(S)}$ and $R_0^{(R)}$ are less than 1. When $R_0^{(R)} < R_0^{(R)}$ with $R_0^{(R)} > 1$, the drug-resistant infected population persists for a very long time, while the drug-sensitive infected population gets eliminated within a very short period. This shows that the ratio of transmission rates α_S and α_R must be limited by a threshold value in order to eliminate the drug-sensitive strain from the system. Otherwise, all the infected population co-exist in the system if $R_0^{(S)} > 1$ and $R_0^{(R)} > R_0^{(R)}$, either at a constant level or vary periodically depending upon the conditions provided in Theorem 4.2.10 and Theorem 4.2.11. This indicates that the recruitment rate of the susceptible population has a direct positive impact on the drug-sensitive infected as well as drug-resistant infected populations. Likewise, a higher transmission rate of the drug-sensitive (or drug-resistant) strain leads to a greater number of individuals being infected with the drug-sensitive (or drug-resistant) variant. The strain replacement is also possible for the system, and it depends on the relative fitness of both strains. The analysis shows that a relatively higher transmission rate of the drug-resistant infected population from the susceptible population is directly linked to the strain replacement.

The analysis of the basic reproduction number for drug-sensitive strain shows that it is negatively correlated with the transfer rates ρ, γ and β_S. Similarly, the basic reproduction number of drug-resistance strain is inversely proportional to the transfer rate β_R. The drug adherence level (ϵ) and the treatment availability (η) are key parameters in deciding the system dynamics as the basic reproduction number is not uniformly dependent on them. Condition (4.2.5), which suggests a positive effect of the treatment availability in eradicating the drug-sensitive strain from the system. In a system, the primary goals of the policymakers are to reduce the disease burden and control the risk factors associated with it. In the presence of the treatment, the equation (4.2.5) suggests that we should focus on reducing the transfer rate β_S rather than ρ or γ to implement the treatment policies successfully. We can bring down the transfer rate β_S by controlling the growth of the drug-sensitive infected population, as a part of them are unaware of their disease status. There are some scenarios where it might be a key factor to reduce the drug-sensitive infected population, in the presence of the treatment, on the cost of an increased number of the drug-resistant infected population to control the overall burden of the disease. These scenarios can be as follows: (a) if we consider that the drug-resistant infected population is aware of their disease status and makes fewer contacts than the drug-sensitive infected population, and (b) if the drug-resistant strain of the virus has less transmissibility, which is backed by several studies [166, 173]. However, a lower transfer rate β_S will put some extra burden on the healthcare system as more people will be under treatment. Still, if the health care system can handle this burden, it is a more effective way to reduce the overall infected population.

We have also performed a comprehensive bifurcation analysis for the proposed model.

The system exhibits forward transcritical bifurcation with respect to the bifurcation parameter α_R. The disease-free equilibrium point exchanges its stability with the drug-resistant strain endemic equilibrium point at a threshold value of the parameter α_R. The forward direction signifies the impact of α_R on the emergence of the endemic. Our focus should be on controlling the parameter α_R to prevent this stability exchange if the disease burden is under control. An extensive theoretical and numerical analysis have been carried out to determine the Hopf-bifurcation with respect to the parameters ϵ and η. Numerical analysis of the model suggests that the co-existence endemic equilibrium point is stable for lower and higher values of these parameters and becomes unstable for medium-level values. The existence of Hopf-bifurcation signifies critical values of these bifurcation parameters where the co-existence endemic equilibrium point shows a shift from stable to oscillatory behaviour and vice versa. It indicates the onset of cyclic epidemic states of the disease for a specific range of these bifurcation parameters. Identifying these critical values is very important for epidemiologists in order to propose an intervention strategy or control policy for the disease. Since HIV/AIDS is a chronic disease and policies are generally proposed for a long time horizon, it is crucial that the system remains in a stable state rather than showing an oscillatory behaviour. To consider appropriate preventive measures, we should know the disease burden levels for a long time period. The oscillatory behaviour of the solutions around the co-existence endemic state is not favourable to propose any control strategy to eradicate the infection from a community.

In summary, we conclude that the persistence of an endemic state exclusively characterized by the presence of the drug-sensitive infected population is not possible. Our study suggests that better treatment availability is not enough to control the overall disease burden, as it can increase the drug-resistance issue under sub-optimal drug adherence. This result is consistent with studies on the transmission of drug resistance within a host [174] and a community [175]. With higher treatment resources, an adequate adherence level is also necessary to curb the disease and prevent any endemic of novel drug-resistant strain. Various strategies for enhancing the drug adherence to ART based on individual and institutional levels have been discussed in the literature [176, 177]. The treatment availability and the drug adherence level are key parameters in the spread dynamics of HIV in a community. There are some cases where it might be helpful to focus more on a particular compartment of the infected population than others as a better control strategy. We have discussed some situations where policy makers should focus on controlling only drug-sensitive infected population to reduce the overall burden of the disease.

Chapter 5

Strategic Control of Drug-Resistant HIV With Treatment Switching

A central challenge in HIV public health policy lies in determining whether to universally expand treatment access, despite the risk of sub-optimal adherence and consequent drug resistance, or to adopt a more strategic allocation of resources that balances treatment coverage with adherence support. This dilemma is further complicated by the need for timely switching to second-line therapy, which is critical for managing treatment failure but imposes additional burdens on limited healthcare resources. In this chapter, we develop and analyze a compartmental model of HIV transmission that incorporates both drug-sensitive and drug-resistant strains, diagnosis status, and treatment progression, including switching to second-line therapy upon detection of resistance. Basic reproduction numbers for both strains are derived, and equilibrium analysis reveals the existence of a disease-free state and two endemic states, where the drug-sensitive strain may be eliminated while the drug-resistant strain persists. Local and global sensitivity analyses are performed, using partial rank correlation coefficient (PRCC) and Sobol methods, to identify key parameters influencing different model outcomes. We extend the model using optimal control theory to assess multiple intervention strategies targeting diagnosis, treatment initiation, and adherence. A novel dynamic control framework is proposed to achieve the UNAIDS 95-95-95 targets through efficient resource allocation. Numerical simulations validate the analytical results and compare the effectiveness and cost-efficiency of control strategies. Our findings highlight that long-term HIV epidemic control depends critically on prioritizing adherence-focused interventions alongside efforts to expand first-line treatment coverage.

5.1 Formulation of the Mathematical Model

To construct a multi-strain mathematical model that represents the transmission dynamics of HIV with multiple treatment options and drug adherence, we use the compartmental modelling framework based on different stages of the infection. The total sexually active population is categorized into eight mutually exclusive compartments: susceptible individuals (S), undiagnosed and infected individuals with the drug-sensitive strain (I_{SU}), diagnosed and infected individuals with the drug-sensitive strain (I_{SD}), individuals receiving first-line treatment (T_1), undiagnosed and infected individuals with the drug-resistant strain (I_{RU}), diagnosed and infected individuals with the drug-resistant strain (I_{RD}), individuals receiving second-line treatment (T_2), and individuals who have progressed to AIDS (A). The transitions of population among these compartments with time are governed by a system of coupled nonlinear ordinary differential equations presented as follows:

$$\begin{aligned}
S' &= \lambda - \alpha_S S(I_{SU} + cI_{SD}) - \alpha_R S(I_{RU} + cI_{RD}) - \mu S,\\
I'_{SU} &= \alpha_S S(I_{SU} + cI_{SD}) - k_S I_{SU} - \theta_1 I_{SU} - \mu I_{SU},\\
I'_{SD} &= k_S I_{SU} - \beta_S \eta_1 I_{SD} - \theta_1(1-\eta_1) I_{SD} - \mu I_{SD},\\
T'_1 &= \beta_S \eta_1 I_{SD} - \gamma(1-\epsilon) T_1 - \theta_2 \epsilon T_1 - \mu T_1,\\
I'_{RU} &= \alpha_R S(I_{RU} + cI_{RD}) + \gamma(1-\epsilon) T_1 - k_R I_{RU} - \theta_1 I_{RU} - \mu I_{RU},\\
I'_{RD} &= k_R I_{RU} - \beta_R \eta_2 I_{RD} - \theta_1(1-\eta_2) I_{RD} - \mu I_{RD},\\
T'_2 &= \beta_R \eta_2 I_{RD} - \theta_2 T_2 - \mu T_2,\\
A' &= \theta_1 I_{SU} + \theta_1(1-\eta_1) I_{SD} + \theta_2 \epsilon T_1 + \theta_1 I_{RU} + \theta_1(1-\eta_2) I_{RD} + \theta_2 T_2 - (\mu + \mu_d) A,
\end{aligned} \tag{5.1.1}$$

with the initial condition $(S(0), I_{SU}(0), I_{SD}(0), T_1(0), I_{RU}(0), I_{RD}(0), T_2(0), A(0))$ to lie within the biologically feasible region $\mathcal{R}$, defined as,

$$\mathcal{R} = \left\{ (S, I_{SU}, I_{SD}, T_1, I_{RU}, I_{RD}, T_2, A) \in \mathbb{R}^8_+ : 0 \leq S + I_{SU} + I_{SD} + T_1 + I_{RU} + I_{RD} + T_2 + A \leq \frac{\lambda}{\mu} \right\},$$

where $\mathbb{R}^8_+$ refers to the non-negative orthant along with its lower-dimensional faces.

The susceptible individuals are recruited into the population at a constant rate λ as new individuals become sexually active. These individuals can become infected through effective contact with both drug-sensitive and drug-resistant infected individuals. We assume that effective contact results in the transmission of the same strain to newly infected individuals. The force of infection, expressed as a function of both susceptible and infected individuals, is a critical component of epidemiological modelling. Based on the principle of mass action, we define the force of infection from drug-sensitive individuals as $\alpha_S(I_{SU} + cI_{SD})$, and from

drug-resistant individuals as $\alpha_R(I_{RU}+cI_{RD})$. The parameter $c \in [0,1]$ captures the reduction in transmission rate of diagnosed individuals compared to undiagnosed ones. This reduction reflects the behavioral change following diagnosis, as individuals who are aware of their HIV positive status are less likely to engage in risk-prone behavior. Once infected, susceptible individuals move into undiagnosed compartments (I_{SU} or I_{RU}) based on whether the infection is acquired from a drug-sensitive or drug-resistant individual. Undiagnosed individuals may get tested and become diagnosed at rates k_S (for I_{SU}) and k_R (for I_{RU}), or may progress directly to the AIDS stage at rate θ_1 if not tested in time, where θ_1 is the conversion rate of untreated infected population to the population in AIDS stage. While diagnosis helps in earlier detection of infection, its impact on transmission remains limited unless it is promptly followed by an effective treatment initiation. We assume that first-line treatment coverage is limited to a fraction (η_1) of the diagnosed drug-sensitive infected population, due to resource constraints. This fraction initiates first-line treatment at rate β_S, while the remaining $(1-\eta_1)$ progresses to the AIDS stage at rate θ_1.

Further, we assume that only a fraction ϵ of individuals receiving first-line treatment are adherent, while the remaining fraction $(1-\epsilon)$ are non-adherent. Individuals under treatment are considered non-infectious, as effective treatment suppresses viral load to levels that prevent onward transmission. However, the non-adherent individuals are assumed to develop drug resistance and, unlike adherent individuals, do not progress directly to the AIDS stage. Instead, they transition to the undiagnosed drug-resistant infected compartment (I_{RU}) at a rate γ. In contrast, adherent individuals progress to the AIDS stage at a reduced rate θ_2, as treatment suppresses but does not cure the infection. Note that the progression rate to AIDS for untreated infected individuals (θ_1) is significantly higher than that of those receiving optimal treatment (θ_2). After the diagnosis of drug-resistant infection, the second-line treatment is given to only a fraction η_2, reflecting constraints in resource availability, at a rate β_R. The remaining fraction of diagnosed drug-resistant infected individuals progresses to the AIDS stage at a rate θ_1. For those receiving second-line treatment, we assume full adherence due to the advanced stage of infection and enhanced medical supervision. Consequently, these individuals progress to the AIDS stage at a rate θ_2. Individuals in the AIDS stage are assumed to be sufficiently aware of their condition to not contribute to further transmission. A natural death rate μ applies uniformly across all compartments. Since these treatments cannot cure the infection but only delay disease progression, all infected individuals are assumed to eventually progress to the AIDS stage unless they die naturally beforehand. Consequently, we consider disease-induced mortality to occur exclusively in the AIDS compartment, with a rate μ_d. All model parameters and their biological interpretations are summarized in Table 5.1, and a schematic representation of the system (5.1.1) is

presented in Figure 5.1.

Parameter	Biological Description
λ	Recruitment rate of susceptible individuals
α_S	Transmission rate per effective contact between a susceptible individual and a drug-sensitive infected individual
α_R	Transmission rate per effective contact between a susceptible individual and a drug-resistant infected individual
k_S	Diagnosis rate of infection among drug-sensitive infected individuals
k_R	Diagnosis rate of infection among drug-resistant infected individuals
c	Relative infectiousness of diagnosed individuals compared to undiagnosed individuals
θ_1	Progression rate of infection in untreated infected individuals to AIDS stage
θ_2	Progression rate of infection in optimally adherent treated infected individuals to AIDS stage
β_S	First-line treatment initiation rate for diagnosed drug-sensitive infected individuals
β_R	Second-line treatment initiation rate for diagnosed drug-resistant infected individuals
γ	Rate at which non-adherent individuals develop drug resistance
η_1	Proportion of diagnosed drug-sensitive infected individuals receiving first-line treatment
η_2	Proportion of diagnosed drug-resistant infected individuals receiving second-line treatment
ϵ	Proportion of individuals receiving first-line treatment who are adherent
μ	Natural death rate
μ_d	Disease-induced death rate

Table 5.1: Parameters and their biological descriptions for the system (5.1.1).

5.2 Mathematical Analysis of the Model

To understand the long-term behavior of the system and its sensitivity to changes in epidemiological parameters, we identify the equilibrium points and analyze their local stability. This section explores the parameter conditions under which the disease either dies out or persists in the population. In addition, we examine whether the coexistence of both drug-sensitive and drug-resistant strains is possible, and if so, determine the conditions that enable

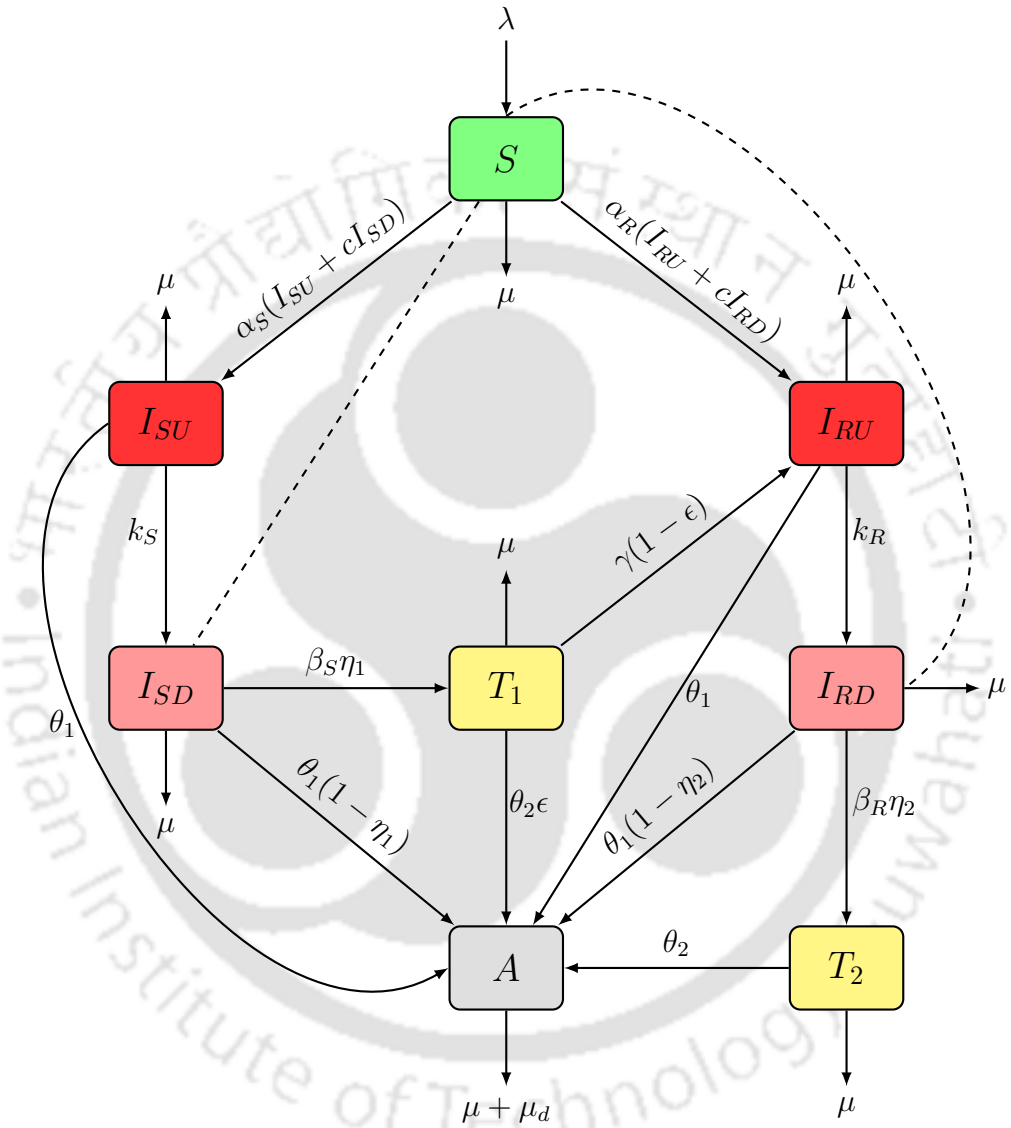

Figure 5.1: Schematic representation of the system (5.1.1). Solid arrows represent direct transitions between compartments resulting from effective contact, while dashed arrows indicate the presence of effective contacts that contribute to infection risk, without resulting in transitions to the contacted compartment.

such coexistence. But first we establish a preliminary result regarding the non-negativity and boundedness of the model solutions, which ensures that the system is biologically well-posed.

5.2.1 Uniqueness, non-negativity and boundedness of the solutions

The right-hand side of the system (5.1.1) is continuous and Lipschitz on $[0, a]$, $a > 0$. Therefore, the system (5.1.1) with the initial condition $(S(0), I_S(0), T(0), I_R(0)) \in \mathbb{R}^4_+$ has a unique solution. To guarantee the biological feasibility, we present the following theorem.

Theorem 5.2.1. *The biologically feasible region $\mathcal{R}$ is a positively invariant set for the system (5.1.1). This implies that any solution $(S(t), I_{SU}(t), I_{SD}(t), T_1(t), I_{RU}(t), I_{RD}(t), T_2(t), A(t))$ of the system, starting from an initial condition $(S(0), I_{SU}(0), I_{SD}(0), T_1(0), I_{RU}(0), I_{RD}(0), T_2(0), A(0)) \in \mathcal{R}$, will remain within the region $\mathcal{R}$ for all $t > 0$.*

Proof. The proof of this theorem follows a similar approach to that of Theorem 4.2.1 of Chapter 4. □

5.2.2 Equilibrium points and their stability properties

In the system (5.1.1), the first seven equations are independent of the AIDS compartment (A). The eighth equation, corresponding to the dynamics of A, can be solved separately and yields a positive value for A whenever the other state variables are positive. Therefore, we focus on the following reduced system for further analysis.

$$\begin{aligned}
S' &= \lambda - \alpha_S S(I_{SU} + cI_{SD}) - \alpha_R S(I_{RU} + cI_{RD}) - \mu S \\
I'_{SU} &= \alpha_S S(I_{SU} + cI_{SD}) - A_1 I_{SU} \\
I'_{SD} &= k_S I_{SU} - A_2 I_{SD} \\
T'_1 &= \beta_S \eta_1 I_{SD} - A_3 T_1 \\
I'_{RU} &= \alpha_R S(I_{RU} + cI_{RD}) + \gamma(1-\epsilon)T_1 - A_4 I_{RU} \\
I'_{RD} &= k_R I_{RU} - A_5 I_{RD} \\
T'_2 &= \beta_R \eta_2 I_{RD} - A_6 T_2
\end{aligned} \tag{5.2.1}$$

where $A_1 = k_S + \theta_1 + \mu$, $A_2 = \beta_S \eta_1 + \theta_1(1-\eta_1) + \mu$, $A_3 = \gamma(1-\epsilon) + \theta_2 \epsilon + \mu$, $A_4 = k_R + \theta_1 + \mu$, $A_5 = \beta_R \eta_2 + \theta_1(1-\eta_2) + \mu$, $A_6 = \theta_2 + \mu$.

Disease elimination and basic reproduction numbers

The elimination of the infection from the system is contingent on the existence of a disease free equilibrium state and its stability. In order to obtain the disease free equilibrium

(DFE) point of the system (5.2.1), we set all variables to zero which are either infectious ($I_{SU},\ I_{SD},\ I_{RU},\ I_{RD}$) or infected ($T_1,\ T_2$) and find the steady state of non-infected variable (S). As a result, the DFE point is given by,

$$\begin{aligned} E^{(0)} &= \left(S^{(0)}, I_{SU}^{(0)}, I_{SD}^{(0)}, T_1^{(0)}, I_{RU}^{(0)}, I_{RD}^{(0)}, T_2^{(0)}\right) \\ &= \left(\frac{\lambda}{\mu}, 0, 0, 0, 0, 0, 0\right). \end{aligned}$$

This indicates that the whole population becomes susceptible to HIV infection once DFE point is achieved. Note that, although, this is an ideal situation which is most likely to be unachievable in short term, we still need further mathematical investigation to derive some conditions under which the solutions of the system (5.2.1) converge to the DFE point. For that, first we determine the basic reproduction number for the system as well as individual viral strains, which will provide crucial insights for the dynamics of the presented model. Since we have four types of infectious individuals in the system, the reduced infection subsystem linearized about the DFE point is as follows

$$\dot{x} = (F + V)x,$$

where $x = (I_{SU}, I_{SD}, I_{RU}, I_{RD})^T \in \mathbb{R}_+^4$. Also, F and V are Jacobian matrices at point $E^{(0)}$, given by

$$F = \begin{pmatrix} \frac{\lambda\alpha_S}{\mu} & \frac{\lambda c\alpha_S}{\mu} & 0 & 0 \\ 0 & 0 & 0 & 0 \\ 0 & 0 & \frac{\lambda\alpha_R}{\mu} & \frac{\lambda c\alpha_R}{\mu} \\ 0 & 0 & 0 & 0 \end{pmatrix}, \quad V = \begin{pmatrix} A_1 & 0 & 0 & 0 \\ -k_S & A_2 & 0 & 0 \\ 0 & 0 & A_4 & 0 \\ 0 & 0 & -k_R & A_5 \end{pmatrix},$$

which correspond to the transmission of the virus, describing the production of newly infected individuals and the transition of infectiousness, describing the change in status of infected individuals, respectively. Therefore, the next generation matrix (FV^{-1}) is obtained as,

$$FV^{-1} = \begin{pmatrix} \frac{\lambda\alpha_S(A_2+ck_S)}{\mu A_1 A_2} & \frac{\lambda c\alpha_S}{\mu A_2} & 0 & 0 \\ 0 & 0 & 0 & 0 \\ 0 & 0 & \frac{\lambda\alpha_R(A_5+ck_R)}{\mu A_4 A_5} & \frac{\lambda c\alpha_R}{\mu A_5} \\ 0 & 0 & 0 & 0 \end{pmatrix}.$$

The basic reproduction number (R_0) for system (5.2.1) is the spectral radius or dominant eigenvalue of the next generation matrix FV^{-1}. Therefore, $R_0 = \max\{R_0^{(S)}, R_0^{(R)}\}$, where

$$R_0^{(S)} = \frac{\lambda\alpha_S\left(A_2 + ck_S\right)}{\mu A_1 A_2} = \frac{\lambda\alpha_S\left(\beta_S\eta_1 + \theta_1(1-\eta_1) + \mu + ck_S\right)}{\mu(k_S + \theta_1 + \mu)(\beta_S\eta_1 + \theta_1(1-\eta_1) + \mu)},$$

and

$$R_0^{(R)} = \frac{\lambda\alpha_R\left(A_5 + ck_R\right)}{\mu A_4 A_5} = \frac{\lambda\alpha_R\left(\beta_R\eta_2 + \theta_1(1-\eta_2) + \mu + ck_R\right)}{\mu(k_R + \theta_1 + \mu)(\beta_R\eta_2 + \theta_1(1-\eta_2) + \mu)}.$$

Additionally, we define the "relative basic reproduction number" as the ratio of $R_0^{(S)}$ and $R_0^{(R)}$. This quantity signifies the strength of the dominance of the sensitive strain over the resistant strain in terms of transmission potential. The relative basic reproduction number is denoted as $R_0^{(SR)}$, which is given by:

$$\begin{aligned} R_0^{(SR)} &= \frac{\alpha_S A_4 A_5 \left(A_2 + ck_S\right)}{\alpha_R A_1 A_2 \left(A_5 + ck_R\right)} \\ &= \frac{\alpha_S \left(\beta_S \eta_1 + \theta_1(1-\eta_1) + \mu + ck_S\right)\left(k_R + \theta_1 + \mu\right)\left(\beta_R \eta_2 + \theta_1(1-\eta_2) + \mu\right)}{\alpha_R \left(\beta_R \eta_2 + \theta_1(1-\eta_2) + \mu + ck_R\right)\left(k_S + \theta_1 + \mu\right)\left(\beta_S \eta_1 + \theta_1(1-\eta_1) + \mu\right)}. \end{aligned}$$

The basic reproduction number $R_0^{(S)}$(or $R_0^{(R)}$) quantifies the average number of secondary infections caused by a single individual infected with the drug-sensitive (or drug-resistant) strain in a fully susceptible population. Each basic reproduction number can be decomposed into two additive components corresponding to transmission from undiagnosed and diagnosed infected individuals. In $R_0^{(S)}$, the term $\frac{\lambda \alpha_S}{\mu A_1}$ captures the contribution from drug-sensitive undiagnosed individuals (I_{SU}), where $\lambda \alpha_S$ reflects the inflow due to new infections and $\frac{1}{\mu A_1}$ shows the effective infectious period, influenced by the removal through progression to other compartments or natural death. The additional term $\frac{\lambda \alpha_S c k_S}{\mu A_1 A_2}$ quantifies the contribution from drug-sensitive diagnosed individuals (I_{SD}). Similarly, $R_0^{(R)}$ includes contributions from the undiagnosed $\left(\frac{\lambda \alpha_R}{\mu A_4}\right)$ and diagnosed $\left(\frac{\lambda \alpha_R c k_R}{\mu A_4 A_5}\right)$ individuals infected with the drug-resistant strain, representing their respective transmission and removal dynamics.

Biologically, these basic reproduction numbers are shaped by various model parameters related to epidemiological, demographic, and behavioral factors. A higher recruitment rate of the susceptible population increases the pool of individuals available for infection, contributing to higher infection levels in the population. The transmission rates α_S and α_R, along with the reduction factor c, directly linked to the disease burden. Diagnosis rates k_S and k_R play a mixed role as they help identify infected individuals early, thereby reducing transmission, but also increase the diagnosed population, which may continue to transmit the infection at a reduced level. As a result, diagnosis contributes both to limiting and sustaining transmission. However, its overall impact remains beneficial in reducing the spread of the disease. The natural death rate μ and the the progression rate to AIDS θ_1 shorten the infectious period, indirectly reducing the average number of secondary cases. Similarly, parameters β_S, β_R, η_1 and η_2 influence the initiation of effective treatment of diagnosed individuals, which in turn reduces overall infectiousness and slows disease progression. In the subsequent analysis, we examine the significance of the basic reproduction numbers in determining the long-term dynamics of the system (5.1.1), as the existence and stability of

equilibrium points depend on these thresholds.

To determine the local behavior of the system (5.2.1) around an equilibrium point, we write the corresponding linearly approximated system as,

$$\dot{X} = J\left(E^{(*)}\right) X,$$

where $X = (S,\ I_{SU},\ I_{SD},\ T_1,\ I_{RU},\ I_{RD},\ T_2)^T$, $E^{(*)} = \left(S^{(*)}, I_{SU}^{(*)}, I_{SD}^{(*)}, T_1^{(*)}, I_{RU}^{(*)}, I_{RD}^{(*)}, T_2^{(*)}\right)$, and $J\left(E^{(*)}\right)$ is the Jacobian matrix of the system (5.2.1) at the equilibrium point $E^{(*)}$, which is given by,

$$J\left(E^{(*)}\right) = \begin{pmatrix} -\alpha_S\left(I_{SU}^{(*)} + cI_{SD}^{(*)}\right) - \alpha_R\left(I_{RU}^{(*)} + cI_{RD}^{(*)}\right) - \mu & -\alpha_S S^{(*)} & -c\alpha_S S^{(*)} & 0 & -\alpha_R S^{(*)} & -c\alpha_R S^{(*)} & 0 \\ \alpha_S\left(I_{SU}^{(*)} + cI_{SD}^{(*)}\right) & \alpha_S S^{(*)} - A_1 & c\alpha_S S^{(*)} & 0 & 0 & 0 & 0 \\ 0 & k_S & -A_2 & 0 & 0 & 0 & 0 \\ 0 & 0 & \beta_S\eta_1 & -A_3 & 0 & 0 & 0 \\ \alpha_R\left(I_{RU}^{(*)} + cI_{RD}^{(*)}\right) & 0 & 0 & \gamma(1-\epsilon) & \alpha_R S^{(*)} - A_4 & c\alpha_R S^{(*)} & 0 \\ 0 & 0 & 0 & 0 & k_R & -A_5 & 0 \\ 0 & 0 & 0 & 0 & 0 & \beta_R\eta_2 & -A_6 \end{pmatrix}. \tag{5.2.2}$$

In order to determine the local stability of the DFE, we calculate the Jacobian matrix $J\left(E^{(0)}\right)$, which has the following characteristic equation,

$$\begin{aligned} p_0(x) =& (x+\mu)(x+A_3)(x+A_6) \\ & \left(\frac{\mu x^2 + (-\lambda\alpha_S + \mu A_1 + \mu A_2)x + (\mu A_1 A_2 - \lambda\alpha_S A_2 - c\lambda k_S\alpha_S)}{\mu}\right) \\ & \left(\frac{\mu x^2 + (-\lambda\alpha_R + \mu A_4 + \mu A_5)x + (\mu A_4 A_5 - \lambda\alpha_R A_5 - c\lambda k_R\alpha_R)}{\mu}\right) = 0. \end{aligned}$$

Clearly, this equation always has three roots with a negative real part $(-\mu, -A_3, -A_6)$. In addition, the remaining four roots will have a negative real part if $R_0^{(S)} < 1$ and $R_0^{(R)} < 1$. From the above discussion, we can propose the following result about the existence and local stability of $E^{(0)}$.

Theorem 5.2.2. *For the system (5.2.1), the disease free equilibrium point $(E^{(0)})$ exists trivially. Further, $E^{(0)}$ is locally asymptotically stable if $R_0 < 1$, otherwise it is unstable.*

Disease persistence

The disease persists in the system if at least one of the drug-sensitive or drug-resistant infected populations maintains a positive level for a long time, which is also referred to as an endemic state. In this subsection, we will discuss all possible endemic states and analyze the conditions necessary for their existence and stability. Based on these conditions, we can determine which parameter to focus on to reduce or eliminate the infection from the system.

The system (5.2.1) has two possible scenarios for disease persistence: one in which only the drug-resistant infected population persists and another in which both drug-sensitive and drug-resistant infected populations coexist.

Drug-resistant strain endemic equilibrium point

To obtain the drug-resistant strain endemic equilibrium point, we set $I_{SU} = 0$ and solve the resulting system of equations derived from the system (5.2.1). The corresponding equilibrium point is given by,

$$E^{(1)} = \left(S^{(1)}, I_{SU}^{(1)}, I_{SD}^{(1)}, T_1^{(1)}, I_{RU}^{(1)}, I_{RD}^{(1)}, T_2^{(1)}, A^{(1)}\right)$$

where,

$$S^{(1)} = \frac{A_4 A_5}{(A_5 + ck_R)\alpha_R},\ I_{SU}^{(1)} = I_{SD}^{(1)} = T_1^{(1)} = 0,\ I_{RU}^{(1)} = \frac{\mu A_5 \left(R_0^{(R)} - 1\right)}{\alpha_R \left(A_5 + ck_R\right)},$$

$$I_{RD}^{(1)} = \frac{\mu k_R \left(R_0^{(R)} - 1\right)}{\alpha_R \left(A_5 + ck_R\right)},\ T_2^{(1)} = \frac{\mu k_R \beta_R \eta_2 \left(R_0^{(R)} - 1\right)}{\alpha_R A_6 \left(A_5 + ck_R\right)}.$$

Note that at the equilibrium state, $I_{SD} = T_1 = 0$, since I_{SU} is the only source compartment for these populations. Clearly, the drug-resistant strain endemic equilibrium point exists if and only if $R_0^{(R)} > 1$. This condition suggests that the transmission and diagnosis rates of the resistant strain, and the availability of second-line therapy play a critical role in determining the existence of $E^{(1)}$. However, the local stability of $E^{(1)}$ may still be influenced by parameters associated with the sensitive strain, even though these compartments are absent in the equilibrium state. To assess the local stability of $E^{(1)}$, we compute the Jacobian matrix $J\left(E^{(1)}\right)$ using (5.2.2). The corresponding characteristic equation is then given by,

$$p_1(x) = (x + A_3)(x + A_6)(x^2 + B_1 x + B_2)(x^3 + C_1 x^2 + C_2 x + C_3) = 0,$$

where

$$B_1 = A_1 + A_2 - \frac{\alpha_S A_4 A_5}{\alpha_R (A_5 + ck_R)},\ B_2 = A_1 A_2 - \frac{\alpha_S A_4 A_5 (A_2 + ck_S)}{\alpha_R (A_5 + ck_R)},$$

$$C_1 = A_5 + \frac{ck_R A_4}{A_5 + ck_R} + \frac{\lambda \alpha_R (A_5 + ck_R)}{A_4 A_5},\ C_2 = \frac{-\mu A_4^2 A_5^2 + \lambda \alpha_R (A_4 + A_5)(A_5 + ck_R)^2}{A_4 A_5 (A_5 + ck_R)},$$

$$C_3 = -\mu A_4 A_5 + \lambda \alpha_R (A_5 + ck_R).$$

Clearly, $p_1(x)$ has two real and negative roots as $-A_3$ and $-A_6$. According to the Routh–Hurwitz criterion [142], $E^{(1)}$ is locally asymptotically stable if the following conditions are satisfied: $B_i > 0$ for $i = 1, 2$; $C_i > 0$ for $i = 1, 2, 3$; and $C_1 C_2 > C_3$.

Let's consider $R_0^{(SR)} < 1$, then we have,

$$\begin{aligned} B_1 &= A_1 + A_2 - \frac{A_1 A_2}{A_2 + ck_S} \frac{R_0^{(S)}}{R_0^{(R)}} \\ &= A_1 \left(1 - \frac{A_2}{A_2 + ck_S} R_0^{(SR)}\right) + A_2 > 0, \\ B_2 &= A_1 A_2 \left(1 - R_0^{(SR)}\right) > 0. \end{aligned}$$

Similarly,

$$\begin{aligned} C_1 &> 0, \\ C_2 &= -\frac{\mu A_4 A_5}{A_5 + ck_R} + \frac{\lambda \alpha_R (A_5 + ck_R)}{A_4} + \frac{\lambda \alpha_R (A_5 + ck_R)}{A_5} \\ &= \frac{-\mu A_4 A_5^2 + \lambda \alpha_R (A_5 + ck_R)^2}{A_5 (A_5 + ck_R)} + \frac{\lambda \alpha_R (A_5 + ck_R)}{A_4} \\ &> \frac{\mu A_4 A_5 \left(R_0^{(R)} - 1\right)}{A_5 + ck_R} > 0, \qquad \left(\because R_0^{(R)} > 1\right) \\ C_3 &= \mu A_4 A_5 \left(R_0^{(R)} - 1\right) > 0. \end{aligned}$$

Also,

$$\begin{aligned} C_1 C_2 - C_3 &= \lambda \alpha_R c k_R - \lambda \alpha_R \mu - \frac{c k_R \mu A_4^2 A_5}{(A_5 + ck_R)^2} + \frac{\lambda \alpha_R c k_R A_4}{A_5} + \frac{\lambda^2 \alpha_R^2 (A_5 + 2ck_R)}{A_4 A_5} \\ &\quad + \frac{c k_R \mu A_4 A_5}{A_5 + ck_R} + \frac{\lambda^2 \alpha_R^2 (A_5 + ck_R)^2}{A_4^2 A_5} + \frac{\lambda \alpha_R (A_5^4 + c k_R A_5^3 + \lambda \alpha_R c^2 k_R^2)}{A_4 A_5^2} \\ &> -\lambda \alpha_R \mu - \frac{c k_R \mu A_4^2 A_5}{(A_5 + ck_R)^2} + \frac{\lambda \alpha_R c k_R A_4}{A_5} + \frac{\lambda^2 \alpha_R^2 (A_5 + 2ck_R)}{A_4 A_5} \\ &> \lambda \alpha_R \mu \left(R_0^{(R)} - 1\right) + \frac{c k_R \mu A_4^2 A_5}{(A_5 + ck_R)^2} \left(R_0^{(R)} - 1\right) > 0. \end{aligned}$$

Based on the above discussion, we propose the following result about the existence and local stability of the drug-resistant strain endemic equilibrium point $E^{(1)}$.

Theorem 5.2.3. *For the system (5.2.1), the drug-resistant strain endemic equilibrium point $E^{(1)}$ exists if and only if $R_0^{(R)} > 1$. Further, $E^{(1)}$ is locally asymptotically stable if $R_0^{(SR)} < 1$, otherwise it is unstable.*

Co-existence endemic equilibrium point

Here, we investigate the simultaneous persistence of drug-sensitive and drug-resistant infected populations by analyzing the co-existence endemic equilibrium of the system (5.2.1).

To identify this equilibrium, we set the right-hand side of the system (5.2.1) to zero and solve the resulting system of algebraic equations, which yields:

$$E^{(*)} = \left(S^{(*)}, I_{SU}^{(*)}, I_{SD}^{(*)}, T_1^{(*)}, I_{RU}^{(*)}, I_{RD}^{(*)}, T_2^{(*)}\right),$$

where

$$S^{(*)} = \frac{A_1 A_2}{(A_2 + ck_S)\alpha_S},$$

$$I_{SU}^{(*)} = \frac{\mu A_1^2 A_2^2 A_3 \left(R_0^{(S)} - 1\right)\left(R_0^{(SR)} - 1\right)}{\alpha_S A_1 (A_2 + ck_S)\left(A_1 A_2 A_3 \left(R_0^{(SR)} - 1\right) + \gamma k_S \beta_S \eta_1 (1-\epsilon)\right)},$$

$$I_{SD}^{(*)} = \frac{\mu k_S A_1^2 A_2^2 A_3 \left(R_0^{(S)} - 1\right)\left(R_0^{(SR)} - 1\right)}{\alpha_S A_1 A_2 (A_2 + ck_S)\left(A_1 A_2 A_3 \left(R_0^{(SR)} - 1\right) + \gamma k_S \beta_S \eta_1 (1-\epsilon)\right)},$$

$$T_1^{(*)} = \frac{\mu k_S \beta_S \eta_1 A_1^2 A_2^2 \left(R_0^{(S)} - 1\right)\left(R_0^{(SR)} - 1\right)}{\alpha_S A_1 A_2 (A_2 + ck_S)\left(A_1 A_2 A_3 \left(R_0^{(SR)} - 1\right) + \gamma k_S \beta_S \eta_1 (1-\epsilon)\right)},$$

$$I_{RU}^{(*)} = \frac{\gamma k_S \beta_S \eta_1 \mu A_5 (1-\epsilon)\left(R_0^{(S)} - 1\right)}{\alpha_R (A_5 + ck_R)\left(A_1 A_2 A_3 \left(R_0^{(SR)} - 1\right) + \gamma k_S \beta_S \eta_1 (1-\epsilon)\right)},$$

$$I_{RD}^{(*)} = \frac{\gamma k_S k_R \beta_S \eta_1 \mu (1-\epsilon)\left(R_0^{(S)} - 1\right)}{\alpha_R (A_5 + ck_R)\left(A_1 A_2 A_3 \left(R_0^{(SR)} - 1\right) + \gamma k_S \beta_S \eta_1 (1-\epsilon)\right)},$$

$$T_2^{(*)} = \frac{\gamma k_S k_R \beta_S \beta_R \eta_1 \eta_2 \mu (1-\epsilon)\left(R_0^{(S)} - 1\right)}{A_6 \alpha_R (A_5 + ck_R)\left(A_1 A_2 A_3 \left(R_0^{(SR)} - 1\right) + \gamma k_S \beta_S \eta_1 (1-\epsilon)\right)}.$$

The co-existence endemic equilibrium point remains in the biologically feasible region if and only if $R_0^{(S)} > 1$ and $R_0^{(SR)} > 1$. These existence conditions suggest that coexistence is feasible only when the drug-sensitive strain maintains dominance in overall incidence relative to the drug-resistant strain.

Now, in order to determine the local asymptotic stability of the equilibrium point $E^{(*)}$, we compute the Jacobian matrix $J\left(E^{(*)}\right)$. The corresponding characteristic equation of this Jacobian takes the form

$$p_*(x) = (x + A_6) q_*(x) = 0, \tag{5.2.3}$$

where $q_*(x)$ is a sixth-degree polynomial given by:

$$q_*(x) = x^6 + a_5 x^5 + a_4 x^4 + a_3 x^3 + a_2 x^2 + a_1 x + a_0.$$

The factor $(x + A_6)$ indicates an eigenvalue as $-A_6$ (< 0), contributing to stability of $E^{(*)}$. The remaining six eigenvalues of $J\left(E^{(*)}\right)$ correspond to the roots of the polynomial $q_*(x)$. However, analytical investigation to determine these roots and derive explicit conditions for local stability is intractable, as the extraction of the coefficients $a_0, \ldots, a_5$ is infeasible due to the highly complex and nested structure of the characteristic polynomial. Therefore, we will investigate the stability of the equilibrium point $E^{(*)}$ numerically for a specific parameter set using the Routh-Hurwitz criterion [142] in Section 5.6.

The Routh array for the polynomial $q_*(x) = x^6 + a_5x^5 + a_4x^4 + a_3x^3 + a_2x^2 + a_1x + a_0$ is:

s^6	1	a_4	a_2	a_0
s^5	a_5	a_3	a_1	0
s^4	b_1	b_2	b_3	0
s^3	c_1	c_2	0	0
s^2	d_1	d_2	0	0
s^1	e_1	0	0	0
s^0	f_1	0	0	0

where the elements are defined as:

$$b_1 = \frac{a_5a_4 - a_3}{a_5}, \quad b_2 = \frac{a_5a_2 - a_1}{a_5}, \quad b_3 = a_0, \quad c_1 = \frac{b_1a_3 - a_5b_2}{b_1}, \quad c_2 = \frac{b_1a_1 - a_5b_3}{b_1},$$
$$d_1 = \frac{c_1b_2 - b_1c_2}{c_1}, \quad d_2 = a_0, \quad e_1 = \frac{d_1c_2 - c_1a_0}{d_1}, \quad f_1 = a_0.$$

According to the Routh-Hurwitz criterion, the equilibrium point is locally asymptotically stable if and only if all elements in the first column of the Routh array are positive. Therefore, the local stability of $E^{(*)}$ holds under the condition:

$$a_5 > 0, \quad b_1 > 0, \quad c_1 > 0, \quad d_1 > 0, \quad e_1 > 0, \quad a_0 > 0 \tag{5.2.4}$$

Based on these results, we we propose the following result about the existence and local stability of the co-existence endemic equilibrium point $E^{(*)}$.

Theorem 5.2.4. *For the system (5.2.1), the co-existence endemic equilibrium point $E^{(*)}$ exists if and only if $R_0^{(R)} > 1$ and $R_0^{(SR)} > 1$. Further, $E^{(*)}$ is locally asymptotically stable under the parameter conditions provided in (5.2.4), otherwise it is unstable.*

The existence and stability conditions of these equilibrium points highlight the critical role of certain parameters in deciding the long-term dynamics of the system. For example, a lower recruitment rate λ reduces the influx of susceptible individuals, leading to a decline in disease burden or even complete elimination over the long time horizon. Similarly, increasing awareness among diagnosed individuals (i.e., reducing c) significantly contributes

to disease control. The relative transmission dynamics of the two strains also plays a key role. Relatively higher transmission rates of the drug-sensitive strain or lower rates for the drug-resistant strain can create a possibility for the coexistence of sensitive and resistant strains, even at a higher treatment coverage. The effects of other parameters involve complex inter-dependencies, which will be explored in detail through a comprehensive sensitivity analysis in Section 5.4.

Remark 5.2.5. *The existence and stability conditions of the equilibrium points $E^{(0)}, E^{(1)}$ and $E^{(*)}$ indicate that the system does not admit multiple regions of asymptotic stability, and no two stable equilibrium states can coexist. This implies the absence of bistability in the system.*

5.3 Epidemiological Parameters and Initial State Values

In this section, we compute the epidemiological parameters of the system (5.1.1), using various studies, including meta-analysis, reviews, and reports. To increase the applicability of the proposed model across different scenarios, we incorporate studies that account for diverse population groups based on factors such as risk behavior, geographic location, and economic status etc. Using these studies, we determine the baseline parameter values along with their ranges of variation. Further, we estimate the initial conditions for each state variable in the system (5.1.1), which will be used for most of numerical simulations.

In Chapter 2, the recruitment rate for India is estimated at 25.31 million per year, calculated based on factors such as births, immigration, emigration, and other processes contributing to new addition of individuals into the sexually active population. The transmission rate α_S (α_R) is the rate of infection per effective contact between susceptible and drug-sensitive (drug-resistant) infected populations. Typically, the infection rate is defined by the change in the infected population resulting from interactions between one unit of both susceptible and infected individuals over a unit of time. For the drug-sensitive infected population, we consider the transmission rate $\alpha_S = 0.000047134$ million^{-1} year^{-1} (see Chapter 2). A mutation in the wild strain of a virus can either increase or decrease its virulence [178], making it essential to consider both scenarios where the transmission rate of the drug-resistant infected population is either higher or lower than that of the drug-sensitive infected population. Therefore, we vary the transmission rate associated with drug-resistant strain within an appropriate range of 0.00001 to 0.00007 million^{-1} year^{-1}, setting the baseline value at $\alpha_R = 0.00002$ million^{-1} year^{-1}. A recent systematic review and meta-analysis study of high-

and upper-middle-income countries estimated that people live with undiagnosed HIV infection for an average of 3 years before receiving a diagnosis [157]. However, despite improved HIV testing facilities, the average time from infection to diagnosis can still range widely, from 0.69 to 10.15 years, depending on different interacting groups and regional factors [158–160]. Therefore, we set the baseline value for the diagnosis rate of infection in drug-sensitive infected population as $k_S = 0.33$ year^{-1}. To assess various scenarios influenced by k_S, we can adjust this parameter within a range of 0.01 to 1.45 per year. For the undiagnosed drug-resistant infected population, we assume that the diagnosis of their resistant status takes less time as compared to the diagnosis of the drug-sensitive infected population, as they are already under medical supervision. Hence, we assume that the diagnosis rate of infection in drug-sensitive infected population as k_R =5 year^{-1}, with a range of variation as 1 to 15 per year. This corresponds to the undiagnosed period for drug-resistant strain, which varies from approximately 3 weeks to 1 year. Undiagnosed individuals are estimated to transmit HIV at a rate three to seven times higher than diagnosed individuals [179]. This variation depends on factors such as the number of at-risk sexual partners, retention in treatment, and viral suppression among diagnosed individuals. Thus, we choose $c = 0.25$ as the baseline value, indicating a 75% reduction in HIV transmissibility after diagnosis. To account for all possible scenarios, we allow c to vary between 0 and 1.

Further, in the absence of treatment, the natural progression of HIV infection to AIDS usually takes about 8 to 10 years [170]. Accordingly, we assume a mean conversion time of $1/\theta_1 = 10$ years (i.e., $\theta_1 = 0.1$ year^{-1}) for an untreated HIV infection case into the AIDS stage. In contrast, when treatment is provided, an adherent patient advances to the AIDS stage far more slowly than a non-adherent or untreated patient. ART significantly increases the life expectancy of AIDS patients, with estimates ranging from 29 to 37.3 years, depending on the age of the patient at which treatment begins [171]. Therefore, we choose a suitable parameter range of 0.025 to 0.05 per year for θ_2, representing an increase of 20 to 40 years in life expectancy for HIV-infected patients as a result of ART. The parameters β_S and β_R are associated with the expected time taken to initiate appropriate treatment after the diagnosis of infection for drug-sensitive and drug-resistant individuals, respectively. A systematic review and meta-analysis suggest that this duration can vary from 5 to 40 days, influenced by factors such as age and gender of patient, and the economic conditions of the country [161]. Another study indicates a broader range, from 20 to 108 days [162]. Consequently, we set these parameters between 4 and 20 per year. A study has shown that the average time for the development of drug resistance in non-adherent patients ($1/\gamma$) is around 6 months after the initiation of treatment [163]. Based on this, we vary the parameter γ between 0.5 and 2 per year, considering different levels of sub-optimality in adherence to

the treatment. The United Nations World Population Prospects 2024 [180] reports that the crude death rate (deaths per 1,000 people per year) ranges from 6.9 to 9.3 across different geographic regions, depending on economic status. Based on this, we assume the natural death rate (μ) can vary between 0.0069 and 0.0093 per year. Regarding the disease induced death rate, the survival probability of a patient declines from 0.48 to 0.26 and further to 0.18 over 2, 4, and 6 years, respectively, following the onset of AIDS [170]. Accordingly, we set the parameter μ_d to lie within the range of 0.16 and 1 per year, representing a potential time frame of 1 to 6 years for patient mortality after AIDS onset.

By the end of 2023, ART coverage among the HIV infected population ranged from 49% in the Middle East and North Africa to 83% in Eastern and Southern Africa, with a global average of 77% [3]. Therefore, we consider the baseline values for the parameters η_1 and η_2 as 0.77 and 0.9, respectively. In a recent study, authors have found that only 53% population is optimally adherent to ART, based on the assumption that the proportion of days covered (PDC) for the study group is greater than 0.95 [181]. Furthermore, if we assume a PDC of 0.90 as the threshold for developing drug resistance in non-adherent patients, approximately 34% of patients are non-adherent to ART. Thus, we set the parameter $\epsilon = 0.66$. For the initial values of each state variable,

We set the initial population sizes as follows: 625 million for the susceptible group, 2.2 million for drug-sensitive infected individuals, 1.5 million for those under treatment, and 1 million for drug-resistant infected individuals, following Chapter 3. A recent study indicates that approximately one-third of infected individuals are unaware of their infection status in underdeveloped and developing countries [182]. Based on this, we allocate 0.7 million to the drug-sensitive undiagnosed group, 1.5 million to the drug-sensitive diagnosed group, 0.3 million to the drug-resistant undiagnosed group, and 0.7 million to the drug-resistant diagnosed group. Additionally, among the 1.5 million individuals under treatment, we assume that 1.2 million are receiving first-line treatment, while 0.3 million are receiving the second-line treatment. Since individuals who progress to the AIDS stage have a short survival period, the population in this stage remains relatively small, estimated at around 0.25 million, as considered in Chapter 4. However, we also vary these initial conditions in our numerical simulations to explore different possible scenarios in dynamics of the proposed model. For each parameter, Table 5.2 provides the unit, baseline value, range of variation, and corresponding references.

Parameter	Unit	Baseline Value	Range of Variation	Reference(s)
λ	million year^{-1}	25.31	[15, 30]	see Chapters 2, 3
α_S	million^{-1} year^{-1}	4.7134×10^{-5}	$[4 \times 10^{-5},\ 3 \times 10^{-4}]$	see Chapters 2, 3
α_R	million^{-1} year^{-1}	2.0×10^{-5}	$[1 \times 10^{-5},\ 3 \times 10^{-3}]$	see Chapters 2, 3
k_S	year^{-1}	0.33	[0.01, 1.45]	[157, 159, 160]
k_R	year^{-1}	5.00	[1, 15]	[157, 159, 160]
c	unitless	0.25	[0, 1]	[179]
θ_1	year^{-1}	0.10	[0.05, 0.5]	[170]
θ_2	year^{-1}	0.03	[0.025, 0.05]	[171]
β_S	year^{-1}	10.00	[4, 20]	[161, 162]
β_R	year^{-1}	15.00	[4, 20]	[161, 162]
γ	year^{-1}	1.00	[0.5, 2]	[163]
η_1	unitless	0.77	[0, 1]	[3]
η_2	unitless	0.90	[0, 1]	Assumed
ϵ	unitless	0.66	[0, 1]	[181]
μ	year^{-1}	0.007	[0.0069, 0.0093]	[180]
μ_d	year^{-1}	0.50	[0.16, 1]	[170]

Table 5.2: Parameter values used in the system (5.1.1) along with their units, baseline values, range of variation, and references.

5.4 Sensitivity Analysis

In the model (5.1.1), the state variables have a complex and non-linear relationship with the epidemiological parameters. The uncertainty in the model inputs and outputs may often attributes to the ambiguous behavior of the model. In such situations, the sensitivity analysis is a tool that identifies the role of uncertainties in the input factors of the model on the variations in different model outputs [183]. The input factors of the model are quantities such as initial values of state variables, model parameters, model parametrization, etc. which can be controlled before the model execution. On the other hand, model outputs, often known as quantities of interest (QoI), refer to variables dependent on model inputs. In epidemiological models, the QoI can be time dependent, such as growth rate of infection, values of state variables or cummulative infections over time, and time independent, such as the basic reproduction numbers, peak infection time and magnitude. Since the model (5.1.1) does not exhibit bi-stable behavior, initial conditions have an insignificant influence on time-dependent QoIs in the longer horizon. However, a small variation might be observed in such model outputs at an early phase for different initial conditions. Therefore, we consider epidemiological parameters as uncertain input quantity for sensitivity analysis.

The sensitivity analysis methods are generally divided into two categories based on the approach used to explore the input space: Local methods, which evaluate the influence of

inputs at a single point, and Global methods, which examine sensitivity at multiple points simultaneously. In this section, we aim to address the following questions: (i). What is the local as well as global impact of each epidemiological parameter on various QoIs? (ii). Is there any difference in the contribution of these parameters in the uncertainties of the short and long-term dynamics of the model (5.1.1)? To thoroughly answer these questions, we conducted both local and global sensitivity analysis, allowing for a detailed evaluation of parameter influence on the dynamics of the system.

5.4.1 Local sensitivity analysis

The initial transmission of drug-sensitive and drug-resistant strains of HIV is largely governed by their respective basic reproduction numbers [184]. In addition, we have observed the importance of the ratio of these basic reproduction numbers in the existence and stability of different equilibrium points in Section 5.2.2. Therefore, we choose the basic reproduction number of both strains and their ratio as our QoIs to assess the local impact of each parameter on the short-term dynamics of the model (5.1.1). Although local sensitivity analysis (LSA) does not provide any information about the interactions between parameters and their combined effect on model output, it works as an initial screening tool to identify the most influential parameters. The normalized forward sensitivity index is a commonly used local sensitivity measure that quantifies the relationship between relative changes in a parameter and the corresponding variations in a variable. If the model output (u) is a differentiable function of the model parameter (α), the normalized forward sensitivity index SI_α^u is defined as:

$$SI_\alpha^u := \frac{\alpha}{u} \times \frac{\partial u}{\partial \alpha}.$$

We calculated the local sensitivity index of $R_0^{(S)}$, $R_0^{(R)}$ and $R_0^{(SR)}$ corresponding to each parameter using their baseline values from Table 5.2. These indices are presented in Table 5.3. Each index represents the ratio of the percentage change in the model output in response to a given percentage change in the model input. The negative sign shows an inverse relationship between the model input and the output. The highlighted values in bold indicate the significant parameters with a sensitivity index magnitude greater than 0.5. Note that the parameters not listed in Table 5.3 have no impact on any of the given QoIs. From this local sensitivity analysis, we observe that λ and α_S are the most influential parameters in positively driving $R_0^{(S)}$, while λ and α_R play a similar role in influencing $R_0^{(R)}$. In contrast, $R_0^{(S)}$ is most negatively sensitive to μ and k_S, whereas μ and k_R have the most negative impact on $R_0^{(R)}$. Except for λ, every listed parameter influences $R_0^{(SR)}$. Among them, α_S and k_R have the strongest positive impact, while α_R and k_S show a negative influence, highlighting

a competitive interaction between these two strains.

QoI	λ	α_S	α_R	c	k_S	k_R	θ_1	β_S	β_R	η_1	η_2	μ
$R_0^{(S)}$	**1.000**	**1.000**	–	0.011	**-0.745**	–	-0.229	-0.011	–	-0.010	–	**-1.016**
$R_0^{(R)}$	**1.000**	–	**1.000**	0.085	–	**-0.894**	-0.020	–	-0.085	–	-0.084	**-1.001**
$R_0^{(SR)}$	–	**1.000**	**-0.952**	-0.074	**-0.745**	**0.894**	-0.209	-0.011	0.085	-0.010	0.084	-0.015

Table 5.3: Normalized forward sensitivity indices of $R_0^{(S)}$, $R_0^{(R)}$, and $R_0^{(SR)}$ with respect to key model parameters. Bold values indicate indices with absolute values greater than 0.5, highlighting parameters with substantial influence on the respective QoIs.

Although LSA gives an initial screening of some most influential parameters at their baseline values and has low computational cost, it is best suited for linear models where these sensitivity results can be extrapolated across the entire parameter space. For a nonlinear model, where state variables and model parameters may interact with each other, LSA may produce misleading conclusions [147]. Therefore, we further extend our analysis by conducting a detailed global sensitivity analysis of the proposed nonlinear model (5.1.1) to assess the impact of interactions among state variables and model parameters on different model outputs.

5.4.2 Global sensitivity analysis

Global sensitivity analysis (GSA) methods typically determine sensitivity indices by applying an appropriate averaging method to model output values for multiple input points in the parameter space. This single averaged value quantifies the overall impact of the input factor on output uncertainty. These indices are often not computable analytically and are instead estimated using numerical approximations based on sampling-based methods. Various sampling procedures are available in the literature for generating input samples across the parameter space, including random sampling [185], Latin hypercube sampling (LHS) [186], and quasi-random sampling [187] etc. The selection of an appropriate sampling technique depends on the specific requirements of the GSA method. In this study, we apply two different GSA methods based on their respective use cases for different QoIs.

Partial rank correlation coefficient method

The partial rank correlation coefficient (PRCC) is a correlation and regression based GSA method that quantifies the monotonic relationship between the model parameters and outputs. PRCC efficiently captures monotonic dependencies, including underlying nonlinear relationships, by transforming data into rank-ordered form and removing linear effects of

other parameters. A rank-based transformation ensures the robustness of the results, particularly when nonlinear relationships exist between input parameters and outputs. The PRCC gives the sensitivity measure as the linear correlation between the residuals $(\mathbf{X_j} - \hat{X}_j)$ and $(\mathbf{Y} - \hat{Y})$. Here, $\mathbf{X_j}$ is the rank-transformed j^{th} input parameter and $\mathbf{Y}$ denotes the rank-transformed output state variable. The terms $\hat{X}_j$ and $\hat{Y}$ are derived from following linear regression models based on k samples:

$$\hat{X}_j = C_0 + \sum_{i=1, i\neq j}^{k} C_i \mathbf{X_i}, \quad \text{and} \quad \hat{Y} = B_0 + \sum_{i=1, i\neq j}^{k} B_i \mathbf{Y_i}.$$

A PRCC index of 1 or -1 indicates that the output is a perfectly monotonic increasing or decreasing function of the inputs, respectively. In contrast, an index of 0 suggests that the output fluctuates between increasing and decreasing at successive data points.

Similar to Section 5.4.1, we select $R_0^{(S)}$, $R_0^{(R)}$ and $R_0^{(SR)}$ as QoIs to access the impact of parameters on early dynamics of the model. Each of these functions is strictly monotonic with respect to all parameters within the specified range of variation given in Table 5.2, a necessary condition to ensure the robustness of the PRCC method. To generate the sample space, we use LHS with $N = 5000$, which is more efficient than random sampling. Here, N represents the number of samples from the feasible range of parameters. LHS requires fewer simulations because it achieves a faster convergence rate. As we do not have any information on the distribution of parameters, we assume a uniform distribution for each parameter. For the generated sample space, the QoIs are first computed and then converted into their rank values along with the parameters. The PRCC values for each parameter are subsequently determined using the procedure described in [188]. These values, corresponding to different QoIs, are displayed in Figure 5.3 using a heatmap representation. In Figure 5.3, the color intensity of each block quantifies the influence of a parameter on the corresponding output. The parameters α_S and λ exhibit the strongest positive influence on $R_0^{(S)}$, whereas $k_S, \theta_1,$ and μ show a significant negative impact on $R_0^{(S)}$. Similarly, variations in parameters α_R, c and λ lead to a directly proportional change in $R_0^{(R)}$, while parameters k_R and η_2 influence it indirectly. Also, $R_0^{(SR)}$ exhibits a direct dependence on α_S, k_R and η_2, and α_R, k_S and c contribute inversely to its variations.

The sensitivity analysis is meaningful only with an assessment of its sampling variability. Quantifying the uncertainty in output values over a given parameter range is a computationally expensive task, as it involves multiple iterations of the entire process. Therefore, we applied the bootstrapping technique for resampling to access the confidence interval (CI) for the PRCC values efficiently. We used the percentile method for constructing CIs to eliminate the effect of skewness in bootstrap distributions, as moment-based methods may lead to poor

estimates in such cases [189]. However, the percentile method requires a larger number of bootstrap resamples to achieve reliable estimates. As suggested in [189], we performed 2000 bootstrap iterations by random resampling with replacement from the original dataset of 5000 points. For each bootstrap sample, we computed the PRCC value for all three outputs and constructed 95% CIs using the percentile approach. Figure 5.4 presents the mean PRCC values for each parameter along with their confidence intervals for different outputs. Parameters with confidence intervals containing 0 are considered to be non-significant. To justify the selection of number of sample points and bootstrap resamples, a detailed convergence test for 3 parameters with highest PRCC values (magnitude) for each output is presented in Figure 5.2. Figure 5.2 presents the convergence analysis of PRCC values for the global sensitivity analysis of the basic reproduction numbers $R_0^{(S)}$, $R_0^{(R)}$, and $R_0^{(SR)}$. For each outcome, the figure shows the three most influential parameters based on their absolute PRCC values across increasing sample sizes. Solid lines with circular markers represent the PRCC estimates, while dashed lines with square markers represent the mean Sequential Relative Change Index (RCI), which quantifies the relative change in PRCC values between consecutive sample sizes. The sample size increases in increments of 500. The RCI is computed as

$$\text{RCI} = \left| \frac{\text{PRCC}_{\text{current}} - \text{PRCC}_{\text{previous}}}{\text{PRCC}_{\text{previous}}} \right|.$$

This metric serves as a convergence criterion, with RCI values below 0.05 typically indicating stabilization of sensitivity estimates. Shaded regions represent 95% confidence intervals, obtained from bootstrap resampling ($n = 2,000$). This analysis demonstrates that a sample size of approximately 5,000 or more is required to achieve convergence, beyond which both PRCC values and their confidence intervals stabilize.

Remark 5.4.1. *PRCC method eliminates the effect of any hidden correlation between parameters by partialling out their shared variance that might arise due to randomness in the sampling procedure. However, certain parameters that do not appear in the expressions for these reproduction numbers still have nonzero PRCC values, though their influence remains negligible.*

To examine the long-term impact of these parameters on the model dynamics, we consider the state variable values at a specific time as the quantity of interest. However, directly applying the PRCC method for global sensitivity analysis may lead to inaccurate results, as the state variables do not necessarily exhibit a monotonic relationship with these parameters. In such cases, variance-based sensitivity analysis methods are more appropriate, providing more reliable results with better interpretability. We apply the Sobol method for GSA,

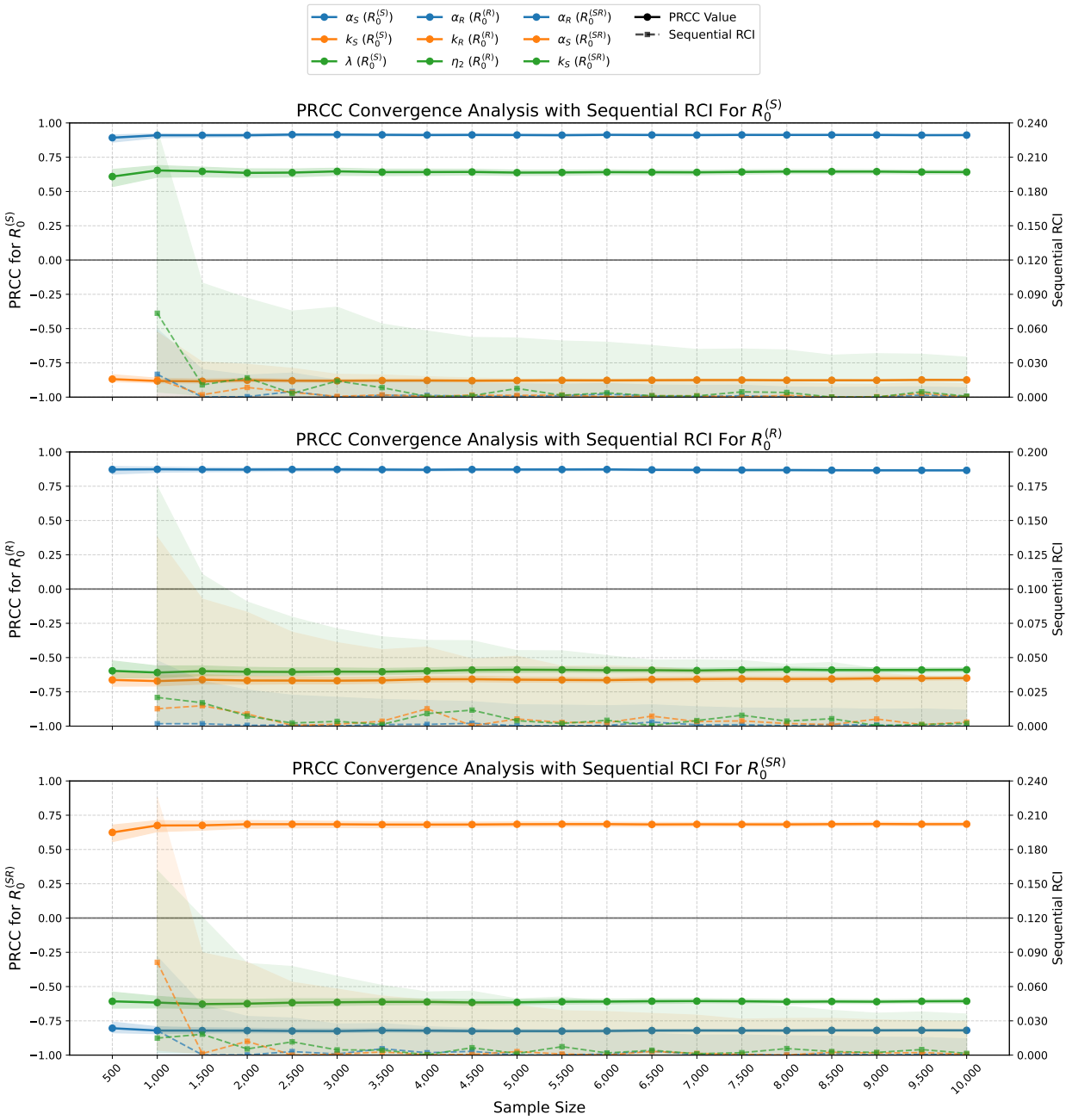

Figure 5.2: Convergence analysis illustrating the stability of PRCC values with increasing sample size for the three most influential parameters affecting each reproduction number. Solid lines with circle represent mean PRCC values, while dashed lines with squares show mean Sequential RCI, quantifying the relative change in PRCC estimates between consecutive sample sizes. The shaded region indicates 95% CI derived from 2000 bootstrap resamples at each sample size.

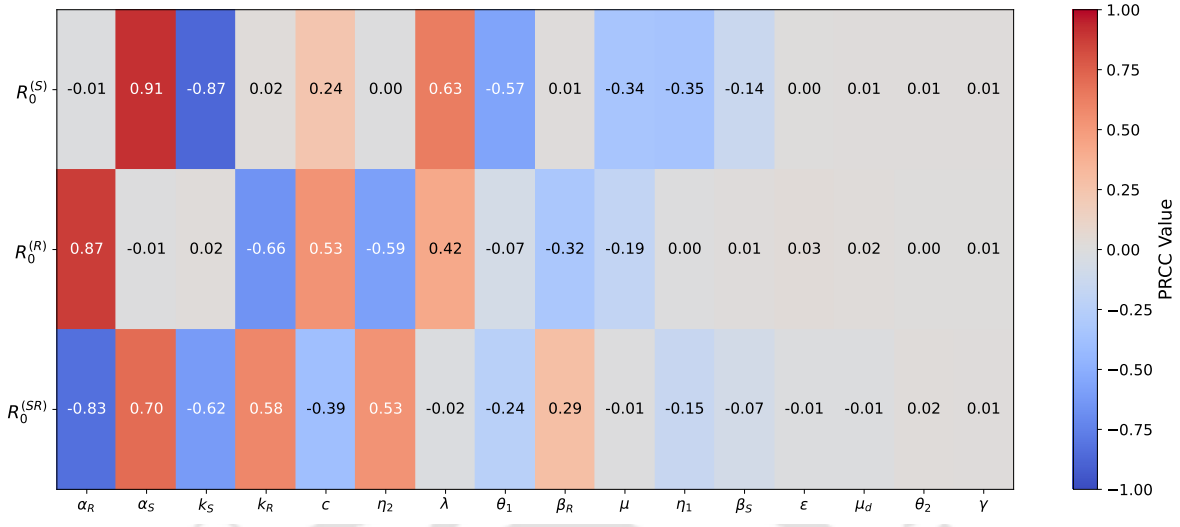

Figure 5.3: Heatmap illustrating PRCC values computed using 5,000 parameter sets generated using LHS for parameters influencing the basic reproduction numbers of sensitive strain ($R_0^{(S)}$), resistant strain ($R_0^{(R)}$), and their ratio ($R_0^{(SR)}$). The color intensity represents the strength of sensitivity, with red indicating positive correlation and blue indicating negative correlation. Parameters are arranged in descending order of mean absolute PRCC values to highlight their relative contribution to early model dynamics.

which characterizes the total variance in output values into contributions from individual parameters and their interactions.

The Sobol method

The Sobol method is a variance-based approach for GSA that quantifies the contribution of individual parameters or a group of parameters to the overall variability of output variables in a non-linear model [148]. However, this method does not provide any insight into the direction of this impact of the parameters. The Sobol indices are derived from the conditional variance. Given Y as the model output, the first-order Sobol index for an input parameter X_i, measuring the direct contribution of i^{th} input to the total variance, is defined as:

$$S_i = \frac{\mathbb{V}_{X_i}[\mathbb{E}_{X_{\sim i}}[Y|X_i]]}{\mathbb{V}[Y]},$$

where $\mathbb{E}$ and $\mathbb{V}$ denote the expectation and variance operators, respectively, and $X_{\sim i}$ represents all parameters except X_i [190]. In the numerator, the expectation of Y is evaluated considering all possible values of $X_{\sim i}$ while keeping X_i fixed, and the outer variance is computed over all possible values of X_i. Another key sensitivity measure is the total-order Sobol index, which captures the overall influence of a parameter X_i by incorporating both its direct contribution and indirect effects arising from interactions with other parameters. The total

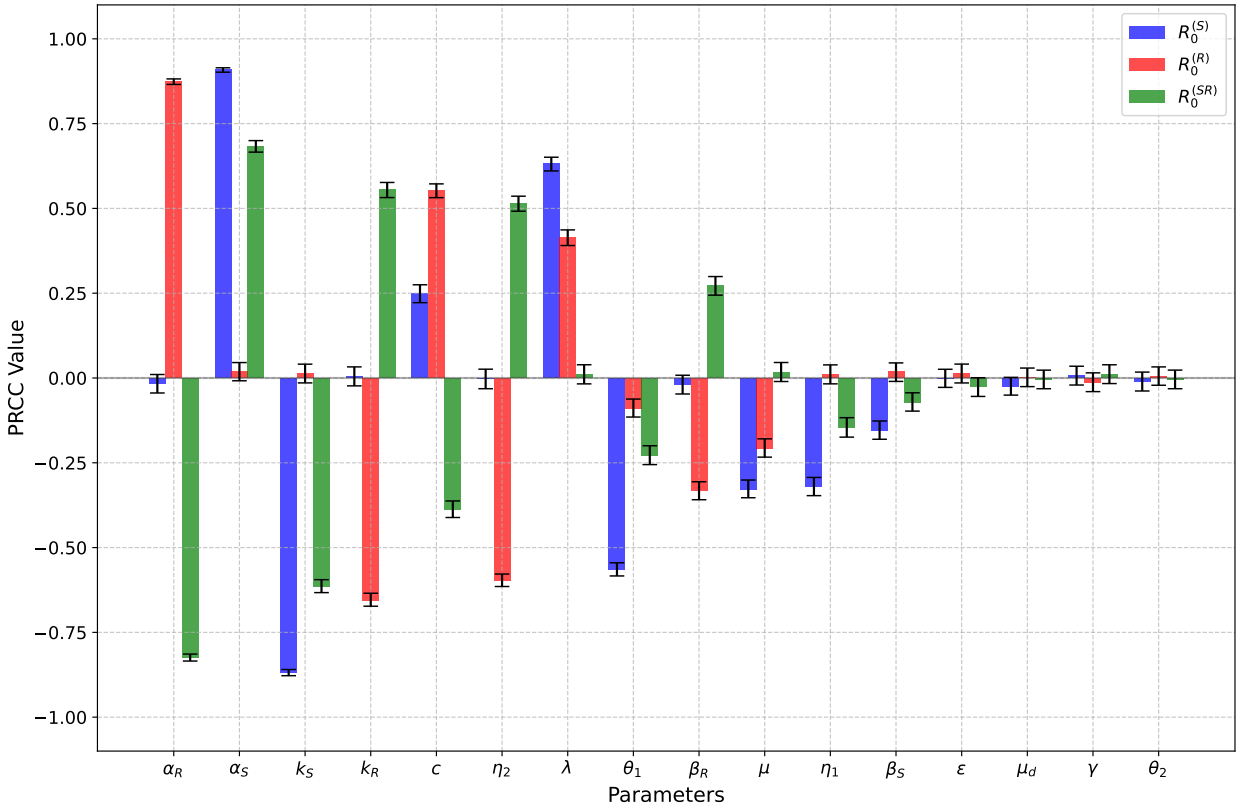

Figure 5.4: Bar plot showing mean PRCC values for parameters influencing the basic reproduction numbers of sensitive strain ($R_0^{(S)}$) in blue, resistant strain ($R_0^{(R)}$) in red, and their ratio ($R_0^{(SR)}$) in green, derived from 2000 bootstrap resamples of 5000 original Latin Hypercube samples. Error bars indicate 95% confidence intervals. Parameters are arranged in descending order of mean absolute PRCC values to highlight their relative contribution to early model dynamics.

order Sobol index for input parameter X_i is defined as [190]:

$$S_{T_i} = \frac{\mathbb{E}_{X_{\sim i}}[\mathbb{V}_{X_i}[Y|X_{\sim i}]]}{\mathbb{V}[Y]}.$$

In this study, we computed only the first-order and total-order sensitivity indices, while higher-order indices were not considered. The total-order index is minimal for non-influential parameters, making it an effective tool for parameter screening, whereas the first-order index serves as a good ranking measure, particularly when parameter interactions are non-significant .

We use the 'SALib' library in Python [191] to generate the sample space and compute Sobol' sensitivity indices for different parameters. The sample space is generated using the Saltelli sampler [190], which is an extension of the Sobol' sequence [192]. Sobol' sequence uses a quasi-random sampling algorithm that strategically distributes new samples to the sequence away from the earlier sampled points. A notable advantage of this sampling method is its superior uniformity compared to random or pseudo-random sampling, making it more suitable for accurately representing a uniform distribution of input parameters. To estimate the first- and total-order Sobol' indices, the Saltelli sampler generates $N \times (P + 2)$ samples [190], where N represents the base sample size and P denotes the number of input parameters. Also, it is recommended to choose the base sample size as an integer power of two to ensure optimal uniformity and better convergence [193].

We define a time-dependent QoI as the total number of infected individuals ($I_{SU} + I_{SD} + I_{RU} + I_{RD}$) at a given time. The time interval is set from 0 to 100, capturing both the short-term and long-term dynamics of the model. To quantify the uncertainty in these time-varying sensitivity indices, the model must be evaluated $N \times (P + 2)$ times per experiment, making this approach computationally expensive. On the other hand, applying standard bootstrap resampling to a single parameter set may produce inaccurate results due to initial sampling bias. This bias can significantly affect outcomes, particularly if the system (5.1.1) has some bifurcation point within this single parameter set. Therefore, we adopted a two-stage approach that integrates ensemble averaging with bootstrap resampling to quantify uncertainty arising from both parameter variability and sampling bias. This approach addresses these challenges by first conducting multiple independent model evaluations ($n = 50$) with different Saltelli's sample sets (with a base sample size of 1024). This produces ensemble average values at different time points, representing more accurate sensitivity indices by eliminating the effects of single sampling bias. Further, we applied bootstrap resampling (1000 resamples) across these independent runs to generate 95% confidence interval. Figure 5.5 presents a detailed illustration of the mean first and total-order Sobol' sensitivity

indices for each parameter, with the shaded region representing the 95% confidence interval, corresponding to the total number of infections at a given time point.

In Figure 5.5, we observe that the influence of most parameters increases over time. The initially low sensitivity indices are expected, given the chronic nature of HIV and its prolonged infectious period, resulting in delayed parameter effects on model dynamics. Parameters such as $\theta_2, \beta_S, \gamma, \epsilon, \mu$ and μ_d have non-significant influence on the output. For most parameters, the large gap between first and total-order indices shows that their impact on the total number of infections is not just through their direct effect but significantly through their interactions with other parameters. Also, the direct impact of individual parameters becomes minimal after a certain time, making interactions between parameters the primary source of variance in the model output. Overall, a substantial shift in sensitivity is observed in the later phase compared to the early phase for most parameters.

5.5 Optimal Control Analysis

In this section, we explore time-dependent control mechanisms that focus on minimizing the infection burden while optimizing the cost of pharmaceutical interventions such as treatment, drug-adherence, and related factors. In section 5.4, we observed that the dynamics of model (5.1.1) is highly sensitive to the parameters k_S and k_R, which are related to the diagnosis of infection. However, HIV diagnosis is not typically classified as a pharmaceutical intervention, it serves as a critical foundation for various interventions, both pharmaceutical and non-pharmaceutical. Therefore, we consider these diagnosis rates for drug-sensitive and drug-resistant infected populations, respectively, as controllable parameters. Furthermore, we consider the parameters η_1, η_2 and ϵ as treatment-related controllable measures.

To construct the optimal control problem, we define the control variables $u_1(t), u_2(t)$, $u_3(t), u_4(t)$ and $u_5(t)$ as bounded and Lebesgue-measurable functions over the interval $[0, t_f]$, where t_f is the final time of interventions. The description of these control variables is as follows:

$u_1(t)$: Intensity of intervention efforts allocated to diagnosing drug-sensitive infected population at time t,

$u_2(t)$: Intensity of intervention efforts allocated to diagnosing drug-resistant infected population at time t,

$u_3(t)$: Intensity of the treatment intervention efforts to initialize first-line therapy among diagnosed drug-sensitive infected individuals at time t,

$u_4(t)$: Intensity of the treatment intervention efforts to initialize first-line therapy among diagnosed drug-sensitive infected individuals at time t,

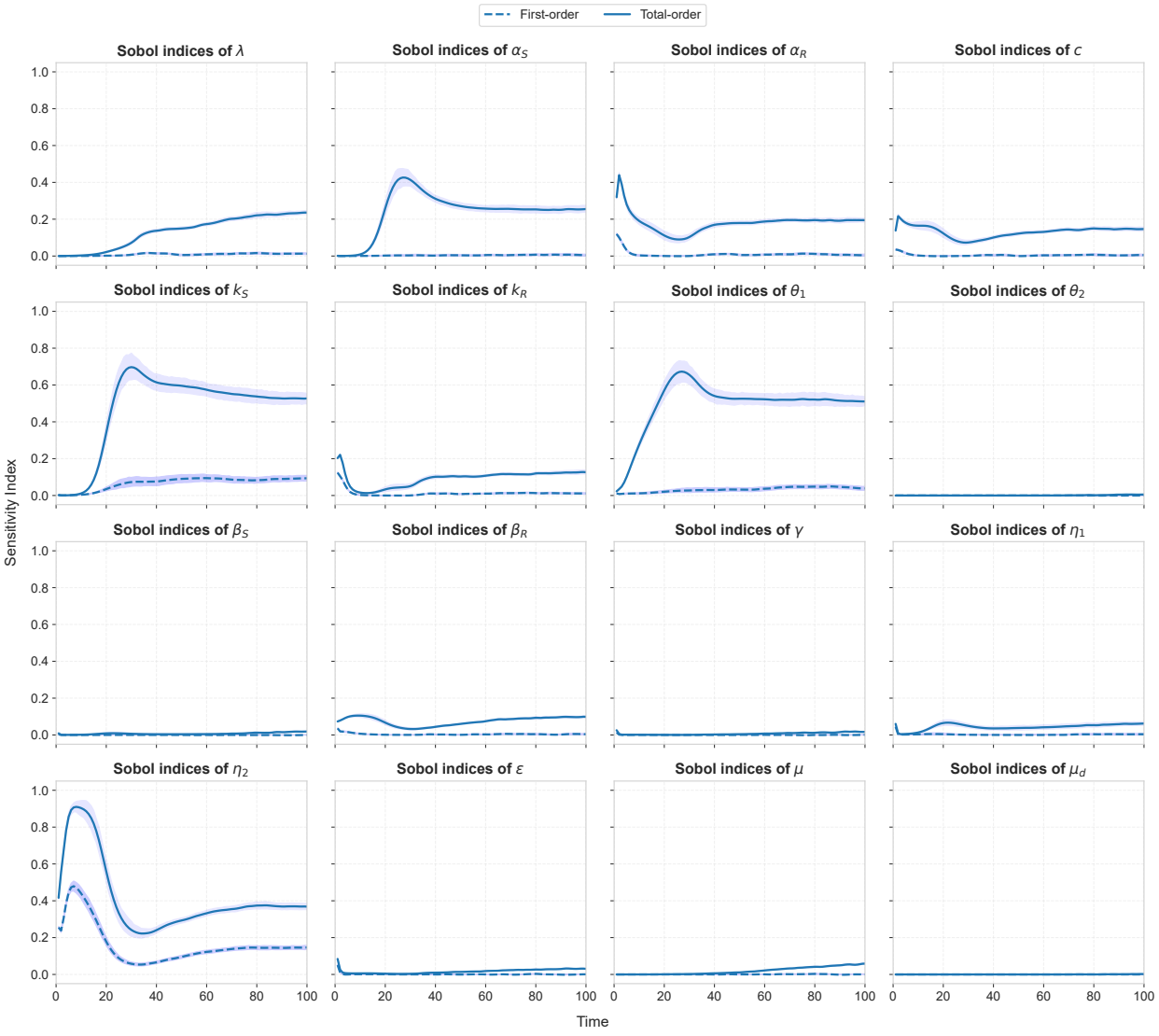

Figure 5.5: Time-dependent global sensitivity analysis of the model (5.1.1) using Sobol' indices. Each sub figure shows the first-order (dashed) and total-order (solid) sensitivity indices for each parameter corresponding to the total number of infected individuals. The shaded region represents the 95% confidence interval.

$u_5(t)$: Intensity of supportive interventions implemented to improve drug-adherence among individuals receiving first-line therapy at time t.

Our primary objective is to determine the optimal control profile $(u_1^*(t), u_2^*(t), u_3^*(t), u_4^*(t), u_5^*(t))$ that minimizes the total associated cost. Note that the optimal allocation of resources is determined by the formulation of the cost function. To achieve the objective described above, we define the following cost functional to be minimized:

$$\begin{aligned} J[\mathcal{U}(t)] &= \int_0^{t_f} \Big[W_1 I_{SU}(t) + W_2 I_{SD}(t) + W_3 I_{RU}(t) + W_4 I_{RD}(t) - W_5 T_1(t) - W_6 T_2(t) \\ &\quad + \frac{1}{2}\big(w_1 u_1^2(t) + w_2 u_2^2(t) + w_3 u_3^2(t) + w_4 u_4^2(t) + w_5 u_5^2(t)\big)\Big] dt, \end{aligned} \tag{5.5.1}$$

where $\mathcal{U}(t) = \{u_1(t), u_2(t), u_3(t), u_4(t), u_5(t) : 0 \leq u_i(t) \leq 1 \text{ for } i = 1, 2, 3, 4, 5; t \in [0, t_f]\}$ is the control set. The integrand $L(I_{SU}, I_{SD}, I_{RU}, I_{RD}, T_1, T_2, u_1(t), u_2(t), u_3(t), u_4(t), u_5(t))$ represents the current cost at time t. The total infected population is defined as the sum of individuals in compartments I_{SU}, I_{SD}, I_{RU} and I_{RD}. While individuals in compartments T_1, T_2 and A are also infected, they do not contribute to the overall disease burden since they are not involved in further transmission. However, treatment-related terms are included in the objective functional to ensure a balanced optimization approach that simultaneously minimizes the untreated infected population while incentivizing treatment enrollment. The positive weight constants W_i $(i = 1, 2, 3, 4)$ represent the relative importance of reducing specific infected classes in controlling disease spread and minimizing its burden, W_5 and W_6 represent the relative importance of maximizing treatment coverage, particularly for vulnerable population with drug-resistant strain, and w_j $(j = 1, 2, 3, 4, 5)$ denote the relative costs of each control intervention, ensuring proper scaling and balance within the cost functional. The impact of efforts to improve HIV diagnosis, treatment availability, and drug adherence is expected to have a nonlinear relationship with the outcomes. Therefore, we use quadratic cost terms for each control variable to appropriately capture these effects, as in [115, 120, 194]. We seek an optimal control solution $\mathcal{U}^*(u_1^*(t), u_2^*(t), u_3^*(t), u_4^*(t), u_5^*(t))$ such that $J(\mathcal{U}^*(t)) = \min\{J(\mathcal{U}(t)\}$, subject to the system,

$$
\begin{aligned}
S' &= \lambda - \alpha_S S(I_{SU} + cI_{SD}) - \alpha_R S(I_{RU} + cI_{RD}) - \mu S,\\
I'_{SU} &= \alpha_S S(I_{SU} + cI_{SD}) - k_{S_{max}}\mathbf{u_1(t)}I_{SU} - \theta_1 I_{SU} - \mu I_{SU},\\
I'_{SD} &= k_{S_{max}}\mathbf{u_1(t)}I_{SU} - \beta_S\mathbf{u_3(t)}I_{SD} - \theta_1(1-\mathbf{u_3(t)})I_{SD} - \mu I_{SD},\\
T'_1 &= \beta_S\mathbf{u_3(t)}I_{SD} - \gamma(1-\mathbf{u_5(t)})T_1 - \theta_2\mathbf{u_5(t)}T_1 - \mu T_1,\\
I'_{RU} &= \alpha_R S(I_{RU} + cI_{RD}) + \gamma(1-\mathbf{u_5(t)})T_1 - k_{R_{max}}\mathbf{u_2(t)}I_{RU} - \theta_1 I_{RU} - \mu I_{RU},\\
I'_{RD} &= k_{R_{max}}\mathbf{u_2(t)}I_{RU} - \beta_R\mathbf{u_4(t)}I_{RD} - \theta_1(1-\mathbf{u_4(t)})I_{RD} - \mu I_{RD},\\
T'_2 &= \beta_R\mathbf{u_4(t)}I_{RD} - \theta_2 T_2 - \mu T_2,\\
A' &= \theta_1 I_{SU} + \theta_1(1-\mathbf{u_3(t)})I_{SD} + \theta_2\mathbf{u_5(t)}T_1 + \theta_1 I_{RU} + \theta_1(1-\mathbf{u_4(t)})I_{RD} + \theta_2 T_2 - (\mu+\mu_d)A
\end{aligned}
\tag{5.5.2}
$$

with non-negative initial conditions. Note that we have substituted the parameters k_S, k_R, η_1, η_2 and ϵ with their respective maximum values within the specified ranges to normalize the newly introduced control variables within the interval $[0, 1]$.

5.5.1 Existence of an optimal control

In this subsection, we establish the presence of optimal control functions that effectively minimize the cost functional within a finite time frame.

Theorem 5.5.1. *For the controlled state system (5.5.2) with non-negative initial conditions, there exists an optimal control set* $(u_1^*, u_2^*, u_3^*, u_4^*, u_5^*)$ *in* $\mathcal{U}$ *such that* $J(u_1^*, u_2^*, u_3^*, u_4^*, u_5^*) = \min\{J(u_1, u_2, u_3, u_4, u_5) : (u_1, u_2, u_3, u_4, u_5) \in \mathcal{U}\}$.

Proof. The existence of an optimal control is ensured if the following three conditions, as stated in Theorem 4.1 (Chapter III) of [195], are satisfied.

i. The solution set of the system (5.5.2) with control functions in $\mathcal{U}$ is non-empty.

ii. The control set $\mathcal{U}$ is closed and convex, and the state system can be written as a linear function of the control variables, with coefficients that depend on both time and state variables.

iii. Integrand L of Eq. (5.5.1) is convex on the control set $\mathcal{U}$. Furthermore, there exists a continuous function g such that

$$L(I_{SU}, I_{SD}, I_{RU}, I_{RD}, T_1, T_2, u_1, u_2, u_3, u_4, u_5) \geq g(u_1, u_2, u_3, u_4, u_5),$$

where

$$|(u_1, u_2, u_3, u_4, u_5)|^{-1} g(u_1, u_2, u_3, u_4, u_5) \to \infty,$$

whenever

$$|(u_1, u_2, u_3, u_4, u_5)| \to \infty.$$

Here, $|.|$ represents the Euclidean norm.

We rewrite the controlled state system (5.5.2) as follows:

$$G(X) = CX + F(X), \tag{5.5.3}$$

where $G(X) = \begin{bmatrix} S' \\ I'_{SU} \\ I'_{SD} \\ T'_1 \\ I'_{RU} \\ I'_{RD} \\ T'_2 \\ A' \end{bmatrix}$, $X = \begin{bmatrix} S \\ I_{SU} \\ I_{SD} \\ T_1 \\ I_{RU} \\ I_{RD} \\ T_2 \\ A \end{bmatrix}$, $F(X) = \begin{bmatrix} \lambda - \alpha_S S(I_{SU} + cI_{SD}) - \alpha_R S(I_{RU} + cI_{RD}) \\ \alpha_S S(I_{SU} + cI_{SD}) \\ 0 \\ 0 \\ \alpha_R S(I_{RU} + cI_{RD}) \\ 0 \\ 0 \\ 0 \end{bmatrix}$,

and

$$C = \begin{bmatrix} -\mu & 0 & 0 & 0 & 0 & 0 & 0 & 0 \\ 0 & -(k_{S_{max}} u_1 + \theta_1 + \mu) & 0 & 0 & 0 & 0 & 0 & 0 \\ 0 & k_{S_{max}} u_1 & -(\beta_S u_3 + \theta_1(1-u_3) + \mu) & 0 & 0 & 0 & 0 & 0 \\ 0 & 0 & \beta_S u_3 & -(\gamma(1-u_5) + \theta_2 u_5 + \mu) & 0 & 0 & 0 & 0 \\ 0 & 0 & 0 & \gamma(1-u_5) & -(k_{R_{max}} u_2 + \theta_1 + \mu) & 0 & 0 & 0 \\ 0 & 0 & 0 & 0 & k_{R_{max}} u_2 & -(\beta_R u_4 + \theta_1(1-u_4) + \mu) & 0 & 0 \\ 0 & 0 & 0 & 0 & 0 & \beta_R u_4 & -(\theta_2 + \mu) & 0 \\ 0 & \theta_1 & \theta_1(1-u_3) & \theta_2 u_5 & \theta_1 & \theta_1(1-u_4) & \theta_2 & -(\mu + \mu_d) \end{bmatrix}.$$

Since the solutions of the system (5.5.2) remain bounded for each bounded control variable in $\mathcal{U}$, applying the triangular inequality will give us

$$|F(X_1) - F(X_2)| \leq p_1|S_1 - S_2| + p_2|I_{SU_1} - I_{SU_2}| + p_3|I_{SD_1} - I_{SD_2}| + p_4|I_{RU_1} - I_{RU_2}| + p_5|I_{RD_1} - I_{RD_2}|,$$

where $p_i > 0$ $(i = 1, 2, 3, 4, 5)$ are constants. Consequently,

$$\begin{aligned} |G(X_1) - G(X_2)| &\leq C|X_1 - X_2| + |F(X_1) - F(X_2)| \\ &\leq p|X_1 - X_2| < \infty, \end{aligned}$$

where $p = ||C|| + \sum_{i=1}^{5} p_i < \infty$. Therefore, the right-hand side functions of the control system (5.5.2) are uniformly Lipschitz continuous. Consequently, by applying the Picard-Lindelöf theorem [196], the system (5.5.2) admits a unique solution, ensuring that condition (i) is satisfied.

Condition (ii) holds trivially, as the control set $\mathcal{U}$ is defined to be closed and convex. Also, the system (5.5.2) is linear with respect to each control variable, with coefficients that depend only on the state variables.

For condition (iii), the integrand L is quadratic in nature with respect to each control variable, and hence, it is convex. Further, since T_1 and T_2 are bounded above, there exists a maximum value M such that $0 \leq W_5T_1 + W_6T_2 \leq M$. Therefore,

$$\begin{aligned} L(I_{SU}, I_{SD}, I_{RU}, I_{RD}, T_1, T_2, u_1, u_2, u_3, u_4, u_5) &= W_1I_{SU} + W_2I_{SD} + W_3I_{RU} + W_4I_{RD} \\ &\quad -W_5T_1 - W_6T_2 + \frac{1}{2}\sum_{i=1}^{5} w_iu_i^2 \\ &\geq -M + \frac{1}{2}\sum_{i=1}^{5} w_iu_i^2 \\ &\geq -M + w_m\left(\sum_{i=1}^{5} u_i^2\right), \end{aligned}$$

where $w_m = \frac{1}{2}\min\{w_1, w_2, w_3, w_4, w_5\}$.
Let

$$g(u_1, u_2, u_3, u_4, u_5) = -M + w_m\left(\sum_{i=1}^{5} u_i^2\right),$$

which is continuous and satisfies $|(u_1, u_2, u_3, u_4, u_5)|^{-1}g(u_1, u_2, u_3, u_4, u_5) \to \infty$ whenever $|(u_1, u_2, u_3, u_4, u_5)| \to \infty$, since the negative term consisting M vanishes while the positive term increases without bound. Therefore, the condition (iii) also holds. The controlled state system (5.5.2) with non-negative initial conditions, along with the cost functional (5.5.1) defined on the control set $\mathcal{U}$ satisfies all three conditions, which shows the existence of an optimal control. □

5.5.2 Characterization of optimal control variables

We next analytically characterize the trajectories of the optimal control variables for the control system (5.5.1)-(5.5.2). Also, we apply the Pontryagin's Maximum Principle [197] to establish the necessary conditions for optimal control. This reformulates the problem (5.5.1)-(5.5.2) into a pointwise minimization of the Hamiltonian H over the control variables $(u_1, u_2, u_3, u_4, u_5)$. We define the Hamiltonian from the control system (5.5.2) and the cost

functional (5.5.1) as follows:

$$\begin{aligned}
H &= L+\sigma_1 S'+\sigma_2 I'_{SU}+\sigma_3 I'_{SD}+\sigma_4 T'_1+\sigma_5 I'_{RU}+\sigma_6 I'_{RD}+\sigma_7 T'_2+\sigma_8 A' \\
&= \left(W_1 I_{SU}+W_2 I_{SD}+W_3 I_{RU}+W_4 I_{RD}-W_5 T_1-W_6 T_2+\frac{1}{2}\sum_{i=1}^{5} w_i u_i^2\right) \\
&\quad +\sigma_1[\lambda-\alpha_S S(I_{SU}+cI_{SD})-\alpha_R S(I_{RU}+cI_{RD})-\mu S] \\
&\quad +\sigma_2[\alpha_S S(I_{SU}+cI_{SD})-k_{S_{max}}u_1(t)I_{SU}-\theta_1 I_{SU}-\mu I_{SU}] \\
&\quad +\sigma_3[k_{S_{max}}u_1(t)I_{SU}-\beta_S u_3(t)I_{SD}-\theta_1(1-u_3(t))I_{SD}-\mu I_{SD}] \\
&\quad +\sigma_4[\beta_S u_3(t)I_{SD}-\gamma(1-u_5(t))T_1-\theta_2 u_5(t)T_1-\mu T_1] \\
&\quad +\sigma_5[\alpha_R S(I_{RU}+cI_{RD})+\gamma(1-u_5(t))T_1-k_{R_{max}}u_2(t)I_{RU}-\theta_1 I_{RU}-\mu I_{RU}] \\
&\quad +\sigma_6[k_{R_{max}}u_2(t)I_{RU}-\beta_R u_4(t)I_{RD}-\theta_1(1-u_4(t))I_{RD}-\mu I_{RD}] \\
&\quad +\sigma_7[\beta_R u_4(t)I_{RD}-\theta_2 T_2-\mu T_2] \\
&\quad +\sigma_8[\theta_1 I_{SU}+\theta_1(1-u_3(t))I_{SD}+\theta_2 u_5(t)T_1+\theta_1 I_{RU}+\theta_1(1-u_4(t))I_{RD} \\
&\quad +\theta_2 T_2-(\mu+\mu_d)A], \qquad (5.5.4)
\end{aligned}$$

where $\sigma_i(t)$'s (for $i=1,2,\ldots,8$) represent the adjoint variables corresponding to the state variables, which will be determined in the subsequent analysis.

Theorem 5.5.2. *Let $(u_1^*,u_2^*,u_3^*,u_4^*,u_5^*)\in\mathcal{U}$ be an optimal control profile with the corresponding optimal state solution $(S^*,I_{SU}^*,I_{SD}^*,T_1^*,I_{RU}^*,I_{RD}^*,T_2^*,A^*)$ subject to the control problem (5.5.1)-(5.5.2). Then there exist adjoint variables σ_i's (for $i=1,2,\ldots,8$) which satisfy,*

$$\begin{aligned}
\sigma'_1 &= \alpha_S(I_{SU}+cI_{SD})(\sigma_1-\sigma_2)+\alpha_R(I_{RU}+cI_{RD})(\sigma_1-\sigma_5)+\mu\sigma_1, \\
\sigma'_2 &= -W_1+\alpha_S S(\sigma_1-\sigma_2)+k_{S_{max}}u_1(\sigma_2-\sigma_3)+\theta_1(\sigma_2-\sigma_8)+\mu\sigma_2, \\
\sigma'_3 &= -W_2+c\alpha_S(\sigma_1-\sigma_2)+\beta_S u_3(\sigma_3-\sigma_4)+\theta_1(1-u_3)(\sigma_3-\sigma_8)+\mu\sigma_3, \\
\sigma'_4 &= W_5+\gamma(1-u_5)(\sigma_4-\sigma_5)+\theta_2 u_5(\sigma_4-\sigma_8)+\mu\sigma_4 \\
\sigma'_5 &= -W_3+\alpha_R S(\sigma_1-\sigma_5)+k_{R_{max}}u_2(\sigma_5-\sigma_6)+\theta_1(\sigma_5-\sigma_8)+\mu\sigma_5, \\
\sigma'_6 &= -W_4+c\alpha_R S(\sigma_1-\sigma_5)+\beta_R u_4(\sigma_6-\sigma_7)+\theta_1(1-u_4)(\sigma_6-\sigma_8)+\mu\sigma_6, \\
\sigma'_7 &= W_6+\theta_2(\sigma_7-\sigma_8)+\mu\sigma_7, \\
\sigma'_8 &= (\mu+\mu_d)\sigma_8, \qquad (5.5.5)
\end{aligned}$$

with transversality conditions $\sigma_i(t_f)=0 \quad \forall i=1,2,\ldots,8$. Further, the solutions of the

optimal control variables are given as,

$$u_1^* = \max\left\{0, \min\left\{\frac{k_{S_{max}}(\sigma_2-\sigma_3)I_{SU}^*}{w_1}, 1\right\}\right\}, \tag{5.5.6}$$

$$u_2^* = \max\left\{0, \min\left\{\frac{k_{R_{max}}(\sigma_5-\sigma_6)I_{RU}^*}{w_2}, 1\right\}\right\}, \tag{5.5.7}$$

$$u_3^* = \max\left\{0, \min\left\{\frac{((\sigma_3-\sigma_4)\beta_S+(\sigma_8-\sigma_3)\theta_1)\,I_{SD}^*}{w_3}, 1\right\}\right\}, \tag{5.5.8}$$

$$u_4^* = \max\left\{0, \min\left\{\frac{((\sigma_6-\sigma_7)\beta_R+(\sigma_8-\sigma_6)\theta_1)\,I_{RD}^*}{w_4}, 1\right\}\right\}, \tag{5.5.9}$$

$$u_5^* = \max\left\{0, \min\left\{\frac{((\sigma_5-\sigma_4)\gamma+(\sigma_4-\sigma_8)\theta_2)\,T_1^*}{w_5}, 1\right\}\right\}. \tag{5.5.10}$$

Proof. Given the existence of an optimal solution, the Pontryagin's Maximum Principle provides the system of differential equations for the adjoint variables, derived by differentiating the Hamiltonian with respect to the state variables and evaluating it at the optimal control. Therefore, the adjoint system is determined by solving the following set of differential equations, subject to the specified boundary conditions:

$$\frac{d\sigma_1}{dt} = -\frac{dH}{dS}, \ \frac{d\sigma_2}{dt} = -\frac{dH}{dI_{SU}}, \ldots, \frac{d\sigma_8}{dt} = -\frac{dH}{dA}, \quad \sigma_i(t_f) = 0 \quad \forall i = 1, 2, \ldots, 8,$$

which results in the adjoint system (5.5.5) for given control problem.

To characterize the optimal controls, we differentiate the Hamiltonian function with respect to the control variables within the interior of the control set $\mathcal{U}$. Applying Pontryagin's Maximum Principle, we derive the following optimality conditions:

$$\begin{aligned}
\frac{dH}{du_1} &= w_1u_1^* - k_{S_{max}}(\sigma_2-\sigma_3)I_{SU}^* = 0,\\
\frac{dH}{du_2} &= w_2u_2^* - k_{R_{max}}(\sigma_5-\sigma_6)I_{RU}^* = 0,\\
\frac{dH}{du_3} &= w_3u_3^* - \beta_S(\sigma_3-\sigma_4)I_{SD}^* - \theta_1(\sigma_8-\sigma_3)I_{SD}^* = 0,\\
\frac{dH}{du_4} &= w_4u_4^* - \beta_R(\sigma_6-\sigma_7)I_{RD}^* - \theta_1(\sigma_8-\sigma_6)I_{RD}^* = 0,\\
\frac{dH}{du_5} &= w_5u_5^* - \gamma(\sigma_5-\sigma_4)T_1^* - \theta_2(\sigma_4-\sigma_8)T_1^* = 0.
\end{aligned} \tag{5.5.11}$$

Solving the system (5.5.11) for $(u_1^*, u_2^*, u_3^*, u_4^*, u_5^*)$ and using the bounds of control set $\mathcal{U}$ yield the optimal control characterizations given in (5.5.6)-(5.5.10) for the control problem (5.5.1)-(5.5.2). □

A comprehensive discussion on various control strategies, their epidemiological outcomes, and the corresponding cost-effectiveness analysis is presented in Section 5.6.

5.6 Numerical Simulations

Dynamic modelling of complex systems depends on numerical simulations to effectively illustrate and support the theoretical findings of the model. In this section, we first validate the analytical results on the existence and stability of equilibrium points through numerical simulations. We then present a comprehensive evaluation of various optimal control strategies, including a dynamic control approach, and their effects on the model outcomes. A detailed cost-effectiveness analysis is carried out, considering both infection reduction and treatment coverage expansion objectives. Additionally, we perform an adjoint-based sensitivity analysis to assess how supplementary resources can be optimally allocated to maximize public health benefits. Finally, to capture both the individual and synergistic contributions of control variables, we include a control contribution analysis using Shapley values, a concept from cooperative game theory.

5.6.1 Existence and stability of equilibrium points

To illustrate the existence and stability of all equilibrium points, we fix the majority of parameters in the system (5.2.1) as outlined in Section 5.3. To explore various scenarios, we vary the parameters α_S and α_R within their feasible ranges, as specified in Table 5.2, since these parameters critically influence the basic reproduction numbers. The initial condition in each time series plot is set as suggested in Section 5.3. First, we set $\alpha_S = 0.000047$ and $\alpha_R = 0.00002$. For this set of parameters, the basic reproduction numbers are computed as $R_0^{(S)} = 0.39\ (< 1)$, $R_0^{(R)} = 0.02\ (< 1)$ and $R_0^{(SR)} = 25.41\ (> 1)$. According to Theorem 5.2.2, this configuration admits a unique disease-free equilibrium point, $E^{(0)} = (3615.7143, 0, 0, 0, 0, 0, 0)$. The eigenvalues of the Jacobian matrix $J(E^{(0)})$ are $-13.5276, -7.7319, -5.024, -0.3668, -0.2652, -0.037$ and -0.007. Since all eigenvalues have a negative real part, $E^{(0)}$ is locally asymptotically stable. This behavior is captured in the time series plot presented in Figure 5.6a.

Next, we consider the parameter set with $\alpha_S = 0.00005$ and $\alpha_R = 0.003$. The corresponding basic reproduction numbers are $R_0^{(S)} = 0.42\ (< 1)$, $R_0^{(R)} = 2.32\ (> 1)$ and $R_0^{(SR)} = 0.18\ (< 1)$. These values satisfy the conditions for the existence and local stability of the drug-resistant strain endemic equilibrium point, as described in Theorem 5.2.3. The equilibrium point in this case is given by $E^{(1)} = (1558.2339, 0, 0, 0, 2.8201, 1.0432, 380.6183)$ and the eigenvalues of the Jacobian matrix $J(E^{(1)})$ are $-0.0008 \pm 0.2137i, -13.9495, -7.7309, -0.3668, -0.3582$ and -0.037. Since all eigenvalues have negative real parts, the local asymptotic stability of $E^{(1)}$ is confirmed, which is further supported by the plot shown in Figure 5.6b. Note that the disease-free equilibrium point also exists for this parameter set, but it

is unstable.

We further explore the system dynamics by considering a new set of parameters with $\alpha_S = 0.0003$ and $\alpha_R = 0.0001$. The basic reproduction numbers are $R_0^{(S)} = 2.51(> 1)$, $R_0^{(R)} = 0.08(< 1)$ and $R_0^{(SR)} = 32.43(> 1)$. Under these conditions, both the co-existence endemic equilibrium point $E^{(*)}$ and the DFE $E^{(1)}$ exist. The $E^{(*)}$ is given by $(1441.2443, 34.0749, 1.4547, 30.5372, 2.0977, 0.7759, 283.1167)$. To examine the local stability of this equilibrium, we compute the characteristic polynomial of the Jacobian matrix $J(E^{(*)})$, which is given by:

$$p_*(x) = (x + 0.037)q_*(x),$$

where

$$q_*(x) = (x^6 + 26.5988x^5 + 219.924x^4 + 598.411x^3 + 201.237x^2 + 6.0169x + 0.8754).$$

The Routh array for the polynomial $q_*(x)$ is:

s^6	1	219.924	201.237	0.8754
s^5	26.5988	598.411	6.0169	0
s^4	197.4262	201.0108	0.8754	0
s^3	571.3298	5.8989	0	0
s^2	198.9724	0.8754	0	0
s^1	3.3852	0	0	0
s^0	0.8754	0	0	0

Note that all the elements in the first column of the Routh array are positive, thereby satisfying the local stability conditions outlined in Theorem 5.2.4. The roots of the characteristic equation $p_*(x) = 0$ are $-0.0086 \pm 0.0673i$, -0.037, -13.5381, -7.7346, -4.9418 and -0.3671. Therefore, the equilibrium point $E^{(*)}$ is locally asymptotically stable, as further supported by the time series plot in Figure 5.6c, which illustrates the convergence of the solutions to the co-existence state over time.

5.6.2 Control strategies

In this discussion, we examine the impact of various control strategies for the proposed optimal control problem (5.5.1)-(5.5.2), with the goal of achieving the 95-95-95 targets set by UNAIDS [137]. Numerical simulations are performed by solving the control system (5.5.1)-(5.5.2) along with the corresponding adjoint system (5.5.5) and the control characterization (5.5.6)-(5.5.10) through an iterative scheme. We employ the forward-backward sweep method, starting with an initial estimate for the control variables, and solve the state system using the classical fourth-order Runge-Kutta method in forward direction over the

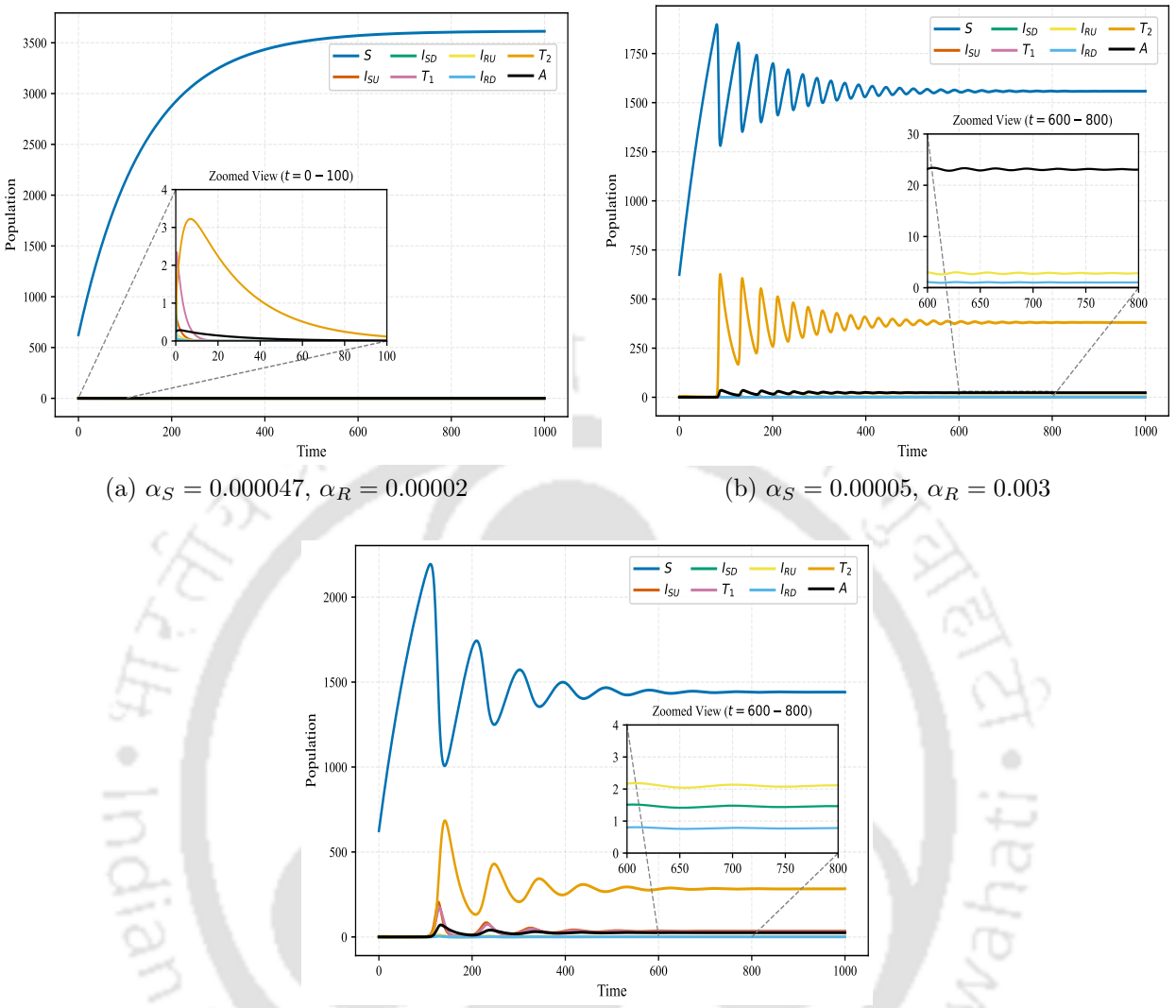

(a) $\alpha_S = 0.000047$, $\alpha_R = 0.00002$

(b) $\alpha_S = 0.00005$, $\alpha_R = 0.003$

(c) $\alpha_S = 0.0003$, $\alpha_R = 0.0001$

Figure 5.6: Time series plots for the system (5.1.1) showing convergence of solutions to (a) the disease-free equilibrium point, (b) the drug-resistant strain endemic equilibrium point, and (c) the coexistence endemic equilibrium point.

simulated time. Subsequently, with the state trajectories determined, the adjoint system is solved backward in time using the transversality conditions $\sigma_i(t_f) = 0 \ \forall i = 1, 2, \ldots, 8$, again applying the Runge-Kutta fourth-order integration. The control variables are updated at each iteration using a convex combination of the previous control values and those derived from the characterization equations to improve numerical stability. This iterative procedure is repeated until successive iterations give negligible differences in the computed values of control variables (for details see [115]).

In general, binary control activation has traditionally been employed in the literature

to differentiate between intervention strategies, where a specific control or a combination of controls is activated while all non-focal controls are set to zero [115, 120, 198]. Although this method effectively isolates the individual or combined effects of interventions, it imposes artificial constraints that poorly reflect real-world public health policy implementation. In practice, interventions are rarely applied in isolation. To address this limitation, we introduce a weight-varying mechanism in the cost functional to distinguish among various strategies for practical advantages. A similar approach has been used in [194, 198, 199]. This approach enables a more effective allocation of resources that accounts for budget and operational constraints. It also ensures that non-focal interventions are maintained at a reduced but non-zero baseline level, rather than being completely excluded. As a result, the complementary benefits of multiple concurrent interventions are preserved that are typically lost under the binary control activation framework. The resulting optimal control profiles represent more balanced strategies, prioritizing key interventions while maintaining essential supportive measures, thereby offering a more realistic application to real-world public health decision-making.

We propose a set of control strategies that target key epidemiological components, including HIV infection diagnosis, initiation and adherence to treatment, and management of drug resistance. The descriptions of these strategies are as following:

Strategy A - Diagnosis focused: This strategy prioritizes finding infected individuals before they can contribute to further transmission, making it particularly effective when early diagnosis substantially reduces onward spread. It is a suitable option in settings where maintaining diagnostic infrastructure is more feasible and cost-effective than providing treatment, particularly in low-income countries. The early diagnosis is prioritized by considering low weights for the costs associated with control u_1 and u_2 while treatment-related costs are maintained at a moderate level.

Strategy B - Treatment focused: Prioritizing treatment-related interventions that enhance treatment availability can be particularly effective in the mature phase of the epidemic, where a substantial proportion of infected individuals are already diagnosed. In some cases, a high prevalence of drug-resistant infections also necessitates the adoption of treatment-focused strategies. We consider lower values for weight constants w_3 and w_4 to illustrate this strategy.

Strategy C - Adherence focused: Once a substantial proportion of the infected population initiates the treatment, it becomes crucial to shift the focus towards adherence-related interventions to prevent the emergence of drug resistance. Consequently, it reduces the prevalence of drug-resistant infections and might be effective when the second-line treat-

ments are limited and costly. This emphasis is captured by assigning a lower weight to the cost constant w_5, which prioritizes adherence-enhancing measures.

Strategy D - Balanced: In resource-rich settings, where multiple interventions can be simultaneously implemented to rapidly reduce the disease burden, a balanced strategy may be adopted. This involves assigning equal weights to all interventions, ensuring uniform emphasis across diagnosis, treatment, and adherence. This approach is also suitable in the final phase of the epidemic, when comprehensive efforts are needed to eliminate remaining transmission.

Strategy E - Dynamic control optimization: A framework for 95-95-95 target achievement: For the optimal achievement of the UNAIDS 95-95-95 targets, we consider a dynamic strategy that combines the key epidemiological components using the model predictive control (MPC) approach, also known as receding horizon control (RHC) [200,201]. In this approach, we define three key metrics based on the values of control and state variables at a given time: the proportion of diagnosed individuals M_1, those under treatment M_2, and those who are virally suppressed M_3 among all HIV-infected individuals. Note that, earlier defined Strategy A improves M_1 by increasing diagnosis rates, Strategy B enhances M_2 by improving treatment initiation, and Strategy C raises M_3 by supporting treatment adherence. Once the 95-95-95 targets are achieved, a balanced strategy is applied, unless any of the metrics drop below the 95% threshold. For this, the total simulation period is partitioned into k sub-intervals, determined by selected decision points where these metrics are recalculated to get feedback from the model. At each decision point, an optimal control problem is solved over the remaining finite prediction horizon, using the current system state as the initial condition. This optimization generates a sequence of optimal control inputs, and only the first portion of the computed control sequence is applied to the system. The process is repeated at subsequent time steps, continuously updating the control strategy based on the evolving values of metrics M_1, M_2 and M_3, thus creating a feedback loop through the state variables. This modified MPC framework ensures the convergence of the optimal control solution by eliminating instabilities that may arise from the strategy-based variations in the cost functional at different phases of the simulation period. For a detailed description of the computational procedure, see Algorithm 2.

For the numerical simulations, we use a representative set of parameters as listed in Table (5.2). The simulation is carried out over a time horizon of $t_f = 25$ years, which is essential for a chronic infection like HIV, where the infectious period is prolonged and the effects of interventions require several years to be observed. The initial population size is $S(0) = 625, I_{SU}(0) = 0.2, I_{SD}(0) = 0.5, T_1(0) = 1.8, I_{RU}(0) = 0.2, I_{RD}(0) = 0.1, T_2(0) =$

Algorithm 2 Dynamic Control Optimization

Require: Simulation time t_f, decision points $D = \{0, 1, \ldots, t_f\}$, model parameters θ, initial conditions y_0, strategy weights W, control bounds $U_b = [0, 1]^5$, convergence tolerance ϵ_c, maximum iterations $k_{\max}$, relaxation parameter α

Initialize: Set $t \leftarrow 0$, $y \leftarrow y_0$, and discretize time grid $t_{\text{total}} = \{t_0, t_1, \ldots, t_N\}$ over $[0, t_f]$ with N points
for each decision point $t_d \in D$ **do**
  Calculate 95-95-95 metrics at t_d:
    $M_1(t_d) \leftarrow \frac{I_{SD}+I_{RD}+T_1+T_2}{I_{SU}+I_{SD}+I_{RU}+I_{RD}+T_1+T_2}$
    $M_2(t_d) \leftarrow \frac{T_1+T_2}{I_{SD}+I_{RD}+T_1+T_2}$
    $M_3(t_d) \leftarrow \frac{u_5^* T_1+T_2}{T_1+T_2}$
  if $M_1(t_d) < 0.95$ **then**
    Select Strategy A (Diagnosis focused)
  else if $M_1(t_d) \geq 0.95$ and $M_2(t_d) < 0.95$ **then**
    Select Strategy B (Treatment focused)
  else if $M_1(t_d) \geq 0.95$ and $M_2(t_d) \geq 0.95$ and $M_3(t_d) < 0.95$ **then**
    Select Strategy C (Adherence focused)
  else
    Select Strategy D (Balanced)
  end if
  Set cost functional weights W based on selected strategy
  Solve optimal control problem from t_d to t_f using backward-forward sweep:
  for $k = 1$ to $k_{\max}$ **do**
    Solve state system $\dot{y} = f(y, u^{(k-1)}, \theta)$ from t_d to t_f with $y(0) = y_0$
    Solve adjoint system $\dot{\sigma} = -\nabla_y H(y, u^{(k-1)}, \sigma, \theta, W)$ from t_f to t_d with $\sigma(t_f) = 0$
    Compute u^{new} using $\frac{\partial H}{\partial u_j} = 0$ for $j = 1, \ldots, 5$
    Update $u^{(k)} \leftarrow (1 - \alpha)u^{(k-1)} + \alpha u^{\text{new}}$
    if $\max_j \|u_j^{(k)} - u_j^{(k-1)}\|_\infty < \epsilon_c$ **then**
      Set $u^* \leftarrow u^{(k)}$
      break
    end if
  end for
  Implement controls until next decision point:
    Set $t_{\text{next}} \leftarrow t_d + 1$ if $t_d < t_f$ else t_f
    Simulate system forward to t_{next} using $u^*(t)$
    Update $y \leftarrow y(t_{\text{next}})$, $t \leftarrow t_{\text{next}}$
end for
return Dynamic optimal control profile $u^*(t)$, state trajectories $y(t)$.

$0.2, A(0) = 0.25$. The weight constants associated with the state variables are fixed as $W_1 = 1$, $W_2 = 0.5$, $W_3 = 5$, $W_4 = 2$, $W_5 = 0.25$ and $W_6 = 0.05$. Note that, these weights are assigned based on the relative burden of infection of each state variable within the community. The values of W_5 and W_6 reflect the prioritization of treatment coverage, even though this may lead to increased costs. Further, the weight constants associated with the control functions, along with the corresponding strategies, are listed in the Table 5.4. It is important to note that the weight constants used in the simulations are theoretical in nature and are primarily intended to illustrate the different control strategies proposed in this study. However, they are roughly scaled based on estimated intervention costs. Higher weights are assigned to the drug-resistant infected population compared to the drug-sensitive group, reflecting the increased cost of managing drug-resistant related interventions. Additionally, given the prolonged nature of HIV treatment, the weights associated with treatment-related interventions are chosen to be relatively higher to account for their long-term resource requirements.

Strategy	w_1	w_2	w_3	w_4	w_5
Strategy A	0.005	0.005	2	5	1
Strategy B	0.5	0.5	0.02	0.05	1
Strategy C	0.5	0.5	2	5	0.01
Strategy D	0.5	0.5	2	5	0.6

Table 5.4: The weight constants associated with the control variables in different control strategies.

The optimal control profiles for each strategy are shown in Figures 5.7-5.11. These figures also illustrate the state trajectories of infected and treated populations, highlighting the differences in population dynamics under various control strategies. In addition, we included two key epidemiological indicators, the proportions of drug-resistant and undiagnosed individuals within the total infected population, to identify the effectiveness of proposed strategies in achieving their individual objectives. In Figure 5.7a, the optimal control profile for Strategy A emphasizes diagnosis-focused interventions. Consequently, the proportion of undiagnosed cases declines significantly from the beginning. As the initiation rate of second-line therapy increases to a certain level, the drug-resistant cases starts to fall (see Figure 5.7b). Note that, the number of diagnosed drug-resistant individuals rises sharply in the early phase (see Figure 5.7c). This is primarily due to an imbalance between the high diagnosis rate, driven by higher values of control u_2, and the limited availability of second-line treatment.

In Strategy B, the optimal control profile reflects a prioritized allocation of resources

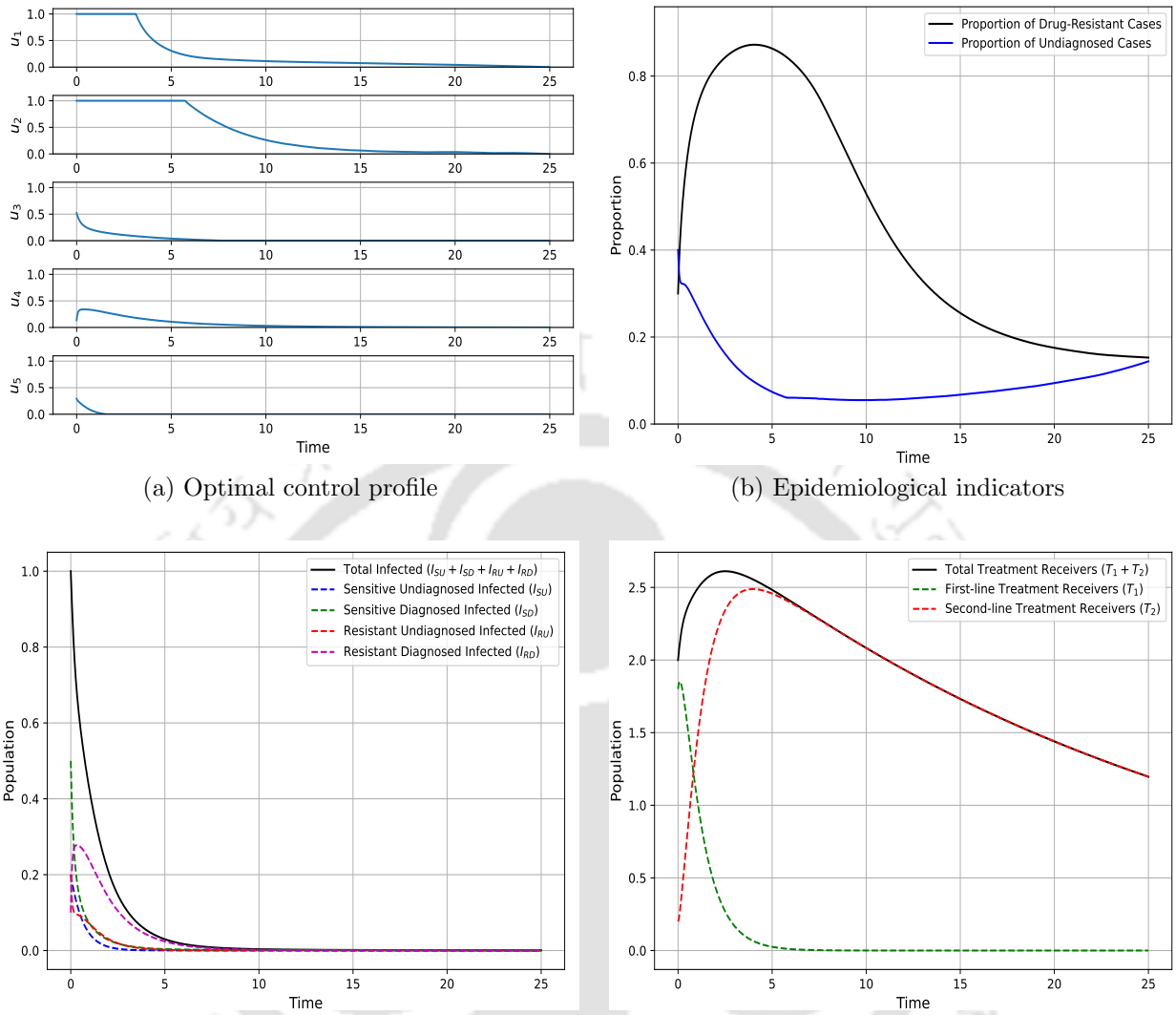

(a) Optimal control profile

(b) Epidemiological indicators

(c) Infected population dynamics

(d) Treatment coverage dynamics

Figure 5.7: State and optimal control dynamics of the optimal control problem (5.5.1)-(5.5.2) for Strategy A.

toward treatment-related interventions (see Figure 5.8). Although this strategy emphasizes treatment, it also focuses on diagnosis in the early phase of the simulation, making the infected population eligible to receive treatment. The proportion of undiagnosed cases remains higher compared to Strategy A (see Figure 5.8b). As observed in Figure 5.8c, however, all infected populations continuously declines following the implementation of this control strategy, makes it more efficient in reducing disease burden relative to Strategy A. As in Strategy A (see Figure 5.7d), the limited efforts in adherence-enhancing interventions reduce efficacy of first-line treatment, leading to the development of drug resistance among some patients

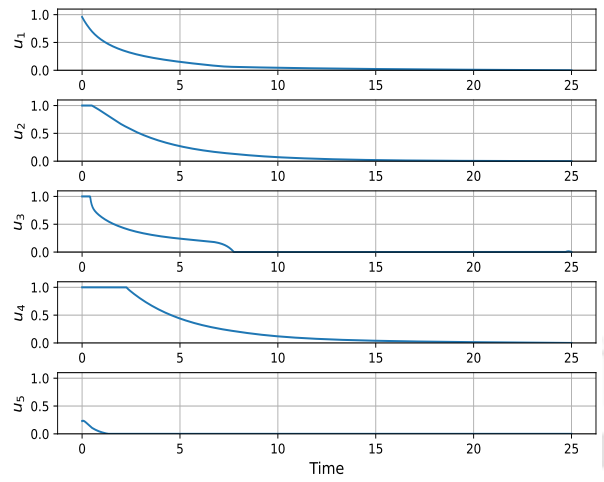

(a) Optimal control profile

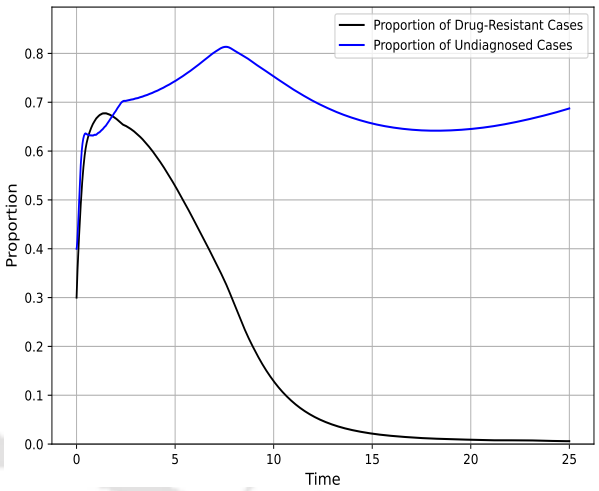

(b) Epidemiological indicators

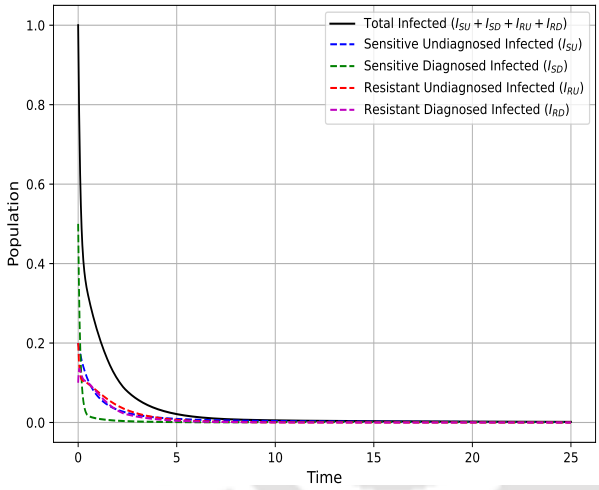

(c) Infected population dynamics

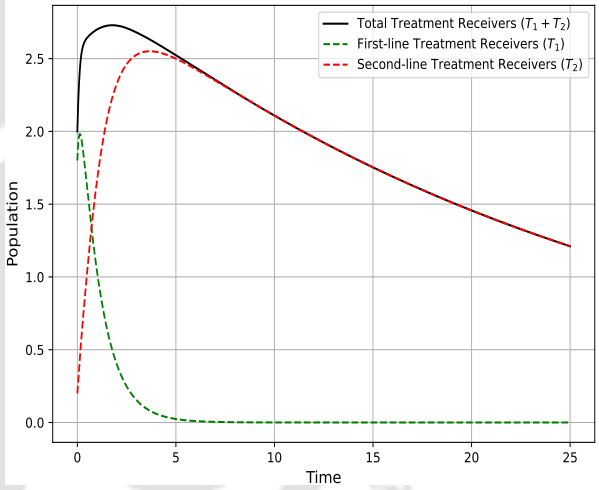

(d) Treatment coverage dynamics

Figure 5.8: State and optimal control dynamics of the optimal control problem (5.5.1)-(5.5.2) for Strategy B.

and their subsequent transition to second-line treatment (see Figure 5.8d).

The optimal controls for Strategy C are presented in Figure 5.9a highlighting the priority to adherence-related control variable u_5. While this strategy leads to a sharp decline in all infected compartments, it does not reduce the proportion of undiagnosed population (see Figure 5.9b, Figure 5.9c). However, higher intensity of control u_5 reduces the development of drug resistance. As a result, after an initial short-term rise, the requirement for second-line therapy decreases. In contrast to Strategies A and B, this approach results in fewer second-line treatment initiations (see Figure 5.9d).

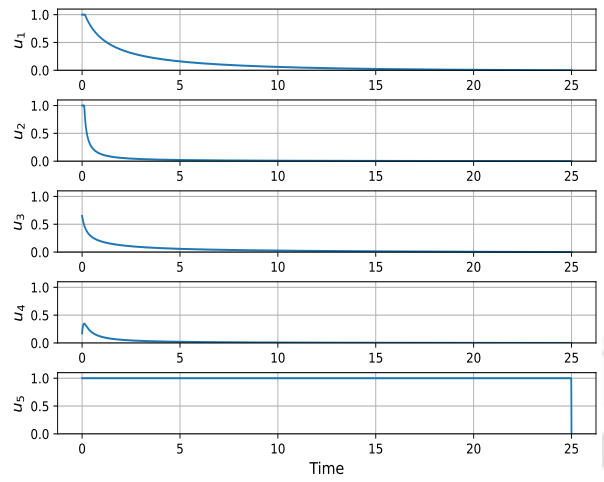

(a) Optimal control profile

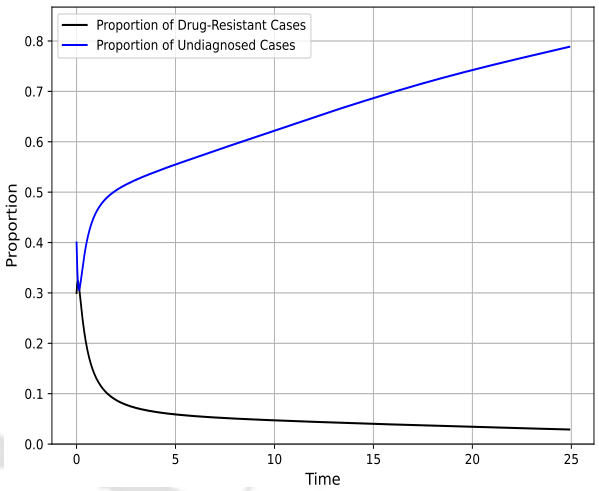

(b) Epidemiological indicators

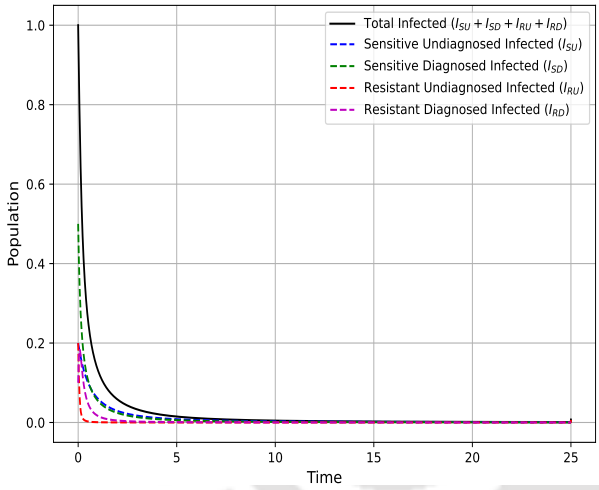

(c) Infected population dynamics

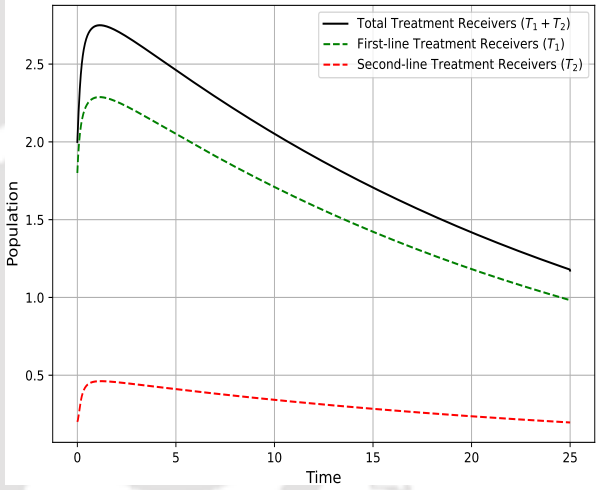

(d) Treatment coverage dynamics

Figure 5.9: State and optimal control dynamics of the optimal control problem (5.5.1)-(5.5.2) for Strategy C.

In Figure 5.10a, the optimal control profile shows a balanced approach by targeting all control variables at different stages of the simulation. In the early phase, all controls are applied simultaneously to maximize the intervention impact. As the number of individuals receiving first-line treatment falls below a certain threshold, the adherence-related control loses its relevance and reduces to zero to achieve the optimality. At the same time, these additional efforts are redirected toward improving the diagnosis of drug-resistant infections and expanding second-line treatment coverage, in response to the sudden increase in drug-resistant cases resulting from non-adherence to first-line treatment (see Figure 5.10b, Figure

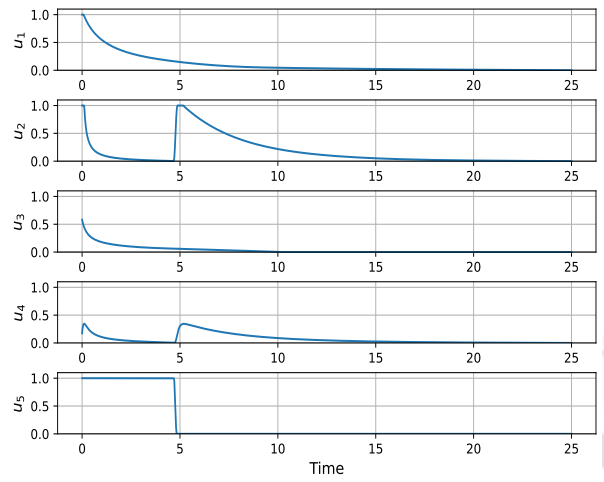

(a) Optimal control profile

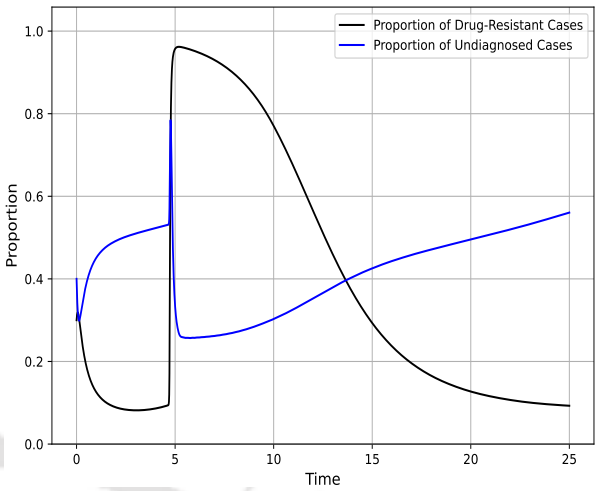

(b) Epidemiological indicators

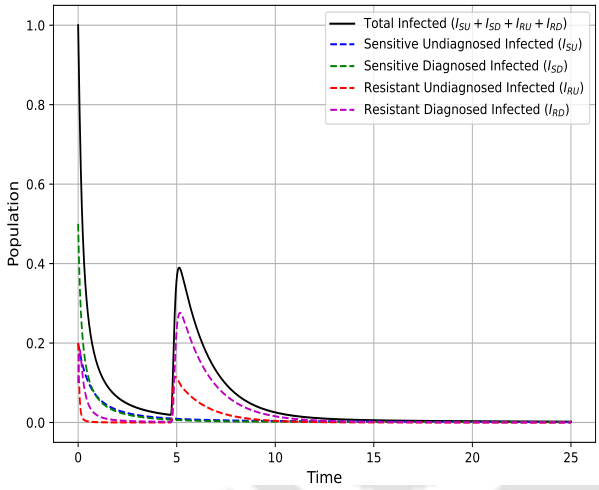

(c) Infected population dynamics

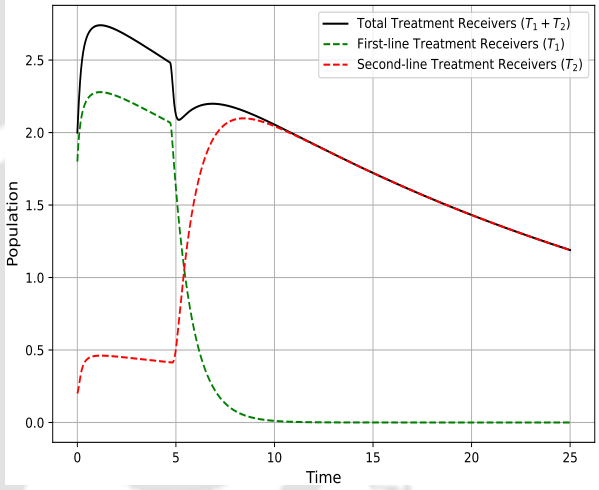

(d) Treatment coverage dynamics

Figure 5.10: State and optimal control dynamics of the optimal control problem (5.5.1)-(5.5.2) for Strategy D.

5.10c). Accordingly, a significant change in treatment coverage dynamics is observed (see Figure 5.10d).

In the dynamic control optimization framework, decision points are set at one-year intervals considering the long-term dynamics of HIV infection. At each decision point, controls are updated based on feedback from the current system state. The optimal control profile in Figure 5.11a shows that the initial efforts starts from the diagnosis focused interventions to achieve the 95-95-95 targets. After a few strategy adjustments, all three targets are achieved within the first five years, followed by the implementation of a balanced strategy for the

remaining simulation period. The color bar at the bottom indicates the specific strategy implemented during each corresponding time interval (see Figure 5.11b). Due to sudden changes in control inputs at each decision point, the state variables exhibit non-smooth trajectories. The results also suggest that while second-line treatment is more optimal than first-line treatment, the required coverage is lower compared to Strategies A, B, and D. (see Figure 5.11b). This dynamic approach suggests that the 95-95-95 targets can be achieved within five years through optimal resource allocation. However, although these targets are reached by the third year, sustaining them requires continuous and judicious allocation of resources across all aspects of HIV management.

We further compared the total number of infected individuals and those receiving treatment under each control strategy with the baseline scenario of no intervention. The corresponding population dynamics for each strategy and the no-control case are illustrated in Figure 5.12. Among all strategies, Strategy C shows highest reduction in infection burden, averting approximately 26.69 million person-years of infection, whereas Strategy D is the least effective, with 25.9 million person-years averted. In terms of treatment coverage, Strategy B leads with 44.02 million person-years of additional treatment, while Strategy D again shows the lowest impact, contributing 42.54 million person-years of treatment. A detailed comparison of infection aversion and treatment additions across strategies is provided in Table 5.5.

5.6.3 Cost-effectiveness analysis

Efficient allocation of resources is crucial for the effective control and elimination of a disease, particularly in resource-limited settings and low-income countries. Cost-effectiveness analysis is a valuable tool for identifying relatively low-cost interventions with substantial potential to reduce the burden of disease [120, 194]. In this section, we evaluate the cost-effectiveness of the control strategies proposed in Section 5.6.2 and rank them according to their effectiveness in reducing infection levels with optimal resource utilization. For this purpose, we consider the average cost-effectiveness ratio (ACER) method [194]. The strategy with the lowest ACER value is ranked as the most cost-effective strategy.

In general, the ACER is defined as the ratio of the total cost factor associated with a control strategy to its corresponding impact on disease reduction. However, accurately estimating the exact cost and impact of implementing a strategy, particularly over a large population and long time horizon, is often impractical. Therefore, we employ proxy metrics to represent these estimates that are most suitable for our modelling framework. The impact of a control strategy can be measured by metrics such as averted total infections, averted

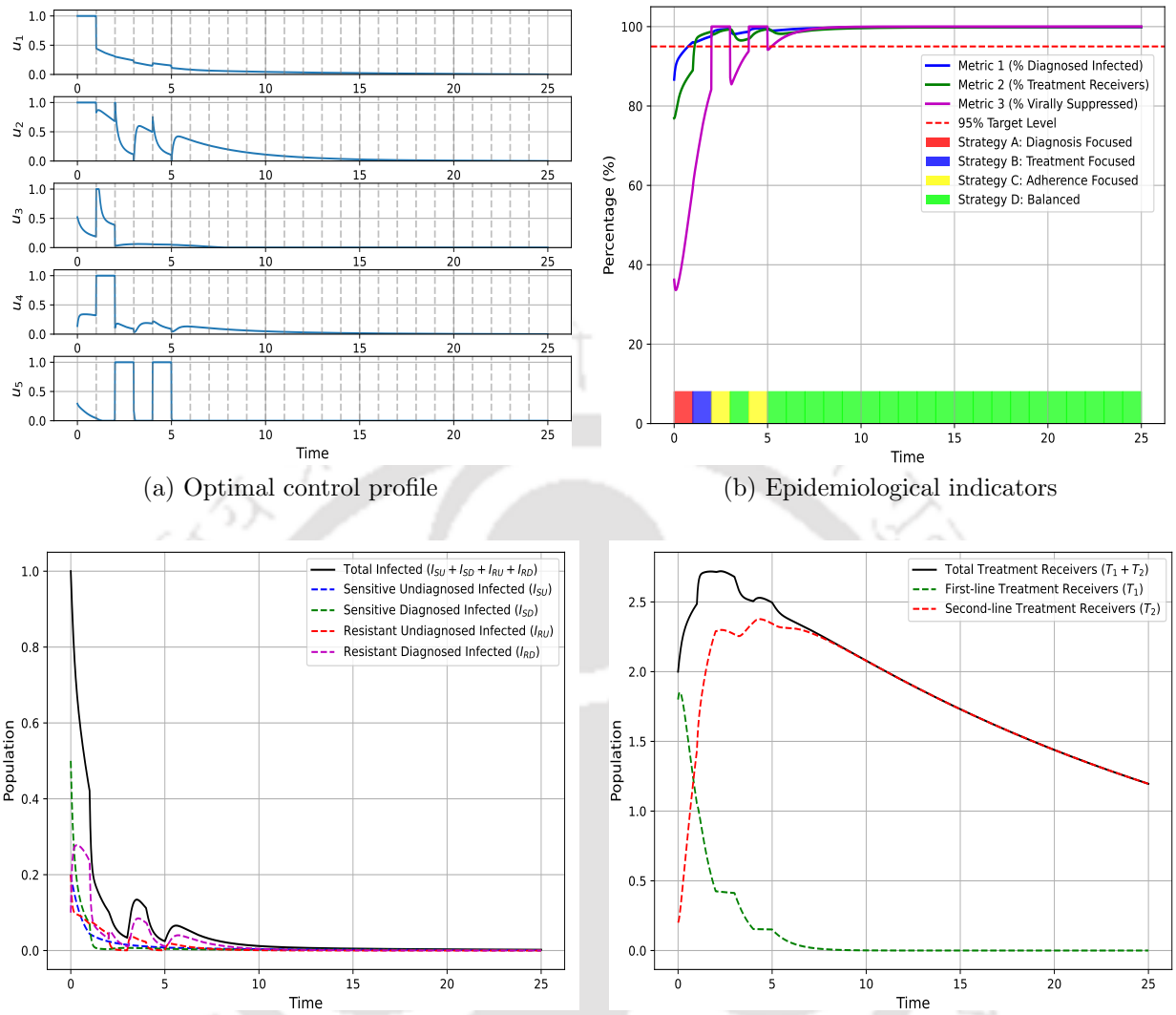

(a) Optimal control profile

(b) Epidemiological indicators

(c) Infected population dynamics

(d) Treatment coverage dynamics

Figure 5.11: State and optimal control dynamics of the optimal control problem (5.5.1)-(5.5.2) for Strategy E.

person-years of infection, or additional person-year of treatment. We use the total averted person-year of infection and additional person-year of treatment, as these are more suitable metrics for the proposed model, which account for the duration individuals remain in a state. It is calculated as the difference in the cumulative number of infected or treated individual with and without control implementation during the simulation period. Further, the cost of a control strategy is calculated as the sum of the integrals of the squared optimal control values (control intensity), each weighted by its respective relative cost factor (RCF), over the simulation period.

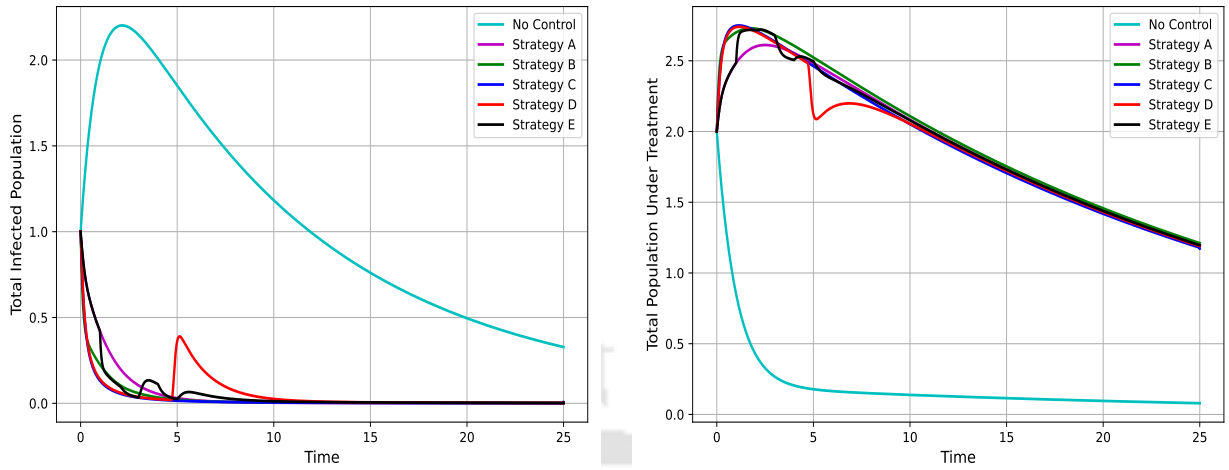

(a) Total infected population under different strategies and no control

(b) Total treated population under different strategies and no control

Figure 5.12: Comparative population dynamics of infected and treated individuals under different control strategies and the no-intervention scenario over the simulation period.

The cost estimates for various control components depend on regional economic conditions and the mode of implementation. Using a relative scale for these estimates reduces this variance. The costs associated with u_1 and u_2 include expenses for testing, infrastructure development, and public awareness campaigns [202]. Among these, diagnosis of drug-resistant cases is significantly more expensive due to the need for specialized tests and advanced equipments. HIV drug-resistance testing at Metropolis Healthcare Limited, one of India's leading diagnostic providers, can cost 5–20 times more than standard HIV testing, depending on the method used. However, this disparity decreases when considering the cost of all components of efforts combined. Accordingly, we set the $RIF(u_1) = 1$ as the base unit and $RIF(u_2) = 5$. Treatment-related efforts, represented by u_3 and u_4, involve training healthcare professionals, expanding treatment facilities, and offering subsidized therapy [203]. In particular, second-line ART incurs higher costs due to more complex protocols and specialized care needs. Based on this, we assign $RIF(u_3) = 10$ and $RIF(u_4) = 15$. Further, efforts to improve drug adherence, such as individual counseling, educational campaigns, reminder systems via SMS or mobile apps, and strengthening medicine supply chains, are major contributors for the cost of u_5 [204]. We assume their relative cost as $RCF(u_5) = 2$. Note that these values are not exact but serve as approximations to reflect the relative cost burden of each control measure.

Based on the control intensities and RCF of each control variable, and the control impact

of each strategy, the ACER for a strategy is given by:

$$\text{ACER} = \frac{\text{Total Cost of Interventions}}{\text{Total Strategy Impact}} = \frac{\sum_{i=1}^{5} (\text{Control Intensity})_i \times (\text{RCF}_i)}{\text{Total Strategy Impact}}.$$

For each strategy, Table 5.5 presents the control intensity for each control, the total cost of interventions, and the respective impact on each infection and treatment classes. Based on these values, the ACER is computed in terms of (i) total person-years of infection averted and (ii) total person-years of treatment added. The total infection-related impact of a strategy is calculated by adding the averted person-years across all infected classes. To reflect the real-world cost implications in treatment impact, particularly in resource-limited settings, we assign a higher weight to first-line treatment in the ACER calculation for treatment coverage. This extra weight accounts for the significant cost difference between first and second-line ART, where second-line ART can be 3 to 9 times more expensive depending on the regional economic state [205]. Consequently, the total impact of a strategy on added person-years of treatment is computed as the sum of 5 times the added person-years for T_1 (assumed for low and lower-middle-income countries) and the added person-years for T_2. Based on this, the ACER for person-year of averted infection and added treatment are listed in Table 5.5.

The ACER values indicate that Strategy D is the most cost-efficient in reducing the infection burden, despite averting the fewest person-years of infection. The lower total implementation cost in this strategy contributes to its high cost-effectiveness. In contrast, Strategy B ranks lowest in cost-efficiency due to the high expenses associated with treatment-focused interventions. While Strategy B significantly reduces the infection burden, this high cost limits its cost-effectiveness. Also, Strategies E, A, and C rank second, third, and fourth, respectively, in terms of cost-effectiveness for infection reduction.

However, when the goal is to increase treatment coverage, Strategy C becomes the most cost-effective. This is because a large share of resources in Strategy C is allocated to adherence-related interventions, enhancing the effectiveness of first-line treatment and reducing the need for more expensive second-line treatment. Similarly, Strategy D, which also prioritizes early focus on in adherence improving interventions, proves cost-effective for improving treatment outcomes, though it is slightly costly then Strategy C. The dynamic control approach, which emphasizes first-line treatment more than Strategies A and B, also demonstrates better cost-efficiency compared to those strategies. Although Strategy B achieves the highest overall treatment coverage, the lack of adherence-enhancing interventions makes it the least cost-effective. Overall, these ACER values suggest that in settings where expanding treatment coverage is feasible, particularly in middle- and upper-middle-income countries, investing in adherence-improving interventions is a more cost-effective

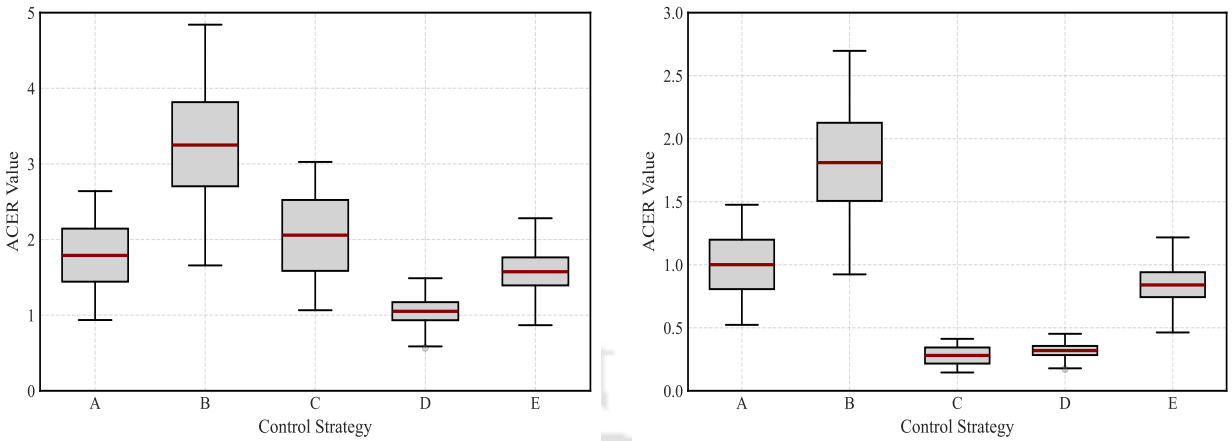

(a) Impact on infection reduction

(b) Impact on treatment expansion

Figure 5.13: Distribution of ACER values for proposed control strategies under (a) infection reduction and (b) treatment expansion objectives. Boxplots show the median (red line), interquartile range, and variability across sampled cost configurations.

approach. Otherwise, a balanced allocation of resources across all intervention components results in a more sustainable and efficient approach.

5.6.4 Robustness of cost-effectiveness rankings

To examine the robustness of the ACER values presented in Table 5 under cost uncertainty, we performed a sensitivity analysis by varying the RCF values of all interventions. A total of 5,000 parameter sets were generated using the LHS method, with RCFs ranging from 50% to 150% of their baseline values as described earlier. For each configuration, the ACER of all five strategies was recalculated for both infection-reduction and treatment-expansion outcomes.

Figure 5.13 presents the resulting ACER distributions. For infection-based impact (see Figure 5.13a), Strateg D consistently exhibited the lowest median ACER and minimal variability, maintaining its dominance across almost all parameter sets. In contrast, Strategy B showed the highest ACER and greatest spread, indicating strong sensitivity to cost fluctuations. For treatment-based impact (see Figure 5.13b), Strategy C achieved the lowest median ACER, followed closely by Strategy D. The narrow interquartile ranges across most strategies indicate that the cost-effectiveness rankings are largely robust to moderate variations in RCFs. Only Strategy B showed notable instability, suggesting that its relative performance depends more strongly on cost assumptions.

To complement the ACER sensitivity results, we examined the frequency of strategy

Strategies	Control Intensity					Total Cost	Strategy Impact						ACER	
	u_1	u_2	u_3	u_4	u_5		I_{SU}	I_{SD}	I_{RU}	I_{RD}	T_1	T_2	Infection	Treatment
Strategy A	3.9842	7.3509	0.1322	0.3003	0.0247	46.6137	2.5841	4.0793	19.1606	0.1837	0.8931	42.0576	1.7923	1.0019
Strategy B	0.9636	2.3083	1.4431	3.9535	0.0203	86.2788	2.4519	4.2578	19.1076	0.6748	0.8828	43.1396	3.2568	1.8143
Strategy C	1.1014	0.2416	0.1663	0.0600	25.0000	54.8731	2.4760	4.1091	19.3202	0.7818	38.2447	4.7120	2.0562	0.2801
Strategy D	1.0069	2.1653	0.1434	0.2972	4.7432	27.2111	2.4556	4.0749	19.1341	0.2335	10.6799	31.8639	0.7089	0.3191
Strategy E	1.3043	2.4865	0.4899	1.2210	2.0251	41.0008	2.4878	4.1075	19.1107	0.3205	1.4350	41.6223	1.5754	0.8402

Table 5.5: Summary of control intensities, total costs, impacts on infection and treatment classes, and ACER values for all control strategies. ACER values are computed considering both infection reduction and treatment coverage expansion objectives.

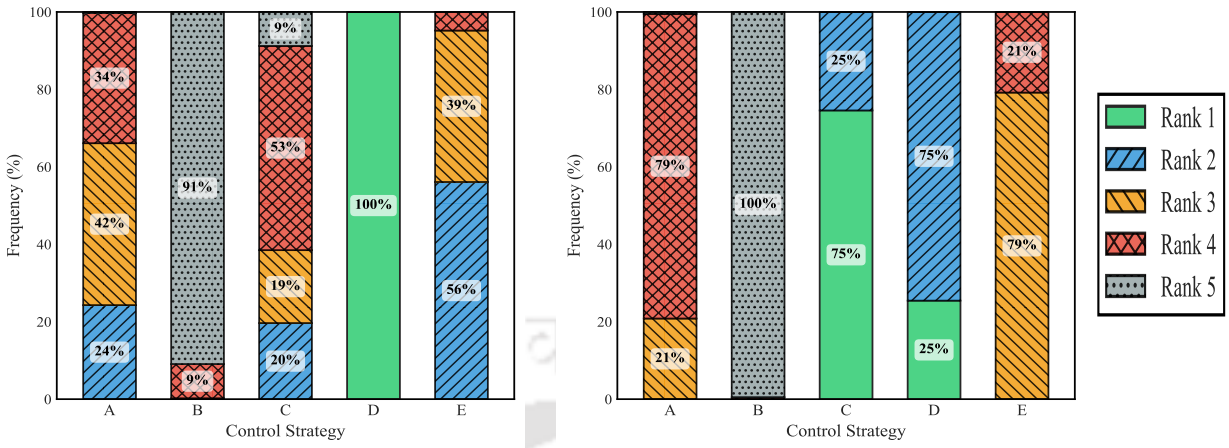

(a) Impact on infection reduction

(b) Impact on treatment expansion

Figure 5.14: Rank frequency distribution of the control strategies under (a) infection reduction and (b) treatment expansion outcomes. Bars indicate the proportion of simulations in which each strategy achieved a given rank.

rankings across 5,000 random RCF samples within ±50% of baseline values (see Figure 5.14). For infection reduction (see Figure 5.14a), Strategy D ranked first in almost all parameter sets, confirming its robust superiority. Strategy E showed stable second-rank performance, while Strategies A and C exhibited moderate variability. Strategy B consistently ranked last in over 90% of simulations. For treatment expansion (see Figure 5.14b), Strategy C ranked first in 75% of cases, followed by Strategy D (25%), indicating both as strong candidates depending on the cost structure. Other strategies remained consistently less cost-effective, while Strategy B almost always ranked last. Overall, these results confirm that although absolute ACER values vary with cost parameters, the ordinal rankings, particularly for the most cost-effective strategies, remain largely stable, showing the robustness of the policy insights derived from the cost-effectiveness analysis.

5.6.5 Adjoint-based sensitivity analysis of state variables

After identifying the most cost-effective control strategy, both in terms of averted infection burden and enhanced treatment coverage, the logical next step is to determine how to optimally allocate any additional resources to maximize public health benefits. This is relevant for particularly middle- and upper-middle income countries, where budgets may permit allocations of resources beyond the cost-effectiveness goals. To address this, we conducted an adjoint-based sensitivity analysis of each state variable with respect to each control vari-

able. This analysis provides forward-looking insights into how small perturbations in control variables influence the cumulative population in each compartment. Controls with higher sensitivity indices, positive for the susceptible and treatment classes and negative for the infected and AIDS classes, are identified as potential priorities for additional investment. A detailed discussion of adjoint-based sensitivity analysis for differential-algebraic equations can be found in [206].

In this section, we analyze the sensitivities of state variables under Strategy C and Strategy D, as these strategies are the most cost-effective for enhancing treatment coverage and reducing infection burden, respectively. In this approach, we begin with solving the optimal control problem (5.5.1)-(5.5.2) for the chosen strategy to obtain the optimal control profile $u_i^*(t)$ and the corresponding state trajectories $x_i^*(t)$ over the time interval $[0, t_f]$. Subsequently, we formulate a new adjoint system for the state variable of interest as follows:

$$\frac{d\sigma_i}{dt} = -\sum_{j=1}^{8} \sigma_j \frac{\partial f_j}{\partial x_i} - \frac{\partial \mathcal{X}}{\partial x_i}, \quad \sigma_i(t_f) = 0. \tag{5.6.1}$$

Here, f_j denotes the j^{th} component of the right-hand side of system (5.5.2) and $\sigma_i(t)$ is the adjoint variable that captures how small perturbations in a state variable $x_i(t)$ propagate through time to affect the state of interest $\mathcal{X}(t)$. The adjoint system is solved backward in time using the previously obtained optimal control profiles $u_i^*(t)$ and the corresponding state trajectories $x_i^*(t)$. The sensitivities of $\mathcal{X}(t)$ to a control variable u_k is then computed using the adjoint variables $\sigma_i(t)$ and the system equations, as follows:

$$\begin{aligned} \frac{\partial \mathcal{X}}{\partial u_k} &= \int_0^{t_f} \sum_{i=1}^{8} \frac{\partial \mathcal{X}}{\partial x_i} \frac{\partial f_i}{\partial u_k} dt \\ &= \int_0^{t_f} \sum_{i=1}^{8} \sigma_i \frac{\partial f_i}{\partial u_k} dt. \end{aligned} \tag{5.6.2}$$

Note that these sensitivities indicate the cumulative effect of small perturbations in the control $u_k(t)$ on the state of interest $\mathcal{X}(t)$. This effect is mediated through the state variables $x_i(t)$, whose contributions are captured by the corresponding adjoint variables $\sigma_i(t)$ for $i = 1, 2, ..., 8$.

The adjoint-based sensitivity indices of each state variable with respect to the control variables for Strategy C and Strategy D are presented in Table 5.6. The relative significance of the control variables is almost similar across these two strategies. All control variables exhibit a positive impact on the susceptible population and a negative impact on the AIDS-infected population, with u_5 showing the highest influence compared to the other controls.

The undiagnosed infected population with the sensitive strain is primarily negatively influenced by u_1, which governs the diagnosis rate. Further, u_3 also shows a small negative effect on I_{SU}, due to its strong negative impact on I_{SD} population, thereby indirectly reducing the prevalence of the sensitive strain. Although u_1 tends to increase I_{SD} by converting I_{SU} to I_{SD}, this is overpowered by the strong negative influence of u_3 on I_{SD}. The controls u_2, u_4, and u_5 do not show any impact on both I_{SU} and I_{SD}. Overall, after achieving the cost-effectiveness objective, control u_3 emerges as the most suitable target for further resource allocation to reduce the drug-sensitive infected population in both strategies

The first-line treatment coverage is most positively influenced by control u_5, which enhances adherence to treatment in both strategies. An Improved adherence helps infected individuals to continue with first-line treatment and reduces the emergence of drug resistance. Consequently, u_5 depicts a strong negative impact on the compartments I_{RU}, I_{RD}, and T_2. In contrast, u_2 and u_4 have negligible influence on these compartments compared to u_5. In Strategy C, controls u_1 and u_3 have no impact on the drug-resistant and second-line treatment compartments, as adherence-improving interventions (through u_5) are applied at their full capacity, and the resistant infections primarily arise through transmission. However, in Strategy D, adherence interventions are focused only in the early phase of the simulation. As a result, drug resistance can also emerge during treatment, making the compartments I_{RU}, I_{RD}, and T_2 sensitive to changes in u_1 and u_3. Nevertheless, this sensitivity remains insignificant when compared to the dominant influence of u_5. Overall, the drug-resistant infected and treatment-receiving populations are predominantly sensitive to control u_5.

State Variables	Strategy C					Strategy D				
	u_1	u_2	u_3	u_4	u_5	u_1	u_2	u_3	u_4	u_5
S	0.5359	0.0179	0.3353	0.0731	27.1014	0.6158	0.0998	0.4373	0.2438	3.0096
I_{SU}	-1.0808	0	-0.0844	0	0	-1.3015	0	-0.1706	0	0
I_{SD}	0.0825	0	-2.0983	0	0	0.1934	0	-3.6801	0	0
T_1	1.3701	0	3.9012	0	409.6203	0.4349	0	1.9751	0	34.0293
I_{RU}	0	-0.0679	0	-0.0125	-156.1592	0.0073	-0.4012	0.4274	-0.0104	-9.7815
I_{RD}	0	-0.0143	0	-1.1285	-63.9923	0.0215	-0.0223	0.4016	-4.0039	-3.6434
T_2	0	0.1489	0	2.1617	-104.9142	1.0426	0.7183	3.3622	7.3432	-9.5087
A	-0.1136	-0.0076	-0.2043	-0.1005	-20.6713	-0.1283	-0.0424	-0.3142	-0.3717	-1.1643

Table 5.6: Adjoint-based sensitivity indices of state variables with respect to each control variable under Strategy C and Strategy D.

Remark 5.6.1. *Note that we have used* $\frac{\partial f_i}{\partial u_k}$ *as an approximation of* $\frac{\partial x_i}{\partial u_k}$ *while applying the chain rule in (5.6.2). This is because the control* u_k *directly modifies the rate of change of*

the state x_i. Thus, $\frac{\partial f_i}{\partial u_k}$ captures the direct and instantaneous effect of u_k on x_i.

5.6.6 Control contribution analysis

In the previous sections, cost-effectiveness and adjoint-based sensitivity analyses helped identify the most efficient strategies and key controls under cost-constrained settings. Although these analyses offer critical insights into the relative efficiency and influence of different strategies, they do not fully capture the individual and synergistic contributions of each control variable. In this section, we quantify the contribution of each control within a given strategy to better understand its specific role, both direct and indirect, in achieving the overall public health objectives, particularly in scenarios where the cost of intervention is not a limiting factor. This analysis provides a broader and more actionable perspective for public health decision-makers, allowing informed allocation of resources.

We use the Shapley Value analysis [149–151], a tool from cooperative game theory, to achieve this objective. In game theory, the Shapley value analysis provides a systematic approach to fairly distribute the total outcome of a cooperative game among its players based on their individual marginal impacts. In the context of this study, the 'players' are the five control variables, and the 'outcome of the game' is the change observed in the state variables with and without the application of these controls. Shapley values quantify the average marginal contribution of each control to a given state variable, calculated across all possible combinations of the remaining controls. This ensures that each control's contribution is evaluated not only in isolation but also in the context of its interactions with all possible subsets of the remaining controls, providing a comprehensive idea about how the effectiveness of one control depends on others.

The calculation of Shapley values involves a combinatorial process that considers all possible coalitions of control variables. For a specific control u_i within a set of n controls (U), its Shapley value $\phi(u_i)$, corresponding to the given state variable, is computed as the weighted average of its marginal contributions across all subsets S of U that exclude u_i. Mathematically, this is expressed as:

$$\phi(u_i) = \sum_{S \subseteq U \setminus u_i} \frac{|S|!(n - |S| - 1)!}{n!} \left(v(S \cup u_i) - v(S)\right),$$

where $v(S)$ denotes the value related to the given state variable under the coalition S, and the term $v(S \cup u_i) - v(S)$ represents the marginal contribution of control u_i when added to coalition S. The weighting factor $\frac{|S|!(n - |S| - 1)!}{n!}$ ensures fairness by accounting for all possible positions that control u_i could occupy in a permutation of the full set of

controls. This normalizes the contributions based on coalition size and ensures that each subset is weighted appropriately. In this study, with five control variables, the process involves evaluating all $2^5 = 32$ possible control combinations, making it computationally feasible while providing a robust and precise attribution of each control's impact on the state variables.

We conducted the Shapley value analysis for Strategy C and Strategy D, given their significance in terms of cost-effectiveness. The objective of this analysis is to quantify the contribution of each control variable to the observed person-year differences in each state variable, calculated with and without the implementation of the respective control strategies. As described in Section 5.6.3, these person-year differences represent the overall impact of a control strategy on disease dynamics. The cumulative person-years for each state variables under different control combinations are summarized in Table 5.7 for strategy C and in Table 5.8 for strategy D. These person-year distributions serve as the basis for computing the marginal contributions of each control variable. These contributions are subsequently used to calculate the Shapley values, which provide a measure of the individual and synergistic impact of each control on the model outcomes. Tables 5.9 and 5.10 present the Shapley value-based decomposition of control contributions to person-years in each state variable under Strategy C and Strategy D, respectively. The sign of the Shapley value indicates the direction of influence, while the percentage contribution, calculated using the absolute values, reflects the relative magnitude of each control's contribution. The detailed procedure for computing these Shapley values is outlined in Algorithm 3.

For Strategy C, which prioritizes adherence-focused interventions, Table 5.9 highlights major contributions from control u_5 across multiple state variables, especially in the treatment compartments. The Shapley values for T_1 and T_2 associated with u_5 are significantly higher (32.30 and –11.48, respectively) compared to other controls. This indicates that strong adherence support significantly influences the accumulation of person-years in treatment stages, enhancing retention in first-line therapy while reducing person-years in second-line treatment due to fewer treatment failures or transitions. In contrast, Strategy D, the balanced control approach, distributes the contribution more evenly across multiple controls. Here, although u_5 still plays a key role, particularly for T_1 (49.11%) in negative direction, the influence of u_2 becomes significantly more pronounced for T_2 (43.36%) and I_{RU} (54.44%), as compared to Strategy C. In addition, the contribution of u_4 also increases significantly for both T_1 and T_2. This redistribution indicates that under a balanced strategy, interventions targeting both adherence support to first-line treatment and resistance management collectively shape the epidemiological results. The switch from a high negative contribution of u_5 in T_2 under Strategy C (–11.48) to a comparatively small negative value (–2.44) under

Control Combination	**S**	$\mathbf{I}_{SU}$	$\mathbf{I}_{SD}$	$\mathbf{T}_1$	$\mathbf{I}_{RU}$	$\mathbf{I}_{RD}$	$\mathbf{T}_2$	**A**
$(0,0,0,0,0)$	21806.0240	2.7202	4.3542	1.7988	19.3376	0.8708	3.2637	5.9055
$(u_1,0,0,0,0)$	21806.8647	0.5731	6.0694	1.7988	19.3377	0.8708	3.2637	5.8290
$(0,u_2,0,0,0)$	21809.3619	2.7204	4.3542	1.7988	0.2398	18.3332	3.2637	5.6092
$(0,0,u_3,0,0)$	21806.0238	2.7199	4.3506	1.7993	19.3414	0.8708	3.2637	5.9055
$(0,0,0,u_4,0)$	21806.0778	2.7202	4.3542	1.7988	19.3117	0.0442	4.8138	5.8268
$(0,0,0,0,u_5)$	21809.9808	2.7204	4.3542	29.3721	1.9883	0.8708	3.2637	4.2294
$(u_1,u_2,0,0,0)$	21810.2029	0.5731	6.0695	1.7988	0.2398	18.3332	3.2637	5.5327
$(u_1,0,u_3,0,0$	21806.8647	0.5731	6.0691	1.7990	19.3377	0.8708	3.2637	5.8290
$(u_1,0,0,u_4,0)$	21806.9186	0.5731	6.0694	1.7988	19.3118	0.0442	4.8138	5.7503
$(u_1,0,0,0,u_5)$	21810.8219	0.5731	6.0695	29.3721	1.9883	0.8708	3.2637	4.1528
$(0,u_2,u_3,0,0)$	21809.3619	2.7204	4.3541	1.7989	0.2398	18.3332	3.2637	5.6092
$(0,u_2,0,u_4,0)$	21810.4071	2.7204	4.3542	1.7988	0.1803	0.5459	35.3498	3.9411
$(0,u_2,0,0,u_5)$	21810.3301	2.7204	4.3542	29.3736	0.0306	2.6599	3.2637	4.1987
$(0,0,u_3,u_4,0)$	21806.0776	2.7200	4.3506	1.7993	19.3155	0.0442	4.8138	5.8267
$(0,0,u_3,0,u_5)$	21810.7239	2.3556	0.1365	37.3270	1.9877	0.8708	3.2637	3.7849
$(0,0,0,u_4,u_5)$	21810.0347	2.7204	4.3542	29.3721	1.9624	0.0442	4.8138	4.1506
$(u_1,u_2,u_3,0,0)$	21810.2029	0.5731	6.0692	1.7991	0.2398	18.3332	3.2637	5.5327
$(u_1,u_2,0,u_4,0)$	21811.2482	0.5731	6.0695	1.7988	0.1803	0.5459	35.3498	3.8646
$(u_1,u_2,0,0,u_5)$	21811.1712	0.5731	6.0695	29.3736	0.0306	2.6599	3.2637	4.1222
$(u_1,0,u_3,u_4,0)$	21806.9186	0.5731	6.0691	1.7990	19.3118	0.0442	4.8138	5.7503
$(u_1,0,u_3,0,u_5)$	21811.7916	0.2443	0.2451	40.0431	1.9874	0.8708	3.2637	3.5545
$(u_1,0,0,u_4,u_5)$	21810.8757	0.5731	6.0695	29.3721	1.9624	0.0442	4.8138	4.0741
$(0,u_2,u_3,u_4,0)$	21811.1308	2.3573	0.1562	2.2836	0.2135	0.6366	42.8143	3.4896
$(0,u_2,u_3,0,u_5)$	21811.0731	2.3557	0.1365	37.3278	0.0306	2.6599	3.2637	3.7543
$(0,u_2,0,u_4,u_5)$	21810.4854	2.7204	4.3542	29.3736	0.0173	0.0890	7.9757	3.9606
$(0,0,u_3,u_4,u_5)$	21810.7778	2.3556	0.1365	37.3271	1.9618	0.0442	4.8138	3.7061
$(u_1,u_2,u_3,u_4,0)$	21812.1756	0.2697	0.3075	2.4480	0.2278	0.6773	45.2534	3.2645
$(u_1,u_2,u_3,0,u_5)$	21812.1408	0.2443	0.2451	40.0434	0.0306	2.6599	3.2637	3.5240
$(u_1,u_2,0,u_4,u_5)$	21811.3264	0.5731	6.0695	29.3736	0.0176	0.0900	7.9733	3.8841
$(u_1,0,u_3,u_4,u_5)$	21811.8455	0.2443	0.2451	40.0429	1.9616	0.0442	4.8138	3.4758
$(0,u_2,u_3,u_4,u_5)$	21811.2283	2.3557	0.1365	37.3278	0.0176	0.0901	7.9731	3.5162
(u_1,u_2,u_3,u_4,u_5)	21812.2960	0.2443	0.2451	40.0434	0.0176	0.0901	7.9731	3.2859

Table 5.7: Person-years in state variables for all control combinations for Strategy C.

Control Combination	S	I_{SU}	I_{SD}	T_1	I_{RU}	I_{RD}	T_2	A
$(0,0,0,0,0)$	21806.0240	2.7202	4.3542	1.7988	19.3376	0.8708	3.2637	5.9055
$(u_1,0,0,0,0)$	21806.8647	0.5731	6.0694	1.7988	19.3377	0.8708	3.2637	5.8290
$(0,u_2,0,0,0)$	21809.3619	2.7204	4.3542	1.7988	0.2398	18.3332	3.2637	5.6092
$(0,0,u_3,0,0)$	21806.0238	2.7199	4.3506	1.7993	19.3414	0.8708	3.2637	5.9055
$(0,0,0,u_4,0)$	21806.0778	2.7202	4.3542	1.7988	19.3117	0.0442	4.8138	5.8268
$(0,0,0,0,u_5)$	21809.9810	2.7204	4.3542	29.3701	1.9907	0.8708	3.2637	4.2292
$(u_1,u_2,0,0,0)$	21810.2029	0.5731	6.0695	1.7988	0.2398	18.3332	3.2637	5.5327
$(u_1,0,u_3,0,0$	21806.8647	0.5731	6.0691	1.7990	19.3377	0.8708	3.2637	5.8290
$(u_1,0,0,u_4,0)$	21806.9186	0.5731	6.0694	1.7988	19.3118	0.0442	4.8138	5.7503
$(u_1,0,0,0,u_5)$	21810.8220	0.5731	6.0695	29.3701	1.9907	0.8708	3.2637	4.1526
$(0,u_2,u_3,0,0)$	21809.3619	2.7204	4.3541	1.7989	0.2398	18.3332	3.2637	5.6092
$(0,u_2,0,u_4,0)$	21810.4071	2.7204	4.3542	1.7988	0.1803	0.5459	35.3498	3.9411
$(0,u_2,0,0,u_5)$	21810.3301	2.7204	4.3542	29.3698	0.0342	2.6602	3.2637	4.1986
$(0,0,u_3,u_4,0)$	21806.0776	2.7200	4.3506	1.7993	19.3155	0.0442	4.8138	5.8267
$(0,0,u_3,0,u_5)$	21810.7240	2.3556	0.1365	37.3250	1.9900	0.8708	3.2637	3.7848
$(0,0,0,u_4,u_5)$	21810.0348	2.7204	4.3542	29.3702	1.9648	0.0442	4.8138	4.1504
$(u_1,u_2,u_3,0,0)$	21810.2029	0.5731	6.0692	1.7991	0.2398	18.3332	3.2637	5.5327
$(u_1,u_2,0,u_4,0)$	21811.2482	0.5731	6.0695	1.7988	0.1803	0.5459	35.3498	3.8646
$(u_1,u_2,0,0,u_5)$	21811.1712	0.5731	6.0695	29.3698	0.0342	2.6602	3.2637	4.1221
$(u_1,0,u_3,u_4,0)$	21806.9186	0.5731	6.0691	1.7990	19.3118	0.0442	4.8138	5.7503
$(u_1,0,u_3,0,u_5)$	21811.7916	0.2443	0.2452	40.0407	1.9898	0.8708	3.2637	3.5544
$(u_1,0,0,u_4,u_5)$	21810.8759	0.5731	6.0695	29.3701	1.9648	0.0442	4.8138	4.0739
$(0,u_2,u_3,u_4,0)$	21811.1308	2.3573	0.1562	2.2836	0.2135	0.6366	42.8143	3.4896
$(0,u_2,u_3,0,u_5)$	21811.0731	2.3557	0.1365	37.3249	0.0334	2.6601	3.2637	3.7542
$(0,u_2,0,u_4,u_5)$	21810.4071	2.7204	4.3542	1.7988	0.1803	0.5459	35.3497	3.9411
$(0,0,u_3,u_4,u_5)$	21810.7779	2.3556	0.1365	37.3251	1.9641	0.0442	4.8138	3.7060
$(u_1,u_2,u_3,u_4,0)$	21812.1756	0.2697	0.3075	2.4480	0.2278	0.6773	45.2534	3.2645
$(u_1,u_2,u_3,0,u_5)$	21812.1408	0.2443	0.2452	40.0406	0.0332	2.6600	3.2637	3.5239
$(u_1,u_2,0,u_4,u_5)$	21811.2482	0.5731	6.0695	1.7988	0.1803	0.5459	35.3497	3.8646
$(u_1,0,u_3,u_4,u_5)$	21811.8455	0.2443	0.2452	40.0407	1.9639	0.0442	4.8138	3.4757
$(0,u_2,u_3,u_4,u_5)$	21811.1414	2.3573	0.1554	10.3456	0.1972	0.6198	34.6006	3.4964
(u_1,u_2,u_3,u_4,u_5)	21812.1960	0.2646	0.2793	12.4787	0.2035	0.6374	35.1276	3.2672

Table 5.8: Person-years in state variables for all control combinations for Strategy D.

State Variables	u_1		u_2		u_3		u_4		u_5	
	Shapley Value	**Contribution (%)**	**Shapley Value**	**Contribution (%)**	**Shapley Value**	**Contribution (%)**	**Shapley Value**	**Contribution (%)**	**Shapley Value**	**Contribution (%)**
S	0.9267	14.78	2.1131	33.69	0.5175	8.25	0.3234	5.16	2.3913	38.13
I_{SU}	-2.1323	86.12	-0.0272	1.10	-0.1977	7.99	-0.0273	1.10	-0.0915	3.70
I_{SD}	1.1018	17.45	-0.4277	6.78	-3.0734	48.69	-0.4280	6.78	-1.2818	20.30
T_1	0.9134	2.39	0.0490	0.13	4.9313	12.89	0.0486	0.13	32.3024	84.46
I_{RU}	0.0004	0.00	-10.5257	54.45	0.0044	0.02	-0.0237	0.12	-8.7754	45.40
I_{RD}	0.0021	0.02	6.2274	46.97	0.0097	0.07	-4.2249	31.86	-2.7950	21.08
T_2	0.1218	0.44	6.8865	24.89	0.7438	2.69	8.4366	30.49	-11.4794	41.49
A	-0.1352	5.16	-0.5265	20.10	-0.3185	12.16	-0.4418	16.87	-1.1976	45.71

Table 5.9: Shapley values for control contribution to person-years in each state variable for Strategy C.

State Variables	u_1		u_2		u_3		u_4		u_5	
	Shapley Value	**Contribution (%)**	**Shapley Value**	**Contribution (%)**	**Shapley Value**	**Contribution (%)**	**Shapley Value**	**Contribution (%)**	**Shapley Value**	**Contribution (%)**
S	0.9241	14.97	2.0822	33.74	0.5127	8.31	0.2925	4.74	2.3605	38.25
I_{SU}	-2.1285	86.68	-0.0231	0.94	-0.1936	7.88	-0.0231	0.94	-0.0873	3.56
I_{SD}	1.1048	17.58	-0.4199	6.68	-3.0656	48.78	-0.4202	6.69	-1.2740	20.27
T_1	0.7969	1.69	-9.1105	19.33	4.9630	10.53	-9.1103	19.33	23.1408	49.11
I_{RU}	0.0017	0.01	-10.4666	54.44	0.0097	0.05	0.0350	0.18	-8.7139	45.32
I_{RD}	0.0055	0.04	6.4014	48.83	0.0316	0.24	-4.0510	30.90	-2.6210	19.99
T_2	0.2274	0.62	15.9301	43.36	0.6621	1.80	17.4802	47.58	-2.4358	6.63
A	-0.1350	5.12	-0.5328	20.19	-0.3184	12.07	-0.4482	16.99	-1.2040	45.64

Table 5.10: Shapley values for control contribution to person-years in each state variable for Strategy D.

Strategy D further supports the idea that spreading the control effort reduces the intensity of adherence-related interventions, consequently increasing the demand for second-line treatment. Furthermore, in both strategies, the primary control affecting I_{SU} is u_1, while I_{SD} is mainly influenced by u_3. Whereas, control u_2 plays a major role in shaping the resistant compartments, I_{RU} and I_{RD}.

The synergetic effects arising from the interaction of multiple control variables across state compartments are also effectively captured by these Shapley values. For instance, controls u_2 and u_4, which target the diagnosis and treatment of drug-resistant infections, also contribute to reducing the burden of sensitive infections. This occurs because effective management of the resistant pool indirectly suppresses the overall transmission dynamics. As resistant and sensitive strains often compete for the same susceptible population, a reduction in the resistant strain can lower the overall force of infection, which benefits the control of sensitive infections. In contrast, controls u_1 and u_3 exhibit a positive contribution to the resistant infected populations, suggesting that the forward flow of individuals through the compartments, such as progression from undiagnosed to diagnosed and then to treatment failure, dominates over any competitive suppression between sensitive and resistant strains. Although these synergetic effects are relatively small, they can significantly enhance the overall effectiveness of intervention strategies. In addition, the combined implementation of u_2 and u_4 significantly reduces the drug resistance burden, compared to their individual effect. Overall, both strategies highlight the dominant influence of control u_5, which remains the primary driver in shaping infection dynamics.

5.7 Conclusion

In this chapter, we developed a compartmental model to explore the transmission dynamics of HIV, incorporating both drug-sensitive and drug-resistant strains, diagnosis status, and treatment switching from first-line to second-line therapy upon resistance detection. The proposed model admits one disease-free equilibrium and two endemic equilibria, where the drug-sensitive strain may be eliminated, while the drug-resistant strain persists at a positive level. Using the next-generation matrix method, we derived the basic reproduction numbers corresponding to both the drug-sensitive and drug-resistant strains. The existence and stability conditions of these equilibrium points highlight the critical role of these basic reproduction numbers in deciding the long-term dynamics of the system. Additionally, the relative transmission dynamics of the two strains significantly influences the outcome: higher transmission rates of the sensitive strain or relatively lower rates for the resistant strain can create the possibility for coexistence of both strains, even at a higher treatment coverage.

Algorithm 3 Control Contribution Analysis using Shapley Values

Require: Simulation time t_f, model parameters θ, initial conditions y_0, strategy weights W, control bounds $U_b = [0,1]^5$, convergence tolerance ϵ, maximum iterations $k_{\max}$, relaxation parameter α

Initialize: Generate all subsets S of the control set $U = \{u_1, u_2, u_3, u_4, u_5\}$, i.e., the power set $\mathcal{P}(U)$.
for each subset $S \in \mathcal{P}(N)$ **do**
  Set controls in $U \setminus S$ to 0.
  Solve the optimal control problem from 0 to t_f using backward-forward sweep:
  for $k = 1$ to $k_{\max}$ **do**
    Solve state system $\dot{y} = f(y, u^{(k-1)}, \theta)$ from 0 to t_f with $y(0) = y_0$
    Solve adjoint system $\dot{\sigma} = -\nabla_y H(y, u^{(k-1)}, \sigma, \theta, W)$ from t_f to 0 with $\sigma(t_f) = 0$
    Compute u^{new} using $\frac{\partial H}{\partial u_i} = 0$ for $i = 1, \ldots, 5$
    Update $u^{(k)} \leftarrow (1-\alpha)u^{(k-1)} + \alpha u^{\text{new}}$
    if $\max_i \|u_i^{(k)} - u_i^{(k-1)}\|_\infty < \epsilon$ **then**
      Set $u^* \leftarrow u^{(k)}$
      break
    end if
  end for
  Simulate the model over $[0, t_f]$ to obtain state trajectories $y_S^{(j)}(t)$ for $j = 1, \ldots, 8$.
  Compute person-years for each state variable $y_S^{(j)}(t)$:

$$v_S^{(j)} = \int_0^{t_f} y_S^{(j)}(t)dt, \quad j = 1, \ldots, 8.$$

end for
for each control $u_i \in U$ and state variable $y^{(j)}$ **do**
  Calculate the Shapley value:

$$\phi^{(j)}(u_i) = \sum_{S \subseteq U \setminus \{u_i\}} \frac{|S|!(n - |S| - 1)!}{n!} \left(v_{S \cup \{u_i\}}^{(j)} - v_S^{(j)} \right), \quad j = 1, \ldots, 8;\ n = 5.$$

end for
return The Shapley values $\phi^{(j)}(u_i)$ for all controls $u_i \in U$ and state variables $y^{(j)} \in y$.

A detailed sensitivity analysis has been conducted for the proposed model in order to identify the most influential parameters in the short-term and long-term dynamics. The PRCC based sensitivity analysis of basic reproduction numbers suggests that the transmission rates of both strains are main governing factors in the early stage of the infection. Time-varying sensitivity analysis was performed to identify the key parameters influencing model dynamics across different phases of disease progression, offering valuable insights for designing targeted intervention strategies. We employed the Sobol method to compute both first-order and total-order sensitivity indices. A significant difference observed between the first- and total-order indices for most parameters highlights the strong influence of parameter interactions on the total number of infections. The direct impact of individual parameters becomes minimal after a certain time, and the variance in model outcomes becomes mainly driven by complex interactions among parameters.

We extended the proposed modelling framework by incorporating optimal control theory to evaluate a set of intervention strategies aimed at improving diagnosis, treatment coverage, and adherence to ART optimally. Instead of using binary control activation, we introduced a weight-varying mechanism in the cost functional to differentiate between various intervention strategies in a more realistic manner. We proposed five different control strategies targeting key epidemiological components: (A) diagnosis focused, (B) treatment focused, (C) adherence focused, (D) a balanced approach, and (E) a dynamic optimization based approach. Among these, Strategy C, centered on improving adherence levels, produced the highest reduction in infection burden, particularly in the drug-resistant population, showing the crucial role of optimal adherence in controlling HIV transmission. Notably, a higher initiation rate of second-line treatment was supported across all strategies except Strategy C. In this case, the first-line treatment remained more effective due to the optimal allocation of resources toward adherence improvement, reducing the need to switch to second-line therapy. Despite this, Strategy C outperformed all other strategies in averting total infection cases. In contrast, Strategy D with the balanced approach proved to be the least effective in both infection reduction and increasing treatment coverage, suggesting that distributing resources evenly may reduce the potential impact of targeted interventions. Strategy B demonstrated the highest improvement in treatment coverage, although it was less effective in reducing overall infections compared to adherence-focused approach. This indicates that if expanding treatment access is the primary goal, Strategy B offers a more effective pathway, provided sufficient resources are available. Also, the dynamic control strategy shows that the 95-95-95 global targets can be achieved within five years through optimally timed and weighted resource allocation. Although these targets are met by the end of the third year, maintaining them requires sustained and judicious investment in all three aspects, which are diagnosis,

treatment initiation, and adherence. This highlights the need for dynamic, adaptable control policies to ensure long-term success in HIV management.

Efficient resource allocation is essential for the effective control and elimination of infectious diseases, particularly in resource-constrained settings. To evaluate the economic viability of the proposed intervention strategies, we performed a cost-effectiveness analysis using two key metrics: total averted person-years of infection and additional person-years of treatment provided. Strategy D emerged as the most cost-efficient in reducing infection burden, despite averting the fewest person-years of infection, while Strategy B ranked lowest due to the high costs associated with treatment-focused interventions. Strategies E, A, and C rank second, third and fourth, respectively, in terms of cost-effectiveness for infection reduction. When the objective shifts to expanding treatment coverage, Strategy C emerged as the most cost-effective option. This is attributed to its strategic allocation of resources towards adherence-focused interventions, which improves the efficacy of first-line therapy and reduces the need for more expensive second-line treatment. Strategy D is cost-effective in improving treatment outcomes, although it is slightly more expensive than Strategy C. The dynamic control strategy, which favors first-line treatment more than Strategies A and B, also demonstrated superior cost-efficiency compared to those strategies. In contrast, despite achieving the highest treatment coverage, Strategy B remained the least cost-effective due to its lack of adherence-enhancing components.

Beyond cost-effectiveness goals, we conducted an adjoint-based sensitivity analysis to identify optimal directions for additional resource allocation, with a focus on middle- and upper-middle-income countries. This analysis was applied to Strategies C and D, as these were the most cost-effective strategies, and examined the sensitivity of each state variable with respect to each control variable. Results indicate that increasing first-line treatment coverage is the most impactful intervention to reduce the drug-sensitive infected population. Additionally, the dynamics of drug-resistant infections and treatment-receiving populations were found to be highly sensitive to adherence-enhancing interventions. These findings suggest that, when considering broader public health objectives beyond cost constraints, prioritizing first-line treatment and adherence support produces the highest returns for improving public health outcomes. To better understand the individual and combined contributions of each control within a given strategy, particularly in settings where intervention costs are not a constraint, we used Shapley value analysis from cooperative game theory. This approach quantified both direct and synergistic effects of each control on achieving public health goals. The analysis revealed that controls targeting the diagnosis and treatment of drug-resistant infections also contributed to reducing the burden of drug-sensitive cases by indirectly suppressing overall transmission dynamics. However, some controls exhibited un-

intended amplification of resistance due to forward flow through compartments. The joint implementation of targeted interventions proved more effective than isolated efforts. Among all controls, adherence-focused intervention consistently emerged as the most influential in shaping long-term epidemic outcomes.

In conclusion, our findings provide valuable insights into the intricate relationship between treatment adherence, the emergence of drug resistance, and the effectiveness of control interventions in shaping the dynamics of the HIV epidemic. While multiple targeted interventions can collectively reduce the burden of both drug-sensitive and drug-resistant HIV strains, the long-term success of epidemic control critically depends on prioritizing adherence-focused strategies alongside efforts to expand first-line treatment coverage. In settings where expanding treatment coverage is feasible, particularly in middle- and upper-middle-income countries, investing in adherence-enhancing interventions emerges as a more cost-effective strategy. Where such expansion is limited, a balanced allocation of resources across all intervention components provides a more sustainable and efficient alternative.

Chapter 6

Epilogue

In this thesis, we developed and analyzed a series of mathematical models to investigate the transmission dynamics of HIV in the presence of drug-sensitive and drug-resistant strains. Beginning with a treatment-free framework, we explored the competitive interactions between the two strains and identified conditions under which one strain dominates or is excluded. We then extended this framework to incorporate treatment, adherence, and treatment-induced resistance, allowing for the possibility of coexistence between strains. Further, we introduced an AIDS compartment to capture late-stage disease dynamics and examined how treatment availability and adherence influence overall disease burden. In the final part of this work, we applied optimal control theory to design and compare intervention strategies targeting diagnosis, treatment coverage, adherence support, and switching to second-line therapy. The analysis combined stability, bifurcation and control theory with extensive numerical simulations and cost-effectiveness evaluations, providing valuable theoretical and practical insights into the design of effective HIV control strategies. The practical implications of the findings from each mathematical model are summarized and discussed in the following Section.

6.1 Summary

The first model of the thesis highlights that, in the absence of treatment, competition between strains prevents their long-term coexistence, leading to the eventual exclusion of one strain. However, the second model of the study shows that treatment availability can facilitate the coexistence of drug-sensitive and drug-resistant strains, underlining the need for careful monitoring of resistance emergence when scaling up ART programs. The inclusion of treatment adherence and treatment-induced resistance in the modelling framework revealed that poor adherence acts as a significant driver of resistance spread. From a policy

perspective, this emphasizes that scaling up ART without parallel investments in adherence support could inadvertently accelerate the burden of drug-resistant infections, threatening the long-term success of treatment programs.

The model incorporating an AIDS compartment provided further insights into the impact of treatment availability on disease progression and population-level outcomes. The results indicate that prioritizing the reduction of the drug-sensitive infected population, particularly those unaware of their status, may be necessary in some scenarios to minimize the overall disease burden, even at the cost of a short-term increase in drug resistance. This highlights the importance of coupling ART scale-up with early diagnosis and linkage-to-care strategies to maximize the impact of treatment.

The final chapter developed an optimal control framework to evaluate alternative intervention strategies under resource constraints. This framework provides evidence-based guidance on how to allocate resources between diagnosis, treatment initiation, adherence support, and second-line switching. In particular, adherence-focused strategies were found to be the most effective in reducing the total number of infections, including resistant cases, whereas treatment-focused strategies were more effective for rapidly increasing treatment coverage. The dynamic optimization approach further demonstrated that the UNAIDS 95–95–95 targets can be achieved within a relatively short time horizon if resources are timed and weighted optimally across the care continuum.

Overall, the findings of this thesis underline the need for a balanced yet adherence-focused approach to HIV control policies. Interventions must not only expand access to ART but also ensure patients are diagnosed early, supported to remain adherent, and switched promptly to second-line therapy when resistance emerges. In resource-limited settings, these results can inform cost-effective prioritization of interventions to achieve sustainable epidemic control.

6.2 Limitations and Future Research Directions

While this thesis provides valuable insights into the transmission dynamics of HIV and the emergence of drug resistance under various treatment strategies, several limitations remain that present opportunities for future research.

First, the current modelling frameworks do not explicitly incorporate preventive measures such as condom use, behavioural change programs, or Pre-Exposure Prophylaxis (PrEP). Although these interventions play a critical role in real-world HIV prevention, they were excluded to focus exclusively on the dynamics of treatment, adherence, and resistance. However, it is well known that PrEP, despite its effectiveness in reducing HIV acquisition, can also drive the emergence of primary drug resistance in certain scenarios [85, 207, 208]. Future

extensions of this work should therefore incorporate PrEP use, alongside first and second-line ART, to more comprehensively capture the interplay between prevention, treatment, and resistance evolution.

Second, the models presented in this thesis assume a homogeneously mixed population, where each individual has an equal probability of contacting every other individual. While this assumption simplifies the analysis and enables analytical tractability, it overlooks the heterogeneity inherent in real-world populations, such as differences in sexual contact patterns, risk behaviours, and adherence levels etc. These factors may substantially influence transmission dynamics and intervention outcomes. To address this limitation, the deterministic compartmental models can be extended to network-based or agent-based frameworks that explicitly incorporate heterogeneity at the individual level [209, 210]. Such approaches would allow for more realistic modelling of complex transmission networks and targeted intervention strategies.

Third, all models in this thesis are deterministic with constant parameter values. Stochastic models could better capture random fluctuations and rare events, which are particularly relevant when modelling the early emergence of drug resistance. Moreover, introducing time-varying parameters, such as dynamic adherence levels, diagnosis rates, or transmission probabilities, would enable the modelling of behavioral or policy-driven changes in response to interventions. Further, in Chapter 5, we employed global sensitivity analysis to identify parameters that most strongly influence epidemiological outcomes, a natural extension of this work is a full uncertainty quantification analysis. This approach would consider key parameters as random variables with particular probability distributions and would quantify the resulting uncertainty in model predictions using sampling-based methods. This would provide predictive confidence intervals and further enhance the utility of presented model for public health planning.

Overall, these future directions aim to refine the modelling framework to be more realistic and data-driven, thereby improving its utility for public health decision-making and contributing to the long-term goal of achieving and sustaining the UNAIDS 95-95-95 targets.

Bibliography

[1] Robert Beaglehole and Ruth Bonita. *Basic epidemiology*. Orient Blackswan, 1993.

[2] Sten H Vermund. Global HIV epidemiology: A guide for strategies in prevention and care. *Current HIV/AIDS Reports*, 11:93–98, 2014.

[3] UNAIDS - Fact Sheet 2024. `https://www.unaids.org/sites/default/files/media_asset/UNAIDS_FactSheet_en.pdf`, 2024.

[4] Liming Cai, Xuezhi Li, Mini Ghosh, and Baozhu Guo. Stability analysis of an HIV/AIDS epidemic model with treatment. *Journal of Computational and Applied Mathematics*, 229(1):313–323, 2009.

[5] Esteban A Hernandez-Vargas and Richard H Middleton. Modeling the three stages in HIV infection. *Journal of Theoretical Biology*, 320:33–40, 2013.

[6] William C Miller, Nora E Rosenberg, Sarah E Rutstein, and Kimberly A Powers. Role of acute and early HIV infection in the sexual transmission of HIV. *Current Opinion in HIV and AIDS*, 5(4):277–282, 2010.

[7] Katharine Gurski and Kathleen Hoffman. Staged HIV transmission and treatment in a dynamic model with long-term partnerships. *Journal of Mathematical Biology*, 86(5):74, 2023.

[8] Paola Paci, Filippo Castiglione, Massimo Bernaschi, and Valentina Baldazzi. A discrete/continuous model of anti-HIV response and therapy. In *Tenth International Conference on Computer Modeling and Simulation (UKSIM 2008)*, pages 481–486. IEEE, 2008.

[9] George M Shaw and Eric Hunter. HIV transmission. *Cold Spring Harbor Perspectives in Medicine*, 2(11):a006965, 2012.

[10] Emily Boardman, Marta Boffito, David R Chadwick, Emily Cheserem, Samuel Kabagambe, Bakita Kasadha, and Cindy Elliott. Tackling late HIV diagnosis: Lessons from the UK in the COVID-19 era. *International Journal of STD & AIDS*, 35(4):244–253, 2024.

[11] Amaury Thiabaud, Isotta Triulzi, Erol Orel, Kali Tal, and Olivia Keiser. Social, behavioral, and cultural factors of HIV in Malawi: Semi-automated systematic review. *Journal of Medical Internet Research*, 22(8):e18747, 2020.

[12] Feny Deya Virdausi, Ferry Efendi, Tiyas Kusumaningrum, Qorinah Estiningtyas Sakilah Adnani, Lisa McKenna, Kadar Ramadhan, and Ika Adelia Susanti. Socio-economic and demographic factors associated with knowledge and attitude of HIV/AIDS among women aged 15–49 years old in Indonesia. In *Healthcare*, volume 10, page 1545. MDPI, 2022.

[13] Late Presentation Working Groups in EuroSIDA and COHERE Kamilla. Estimating the burden of HIV late presentation and its attributable morbidity and mortality across Europe 2010–2016. *BMC Infectious Diseases*, 20(1):728, 2020.

[14] Sara Croxford, Annemarie Rinder Stengaard, Johanna Brännström, Lauren Combs, Nikos Dedes, Enrico Girardi, Sophie Grabar, Ole Kirk, Giorgi Kuchukhidze, Jeffrey V Lazarus, et al. Late diagnosis of HIV: An updated consensus definition. *HIV Medicine*, 23(11):1202–1208, 2022.

[15] Tahilin Sanchez Karver, Kaitlyn Atkins, Virginia A Fonner, Carlos E Rodriguez-Diaz, Michael D Sweat, Tamara Taggart, Ping Teresa Yeh, Caitlin E Kennedy, and Deanna Kerrigan. HIV-related intersectional stigma and discrimination measurement: State of the science. *American Journal of Public Health*, 112(S4):S420–S432, 2022.

[16] Indrajit Ghosh, Pankaj Kumar Tiwari, Sudip Samanta, Ibrahim M Elmojtaba, Nasser Al-Salti, and Joydev Chattopadhyay. A simple SI-type model for HIV/AIDS with media and self-imposed psychological fear. *Mathematical Biosciences*, 306:160–169, 2018.

[17] Ling Xue, Kai Zhang, and Hao Wang. Long-term forecast of HIV/AIDS epidemic in china with fear effect and 90-90-90 strategies. *Bulletin of Mathematical Biology*, 84(11):132, 2022.

[18] Jared M Baeten, Jessica E Haberer, Albert Y Liu, and Nirupama Sista. Preexposure prophylaxis for HIV prevention: Where have we been and where are we going? *JAIDS Journal of Acquired Immune Deficiency Syndromes*, 63:S122–S129, 2013.

[19] Geeta Rao Gupta, Justin O Parkhurst, Jessica A Ogden, Peter Aggleton, and Ajay Mahal. Structural approaches to HIV prevention. *The Lancet*, 372(9640):764–775, 2008.

[20] James Cutrell, Tomasz Jodlowski, and Roger Bedimo. The management of treatment-experienced HIV patients (including virologic failure and switches). *Therapeutic Advances in Infectious Disease*, 7:1–15, 2020.

[21] David L Paterson, Susan Swindells, Jeffrey Mohr, Michelle Brester, Emanuel N Vergis, Cheryl Squier, Marilyn M Wagener, and Nina Singh. Adherence to protease inhibitor therapy and outcomes in patients with HIV infection. *Annals of Internal Medicine*, 133(1):21–30.

[22] Pietro L Vernazza, Joseph J Eron, Susan A Fiscus, and Myron S Cohen. Sexual transmission of HIV: Infectiousness and prevention. *AIDS*, 13(2):155–166, 1999.

[23] Myron S Cohen, Ying Q Chen, Marybeth McCauley, Theresa Gamble, Mina C Hosseinipour, Nagalingeswaran Kumarasamy, James G Hakim, Johnstone Kumwenda, Beatriz Grinsztejn, Jose HS Pilotto, et al. Prevention of HIV-1 infection with early antiretroviral therapy. *New England Journal of Medicine*, 365(6):493–505, 2011.

[24] P Richard Harrigan, Robert S Hogg, Winnie WY Dong, Benita Yip, Brian Wynhoven, Justin Woodward, Chanson J Brumme, Zabrina L Brumme, Theresa Mo, Chris S Alexander, and Julio S. G. Montaner. Predictors of HIV drug-resistance mutations in a large antiretroviral-naive cohort initiating triple antiretroviral therapy. *The Journal of Infectious Diseases*, 191(3):339–347, 2005.

[25] Jean B Nachega, Vincent C Marconi, Gert U van Zyl, Edward M Gardner, Wolfgang Preiser, Steven Y Hong, Edward J Mills, and Robert Gross. HIV treatment adherence, drug resistance, virologic failure: Evolving concepts. *Infectious Disorders-Drug Targets (Formerly Current Drug Targets-Infectious Disorders)*, 11(2):167–174, 2011.

[26] Evan Wood, Robert S Hogg, Benita Yip, P Richard Harrigan, Michael V O'Shaughnessy, and Julio SG Montaner. Is there a baseline CD4 cell count that precludes a survival response to modern antiretroviral therapy? *AIDS*, 17(5):711–720, 2003.

[27] Kathy K Byrd, John G Hou, Ron Hazen, Heather Kirkham, Sumihiro Suzuki, Patrick G Clay, Tim Bush, Nasima M Camp, Paul J Weidle, and Ambrose Delpino. Antiretroviral adherence level necessary for HIV viral suppression using real-world data. *Journal of Acquired Immune Deficiency Syndromes*, 82(3):245–251, 2019.

[28] Linda Fogarty, Debra Roter, Susan Larson, Jessica Burke, Jeanne Gillespie, and Richard Levy. Patient adherence to HIV medication regimens: a review of published and abstract reports. *Patient Education and Counseling*, 46(2):93–108, 2002.

[29] Basavaprabhu Achappa, Deepak Madi, Unnikrishnan Bhaskaran, John T Ramapuram, Satish Rao, and Soundarya Mahalingam. Adherence to antiretroviral therapy among people living with HIV. *North American Journal of Medical Sciences*, 5(3):220, 2013.

[30] Beena Joshi, Sanjay Chauhan, Achhelal Pasi, Ragini Kulkarni, Nithya Sunil, Damodar Bachani, Ranjit Mankeshwar, ART Adherence Study Group, et al. Level of suboptimal adherence to first line antiretroviral treatment & its determinants among HIV positive people in India. *The Indian Journal of Medical Research*, 140(1):84, 2014.

[31] Maria L Ekstrand, Elsa Heylen, Amanda Mazur, Wayne T Steward, Catherine Carpenter, Kartik Yadav, Sanjeev Sinha, and Adey Nyamathi. The role of HIV stigma in ART adherence and quality of life among rural women living with HIV in India. *AIDS and Behavior*, 22(12):3859–3868, 2018.

[32] Mark S Dworkin, Apurba Chakraborty, Diana Zychowski, Geri Donenberg, Richard Novak, and Robert Garofalo. Self-efficacy and ability to read as factors associated with antiretroviral therapy adherence in an HIV-infected population. *International Journal of STD & AIDS*, 29(12):1154–1164, 2018.

[33] Virender Kumar and William Encinosa. Effects of HIV medication complexity and depression on adherence to HIV medication. *The Patient: Patient-Centered Outcomes Research*, 3(1):59–69, 2010.

[34] Hongbo Jiang, Yi Zhou, and Weiming Tang. Maintaining HIV care during the COVID-19 pandemic. *The Lancet HIV*, 7(5):e308–e309, 2020.

[35] Britta L Jewell, Edinah Mudimu, John Stover, Debra Ten Brink, Andrew N Phillips, Jennifer A Smith, Rowan Martin-Hughes, Yu Teng, Robert Glaubius, Severin Guy Mahiane, et al. Potential effects of disruption to HIV programmes in sub-Saharan Africa caused by COVID-19: Results from multiple mathematical models. *The Lancet HIV*, 7(9):e629–e640, 2020.

[36] Jamile Ballivian, Maria L Alcaide, Diego Cecchini, Deborah L Jones, John M Abbamonte, and Isabel Cassetti. Impact of COVID–19-related stress and lockdown on mental health among people living with HIV in Argentina. *JAIDS Journal of Acquired Immune Deficiency Syndromes*, 85(4):475–482, 2020.

[37] Susan J Little, Sarah Holte, Jean-Pierre Routy, Eric S Daar, Marty Markowitz, Ann C Collier, Richard A Koup, John W Mellors, Elizabeth Connick, Brian Conway, et al. Antiretroviral-drug resistance among patients recently infected with HIV. *New England Journal of Medicine*, 347(6):385–394, 2002.

[38] William L Trebelcock, Javier R Lama, Ann Duerr, Hugo Sanchez, Robinson Cabello, Trupti Gilada, Patricia Segura, Sari L Reisner, Kenneth H Mayer, James Mullins, et al. HIV pretreatment drug resistance among cisgender MSM and transgender women from Lima, Peru. *Journal of the International AIDS Society*, 22(11):e25411, 2019.

[39] Ross S Milne, Rachel A Silverman, Ingrid A Beck, Jennifer Mckernan-Mullin, Wenjie Deng, Thomas R Sibley, Sandra Dross, James N Kiarie, Samah R Sakr, Robert W Coombs, et al. Minority and majority pre-treatment HIV-1 drug resistance associated with failure of 1^{st}-line NNRTI Art in Kenyan women. *AIDS (London, England)*, 2019.

[40] Aleksandr N Shchemelev, Aleksandr V Semenov, Yu V Ostankova, Elena B Zueva, Diana E Valutite, Daria A Semenova, Vladimir S Davydenko, and Areg A Totolian. Genetic diversity and drug resistance mutations of HIV-1 in Leningrad Region. *Journal of Microbiology, Epidemiology and Immunobiology*, 99(1):28–37, 2022.

[41] Andrea Calcagno, Jessica Cusato, Antonio D'Avolio, and Stefano Bonora. Genetic polymorphisms affecting the pharmacokinetics of antiretroviral drugs. *Clinical Pharmacokinetics*, 56:355–369, 2017.

[42] Panel on Antiretroviral Guidelines for Adults and Adolescents. Guidelines for the Use of Antiretroviral Agents in Adults and Adolescents with HIV. `https://clinicalinfo.hiv.gov/en/guidelines/adult-and-adolescent-arv`, 2024.

[43] Second-Line Study Group et al. Ritonavir-boosted lopinavir plus nucleoside or nucleotide reverse transcriptase inhibitors versus ritonavir-boosted lopinavir plus raltegravir for treatment of HIV-1 infection in adults with virological failure of a standard first-line ART regimen (SECOND-LINE): a randomised, open-label, non-inferiority study. *The Lancet*, 381(9883):2091–2099, 2013.

[44] Michael Aboud, Richard Kaplan, Johannes Lombaard, Fujie Zhang, José A Hidalgo, Elmira Mamedova, Marcelo H Losso, Ploenchan Chetchotisakd, Carlos Brites, Jörg Sievers, et al. Dolutegravir versus ritonavir-boosted lopinavir both with dual nucleoside reverse transcriptase inhibitor therapy in adults with HIV-1 infection in whom first-line therapy has failed (DAWNING): An open-label, non-inferiority, phase 3b trial. *The Lancet Infectious Diseases*, 19(3):253–264, 2019.

[45] John Graunt and Walter Francis Willcox. *Natural and Political Observations Made upon the Bills of Mortality*. Johns Hopkins Press, 1939.

[46] Klaus Dietz and JAP Heesterbeek. Daniel Bernoulli's epidemiological model revisited. *Mathematical Biosciences*, 180(1-2):1–21, 2002.

[47] Ronald Ross. On some peculiar pigmented cells found in two mosquitos fed on malarial blood. *British Medical Journal*, 2(1929):1786, 1897.

[48] William Ogilvy Kermack and Anderson G McKendrick. A contribution to the mathematical theory of epidemics. *Proceedings of the Royal Society of London (Series A)*, 115(772):700–721, 1927.

[49] Leonid A Rvachev and Ira M Longini Jr. A mathematical model for the global spread of influenza. *Mathematical Biosciences*, 75(1):3–22, 1985.

[50] Gerardo Chowell, Nick W Hengartner, Carlos Castillo-Chavez, Paul W Fenimore, and Jim Michael Hyman. The basic reproductive number of Ebola and the effects of public health measures: the cases of Congo and Uganda. *Journal of Theoretical Biology*, 229(1):119–126, 2004.

[51] RM Anderson, GF Medley, RM May, and AM Johnson. A preliminary study of the transmission dynamics of the human immunodeficiency virus (HIV), the causative agent of AIDS. *Mathematical Medicine and Biology: a Journal of the IMA*, 3(4):229–263, 1986.

[52] Alan S Perelson and Patrick W Nelson. Mathematical analysis of HIV-1 dynamics in vivo. *SIAM Review*, 41(1):3–44, 1999.

[53] Adam J Kucharski, Timothy W Russell, Charlie Diamond, Yang Liu, John Edmunds, Sebastian Funk, Rosalind M Eggo, Fiona Sun, Mark Jit, James D Munday, et al. Early dynamics of transmission and control of COVID-19: a mathematical modelling study. *The Lancet Infectious Diseases*, 20(5):553–558, 2020.

[54] Oliver J Watson, Gregory Barnsley, Jaspreet Toor, Alexandra B Hogan, Peter Winskill, and Azra C Ghani. Global impact of the first year of COVID-19 vaccination: a mathematical modelling study. *The Lancet Infectious Diseases*, 22(9):1293–1302, 2022.

[55] Linda JS Allen. An introduction to stochastic epidemic models. In *Mathematical Epidemiology*, pages 81–130. Springer, 2008.

[56] Hakan Andersson and Tom Britton. *Stochastic Epidemic Models and Their Statistical Analysis*, volume 151. Springer Science & Business Media, 2012.

[57] Martina Morris. Epidemiology and social networks: Modeling structured diffusion. *Sociological Methods & Research*, 22(1):99–126, 1993.

[58] Matt J Keeling and Ken TD Eames. Networks and epidemic models. *Journal of the Royal Society Interface*, 2(4):295–307, 2005.

[59] Liliana Perez and Suzana Dragicevic. An agent-based approach for modeling dynamics of contagious disease spread. *International Journal of Health Geographics*, 8(1):50, 2009.

[60] Tomas Philipson. Economic epidemiology and infectious diseases. *Handbook of Health Economics*, 1:1761–1799, 2000.

[61] Shweta Bansal, Bryan T Grenfell, and Lauren Ancel Meyers. When individual behaviour matters: Homogeneous and network models in epidemiology. *Journal of the Royal Society Interface*, 4(16):879–891, 2007.

[62] Chris Bauch, Alberto d'Onofrio, and Piero Manfredi. Behavioral epidemiology of infectious diseases: an overview. *Modeling the Interplay between Human Behavior and the Spread of Infectious Diseases*, pages 1–19, 2012.

[63] Martin S Eichenbaum, Sergio Rebelo, and Mathias Trabandt. The macroeconomics of epidemics. *The Review of Financial Studies*, 34(11):5149–5187, 2021.

[64] Gerardo Chowell, Doracelly Hincapie-Palacio, Juan Ospina, Bruce Pell, Amna Tariq, Sushma Dahal, Seyed Moghadas, Alexandra Smirnova, Lone Simonsen, and Cécile Viboud. Using phenomenological models to characterize transmissibility and forecast patterns and final burden of Zika epidemics. *PLoS Currents*, 8, 2016.

[65] Bruce Pell, Yang Kuang, Cecile Viboud, and Gerardo Chowell. Using phenomenological models for forecasting the 2015 Ebola challenge. *Epidemics*, 22:62–70, 2018.

[66] Emily Chen, Kristina Lerman, Emilio Ferrara, et al. Tracking social media discourse about the COVID-19 pandemic: Development of a public coronavirus twitter data set. *JMIR Public Health and Surveillance*, 6(2):e19273, 2020.

[67] Robert M May and Roy M Anderson. Commentary transmission dynamics of HIV infection. *Nature*, 326(137):10–1038, 1987.

[68] John A Jacquez, James S Koopman, Carl P Simon, and Ira M Longini Jr. Role of the primary infection in epidemics of HIV infection in gay cohorts. *JAIDS Journal of Acquired Immune Deficiency Syndromes*, 7(11):1169–1184, 1994.

[69] Francisco Antônio Bezerra Coutinho, LF Lopez, Marcelo Nascimento Burattini, and Eduardo Massad. Modelling the natural history of HIV infection in individuals and its epidemiological implications. *Bulletin of Mathematical Biology*, 63(6):1041–1062, 2001.

[70] T Déirdre Hollingsworth, Roy M Anderson, and Christophe Fraser. HIV-1 transmission: by stage of infection. *The Journal of Infectious Diseases*, 198(5):687–693, 2008.

[71] Martina Morris and Mirjam Kretzschmar. Concurrent partnerships and the spread of HIV. *AIDS*, 11(5):641–648, 1997.

[72] James M Hyman, Jia Li, and E Ann Stanley. The differential infectivity and staged progression models for the transmission of hiv. *Mathematical Biosciences*, 155(2):77–109, 1999.

[73] Francisco Antônio Bezerra Coutinho, Eduardo Massad, Luis Fernandez Lopez, Marcelo Nascimento Burattini, Claudio J Struchiner, and Raymundo Soares de Azevedo-Neto. Modelling heterogeneities in individual frailties in epidemic models. *Mathematical and Computer Modelling*, 30(1-2):97–115, 1999.

[74] Kimberly A Powers, Azra C Ghani, William C Miller, Irving F Hoffman, Audrey E Pettifor, Gift Kamanga, Francis EA Martinson, and Myron S Cohen. The role of acute and early HIV infection in the spread of HIV and implications for transmission prevention strategies in Lilongwe, Malawi: a modelling study. *The Lancet*, 378(9787):256–268, 2011.

[75] Sharmistha Mishra, Richard Steen, Antonio Gerbase, Ying-Ru Lo, and Marie-Claude Boily. Impact of high-risk sex and focused interventions in heterosexual HIV epidemics: a systematic review of mathematical models. *PLoS One*, 7(11):e50691, 2012.

[76] Megan Coffee, Mark N Lurie, and Geoff P Garnett. Modelling the impact of migration on the HIV epidemic in South Africa. *Aids*, 21(3):343–350, 2007.

[77] Gabriela B Gomez, Annick Borquez, Kelsey K Case, Ana Wheelock, Anna Vassall, and Catherine Hankins. The cost and impact of scaling up pre-exposure prophylaxis for HIV prevention: a systematic review of cost-effectiveness modelling studies. *PLoS Medicine*, 10(3):e1001401, 2013.

[78] SK Sharma, Alladi Mohan, and Tamilarasu Kadhiravan. HIV-TB co-infection: Epidemiology, diagnosis & management. *Indian Journal of Medical Research*, 121(4):550–567, 2005.

[79] Zindoga Mukandavire, Abba B Gumel, Winston Garira, and Jean Michel Tchuenche. Mathematical analysis of a model for HIV-malaria co-infection. *Mathematical Biosciences and Engineering*, 2009.

[80] Andrzej Pawlowski, Marianne Jansson, Markus Sköld, Martin E Rottenberg, and Gunilla Källenius. Tuberculosis and HIV co-infection. *PLoS Pathogens*, 8(2):e1002464, 2012.

[81] Amparo Yovanna Castro Sanchez, Marc Aerts, Ziv Shkedy, Peter Vickerman, Fabrizio Faggiano, Guiseppe Salamina, and Niel Hens. A mathematical model for HIV and hepatitis C co-infection and its assessment from a statistical perspective. *Epidemics*, 5(1):56–66, 2013.

[82] Athena P Kourtis, Marc Bulterys, Dale J Hu, and Denise J Jamieson. HIV–HBV coinfection: a global challenge. *New England Journal of Medicine*, 366(19):1749–1752, 2012.

[83] Engida Endriyas Endashaw and Temesgen Tibebu Mekonnen. Modeling the effect of vaccination and treatment on the transmission dynamics of hepatitis B virus and HIV/AIDS coinfection. *Journal of Applied Mathematics*, 2022(1):5246762, 2022.

[84] Fatuh Inayaturohmat, Nursanti Anggriani, Asep K Supriatna, and Md Haider Ali Biswas. A systematic literature review of mathematical models for coinfections: Tuberculosis, malaria, and HIV/AIDS. *Journal of Multidisciplinary Healthcare*, pages 1091–1109, 2024.

[85] Emmanuel F Drabo, Joel W Hay, Raffaele Vardavas, Zachary R Wagner, and Neeraj Sood. A cost-effectiveness analysis of preexposure prophylaxis for the prevention of

HIV among Los Angeles County men who have sex with men. *Clinical Infectious Diseases*, 63(11):1495–1504, 2016.

[86] Leigh F Johnson and Nathan Geffen. A comparison of two mathematical modeling frameworks for evaluating sexually transmitted infection epidemiology. *Sexually Transmitted Diseases*, 43(3):139–146, 2016.

[87] EO Omondi, RW Mbogo, and LS Luboobi. A mathematical model of HIV transmission between commercial sex workers and injection drug users. *Research in Mathematics*, 9(1):2082044, 2022.

[88] Bertran Auvert, Dirk Taljaard, Emmanuel Lagarde, Joelle Sobngwi-Tambekou, Rémi Sitta, and Adrian Puren. Randomized, controlled intervention trial of male circumcision for reduction of HIV infection risk: the ANRS 1265 Trial. *PLoS Medicine*, 2(11):e298, 2005.

[89] Victor C Matos, Thiago S Torres, and Paula M Luz. Adherence to antiretroviral therapy among cisgender gay, bisexual and other men who have sex with men in Brazil: Evaluating the role of HIV-related stigma dimensions. *PLoS One*, 19(8):e0308443, 2024.

[90] Andrew R Zolopa. The evolution of HIV treatment guidelines: Current state-of-the-art of ART. *Antiviral Research*, 85(1):241–244, 2010.

[91] Kyeongah Nah, Hiroshi Nishiura, Naho Tsuchiya, Xiaodan Sun, Yusuke Asai, and Akifumi Imamura. Test-and-treat approach to HIV/AIDS: a primer for mathematical modeling. *Theoretical Biology and Medical Modelling*, 14(1):16, 2017.

[92] J Mushanyu. A note on the impact of late diagnosis on HIV/AIDS dynamics: a mathematical modelling approach. *BMC Research Notes*, 13(1):340, 2020.

[93] Cristiana J Silva and Delfim FM Torres. A SICA compartmental model in epidemiology with application to HIV/AIDS in Cape Verde. *Ecological Complexity*, 30:70–75, 2017.

[94] Daniel IS Rosenbloom, Alison L Hill, S Alireza Rabi, Robert F Siliciano, and Martin A Nowak. Antiretroviral dynamics determines HIV evolution and predicts therapy outcome. *Nature Medicine*, 18(9):1378–1385, 2012.

[95] R Scott Braithwaite, Mark S Roberts, Matthew Bidwell Goetz, Cynthia L Gibert, Maria C Rodriguez-Barradas, Kimberly Nucifora, and Amy C Justice. Do benefits

of earlier antiretroviral treatment initiation outweigh harms for individuals at risk for poor adherence? *Clinical Infectious Diseases*, 48(6):822–826, 2009.

[96] Hao Lai, Rui Li, Zengbin Li, Baoming Zhang, Chao Li, Chang Song, Quanbi Zhao, Jinghua Huang, Qiuying Zhu, Shujia Liang, et al. Modelling the impact of treatment adherence on the transmission of HIV drug resistance. *Journal of Antimicrobial Chemotherapy*, 78(8):1934–1943, 2023.

[97] Sally M Blower, AN Aschenbach, HB Gershengorn, and JO Kahn. Predicting the unpredictable: Transmission of drug-resistant HIV. *Nature Medicine*, 7(9):1016–1020, 2001.

[98] O Sharomi and AB Gumel. Dynamical analysis of a multi-strain model of HIV in the presence of anti-retroviral drugs. *Journal of Biological Dynamics*, 2(3):323–345, 2008.

[99] Miguel Fudolig and Reka Howard. The local stability of a modified multi-strain SIR model for emerging viral strains. *PLoS One*, 15(12):e0243408, 2020.

[100] Md Abdul Kuddus, Emma S McBryde, Adeshina I Adekunle, Lisa J White, and Michael T Meehan. Mathematical analysis of a two-strain disease model with amplification. *Chaos, Solitons & Fractals*, 143:110594, 2021.

[101] Dennis N Makau, Samantha Lycett, Matthew Michalska-Smith, Igor AD Paploski, Maxim C-J Cheeran, Meggan E Craft, Rowland R Kao, Declan C Schroeder, Andrea Doeschl-Wilson, and Kimberly VanderWaal. Ecological and evolutionary dynamics of multi-strain RNA viruses. *Nature Ecology & Evolution*, 6(10):1414–1422, 2022.

[102] Sally M Blower, Hayley B Gershengorn, and RM Grant. A tale of two futures: HIV and antiretroviral therapy in San Francisco. *Science*, 287(5453):650–654, 2000.

[103] Raph L Hamers, Tobias F Rinke de Wit, and Charles B Holmes. HIV drug resistance in low-income and middle-income countries. *The Lancet HIV*, 5(10):e588–e596, 2018.

[104] Daniel Keebler, Paul Revill, Scott Braithwaite, Andrew Phillips, Nello Blaser, Annick Borquez, Valentina Cambiano, Andrea Ciaranello, Janne Estill, Richard Gray, et al. Cost-effectiveness of different strategies to monitor adults on antiretroviral treatment: a combined analysis of three mathematical models. *The Lancet Global Health*, 2(1):e35–e43, 2014.

[105] Ruanne V Barnabas, Paul Revill, Nicholas Tan, and Andrew Phillips. Cost-effectiveness of routine viral load monitoring in low-and middle-income countries: a systematic review. *Journal of the International AIDS Society*, 20:e25006, 2017.

[106] Tracy Glass, Landon Myer, and Maia Lesosky. The role of HIV viral load in mathematical models of HIV transmission and treatment: a review. *BMJ Global Health*, 5(1), 2020.

[107] Minh D Pham, Huy V Nguyen, David Anderson, Suzanne Crowe, and Stanley Luchters. Viral load monitoring for people living with HIV in the era of test and treat: Progress made and challenges ahead–a systematic review. *BMC Public Health*, 22(1):1203, 2022.

[108] Mingwang Shen, Yanni Xiao, Libin Rong, Lauren Ancel Meyers, and Steven E Bellan. Early antiretroviral therapy and potent second-line drugs could decrease HIV incidence of drug resistance. *Proceedings of the Royal Society B: Biological Sciences*, 284(1857):20170525, 2017.

[109] Janne Estill, Nathan Ford, Luisa Salazar-Vizcaya, Andreas D Haas, Nello Blaser, Vincent Habiyambere, and Olivia Keiser. The need for second-line antiretroviral therapy in adults in sub-Saharan Africa up to 2030: a mathematical modelling study. *The Lancet HIV*, 3(3):e132–e139, 2016.

[110] K Wickwire. Mathematical models for the control of pests and infectious diseases: a survey. *Theoretical Population Biology*, 11(2):182–238, 1977.

[111] Horst Behncke. Optimal control of deterministic epidemics. *Optimal Control Applications and Methods*, 21(6):269–285, 2000.

[112] Margaret L Brandeau. Allocating resources to control infectious diseases. *Operations Research and Health Care: A Handbook of Methods and Applications*, pages 443–464, 2005.

[113] Erik Verriest, Florent Delmotte, and Magnus Egerstedt. Control of epidemics by vaccination. In *American Control Conference, 2005*, pages 985–990. IEEE, 2005.

[114] Cesar Castilho. Optimal control of an epidemic through educational campaigns. *Electronic Journal of Differential Equations (EJDE)*, 2006:1–11, 2006.

[115] Suzanne Lenhart and John T Workman. *Optimal Control Applied to Biological Models*. Chapman and Hall/CRC, 2007.

[116] Denise Kirschner, Suzanne Lenhart, and Steve Serbin. Optimal control of the chemotherapy of HIV. *Journal of Mathematical Biology*, 35(7):775–792, 1997.

[117] Hem Raj Joshi. Optimal control of an HIV immunology model. *Optimal Control Applications and Methods*, 23(4):199–213, 2002.

[118] Rebecca V Culshaw, Shigui Ruan, and Raymond J Spiteri. Optimal HIV treatment by maximising immune response. *Journal of Mathematical Biology*, 48(5):545–562, 2004.

[119] Steven M Shechter, Matthew D Bailey, Andrew J Schaefer, and Mark S Roberts. The optimal time to initiate HIV therapy under ordered health states. *Operations Research*, 56(1):20–33, 2008.

[120] Kazeem Oare Okosun, OD Makinde, and I Takaidza. Impact of optimal control on the treatment of HIV/AIDS and screening of unaware infectives. *Applied Mathematical Modelling*, 37(6):3802–3820, 2013.

[121] I Takaidza, OD Makinde, and KO Okosun. Computational modelling and optimal control of HIV/AIDS transmission in a community with substance abuse problem. In *Advances in Applied Mathematics*, pages 31–40. Springer, 2014.

[122] Gordon Akudibillah, Abhishek Pandey, and Jan Medlock. Optimal control for HIV treatment. *Mathematical Biosciences and Engineering*, 16(1):373–396, 2018.

[123] Tigabu Kasia Ayele, Emile Franc Doungmo Goufo, and Stella Mugisha. Mathematical modeling of HIV/AIDS with optimal control: a case study in Ethiopia. *Results in Physics*, 26:104263, 2021.

[124] Rinlapas Wattanasirikosone and Chairat Modnak. Analysing transmission dynamics of HIV/AIDS with optimal control strategy and its controlled state. *Journal of Biological Dynamics*, 16(1):499–527, 2022.

[125] Eshetu Dadi Gurmu, Boka Kumsa Bole, and Purnachandra Rao Koya. Mathematical modelling of HIV/AIDS transmission dynamics with optimal control strategy. *International Journal of Mathematcs and Computer Research*, 9(04):2237–2254, 2021.

[126] Hossein Kheiri and Mohsen Jafari. Optimal control of a fractional-order model for the HIV/AIDS epidemic. *International Journal of Biomathematics*, 11(07):1850086, 2018.

[127] Hossein Kheiri and Mohsen Jafari. Fractional optimal control of an HIV/AIDS epidemic model with random testing and contact tracing. *Journal of Applied Mathematics and Computing*, 60(1):387–411, 2019.

[128] Nouar Chorfi, Samir Bendoukha, and Salem Abdelmalek. The optimal control of an HIV/AIDS reaction-diffusion epidemic model. *Discrete and Continuous Dynamical Systems-S*, pages 0–0, 2024.

[129] Anwarud Din and Yongjin Li. Optimizing HIV/AIDS dynamics: Stochastic control strategies with education and treatment. *The European Physical Journal Plus*, 139(9):812, 2024.

[130] Folashade B Agusto and AI Adekunle. Optimal control of a two-strain tuberculosis-HIV/AIDS co-infection model. *Biosystems*, 119:20–44, 2014.

[131] Cristiana J Silva and Delfim FM Torres. A TB-HIV/AIDS coinfection model and optimal control treatment. *Discrete and Continuous Dynamical Systems*, 35(9):4639–4663, 2015.

[132] Abhishek Mallela, Suzanne Lenhart, and Naveen K Vaidya. HIV–TB co-infection treatment: Modeling and optimal control theory perspectives. *Journal of Computational and Applied Mathematics*, 307:143–161, 2016.

[133] Fatmawati, Windarto, and Lathifah Hanif. Application of optimal control strategies to HIV-malaria co-infection dynamics. In *Journal of Physics: Conference Series*, volume 974, page 012057. IOP Publishing, 2018.

[134] Madhuri Majumder, Pankaj Kumar Tiwari, and Samares Pal. Impact of saturated treatments on HIV-TB dual epidemic as a consequence of COVID-19: Optimal control with awareness and treatment. *Nonlinear Dynamics*, 109(1):143–176, 2022.

[135] Tesfaneh Debele Batu and Legesse Lemecha Obsu. Optimal control strategies for HIV and COVID-19 co-infection: a cost-effectiveness analysis. *Frontiers in Applied Mathematics and Statistics*, 10:1439284, 2024.

[136] Shewafera Wondimagegnhu Teklu and Abushet Hayalu Workie. HIV/AIDS and HBV co-infection with optimal control strategies and cost-effectiveness analyses using integer order model. *Scientific Reports*, 15(1):4004, 2025.

[137] UNAIDS. Fast-track - Ending the AIDS epidemic by 2030, 2014.

[138] Maia Martcheva. *An Introduction to Mathematical Epidemiology*, volume 61. Springer, 2015.

[139] Pauline Van den Driessche and James Watmough. Reproduction numbers and subthreshold endemic equilibria for compartmental models of disease transmission. *Mathematical Biosciences*, 180(1-2):29–48, 2002.

[140] Paul Van den Driessche and James Watmough. Further notes on the basic reproduction number. In *Mathematical Epidemiology*, pages 159–178. Springer, 2008.

[141] Hassan K Khalil and Jessy W Grizzle. *Nonlinear Systems*, volume 3. Prentice Hall Upper Saddle River, NJ, 2002.

[142] Xiaojing Yang. Generalized form of Hurwitz-Routh criterion and Hopf bifurcation of higher order. *Applied Mathematics Letters*, 15(5):615–621, 2002.

[143] Joseph P La Salle. *The Stability of Dynamical Systems*. SIAM, 1976.

[144] Lawrence Perko. *Differential Equations and Dynamical Systems*, volume 7. Springer Science & Business Media, 2013.

[145] John Michael Tutill Thompson and H Bruce Stewart. *Nonlinear Dynamics and Chaos*. John Wiley & Sons, 2002.

[146] Steven H Strogatz. *Nonlinear Dynamics and Chaos: with Applications to Physics, Biology, Chemistry, and Engineering*. Chapman and Hall/CRC, 2024.

[147] George Qian and Adam Mahdi. Sensitivity analysis methods in the biomedical sciences. *Mathematical Biosciences*, 323:108306, 2020.

[148] Ilya M Sobol. Global sensitivity indices for nonlinear mathematical models and their Monte Carlo estimates. *Mathematics and Computers in Simulation*, 55(1):271–280, 2001.

[149] Stan Lipovetsky and Michael Conklin. Analysis of regression in game theory approach. *Applied Stochastic Models in Business and Industry*, 17(4):319–330, 2001.

[150] Scott M Lundberg and Su-In Lee. A unified approach to interpreting model predictions. *Advances in Neural Information Processing Systems*, 30, 2017.

[151] Massimo Cavallaro, Haseeb Moiz, Matt J Keeling, and Noel D McCarthy. Contrasting factors associated with COVID-19-related ICU admission and death outcomes in hospitalised patients by means of Shapley values. *PLoS Computational Biology*, 17(6):e1009121, 2021.

[152] United Nations- World Population Prospectus, 2019. `https://population.un.org/wpp/Download/Standard/Population/`.

[153] India HIV Estimate Report (2019), NACO. `http://naco.gov.in/sites/default/files/INDIA%20HIV%20ESTIMATES.pdf`.

[154] Hassan Reza Mohammadi-Moein, Mohammad Reza Maracy, and Katayoun Tayeri. Life expectancy after HIV diagnosis based on data from the counseling center for behavioral diseases. *Journal of Research in Medical Sciences: the Official Journal of Isfahan University of Medical Sciences*, 18(12):1040, 2013.

[155] Carlos Castillo-Chavez and Baojun Song. Dynamical models of tuberculosis and their applications. *Mathematical Biosciences & Engineering*, 1(2):361, 2004.

[156] M Cavani and M Farkas. Bifurcations in a predator-prey model with memory and diffusion. I: Andronov-Hopf bifurcation. *Acta Mathematica Hungarica*, 63(3):213–229, 1994.

[157] Semiu O Gbadamosi, Mary Jo Trepka, Rahel Dawit, Rime Jebai, and Diana M Sheehan. A systematic review and meta-analysis to estimate the time from HIV infection to diagnosis for people with HIV. *AIDS Reviews*, 24(1):32, 2022.

[158] Handan Wand, David Wilson, Ping Yan, Andrea Gonnermann, Ann McDonald, John Kaldor, and Matthew Law. Characterizing trends in HIV infection among men who have sex with men in Australia by birth cohorts: Results from a modified back-projection method. *Journal of the International AIDS Society*, 12:1–8, 2009.

[159] H Irene Hall, Ruiguang Song, Célia Landmann Szwarcwald, and Timothy Green. Brief report: Time from infection with the human immunodeficiency virus to diagnosis, United States. *JAIDS Journal of Acquired Immune Deficiency Syndromes*, 69(2):248–251, 2015.

[160] Andre F Dailey. Vital signs: Human immunodeficiency virus testing and diagnosis delays—United States. *Morbidity and Mortality Weekly Report*, 66, 2017.

[161] Yan Tao, Xueling Xiao, Ci Zhang, Ying Xie, and Honghong Wang. Prevalence of delayed antiretroviral therapy initiation among people living with HIV: A systematic review and meta-analysis. *PLoS One*, 18(10):e0286476, 2023.

[162] Vanessa Nicolau, Rui Cortes, Maria Lopes, Ana Virgolino, Osvaldo Santos, António Martins, Nancy Faria, Ana Paula Reis, Catarina Santos, Fernando Maltez, et al. HIV infection: Time from diagnosis to initiation of antiretroviral therapy in Portugal, a multicentric study. In *Healthcare*, volume 9, page 797. MDPI, 2021.

[163] Kathryn M Stadeli and Douglas D Richman. Rates of emergence of HIV drug resistance in resource-limited settings: a systematic review. *Antiviral Therapy*, 18(1):115–123, 2013.

[164] Global HIV & AIDS statistics — Fact sheet, 2020. `https://www.unaids.org/en/resources/fact-sheet`, 2020.

[165] David R Bangsberg, Andrew R Moss, and Steven G Deeks. Paradoxes of adherence and drug resistance to HIV antiretroviral therapy. *Journal of Antimicrobial Chemotherapy*, 53(5):696–699, 2004.

[166] Jose M Munita and Cesar A Arias. Mechanisms of antibiotic resistance. *Microbiology Spectrum*, 4(2):4–2, 2016.

[167] James A Yorke. Invariance for ordinary differential equations. *Mathematical Systems Theory*, 1(4):353–372, 1967.

[168] George T Gilbert. Positive definite matrices and Sylvester's criterion. *The American Mathematical Monthly*, 98(1):44–46, 1991.

[169] Wei-Min Liu. Criterion of Hopf bifurcations without using eigenvalues. *Journal of Mathematical Analysis and Applications*, 182(1):250–256, 1994.

[170] Jalal Poorolajal, Elham Hooshmand, Hossein Mahjub, Nader Esmailnasab, and Ensiyeh Jenabi. Survival rate of AIDS disease and mortality in HIV-infected patients: a meta-analysis. *Public Health*, 139:3–12, 2016.

[171] S Teeraananchai, SJ Kerr, J Amin, K Ruxrungtham, and MG Law. Life expectancy of HIV-positive people after starting combination antiretroviral therapy: A meta-analysis. *HIV Medicine*, 18(4):256–266, 2017.

[172] Global HIV & AIDS statistics — Fact sheet, 2022. `https://www.unaids.org/sites/default/files/media_asset/UNAIDS_FactSheet_en.pdf`, 2022.

[173] Palanee Ammaranond, Philip Cunningham, Robert Oelrichs, Kazuo Suzuki, Claire Harris, Leakhena Leas, Andrew Grulich, David A Cooper, and Anthony D Kelleher.

Rates of transmission of antiretroviral drug resistant strains of HIV-1. *Journal of Clinical Virology*, 26(2):153–161, 2003.

[174] Purity Ngina, Rachel Waema Mbogo, and Livingstone S Luboobi. HIV drug resistance: Insights from mathematical modelling. *Applied Mathematical Modelling*, 75:141–161, 2019.

[175] Xin Jin, Zhen Wang, Zhiyuan Zhang, Hui Wu, Yuhua Ruan, Chen Zhang, Ruihua Kang, Hui Xing, and Jie Lou. The transmission of drug-resistant strains of HIV in heterosexual populations based on genetic sequences. *PLoS One*, 16(12):e0259023, 2021.

[176] Jane M Simoni, K Rivet Amico, Cynthia R Pearson, and Robert Malow. Strategies for promoting adherence to antiretroviral therapy: a review of the literature. *Current Infectious Disease Reports*, 10(6):515–521, 2008.

[177] Maithe Enriquez and David S McKinsey. Strategies to improve HIV treatment adherence in developed countries: Clinical management at the individual level. *HIV/AIDS-Research and Palliative Care*, pages 45–51, 2011.

[178] Roy M Anderson and Robert M May. *Infectious Diseases of Humans: Dynamics and Control*. Oxford University Press, 1991.

[179] H Irene Hall, David R Holtgrave, and Catherine Maulsby. Hiv transmission rates from persons living with HIV who are aware and unaware of their infection. *AIDS*, 26(7):893–896, 2012.

[180] United Nations - World Population Prospects 2024. `https://population.un.org/wpp/Download/SpecialAggregates/EconomicTrading/`, 2024.

[181] Pengxiang Li, Girish Prajapati, Zhi Geng, Vrushabh P Ladage, Jean Marie Arduino, Dovie L Watson, Robert Gross, and Jalpa A Doshi. Antiretroviral treatment gaps and adherence among people with HIV in the US Medicare program. *AIDS and Behavior*, 28(3):1002–1014, 2024.

[182] Maya Mahmoud, Tala Ballouz, Chloe Lahoud, Jana Adnan, Paola Abi Habib, Reem Saab, Haya Farhat, Mohammad El Hussein, and Nesrine Rizk. Late presentations and missed opportunities among newly diagnosed HIV patients presenting to a specialty clinic in Lebanon. *Scientific Reports*, 14(1):8296, 2024.

[183] Francesca Pianosi, Keith Beven, Jim Freer, Jim W Hall, Jonathan Rougier, David B Stephenson, and Thorsten Wagener. Sensitivity analysis of environmental models: A systematic review with practical workflow. *Environmental Modelling & Software*, 79:214–232, 2016.

[184] Nakul Chitnis, Hyman James M., and Cushing Jim M. Determining important parameters in the spread of malaria through the sensitivity analysis of a mathematical model. *Bulletin of Mathematical Biology*, 70:1272–1296, 2008.

[185] George Fishman. *Monte Carlo: Concepts, Algorithms, and Applications*. Springer Science & Business Media, 2013.

[186] Jon C Helton and Freddie Joe Davis. Latin hypercube sampling and the propagation of uncertainty in analyses of complex systems. *Reliability Engineering & System Safety*, 81(1):23–69, 2003.

[187] Russel E Caflisch. Monte Carlo and quasi-Monte Carlo methods. *Acta Numerica*, 7:1–49, 1998.

[188] Simeone Marino, Ian B Hogue, Christian J Ray, and Denise E Kirschner. A methodology for performing global uncertainty and sensitivity analysis in systems biology. *Journal of Theoretical Biology*, 254(1):178–196, 2008.

[189] GEB Archer, Andrea Saltelli, and Ilya Meyerovich Sobol. Sensitivity measures, ANOVA-like techniques and the use of bootstrap. *Journal of Statistical Computation and Simulation*, 58(2):99–120, 1997.

[190] Andrea Saltelli, Paola Annoni, Ivano Azzini, Francesca Campolongo, Marco Ratto, and Stefano Tarantola. Variance based sensitivity analysis of model output. Design and estimator for the total sensitivity index. *Computer Physics Communications*, 181(2):259–270, 2010.

[191] Jon Herman and Will Usher. SALib: An open-source Python library for sensitivity analysis. *Journal of Open Source Software*, 2(9):97, 2017.

[192] Ilya M Sobol. Uniformly distributed sequences with an additional uniform property. *USSR Computational Mathematics and Mathematical Physics*, 16(5):236–242, 1976.

[193] Art B Owen. On dropping the first Sobol'point. In *International Conference on Monte Carlo and quasi-Monte Carlo Methods in Scientific Computing*, pages 71–86. Springer, 2020.

[194] FB Agusto and MCA Leite. Optimal control and cost-effective analysis of the 2017 meningitis outbreak in Nigeria. *Infectious Disease Modelling*, 4:161–187, 2019.

[195] Wendell H Fleming and Raymond W Rishel. *Deterministic and Stochastic Optimal Control*, volume 1. Springer, New York, 1975.

[196] Earl A Coddington, Norman Levinson, and T Teichmann. *Theory of Ordinary Differential Equations*. American Institute of Physics, 1956.

[197] Lev Semenovich Pontryagin. *Mathematical Theory of Optimal Processes*. Routledge, 2018.

[198] Tunde T Yusuf and Afeez Abidemi. Effective strategies towards eradicating the tuberculosis epidemic: An optimal control theory alternative. *Healthcare Analytics*, 3:100–131, 2023.

[199] Tamás Péni, Balázs Csutak, Gábor Szederkényi, and Gergely Röst. Nonlinear model predictive control with logic constraints for COVID-19 management. *Nonlinear Dynamics*, 102:1965–1986, 2020.

[200] David Q Mayne, James B Rawlings, Christopher V Rao, and Pierre OM Scokaert. Constrained model predictive control: Stability and optimality. *Automatica*, 36(6):789–814, 2000.

[201] Ryan Zurakowski and Andrew R Teel. A model predictive control based scheduling method for HIV therapy. *Journal of Theoretical Biology*, 238(2):368–382, 2006.

[202] Radhika Sundararajan, Matthew Ponticiello, Denis Nansera, Kidola Jeremiah, and Winnie Muyindike. Interventions to increase HIV testing uptake in global settings. *Current HIV/AIDS Reports*, 19(3):184–193, 2022.

[203] Michael J Mugavero, Wynne E Norton, and Michael S Saag. Health care system and policy factors influencing engagement in HIV medical care: piecing together the fragments of a fractured health care delivery system. *Clinical Infectious Diseases*, 52(suppl_2):S238–S246, 2011.

[204] Lawrence Mbuagbaw, Bhairavi Sivaramalingam, Tamara Navarro, Nicholas Hobson, Arun Keepanasseril, Nancy J Wilczynski, R Brian Haynes, and Patient Adherence Review (PAR) Team. Interventions for enhancing adherence to antiretroviral therapy (ART): A systematic review of high quality studies. *AIDS Patient Care and STDs*, 29(5):248–266, 2015.

[205] D Mattur and V Habiyambere. Variation in average unit prices (2020) of antiretroviral drugs in generic accessible low- and middle-income countries. In *Journal of the International AIDS Society*, volume 25, pages 50–52. John Wiley & Sons Ltd., The Atrium, Southern Gate, Chichester, 2022.

[206] Yang Cao, Shengtai Li, Linda Petzold, and Radu Serban. Adjoint sensitivity analysis for differential-algebraic equations: The adjoint DAE system and its numerical solution. *SIAM Journal on Scientific Computing*, 24(3):1076–1089, 2003.

[207] Lindsay Simpson and Abba B Gumel. Mathematical assessment of the role of pre-exposure prophylaxis on HIV transmission dynamics. *Applied Mathematics and Computation*, 293:168–193, 2017.

[208] Kevin M Gibas, Polly van den Berg, Victoria E Powell, and Douglas S Krakower. Drug resistance during HIV pre-exposure prophylaxis. *Drugs*, 79(6):609–619, 2019.

[209] Samuel M Jenness, Jordan A Johnson, Karen W Hoover, Dawn K Smith, and Kevin P Delaney. Modeling an integrated HIV prevention and care continuum to achieve the ending of the HIV epidemic goals. *AIDS*, 34(14):2103–2113, 2020.

[210] Rodrigo Volmir Anderle, Robson Bruniera de Oliveira, Felipe Alves Rubio, James Macinko, Ines Dourado, and Davide Rasella. Modelling HIV/AIDS epidemiological complexity: A scoping review of Agent-Based Models and their application. *PLoS One*, 19(2):e0297247, 2024.

List of Published Papers

Based on the work in this thesis, the following research articles have been published.

1. Ashish Poonia and Siddhartha P. Chakrabarty, Two strains and drug adherence: An HIV model in the paradigm of community transmission, Nonlinear Dynamics, vol. 108, pp. 2767-2792, 2022.
2. Ashish Poonia and Siddhartha P. Chakrabarty, Dynamics of a multi-strain HIV/AIDS epidemic model with treatment and its adherence, The European Physical Journal Plus, vol. 139, no. 8, pp. 769, 2024.
3. Ashish Poonia and Siddhartha P. Chakrabarty, Strategic control of drug-resistant HIV: Multi-strain modeling with diagnosis, adherence, and treatment switching, Bulletin of Mathematical Biology, vol. 87, no. 12, pp. 173, 2025.